

Gas Absorption and Gas-Liquid System Design*

James R. Fair, Ph.D., P.E., Professor of Chemical Engineering, University of Texas; Fellow, American Institute of Chemical Engineers; Member, American Chemical Society, American Society for Engineering Education, National Society of Professional Engineers. (Section Editor, Absorption, Gas-Liquid Contacting)

D. E. Steinmeyer, M.A., M.S., P.E., Distinguished Fellow, Monsanto Company; Fellow, American Institute of Chemical Engineers; Member, American Chemical Society. (Liquid-in-Gas Dispersions)

W. R. Penney, Ph.D., P.E., Professor of Chemical Engineering, University of Arkansas; Member, American Institute of Chemical Engineers. (Gas-in-Liquid Dispersions)

B. B. Crocker, S.M., P.E., Consulting Chemical Engineer; Fellow, American Institute of Chemical Engineers; Member, Air Pollution Control Association. (Phase Separation)

INTRODUCTION

Definitions	14-4	Use of Operating Curve	14-8
Equipment	14-4	Calculation of Transfer Units	14-9
Design Procedures	14-4	Stripping Equations	14-9
Data Sources in the Handbook	14-4	Example 3: Air Stripping of VOCs from Water	14-10
Equilibrium Data	14-4	Use of HTU and K_{CO} Data	14-10
		Use of HETP Data for Absorber Design	14-10

DESIGN OF GAS-ABSORPTION SYSTEMS

General Design Procedure	14-5	PLATE-TOWER DESIGN	
Selection of Solvent	14-5	Graphical Design Procedure	14-11
Selection of Solubility Data	14-5	Algebraic Method for Dilute Gases	14-11
Example 1: Gas Solubility	14-5	Algebraic Method for Concentrated Gases	14-11
Calculation of Liquid-to-Gas Ratio	14-5	Stripping Equations	14-11
Selection of Equipment	14-6	Tray Efficiencies in Plate Absorbers and Strippers	14-12
Column Diameter and Pressure Drop	14-6	Example 4: Actual Plates for Steam Stripping	14-12
Computation of Tower Height	14-6		
Selection of Stripper-Operating Conditions	14-6		
Design of Absorber-Stripper Systems	14-6		
Importance of Design Diagrams	14-6		

PACKED-TOWER DESIGN

Use of Mass-Transfer-Rate Expressions	14-8	HEAT EFFECTS IN GAS ABSORPTION	
Example 2: Packed Height Requirement	14-8	Overview	14-12

		Effects of Operating Variables	14-13
		Equipment Considerations	14-13
		Classical Isothermal Design Method	14-14
		Classical Adiabatic Design Method	14-14
		Rigorous Design Methods	14-14

* Much of the material on absorption is taken from Sec. 14 of the sixth edition, and credit is due to Dr. William M. Edwards, editor of that section.

14-2 GAS ABSORPTION AND GAS-LIQUID SYSTEM DESIGN

Direct Comparison of Design Methods	14-14	Plates versus Packings	14-59
Example 5: Packed Absorber, Acetone into Water	14-14	Optimization	14-61
Example 6: Solvent Rate for Absorption	14-14	PHASE DISPERSION	
MULTICOMPONENT SYSTEMS			
Example 7: Multicomponent Absorption, Dilute Case	14-15	General References	14-62
Graphical Design Methods for Dilute Systems	14-16	Liquid-in-Gas Dispersions	14-62
Algebraic Design Method for Dilute Systems	14-16	Liquid Breakup into Droplets	14-62
Example 8: Multicomponent Absorption, Concentrated Case	14-16	Droplet Breakup—High Turbulence	14-62
ABSORPTION WITH CHEMICAL REACTION			
Introduction	14-17	Liquid-Column Breakup	14-62
Recommended Overall Design Strategy	14-17	Liquid-Sheet Breakup	14-62
Applicability of Physical Design Methods	14-17	Isolated Droplet Breakup—in a Velocity Field	14-62
Traditional Design Method	14-18	Droplet Size Distribution	14-63
Scaling Up from Laboratory or Pilot-Plant Data	14-19	Atomizers	14-63
Principles of Rigorous Absorber Design	14-20	Hydraulic (Pressure) Nozzles	14-63
Estimation of k_L for Irreversible Reactions	14-21	Effect of Physical Properties on Drop Size	14-63
Estimation of k_L for Reversible Reactions	14-22	Effect of Pressure Drop and Nozzle Size	14-64
Simultaneous Absorption of Two Reacting Gases	14-22	Spray Angle	14-66
Desorption with Chemical Reaction	14-23	Two-Fluid (Pneumatic) Atomizers	14-66
Use of Literature for Specific Systems	14-23	Rotary Atomizers	14-66
GAS-LIQUID CONTACTING SYSTEMS			
Plate Columns	14-24	Pipeline Contactors	14-66
Plate Types	14-24	Entrainment Due to Gas Bubbling/Jetting through a Liquid	14-66
Plate-Column Capacity	14-25	Fog Condensation	14-67
Example 9: Loading/Flooding of a Distillation Plate	14-28	Spontaneous (Homogeneous) Nucleation	14-68
Example 10: Entrainment Effect on Plate Efficiency	14-29	Growth on Foreign Nuclei	14-68
Plate Layouts	14-29	Dropwise Distribution	14-68
Pressure Drop	14-30	Gas-in-Liquid Dispersions	14-69
Example 11: Pressure Drop, Sieve Plate	14-33	General References	14-69
Phase Inversion	14-34	Objectives of Gas Dispersion	14-69
Plate Efficiency	14-34	Theory of Bubble and Foam Formation	14-70
Example 12: Estimation of Plate Efficiency	14-36	Characteristics of Dispersion	14-72
Packed Columns	14-38	Methods of Gas Dispersion	14-73
Introduction	14-38	Equipment Selection	14-76
Packed Columns versus Plate Columns	14-39	Mass Transfer	14-79
Packed-Column Hydraulics	14-40	Axial Dispersion	14-80
Flooding and Loading	14-41	PHASE SEPARATION	
Pressure Drop	14-42	Gas-Phase Continuous Systems	14-81
Example 13: Packed Column Pressure Drop	14-44	General References	14-81
Support Plates	14-46	Definitions: Mist and Spray	14-81
Liquid Holdup	14-46	Gas Sampling	14-81
Liquid Distribution	14-48	Particle-Size Analysis	14-82
Maldistribution	14-50	Collection Mechanisms	14-82
End Effects	14-50	Procedures for Design and Selection of Collection Devices	14-82
Interfacial Area	14-51	Collection Equipment	14-83
Mass Transfer	14-52	Energy Requirements for Inertial-Impaction Efficiency	14-93
Behavior of Various Systems and Packings	14-52	Collection of Fine Mists	14-93
Distillation Applications	14-52	Fiber Mist Eliminators	14-93
Liquid-Dispersed Contactors	14-54	Electrostatic Precipitators	14-94
Introduction	14-54	Electrically Augmented Collectors	14-94
Heat-Transfer Applications	14-55	Particle Growth and Nucleation	14-95
Theoretical Transfer Model	14-55	Other Collectors	14-95
Countercurrent, Cocurrent, or Backmixed	14-56	Continuous Phase Uncertain	14-95
Empirical Approach	14-56	Liquid-Phase Continuous Systems	14-95
Wetted-Wall Columns	14-56	General References	14-95
Gas-Liquid-Column Economics	14-58	Types of Gas-in-Liquid Dispersions	14-95
Cost of Internals	14-58	Separation of Unstable Systems	14-95
Cost of Column	14-58	Separation of Foam	14-96
		Physical Defoaming Techniques	14-97
		Chemical Defoaming Techniques	14-97
		Foam Prevention	14-98
		Automatic Foam Control	14-98

Nomenclature

a_e	Effective interfacial area	m^2/m^3	ft^2/ft^3	L_w	Weir length	m	ft
A	Cross sectional area	m^2	ft^2	m	Slope of equilibrium curve = dy^o/dx	-/-	-/-
A_f	Fractional open area	-/-	-/-	M	Molecular weight	kg/kmol	$\text{lb}/\text{lb-mol}$
A	Absorption factor	-/-	-/-	nA	Rate of solute transfer	kmol/s	lb-mol/s
A_e, A'	Effective absorption factor (Edmister)	-/-	-/-	p	Partial pressure	kPa	atm
c	Concentration	kg-moles/m^3	lb-mol/ft^3	P, p_T	Total pressure	kPa	atm
c'	Stokes-Cunningham correction factor for terminal settling velocity	-/-	-/-	q	Volumetric flow rate of liquid	m^3/s	ft^3/s
C_{sb}, C_s	Flooding coefficient	m/s	ft/s	Q	Volumetric flow rate of gas or vapor	m^3/s	ft^3/s
C_v	Discharge coefficient	-/-	-/-	R	Gas constant		
d	Diameter	m	ft	R_h	Hydraulic radius	m	ft
d_b	Bubble diameter	m	ft	s	Length of corrugation side, structured packing	m	ft
d_h	Hole diameter	m	ft	S	Stripping factor	-/-	-/-
d_o	Orifice diameter	m	ft	S_e, S'	Effective stripping factor (Edmister)	-/-	-/-
d_{pe}	Cut size of a particle collected in a device, 50% mass efficiency	μm	ft	T	Absolute temperature	K	°F
d_{psd}	Mass median size particle in the pollutant gas	μm	ft	TS	Tray or plate spacing	m	ft
d_{pa50}	Aerodynamic diameter of a real median size particle	μm	ft	U	Linear velocity of gas	m/s	ft/s
D	Diffusion coefficient	m^2/s	ft^2/s	U_a	Velocity of gas through active area	m/s	ft/s
D_{32}	Sauter mean diameter	m	ft	U_n	Velocity of gas through net area	m/s	ft/s
D_{vm}	Volume mean diameter	m	ft	x	Mole fraction, liquid phase condition	-/-	-/-
e	Entrainment, mass liquid/mass gas	kg/kg	lb/lb	y	Mole fraction, gas or vapor phase	-/-	-/-
E	Plate or stage efficiency, fractional	-/-	-/-	y^*	Gas mole fraction, equilibrium condition	-/-	-/-
E	Power dissipation per mass	W	btu/lb	Z	Height, plate spacing	m	ft
E_a	Murphree plate efficiency, with entrainment, gas concentrations, fractional	-/-	-/-				
E_g	Point efficiency, gas phase only, fractional	-/-	-/-				
E_{oc}	Overall column efficiency, fractional	-/-	-/-				
E_{og}	Overall point efficiency, gas concentrations, fractional	-/-	-/-				
E_{mv}	Murphree plate efficiency, gas concentrations, fractional	-/-	-/-				
f	Fractional approach to flood	-/-	-/-				
F	F-factor for gas loading	$\text{m/s}(\text{kg}/\text{m}^3)^{0.5}$	$\text{ft/s}(\text{lb}/\text{ft}^3)^{0.5}$				
F_{LG}	Flow parameter	-/-	-/-				
g	Gravitational constant	m/s^2	ft/s^2				
g_c	Conversion factor	1.0 ($\text{kg}\cdot\text{m}/\text{N}\cdot\text{s}^2$)	$32.2(\text{lb}\cdot\text{ft})/(\text{lb}_f\cdot\text{s}^2)$				
G	Gas phase mass velocity	$\text{kg/s}\cdot\text{m}^2$	$\text{lb/hr}\cdot\text{ft}^2$				
G_M	Gas phase molar velocity	$\text{kg-moles/s}\cdot\text{m}^2$	$\text{lb-mol/hr}\cdot\text{ft}^2$				
h	Pressure head	mm	ft				
h_f	Height of froth	m	ft				
h_T	Height of contacting	m	ft				
H	Henry's law constant						
H'	Henry's law constant						
H	Height of a transfer unit	m	ft				
H_g	Height of a gas phase transfer unit	m	ft				
H_{og}	Height of an overall transfer unit, gas phase concentrations	m	ft				
H_{OL}	Height of an overall transfer unit, liquid phase concentrations	m	ft				
H_L	Height of a liquid phase transgrafer unit	m	ft				
H'	Henry's law coefficient	kPa/mole	atm/mole				
HETP	Height equivalent to a theoretical plate or stage	m	ft				
k_1	First order reaction velocity constant	1/s	1/sec				
k_2	Second order reaction velocity constant	$\text{m}^3/(\text{s}\cdot\text{kmol})$	$\text{ft}^3/(\text{h}\cdot\text{lb}\cdot\text{mol})$				
k	Individual phase mass transfer coefficient	m/s	ft/sec				
k_G	gas phase mass transfer coefficient	m/s	ft/sec				
k_L	liquid phase mass transfer coefficient	m/s	ft/sec				
K	Vapor-liquid equilibrium ratio	-/-	-/-				
K_{OG}, K_C	Overall mass transfer coefficient, gas concentrations	m/s	ft/sec				
K_{OL}	Overall mass transfer coefficient, liquid concentrations	m/s	ft/sec				
L	Liquid mass velocity	$\text{kg}/\text{m}^2\cdot\text{s}$	$\text{lb}/\text{ft}^2\cdot\text{s}$				
L_M	Liquid molar mass velocity	$\text{kmoles}/\text{m}^2\cdot\text{s}$	$\text{lb-mol}/\text{ft}^2\cdot\text{s}$				
Greek symbols							
α	Relative volatility	-/-	-/-				
β	Aeration factor	-/-	-/-				
ϵ	Void fraction	-/-	-/-				
ϕ	Relative froth density	-/-	-/-				
γ	Activity coefficient	-/-	-/-				
Γ	Flow rate per length	$\text{kg}/(\text{s}\cdot\text{m})$	$\text{lb}/(\text{s}\cdot\text{ft})$				
δ	Effective film thickness	m	ft				
η	Collection efficiency, fractional	-/-	-/-				
λ	Stripping factor = $m/(L_M/G_M)$	-/-	-/-				
μ	Absolute viscosity	$\text{Pa}\cdot\text{s}$	$\text{lb}/(\text{ft}\cdot\text{s})$				
μm	Microns	m	ft				
ν	Kinematic viscosity	m^2/s	ft^2/s				
π	3.1416 . . .	-/-	-/-				
θ	Residence time	s	s				
ρ	Density	kg/m^3	lb/ft^3				
σ	Surface tension	mN/m	dyn/cm				
ψ	Fractional entrainment	-/-	-/-				
Subscripts							
A	Species A						
AB	Species A diffusing through species B						
B	Species B						
e	Effective value						
i	Interface value						
G	Gas or vapor						
L	Liquid						
p	Particle						
w	water						
1	Tower bottom						
2	Tower top						
Dimensionless Groups							
N_{Fr}	Froude number = $(U_L^2)/(Sg)$						
N_{Re}	Reynolds number = $(SU_{ge}\rho_C)/(\mu_G)$						
N_{Sc}	Schmidt number = $\mu/(\rho D)$						
N_{We}	Weber number = $(U_L^2\rho_L S)/(\sigma g_c)$						

GENERAL REFERENCES: Astarita, G., *Mass Transfer with Chemical Reaction*, Elsevier, New York, 1967. Astarita, G., D. W. Savage and A. Bisio, *Gas Treating with Chemical Solvents*, Wiley, New York, 1983. Billet, R., *Distillation Engineering*, Chemical Publishing Co., New York, 1979. Danckwerts, P. V., *Gas-Liquid Reactions*, McGraw-Hill, New York, 1970. *Distillation and Absorption* 1987, Rugby, U.K., Institution of Chemical Engineers, 1988. *Distillation and Absorption* 1992, Rugby, U.K., Institution of Chemical Engineers, 1992. Hines,

A. L. and R. N. Maddox, *Mass Transfer—Fundamentals and Applications*, Prentice Hall, Englewood Cliffs, New Jersey, 1985. Kister, H. Z., *Distillation Design*, McGraw-Hill, New York, 1992. Lockett, M. J., *Distillation Tray Fundamentals*, Cambridge, U.K., Cambridge University Press, 1986. Kohl, A. L. and F. C. Riesenfeld, *Gas Purification*, 4th ed., Gulf, Houston, 1985. Sherwood, T. K., R. L. Pigford, C. R. Wilke, *Mass Transfer*, McGraw-Hill, New York, 1975. Treybal, R. E., *Mass Transfer Operations*, McGraw-Hill, New York, 1980.

INTRODUCTION

Definitions Gas absorption is a unit operation in which soluble components of a gas mixture are dissolved in a liquid. The inverse operation, called stripping or desorption, is employed when it is desired to transfer volatile components from a liquid mixture into a gas. Both absorption and stripping, in common with distillation (Sec. 13), make use of special equipment for bringing gas and liquid phases into intimate contact. This section is concerned with the design of gas-liquid contacting equipment, as well as with the design of absorption and stripping processes.

Equipment Absorption, stripping, and distillation operations are usually carried out in vertical, cylindrical columns or towers in which devices such as plates or packing elements are placed. The gas and liquid normally flow countercurrently, and the devices serve to provide the contacting and development of interfacial surface through which mass transfer takes place. Background material on this mass transfer process is given in Sec. 5.

Design Procedures The procedures to be followed in specifying the principal dimensions of gas absorption and distillation equipment are described in this section and are supported by several worked-out examples. The experimental data required for executing the designs are keyed to appropriate references or to other sections of the handbook.

For absorption, stripping, and distillation, there are three main steps involved in design:

1. *Data on the gas-liquid or vapor-liquid equilibrium for the system at hand.* If absorption, stripping, and distillation operations are considered equilibrium-limited processes, which is the usual approach, these data are critical for determining the maximum possible separation. In some cases, the operations are considered rate-based (see Sec. 13) but require knowledge of equilibrium at the phase interface. Other data required include physical properties such as viscosity and density and thermodynamic properties such as enthalpy. Section 2 deals with sources of such data.

2. *Information on the liquid- and gas-handling capacity of the contacting device chosen for the particular separation problem.* Such information includes pressure drop characteristics of the device, in order that an optimum balance between capital cost (column cross section) and energy requirements might be achieved. Capacity and pressure drop characteristics of the available devices are covered later in this Sec. 14.

3. *Determination of the required height of contacting zone for the separation to be made as a function of properties of the fluid mixtures and mass-transfer efficiency of the contacting device.* This determination involves the calculation of mass-transfer parameters such as heights of transfer units and plate efficiencies as well as equilibrium or rate parameters such as theoretical stages or numbers of transfer units. An additional consideration for systems in which chemical reaction occurs is the provision of adequate residence time for desired reactions to occur, or minimal residence time to prevent undesired reactions from occurring. For equilibrium-based operations, the parameters for required height are covered in the present section.

Data Sources in the Handbook Sources of data for the analysis or design of absorbers, strippers, and distillation columns are mani-

fold, and a detailed listing of them is outside the scope of the presentation in this section. Some key sources within the handbook are shown in Table 14-1.

Equilibrium Data Finding reliable gas-liquid and vapor-liquid equilibrium data may be the most time-consuming task associated with the design of absorbers and other gas-liquid contactors, and yet it may be the most important task at hand. For gas solubility, an important data source is the set of volumes edited by Kertes et al., *Solubility Data Series*, published by Pergamon Press (1979 ff.). In the introduction to each volume, there is an excellent discussion and definition of the various methods by which gas solubility data have been reported, such as the Bunsen coefficient, the Kuenen coefficient, the Ostwald coefficient, the absorption coefficient, and the Henry's law coefficient. The fourth edition of *The Properties of Gases and Liquids* by Reid, Prausnitz and Poling (McGraw-Hill, New York, 1987) provides data and recommended estimation methods for gas solubility as well as the broader area of vapor-liquid equilibrium. Finally, the Chemistry Data Series by Gmehling et al., especially the title *Vapor-Liquid Equilibrium Collection* (DECHEMA, Frankfurt, Germany, 1979 ff.), is a rich source of data evaluated against the various models used for interpolation and extrapolation. Section 13 of this handbook presents a good discussion of equilibrium K values.

TABLE 14-1 Directory to Key Data for Absorption and Gas-Liquid Contactor Design

Type of data	Section
Phase equilibrium data	
Gas solubilities	2
Pure component vapor pressures	2
Equilibrium K values	13
Thermal data	
Heats of solution	2
Specific heats	2
Latent heats of vaporization	2
Transport property data	
Diffusion coefficients	
Liquids	2
Gases	2
Viscosities	
Liquids	2
Gases	2
Densities	
Liquids	2
Gases	2
Surface tensions	2
Packed tower data	
Pressure drop and flooding	14
Mass transfer coefficients	5
HTU, physical absorption	5
HTU with chemical reaction	14
Height equivalent to a theoretical plate (HETP)	
Plate tower data	
Pressure drop and flooding	14
Plate efficiencies	14
Costs of gas-liquid contacting equipment	14

DESIGN OF GAS-ABSORPTION SYSTEMS

General Design Procedure The designer ordinarily is required to determine (1) the best solvent; (2) the best gas velocity through the absorber, namely the vessel diameter; (3) the height of the vessel and its internal members, which is the height and type of packing or the number of contacting trays; (4) the optimum solvent circulation through the absorber and stripper; (5) the temperatures of streams entering and leaving the absorber and the quantity of heat to be removed to account for heat of solution and other thermal effects; (6) the pressures at which the absorber and stripper will operate; and (7) the mechanical design of the absorption and stripping vessels (normally columns or towers), including flow distributors, packing supports, and so on. This section is concerned with all these choices.

The problem presented to the designer of a gas-absorption unit usually specifies the following quantities: (1) gas flow rate; (2) gas composition, at least with respect to the component or components to be absorbed; (3) operating pressure and allowable pressure drop across the absorber; (4) minimum degree of recovery of one or more solutes; and, possibly, (5) the solvent to be employed. Items 3, 4, and 5 may be subject to economic considerations and therefore are sometimes left up to the designer. For determining the number of variables that must be specified in order to fix a unique solution for the design of an absorber one can use the same phase-rule approach described in Sec. 13 for distillation systems.

Recovery of the solvent, sometimes by chemical means but more often by distillation, is almost always required, and the recovery system ordinarily is considered an integral part of the absorption-system process design. A more efficient solvent-stripping operation normally will result in a less costly absorber because of smaller concentration of residual dissolved solute in the regenerated solvent; however, this may increase the overall cost of solvent recovery. A more detailed discussion of these and other economic considerations is presented later in this section.

Selection of Solvent When choice is possible, preference is given to liquids with high solubilities for the solute; a high solubility reduces the amount of solvent to be circulated. The solvent should be relatively nonvolatile, inexpensive, noncorrosive, stable, nonviscous, nonfoaming, and preferably nonflammable. Since the exit gas normally leaves saturated with solvent, solvent loss can be costly and may present environmental contamination problems. Thus, low-cost solvents may be chosen over more expensive ones of higher solubility or lower volatility.

Water generally is used for gases fairly soluble in water, oils for light hydrocarbons, and special chemical solvents for acid gases such as CO₂, SO₂, and H₂S. Sometimes a reversible chemical reaction will result in a very high solubility and a minimum solvent rate. Data on actual systems are desirable when chemical reactions are involved, and those available are referenced later under "Absorption with Chemical Reaction."

Selection of Solubility Data Solubility values determine the liquid rate necessary for complete or economic solute recovery and so are essential to design. Equilibrium data generally will be found in one of three forms: (1) solubility data expressed either as solubility in weight or mole percent or as Henry's-law coefficients, (2) pure-component vapor pressures, or (3) equilibrium distribution coefficients (*K* values). Data for specific systems may be found in Sec. 2; additional references to sources of data are presented in this section.

In order to define completely the solubility of a gas in a liquid, it generally is necessary to state the temperature, the equilibrium partial pressure of the solute gas in the gas phase, and the concentration of the solute gas in the liquid phase. Strictly speaking, the total pressure on the system also should be stated, but for low total pressures, less than about 507 kPa (5 atm), the solubility for a particular partial pressure of solute gas normally will be relatively independent of the total pressure of the system.

For dilute concentrations of many gases and over a fairly wide range for some gases, the equilibrium relationship is given by Henry's law, which relates the partial pressure developed by a dissolved solute A in a liquid solvent B by one of the following equations:

$$p_A = Hx_A \quad (14-1)$$

$$\text{or} \quad P_A = H'c_A \quad (14-2)$$

where *H* is the Henry's law coefficient expressed in kilopascals per mole-fraction solute in liquid and *H'* is the Henry's law coefficient expressed in kilopascals per kilomole per cubic meter.

Although quite useful when it can be applied, this law should be checked experimentally to determine the accuracy with which it can be used. If Henry's law holds, the solubility is defined by stating the value of the constant *H* (or *H'*) along with the temperature and the solute partial pressure for which it is to be employed.

For quite a number of gases, Henry's law holds very well when the partial pressure of the solute is less than about 100 kPa (1 atm). For partial pressures of the solute gas greater than 100 kPa, *H* seldom is independent of the partial pressure of the solute gas, and a given value of *H* can be used over only a narrow range of partial pressures. There is a strongly nonlinear variation of Henry's-law constants with temperature as discussed by Schulze and Prausnitz [*Ind. Eng. Chem. Fundam.*, **20**, 175 (1981)]. Consultation of this reference is recommended before considering temperature extrapolations of Henry's-law data.

Additional data and information on the applicability of Henry's-law constants can be found in the references cited earlier in the subsection "Directory to Key Gas-Absorption Data." The use of Henry's-law constants is illustrated by the following examples.

Example 1: Gas Solubility It is desired to find out how much hydrogen can be dissolved in 100 weights of water from a gas mixture when the total pressure is 101.3 kPa (760 torr; 1 atm), the partial pressure of H₂ is 26.7 kPa (200 torr), and the temperature is 20°C. For partial pressures up to about 100 kPa the value of *H* is given in Sec. 3 as 6.92×10^6 kPa (6.83×10^3 atm) at 20°C. According to Henry's law,

$$x_{\text{H}_2} = p_{\text{H}_2}/H_{\text{H}_2} = 26.7/6.92 \times 10^6 = 3.86 \times 10^{-6}$$

The mole fraction *x* is the ratio of the number of moles of H₂ in solution to the total moles of all constituents contained. To calculate the weights of H₂ per 100 weights of H₂O, one can use the following formula, where the subscripts A and w correspond to the solute (hydrogen) and solvent (water):

$$\begin{aligned} \left(\frac{x_A}{1 - x_A} \right) \frac{M_A}{M_w} 100 &= \left(\frac{3.86 \times 10^{-6}}{1 - 3.86 \times 10^{-6}} \right) \frac{2.02}{18.02} 100 \\ &= 4.33 \times 10^{-5} \text{ weights H}_2/100 \text{ weights H}_2\text{O} \\ &= 0.43 \text{ parts per million weight} \end{aligned}$$

Pure-component vapor pressures can be used for predicting solubilities for systems in which **Raoult's law** is valid. For such systems $p_A = p_A^\circ x_A$, where p_A° is the pure-component vapor pressure of the solute and p_A is its partial pressure. Extreme care should be exercised when attempting to use pure-component vapor pressures to predict gas-absorption behavior. Both liquid-phase and vapor-phase nonidealities can cause significant deviations from the behavior predicted from pure-component vapor pressures in combination with Raoult's law. Vapor-pressure data are available in Sec. 3 for a variety of materials.

Whenever data are available for a given system under similar conditions of temperature, pressure, and composition, **equilibrium distribution coefficients** (*K* = *y/x*) provide a much more reliable tool for predicting vapor-liquid distributions. A detailed discussion of equilibrium *K* values is presented in Sec. 13.

Calculation of Liquid-to-Gas Ratio The minimum possible liquid rate is readily calculated from the composition of the entering gas and the solubility of the solute in the exit liquor, saturation being assumed. It may be necessary to estimate the temperature of the exit liquid based on the heat of solution of the solute gas. Values of latent and specific heats and values of heats of solution (at infinite dilution) are given in Sec. 2.

The actual liquid-to-gas ratio (solvent-circulation rate) normally will be greater than the minimum by as much as 25 to 100 percent and may be arrived at by economic considerations as well as by judgment and experience. For example, in some packed-tower applications involving very soluble gases or vacuum operation, the minimum quantity of solvent needed to dissolve the solute may be insufficient to keep the packing surface thoroughly wet, leading to poor distribution of the liquid stream.

14-6 GAS ABSORPTION AND GAS-LIQUID SYSTEM DESIGN

When the solute concentration in the inlet gas is low and when nearly all the solute is being absorbed (this is the usual case), the approximation

$$y_1 G_M \doteq x_1 L_M \doteq (y^{\circ}/m) L_M \quad (14-3)$$

leads to the conclusion that the ratio mG_M/L_M represents the fractional approach of the exit liquid to saturation with the inlet gas, i.e.,

$$mG_M/L_M = y^{\circ}/y_1 \quad (14-4)$$

Optimization of the liquid-to-gas ratio in terms of total annual costs often suggests that the molar liquid-to-gas ratio L_M/G_M should be about 1.2 to 1.5 times the theoretical minimum corresponding to equilibrium at the rich end of the tower (infinite height), provided flooding is not a problem. This would be an alternative to assuming that $L_M/G_M \doteq m/0.7$, for example.

When the exit-liquor temperature rises owing to the heat of absorption of the solute, the value of m changes through the tower, and the liquid-to-gas ratio must be chosen to give reasonable values of $m_1 G_M/L_M$ and $m_2 G_M/L_M$, where the subscripts 1 and 2 refer to the bottom and top of the absorption tower respectively. For this case the value of $m_2 G_M/L_M$ will be taken to be somewhat less than 0.7, so that the value of $m_1 G_M/L_M$ will not approach unity too closely. This rule-of-thumb approach is useful only when low solute concentrations and mild heat effects are involved.

When the solute has a large heat of solution or when the feed gas contains high percentages of the solute, one should consider the use of internal cooling coils or intermediate external heat exchangers in a plate-type tower to remove the heat of absorption. In a packed tower, one could consider the use of multiple packed sections with intermediate liquid-withdrawal points so that the liquid could be cooled by external heat exchange.

Selection of Equipment Packed columns usually are chosen for very corrosive materials, for liquids that foam badly, for either small- or large-diameter towers involving very low allowable pressure drops, and for small-scale operations requiring diameters of less than 0.6 m (2 ft). The type of packing is selected on the basis of resistance to corrosion, mechanical strength, capacity for handling the required flows, mass-transfer efficiency, and cost. Economic factors are discussed later in this section.

Plate columns may be economically preferable for large-scale operations and are needed when liquid rates are so low that packing would be inadequately wetted, when the gas velocity is so low (owing to a very high L/G) that axial dispersion or "pumping" of the gas back down the (packed) column can occur, or when intermediate cooling is desired. Also, plate towers may have a better turndown ratio and are less subject to fouling by solids than are packed towers. Details on the operating characteristics of plate towers are given later in this section.

Column Diameter and Pressure Drop Flooding determines the minimum possible diameter of the absorber column, and the usual design is for 60 to 80 percent of the flooding velocity. Maximum allowable pressure drop may be determined by the cost of energy for compression of the feed gas. For systems having a significant tendency to foam, the maximum allowable velocity will be lower than estimated flooding velocity, especially for plate towers. The safe range of operating velocities should include the velocity one would derive from economic considerations, as discussed later. Methods for predicting flooding velocities and pressure drops are given later in this section.

Computation of Tower Height The required height of a gas-absorption or stripping tower depends on (1) the phase equilibria involved, (2) the specified degree of removal of the solute from the gas, and (3) the mass-transfer efficiency of the apparatus. These same considerations apply both to plate towers and to packed towers. Items 1 and 2 dictate the required number of theoretical stages (plate tower) or transfer units (packed tower). Item 3 is derived from the tray efficiency and spacing (plate tower) or from the height of one transfer unit (packed tower). Solute-removal specifications normally are derived from economic considerations.

For plate towers, the approximate design methods described below may be used in estimating the number of theoretical stages, and the tray efficiencies and spacings for the tower can be specified on the basis of the information given later. Considerations involved in the rigorous design of theoretical stages for plate towers are treated in Sec. 13.

For packed towers, the continuous differential nature of the contact between gas and liquid leads to a design procedure involving the solution of differential equations, as described in the next subsection.

It should be noted that the design procedures discussed in this section are not applicable to reboiled absorbers, which should be designed according to the methods described in Sec. 13.

Caution is advised in distinguishing between systems involving pure physical absorption and those in which a chemical reaction can significantly affect design procedures.

Selection of Stripper-Operating Conditions Stripping involves the removal of one or more volatile components from a liquid by contacting it with a gas such as steam, nitrogen, or air. The operating conditions chosen for stripping normally result in a low solubility of the solute (i.e., a high value of m), so that the ratio mG_M/L_M will be larger than unity. A value of 1.4 may be used for rule-of-thumb calculations involving pure physical desorption. For plate-tower calculations the stripping factor $S = KG_M/L_M$, where $K = y^{\circ}/x$, usually is specified for each tray.

When the solvent from an absorption operation must be regenerated for recycling back to the absorber, one may employ a "pressure-swing concept," a "temperature-swing concept," or a combination of both in specifying stripping conditions. In pressure-swing operation the temperature of the stripper is about the same as that of the absorber, but the stripping pressure is much lower. In temperature-swing operation the pressures are about equal, but the stripping temperature is much higher than the absorption temperature.

In pressure-swing operation a portion of the dissolved gas may be "sprung" from the liquid by the use of a flash drum upstream of the stripping-tower feed point. This type of operation is discussed by Burrows and Preece [*Trans. Inst. Chem. Eng.*, **32**, 99 (1954)] and by Langley and Haselden [*Inst. Chem. Eng. Symp. Ser. (London)*, no. 28 (1968)]. If the flashing of the feed liquid takes place inside the stripping tower, this effect must be accounted for in the design of the upper section in order to avoid overloading and flooding near the top of the tower.

More often than not the rate at which residual absorbed gas can be driven from the liquid in a stripping tower is limited by the rate of a chemical reaction, in which case the liquid-phase residence time (and hence, the tower liquid holdup) becomes the most important design factor. Thus, many stripper-regenerators are designed on the basis of liquid holdup rather than on the basis of mass transfer rate.

Approximate design equations applicable only to the case of pure physical desorption are developed later in this section for both packed and plate stripping towers. A more rigorous approach using distillation concepts may be found in Sec. 13. A brief discussion of desorption with chemical reaction is given in the subsection "Absorption with Chemical Reaction."

Design of Absorber-Stripper Systems The solute-rich liquor leaving a gas absorber normally is distilled or stripped to regenerate the solvent for recirculation back to the absorber, as depicted in Fig. 14-1. It is apparent that the conditions selected for the absorption step (e.g., temperature, pressure, L_M/G_M) will affect the design of the stripping tower, and, conversely, a selection of stripping conditions will affect the absorber design. The choice of optimum operating conditions for an absorber-stripper system therefore involves a combination of economic factors and practical judgments as to the operability of the system within the context of the overall process flow sheet. Note that in Fig. 14-1 the stripping vapor is provided by a reboiler; alternately, an extraneous stripping gas may be used.

An appropriate procedure for executing the design of an absorber-stripper system is to set up a carefully selected series of design cases and then evaluate the investment costs, the operating costs, and the operability of each case. Some of the economic factors that need to be considered in selecting the optimum absorber-stripper design are discussed later in the subsection "Economic Design of Absorption Systems."

Importance of Design Diagrams One of the first things a designer should try to do is lay out a carefully constructed equilibrium curve, $y^{\circ} = F(x)$, on an xy diagram, as shown in Fig. 14-2. A horizontal line corresponding to the inlet-gas composition y_1 is then the locus of feasible outlet-liquor compositions, and a vertical line corresponding to the inlet-solvent-liquor composition x_2 is the locus of feasible out-

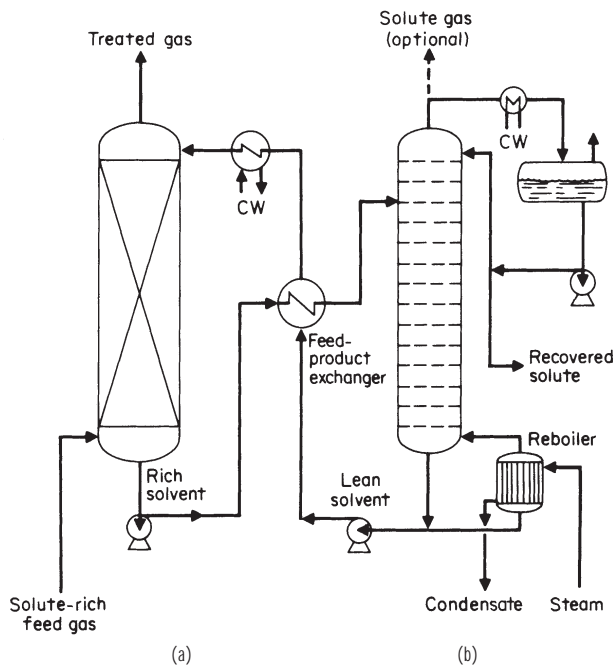


FIG. 14-1 Gas absorber using a solvent regenerated by stripping. (a) Absorber. (b) Stripper.

let-gas compositions. These lines are indicated as $y = y_1$ and $x = x_2$ respectively on Fig. 14-2.

For gas absorption, the region of feasible operating lines lies above the equilibrium curve; for stripping, the feasible region for operating lines lies below the equilibrium curve. These feasible regions are bounded by the equilibrium curve and by the lines $x = x_2$ and $y = y_1$. By inspection, one should be able to visualize those operating lines that are feasible and those that would lead to "pinch points" within the tower. Also, it is possible to determine if a particular proposed design for solute recovery falls within the feasible envelope.

Once the design recovery for an absorber has been established, the operating curve can be constructed by first locating the point x_2, y_2 on the diagram. The intersection of the horizontal line corresponding to the inlet gas composition y_1 with the equilibrium curve $y^* = F(x)$

defines the theoretical minimum liquid-to-gas ratio for systems in which there are no intermediate pinch points. The operating line which connects this point with the point x_2, y_2 corresponds to the minimum value of L_M/G_M . The actual design value of L_M/G_M normally should be around 1.2 to 1.5 times this minimum. Thus, the actual design operating line for a gas absorber will pass through the point x_2, y_2 and will intersect the line $y = y_1$ to the left of the equilibrium curve.

For stripping one begins by using the design specification to locate the point x_1, y_1 . Then the intersection of the vertical line $x = x_2$ with the equilibrium curve $y^* = F(x)$ defines the theoretical minimum gas-to-liquid ratio. The actual value of G_M/L_M is chosen to be about 20 to 50 percent higher than this minimum, so the actual design operating line will intersect the line $x = x_2$ at a point somewhat below the equilibrium curve.

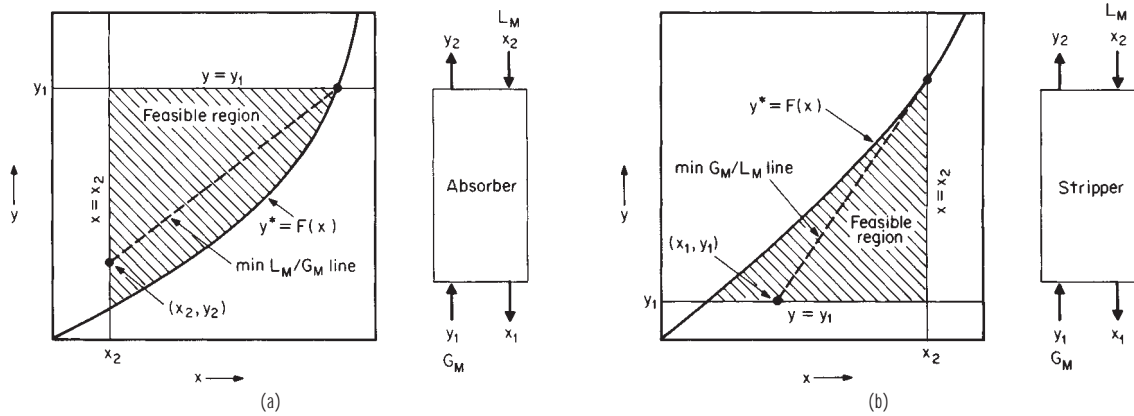


FIG. 14-2 Design diagrams for (a) absorption and (b) stripping.

14-8 GAS ABSORPTION AND GAS-LIQUID SYSTEM DESIGN

Design diagrams minimize the possibility of making careless mistakes and allow one to assess easily the effects of operating variable changes on the operability of the system relative to pinch points, etc. Whenever analytical calculations or computer programs are being used for the design of gas-absorption systems, the construction of

design diagrams based either on calculation results or on computer printouts may reveal problem areas or even errors in the design concept. It is strongly recommended that design diagrams be employed whenever possible.

PACKED-TOWER DESIGN

Methods for estimating the height of the active section of **counterflow differential contactors** such as packed towers, spray towers, and falling-film absorbers are based on rate expressions representing mass transfer at a point on the gas-liquid interface and on material balances representing the changes in bulk composition in the two phases that flow past each other. The rate expressions are based on the interphase mass-transfer principles described in Sec. 5. Combination of such expressions leads to an integral expression for the number of transfer units or to equations related closely to the number of theoretical plates. The paragraphs which follow set forth convenient methods for using such equations, first in a general case and then for cases in which simplifying assumptions are valid.

Use of Mass-Transfer-Rate Expression Figure 14-3 shows a section of a packed absorption tower together with the nomenclature that will be used in developing the equations which follow. In a differential section dh , we can equate the rate at which solute is lost from the gas phase to the rate at which it is transferred through the gas phase to the interface as follows:

$$-d(G_M y) = -G_M dy - y dG_M = N_A a dh \quad (14-5)$$

When only one component is transferred,

$$dG_M = -N_A a dh \quad (14-6)$$

Substitution of this relation into Eq. (14-5) and rearranging yields

$$dh = -\frac{G_M dy}{N_A a(1-y)} \quad (14-7)$$

For this derivation we use the gas-phase rate expression $N_A = k_G(y - y_i)$ and integrate over the tower to obtain

$$h_T = \int_{y_2}^{y_1} \frac{G_M dy}{k_G a(1-y)(y-y_i)} \quad (14-8)$$

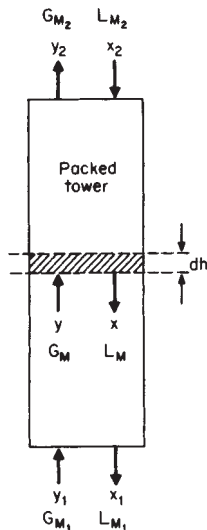


FIG. 14-3 Nomenclature for material balances in a packed-tower absorber or stripper.

Multiplying and dividing by y_{BM} place Eq. (14-8) into the $H_G N_G$ format

$$\begin{aligned} h_T &= \int_{y_2}^{y_1} \left[\frac{G_M}{k_G a y_{BM}} \right] \frac{y_{BM} dy}{(1-y)(y-y_i)} \\ &= H_{G,av} \int_{y_2}^{y_1} \frac{y_{BM} dy}{(1-y)(y-y_i)} = H_{G,av} N_G \end{aligned} \quad (14-9)$$

The general expression given by Eq. (14-8) is more complex than normally is required, but it must be used when the mass-transfer coefficient varies from point to point, as may be the case when the gas is not dilute or when the gas velocity varies as the gas dissolves. The values of y_i to be used in Eq. (14-8) depend on the local liquid composition x_i and on the temperature. This dependency is best represented by using the operating and equilibrium lines as discussed later.

Example 3 illustrates the use of Eq. (14-8) for scrubbing chlorine from air with aqueous caustic solution. For this case one can make the simplifying assumption that y_i , the interfacial partial pressure of chlorine over the aqueous caustic solution, is zero owing to the rapid and complete reaction of the chlorine after it dissolves. We note that the feed gas is not dilute.

Example 2: Packed Height Requirement Let us compute the height of packing needed to reduce the chlorine concentration of 0.537 kg/(s·m²), or 396 lb/(h·ft²), of a chlorine-air mixture containing 0.503 mole-fraction chlorine to 0.0403 mole fraction. On the basis of test data described by Sherwood and Pigford (*Absorption and Extraction*, McGraw-Hill, 1952, p. 121) the value of $k_G a y_{BM}$ at a gas velocity equal to that at the bottom of the packing is equal to 0.1175 kmol/(s·m³), or 26.4 lb·mol/(h·ft³). The equilibrium back pressure y_i can be assumed to be negligible.

Solution. By assuming that the mass-transfer coefficient varies as the 0.8 power of the local gas mass velocity, we can derive the following relation:

$$\hat{K}_G a = k_G a y_{BM} = 0.1175 \left[\frac{71y + 29(1-y)}{71y_1 + 29(1-y_1)} \right]^{0.8}$$

where 71 and 29 are the molecular weights of chlorine and air respectively. Noting that the inert-gas (air) flow rate is given by $G'_M = G_M(1-y) = 5.34 \times 10^{-3}$ kmol/(s·m²), or 3.94 lb·mol/(h·ft²), and introducing these expressions into the integral gives

$$h_T = 1.82 \int_{0.0403}^{0.503} \left[\frac{1-y}{29+42y} \right]^{0.8} \frac{dy}{(1-y)^2 \ln [1/(1-y)]}$$

This definite integral can be evaluated numerically by the use of Simpson's rule to obtain $h_T = 0.305$ m (1 ft).

Use of Operating Curve Frequently, it is not possible to assume that $y_i = 0$ as in Example 2, owing to diffusional resistance in the liquid phase or to the accumulation of solute in the liquid stream. When the back pressure cannot be neglected, it is necessary to supplement the equations with a material balance representing the operating line or curve. In view of the countercurrent flows into and from the differential section of packing shown in Fig. 14-3, a steady-state material balance leads to the following equivalent relations:

$$d(G_M y) = d(L_M x) \quad (14-10)$$

$$G'_M \frac{dy}{(1-y)^2} = L'_M \frac{dx}{(1-x)^2} \quad (14-11)$$

where L'_M = molar mass velocity of the inert-liquid component and G'_M = molar mass velocity of the inert gas. L_M , L'_M , G_M , and G'_M are superficial velocities based on the total tower cross section.

Equation (14-11) is the differential equation of the operating curve, and its integral around the upper portion of the packing is the equation for the operating curve

$$G'_M \left[\frac{y}{1-y} - \frac{y_2}{1-y_2} \right] = L'_M \left[\frac{x}{1-x} - \frac{x_2}{1-x_2} \right] \quad (14-12)$$

For dilute solutions in which the mole fractions of x and y are small, the total molar flows G_M and L_M will be very nearly constant, and the operating-curve equation is

$$G_M(y - y_2) = L_M(x - x_2) \quad (14-13)$$

This equation gives the relation between the bulk compositions of the gas and liquid streams at each level in the tower for conditions in which the operating curve can be approximated by a straight line.

Figure 14-4 shows the relationship between the operating curve and the equilibrium curve $y_i = F(x_i)$ for a typical example involving solvent recovery, where y_i and x_i are the interfacial compositions (assumed to be in equilibrium). Once y is known as a function of x along the operating curve, y_i can be found at corresponding points on the equilibrium curve by

$$(y - y_i)/(x_i - x) = k_L/k_G = k'_L \bar{\rho}_L / k'_G p_T = L_M H_G / G_M H_L \quad (14-14)$$

where L_M = molar liquid mass velocity, G_M = molar gas mass velocity, H_L = height of one transfer unit based on liquid-phase resistance, and H_G = height of one transfer unit based on gas-phase resistance. Thence, the integral in Eq. (14-8) can be evaluated.

Calculation of Transfer Units In the general case the equations described above must be employed in calculating the height of packing required for a given separation. However, if the local mass-transfer coefficient $k_C a y_{BM}$ is approximately proportional to the first power of the local gas velocity G_M , then the height of one gas-phase transfer unit, defined as $H_G = G_M / k_C a y_{BM}$, will be constant in Eq. (14-9). Similar considerations lead to an assumption that the height of one overall gas-phase transfer unit H_{OG} may be taken as constant. The height of packing required is then calculated according to the relation

$$h_T = H_G N_G = H_{OG} N_{OG} \quad (14-15)$$

where N_G = number of gas-phase transfer units and N_{OG} = number of overall gas-phase transfer units. When H_G and H_{OG} are not constant, it may be valid to employ averaged values between the top and bottom of the tower and the relation

$$h_T = H_{G,av} N_G = H_{OG,av} N_{OG} \quad (14-16)$$

In these equations, the terms N_G and N_{OG} are defined by

$$N_G = \int_{y_2}^{y_1} \frac{y_{BM} dy}{(1-y)(y-y_i)} \quad (14-17)$$

and by $N_{OG} = \int_{y_2}^{y_1} \frac{y_{BM}^o dy}{(1-y)(y-y^o)}$ (14-18)

respectively.

Equation (14-18) is the more useful one in practice; it requires either actual experimental H_{OG} data or values estimated by combining

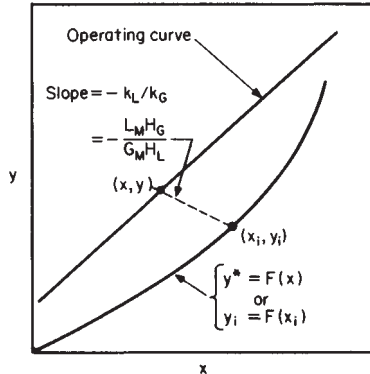


FIG. 14-4 Relationship between equilibrium curve and operating curve in a packed absorber; computation of interfacial compositions.

individual measurements of H_G and H_L by Eq. (14-19). Correlations for predicting H_G , H_L , and H_{OG} in nonreacting systems are presented in Sec. 5.

$$H_{OG} = \frac{y_{BM}}{y_{BM}^o} H_G + \frac{mG_M}{L_M} \frac{x_{BM}}{y_{BM}^o} H_L \quad (14-19a)$$

$$H_{OL} = \frac{x_{BM}}{x_{BM}^o} H_L + \frac{L_M}{mG_M} \frac{y_{BM}}{x_{BM}^o} H_G \quad (14-19b)$$

On occasion the changes in gas flow and in the mole fraction of inert gas are so small that the inclusion of terms such as $(1-y)$ and y_{BM}^o can be neglected or at least can be included in an approximate way. This leads to some of the simplified procedures described later.

One such simplification was suggested by Wiegand [Trans. Am. Inst. Chem. Eng., 36, 679 (1940)], who pointed out that the logarithmic-mean mole fraction of inert gas y_{BM}^o (or y_{BM}) is often very nearly equal to the arithmetic mean. Thus, substitution of the relation

$$\frac{y_{BM}^o}{(1-y)} \doteq \frac{(1-y^o) + (1-y)}{2(1-y)} = \frac{y - y^o}{2(1-y)} + 1 \quad (14-20)$$

into the equations presented earlier leads to the simplified forms

$$N_G = \frac{1}{2} \ln \frac{1-y_2}{1-y_1} + \int_{y_2}^{y_1} \frac{dy}{y-y_i} \quad (14-21)$$

$$N_{OG} = \frac{1}{2} \ln \frac{1-y_2}{1-y_1} + \int_{y_2}^{y_1} \frac{dy}{y-y^o} \quad (14-22)$$

The second (integral) terms represent the numbers of transfer units for an infinitely dilute gas. The first terms, frequently amounting to only small corrections, give the effect of a finite level of gas concentration.

The procedure for applying Eqs. (14-21) and (14-22) involves two steps: (1) evaluation of the integrals and (2) addition of the correction corresponding to the first (logarithmic) term. The discussion which follows deals only with the evaluation of the integral terms (first step).

The simplest possible case occurs when (1) both the operating and the equilibrium lines are straight (i.e., there are dilute solutions), (2) Henry's law is valid ($y^o x = y_i/x_i = m$), and (3) absorption heat effects are negligible. Under these conditions, the integral term in Eq. (14-20) may be computed by Colburn's equation [Trans. Am. Inst. Chem. Eng., 35, 211 (1939)]:

$$N_{OG} = \frac{1}{1 - (mG_M/L_M)} \ln \left[\left(1 - \frac{mG_M}{L_M} \right) \left(\frac{y_1 - mx_2}{y_2 - mx_2} \right) + \frac{mG_M}{L_M} \right] \quad (14-23)$$

Figure 14-5 is a plot of Eq. (14-23) from which the value of N_{OG} can be read directly as a function of mG_M/L_M and the ratio of concentrations. This plot and Eq. (14-23) are equivalent to the use of a logarithmic mean of terminal driving forces, but they are more convenient because one does not need to compute the exit-liquor concentration x_1 .

In many practical situations involving nearly complete cleanup of the gas, an approximate result can be obtained from the equations just presented even when solutions are concentrated or when absorption heat effects are present. In such cases the driving forces in the upper part of the tower are very much smaller than those at the bottom, and the value of mG_M/L_M used in the equations should be the ratio of the slopes of the equilibrium line m and the operating line L_M/G_M in the low-concentration range near the top of the tower.

Another approach is to divide the tower arbitrarily into a lean section (near the top), where approximate methods are valid, and to deal with the rich section separately. If the heat effects in the rich section are appreciable, consideration could be given to installing cooling units near the bottom of the tower. In any event a design diagram showing the operating and equilibrium curves should be prepared to check on the applicability of any simplified procedure. Figure 14-8, presented in Example 6 is one such diagram for an adiabatic absorption tower.

Stripping Equations Stripping, or desorption, involves the removal of a volatile component from the liquid stream by contact with an inert gas such as nitrogen or steam. In this case the change in concentration of the liquid stream is of prime importance, and it

14-10 GAS ABSORPTION AND GAS-LIQUID SYSTEM DESIGN

is more convenient to formulate the rate equation analogous to Eq. (14-6) in terms of the liquid composition x . This leads to the following equations defining numbers of transfer units and heights of transfer units based on liquid-phase resistance:

$$h_T = H_L \int_{x_2}^{x_1} \frac{x_{BM} dx}{(1-x)(x_i-x)} = H_L N_L \quad (14-24)$$

$$h_T = H_{OL} \int_{x_2}^{x_1} \frac{x_{BM}^{\circ} dx}{(1-x)(x^{\circ}-x)} = H_{OL} N_{OL} \quad (14-25)$$

where, as before, subscripts 1 and 2 refer to the bottom and top of the tower respectively (see Fig. 14-3).

In situations in which one cannot assume that H_L and H_{OL} are constant, these terms must be incorporated inside the integrals in Eqs. (14-24) and (14-25), and the integrals must be evaluated graphically or numerically (by using Simpson's rule, for example). In the normal case involving stripping without chemical reactions, the liquid-phase resistance will dominate, making it preferable to use Eq. (14-25) in conjunction with the relation $H_L = H_{OL}$.

The Wiegand approximations of the above integrals in which arithmetic means are substituted for the logarithmic means x_{BM} and x_{BM}° are

$$N_L = \frac{1}{2} \ln \frac{1-x_1}{1-x_2} + \int_{x_1}^{x_2} \frac{dx}{x-x_i} \quad (14-26)$$

$$N_{OL} = \frac{1}{2} \ln \frac{1-x_1}{1-x_2} + \int_{x_1}^{x_2} \frac{dx}{x-x^{\circ}} \quad (14-27)$$

In these equations, the first term is a correction for finite liquid-phase concentrations, and the integral term represents the numbers of transfer units required for dilute solutions. It would be very unusual in practice to find an example in which the first (logarithmic) term is of any significance in a stripper design.

For dilute solutions in which both the operating and the equilibrium lines are straight and in which heat effects can be neglected, the integral term in Eq. (14-27) is

$$N_{OL} = \frac{1}{(1-L_M/mG_M)} \ln \left[\left(1 - \frac{L_M}{mG_M} \right) \left(\frac{x_2 - y_1/m}{x_1 - y_1/m} \right) + \frac{L_M}{mG_M} \right] \quad (14-28)$$

This equation is identical in form to Eq. (14-23). Thus, Fig. 14-5 is applicable if the concentration ratio $(x_2 - y_1/m)/(x_1 - y_1/m)$ is substituted for the abscissa and if the parameter on the curves is identified as L_M/mG_M .

Example 3: Air Stripping of VOCs from Water A 0.45-m diameter packed column was used by Dvorack et al. [Environ. Sci. Tech. 20, 945 (1996)] for removing trichloroethylene (TCE) from wastewater by stripping with atmospheric air. The column was packed with 2.5-cm Pall rings, fabricated from propylene, to a height of 3.0 m. The TCE concentration in the entering water was 38 parts per million by weight (ppmw). A molar ratio of entering water to entering air was kept at 23.7. What degree of removal was to be expected? The temperatures of water and air were 20°C. Pressure was atmospheric.

Solution. For TCE in water, the Henry's law coefficient may be taken as 417 atm/mf at 20°C. In this low-concentration region, the coefficient is constant and equal to the slope of the equilibrium line m . The solubility of TCE in water, based on $H = 417$, is 2390 ppm. Because of this low solubility, the entire resistance to mass transfer resides in the liquid phase. Thus, Eq. (14-25) may be used to obtain N_{OL} , the number of overall liquid phase transfer units.

In the equation, the ratio $x_{BM}/(1-x)$ is unity because of the very dilute solution. It is necessary to have a value of H_L for the packing used, at given flow rates of liquid and gas. Methods for estimating H_L may be found in Sec. 5. Dvorack et al. found $H_{OL} = 0.8$ m. Then, for $h_T = 3.0$ m, $N_L = N_{OL} = 3.0/0.8 = 3.75$ transfer units.

Transfer units may be calculated from Eq. 14-25, replacing mole fractions with ppm concentrations, and since the operating and equilibrium lines are straight,

$$N_{OL} = \frac{38 - (\text{ppm})_{\text{exit}}}{\ln 38/(\text{ppm})_{\text{exit}}} = 3.75$$

Solving, $(\text{ppm})_{\text{exit}} = 0.00151$. Thus, the stripped water would contain 1.51 parts per billion of TCE.

Use of HTU and K_{ca} Data In estimating the size of a commercial gas absorber or liquid stripper it is desirable to have data on the

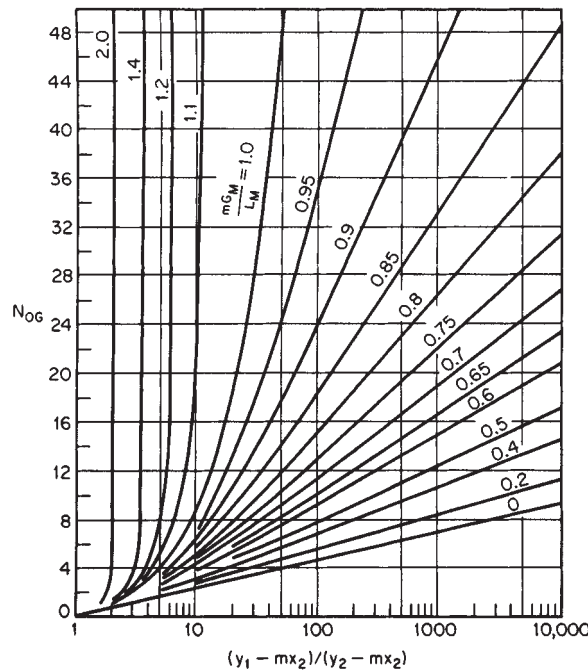


FIG. 14-5 Number of overall gas-phase mass-transfer units in a packed absorption tower for constant mG_M/L_M ; solution of Eq. (14-23). (From Sherwood and Pigford, Absorption and Extraction, McGraw-Hill, New York, 1952.)

overall mass transfer coefficients (or heights of transfer units) for the system of interest, and at the desired conditions of temperature, pressure, solute concentration, and fluid velocities. Such data should be obtained in an apparatus of pilot-plant or semiworks size to avoid abnormalities of scaleup. It must be remembered that values of the mass-transfer parameters are dependent not only on the phase properties and mass throughput in the contactor but also on the type of device used. Within the packing category, there are both random and ordered (structured) type packing elements. Physical characteristics of these devices will be described later.

When no K_{ca} or HTU data are available, their values may be estimated by means of a generalized model. A summary of useful models is given in Section 5, Table 5-28. The values obtained may then be combined by the use of Eq. 14-19 to obtain values of H_{OG} and H_{OL} . This procedure is not valid, however, when the rate of absorption is limited by a chemical reaction.

Use of HETP Data for Absorber Design Distillation design methods (see Sec. 13) normally involve determination of the number of theoretical equilibrium stages or plates N . Thus, when packed towers are employed in distillation applications, it is common practice to rate the efficiency of tower packings in terms of the height of packing equivalent to one theoretical plate (HETP).

The HETP of a packed-tower section, valid for either distillation or dilute-gas absorption and stripping systems in which constant molal overflow can be assumed and in which no chemical reactions occur, is related to the height of one overall gas-phase mass-transfer unit H_{OG} by the equation

$$\text{HETP} = H_{OG} \frac{\ln (mG_M/L_M)}{(mG_M/L_M - 1)} \quad (14-29)$$

For gas-absorption systems in which the inlet gas is concentrated, the correct equation is

$$\text{HETP} = \left(\frac{y_{BM}^{\circ}}{1-y} \right)_{av} H_{OG} \frac{\ln (mG_M/L_M)}{mG_M/L_M - 1} \quad (14-30)$$

where the correction term $y_{BM}^{\circ}/(1 - y)$ is averaged over each individual theoretical plate. The equilibrium compositions corresponding to each theoretical plate may be estimated by the methods described in the subsection "Plate-Tower Design." These compositions are used in conjunction with the local values of the gas and liquid flow rates and

the equilibrium slope m to obtain values for H_C , H_L , and H_{OC} corresponding to the conditions on each theoretical stage, and the local values of the HETP are then computed by Eq. (14-30). The total height of packing required for the separation is the summation of the individual HETPs computed for each theoretical stage.

PLATE-TOWER DESIGN

The design of a plate tower for gas-absorption or gas-stripping operations involves many of the same principles employed in distillation calculations, such as the determination of the number of theoretical plates needed to achieve a specified composition change (see Sec. 13). Distillation differs from gas absorption in that it involves the separation of components based on the distribution of the various substances between a gas phase and a liquid phase when all the components are present in both phases. In distillation, the new phase is generated from the original feed mixture by vaporization or condensation of the volatile components, and the separation is achieved by introducing reflux to the top of the tower.

In gas absorption, the new phase consists of an inert nonvolatile solvent (absorption) or an inert nonsoluble gas (stripping), and normally no reflux is involved. The following paragraphs discuss some of the considerations peculiar to gas-absorption calculations for plate towers and some of the approximate design methods that can be employed when simplifying assumptions are valid.

Graphical Design Procedure Construction of design diagrams (xy) diagrams showing the equilibrium and operating curves) should be an integral part of any design involving the distribution of a single solute between an inert solvent and an inert gas. The number of theoretical plates can be stepped off rigorously provided the curvatures of the operating and equilibrium lines are correctly accounted for in the diagram. This procedure is valid even though an insoluble inert gas is present in the gas phase and an inert nonvolatile solvent is present in the liquid phase.

Figure 14-6 illustrates the graphical method for a three-theoretical-plate system. Note that in gas absorption the operating line is above the equilibrium curve, whereas in distillation this does not happen. In gas stripping, the operating line will be below the equilibrium curve.

On Fig. 14-6, note that the stepping-off procedure begins on the operating line. The starting point x_f, y_3 represents the compositions of the entering lean wash liquor and of the gas exiting from the top of the tower, as determined by the design specifications. After three steps one reaches the point x_1, y_f representing the compositions of the solute-rich feed gas y_f and of the solute-rich liquor leaving the bottom of the tower x_1 .

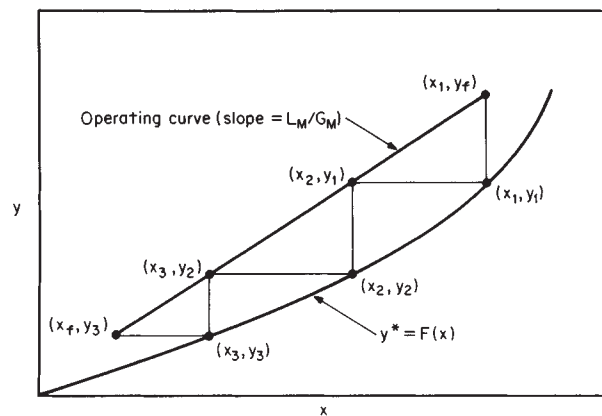


FIG. 14-6 Graphical method for a three-theoretical-plate gas-absorption tower with inlet-liquor composition x_f and inlet-gas composition y_f .

Algebraic Method for Dilute Gases By assuming that the operating and equilibrium curves are straight lines and that heat effects are negligible, Souders and Brown [Ind. Eng. Chem., **24**, 519 (1932)] developed the following equation:

$$(y_1 - y_2)/(y_1 - y_2^{\circ}) = (A^{N+1} - A)/(A^{N+1} - 1) \quad (14-31)$$

where N = number of theoretical plates, y_1 = mole-fraction solute in the entering gas, y_2 = mole-fraction solute in the leaving gas, $y_2^{\circ} = mx_2$ = mole-fraction solute in equilibrium with the incoming solvent liquor (zero for a pure solvent), and A = absorption factor = L_M/mG_M . Note that the absorption factor is the reciprocal of the expression given in Eq. (14-4) for packed columns.

When $A = 1$, Eq. (14-31) is indeterminate, and for this case the solution is given by

$$(y_1 - y_2)/(y_1 - y_2^{\circ}) = N/(N + 1) \quad (14-32)$$

Although Eq. (14-31) is convenient for computing the composition of the exit gas as a function of the number of theoretical stages, an alternative equation derived by Colburn [Trans. Am. Inst. Chem. Eng., **35**, 211 (1939)] is more useful when the number of theoretical plates is the unknown:

$$N = \frac{\ln [(1 - A^{-1})(y_1 - y_2^{\circ})/(y_2 - y_2^{\circ}) + A^{-1}]}{\ln (A)} \quad (14-33)$$

The numerical results obtained by using either Eq. (14-31) or Eq. (14-33) are identical. Thus, the two equations may be used interchangeably as the need arises.

Comparison of Eqs. (14-33) and (14-23) shows that

$$N_{OC}/N = \ln (A)/(1 - A^{-1}) \quad (14-34)$$

thus revealing the close relationship between theoretical stages in a plate tower and mass-transfer units in a packed tower. Equations (14-23) and (14-33) are related to each other by virtue of the relation

$$h_T = H_{OC}N_{OC} = (HETP)N \quad (14-35)$$

Algebraic Method for Concentrated Gases When the feed gas is concentrated, the absorption factor, which is defined in general as $A = L_M/KG_M$ where $K = y^{\circ}/x$, can vary throughout the tower owing to changes in the equilibrium K values due to temperature increases. An approximate solution to this problem can be obtained by substitution of the "effective" absorption factors A_e and A' derived by Edmister [Ind. Eng. Chem., **35**, 837 (1943)] into the equation

$$\frac{y_1 - y_2}{y_1} = \left[1 - \frac{1}{A'} \frac{(L_Mx)_2}{(G_My)_1} \right] \frac{A_e^{N+1} - A_e}{A_e^{N+1} - 1} \quad (14-36)$$

where subscripts 1 and 2 refer to the bottom and top of the tower respectively and the absorption factors are defined by the equations

$$A_e = \sqrt{A_1(A_2 + 1) + 0.25} - 0.5 \quad (14-37)$$

$$A' = A_1(A_2 + 1)/(A_1 + 1) \quad (14-38)$$

This procedure has been applied to the absorption of C_5 and lighter hydrocarbon vapors into a lean oil, for example.

Stripping Equations When the liquid feed is dilute and the operating and equilibrium curves are straight lines, the stripping equations analogous to Eqs. (14-31) and (14-33) are

$$(x_2 - x_1)/(x_2 - x_1^{\circ}) = (S^{N+1} - S)/(S^{N+1} - 1) \quad (14-39)$$

where $x_1^{\circ} = y_1/m$; $S = mG_M/L_M = A^{-1}$; and

14-12 GAS ABSORPTION AND GAS-LIQUID SYSTEM DESIGN

$$N = \frac{\ln [(1-A)(x_2 - x_1^0)/(x_1 - x_1^0) + A]}{\ln (S)} \quad (14-40)$$

For systems in which the concentrations are large and the stripping factor S may vary along the tower, the following Edmister equations [Ind. Eng. Chem., 35, 837 (1943)] are applicable:

$$\frac{x_2 - x_1}{x_2} = \left[1 - \frac{1}{S' (L_M x)_2} \right] \frac{S_e^{N+1} - S_e}{S_e^{N+1} - 1} \quad (14-41)$$

where $S_e = \sqrt{S_2(S_1 + 1) + 0.25} - 0.5$ (14-42)

$$S' = S_2(S_1 + 1)/(S_2 + 1) \quad (14-43)$$

and the subscripts 1 and 2 refer to the bottom and top of the tower respectively.

Equations (14-37) and (14-42) represent two different ways of obtaining an effective factor, and a value of A_e obtained by taking the reciprocal of S_e from Eq. (14-42) will not check exactly with a value of A_e derived by substituting $A_1 = 1/S_1$ and $A_2 = 1/S_2$ into Eq. (14-37). Regardless of this fact, the equations generally give reasonable results for approximate design calculations.

It should be noted that throughout this section the subscripts 1 and 2 refer to the bottom and to the top of the apparatus respectively regardless of whether it is an absorber or a stripper. This has been done to maintain internal consistency among all the equations and to prevent the confusion created in some derivations in which the numbering system for an absorber is different from the numbering system for a stripper.

Tray Efficiencies in Plate Absorbers and Strippers Computations of the number of theoretical plates N assume that the liquid on each plate is completely mixed and that the vapor leaving the plate is in equilibrium with the liquid. In actual practice a condition of complete equilibrium cannot exist since interphase mass transfer requires a finite driving-force difference. This leads to the definition of an overall plate efficiency

$$E = N_{\text{theoretical}}/N_{\text{actual}} \quad (14-44)$$

which can be correlated to system design variables.

Mass-transfer theory indicates that for trays of a given design the factors most likely to influence E in absorption and stripping towers are the physical properties of the fluids and the dimensionless ratio mG_M/L_M . Systems in which the mass transfer is gas-film-controlled may be expected to have plate efficiencies as high as 50 to 100 percent, whereas plate efficiencies as low as 1 percent have been reported for the absorption of gases of low solubility (large m) into solvents of relatively high viscosity.

The fluid properties are represented by the Schmidt numbers of the gas and liquid phases. For gases, the Schmidt numbers normally are close to unity and are independent of temperature and pressure. Thus, the gas-phase mass-transfer coefficients are relatively independent of the system.

By contrast, the liquid-phase Schmidt numbers range from about 10^2 to 10^4 and depend strongly on the temperature. The effect of temperature on the liquid-phase mass-transfer coefficient is related primarily to changes in the liquid viscosity with temperature, and this derives primarily from the strong dependency of the liquid-phase Schmidt number upon viscosity.

Consideration of the preceding discussion in connection with the relationship between mass-transfer coefficients (see Sec. 5):

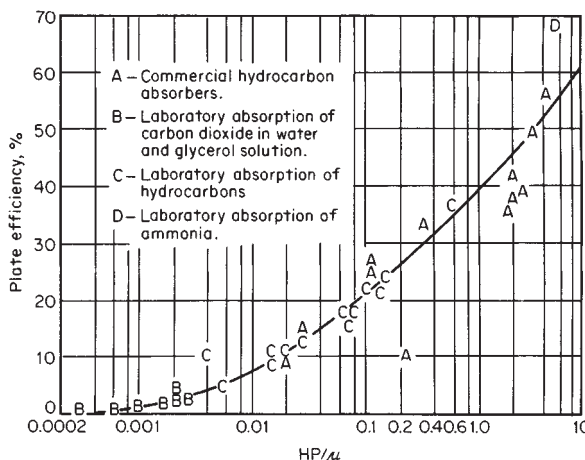


FIG. 14-7 O'Connell correlation for overall column efficiency E_{oc} for absorption. To convert HP/μ in pound-moles per cubic foot-centipoise to kilogram-moles per cubic meter-pascal-second, multiply by 1.60×10^4 . [O'Connell, Trans. Am. Inst. Chem. Eng., 42, 741 (1946).]

$$1/K_G = (1/k_G + m/k_L) \quad (14-45)$$

indicates that variations in the overall resistance to mass transfer in absorbers and strippers are related primarily to variations in the liquid-phase viscosity μ and to variations in the slope m . A correlation of the efficiency of plate absorbers in terms of the viscosity of the liquid solvent and the solubility of the solute gas was developed by O'Connell [Trans. Am. Inst. Chem. Eng., 42, 741 (1946)]. The O'Connell correlation for plate absorbers is presented here as Fig. 14-7.

The best procedure for making plate-efficiency corrections (which obviously can be quite large) is to use experimental-test data from a prototype system that is large enough to be representative of an actual commercial tower.

Example 4: Actual Plates for Steam Stripping The number of actual plates required for steam-stripping an acetone-rich liquor containing 0.573 mole percent acetone in water is to be estimated. The design overhead recovery of acetone is 99.9 percent, leaving 18.5 ppm weight of acetone in the stripper bottoms. The design operating temperature and pressure are 101.3 kPa and 94°C respectively, the average liquid-phase viscosity is 0.30 cP, and the average value of $K = y^0/x$ for these conditions is 33.

By choosing a value of $mG_M/L_M = S = A^{-1} = 1.4$ and noting that the stripping medium is pure steam (i.e., $x_1^0 = 0$), the number of theoretical trays according to Eq. (14-40) is

$$N = \frac{\ln [(1 - 0.714)(1000) + 0.714]}{\ln (1.4)} = 16.8$$

The O'Connell parameter for gas absorbers is $\rho_L/KM\mu_L$, where ρ_L is the liquid density, lb/ft³; μ_L is the liquid viscosity, cP; M is the molecular weight of the liquid; and $K = y^0/x$. For the present design

$$\rho_L/KM\mu_L = 60.1/(33 \times 18 \times 0.30) = 0.337$$

and according to the O'Connell graph for absorbers (Fig. 14-7) the overall tray efficiency for this case is estimated to be 30 percent. Thus, the required number of actual trays is $16.8/0.3 = 56$ trays.

HEAT EFFECTS IN GAS ABSORPTION

Overview One of the most important considerations involved in designing gas-absorption towers is to determine whether or not temperatures will vary along the length of the tower because of heat effects, since the solubility of the solute gas normally depends strongly upon the temperature. When heat effects can be neglected, computation of the tower dimensions and required flows is relatively straight-

forward, as indicated by the simplified design methods discussed earlier for both packed and plate absorbers and strippers. When heat effects cannot be neglected, the computational problem becomes much more difficult.

Heat effects that may cause temperatures to vary from point to point in a gas absorber are (1) the heat of solution of the solute

(including heat of condensation, heat of mixing, and heat of reaction), which can lead to a rise in the liquid temperature; (2) the heat of vaporization or condensation of the solvent; (3) the exchange of sensible heat between the gas and liquid phases; and (4) the loss of sensible heat from the fluids to internal or external cooling coils or to the atmosphere via the tower walls.

Y. T. Shah (*Gas-Liquid-Solid Reactor Design*, McGraw-Hill, New York, 1979, p. 51) has reviewed the literature concerning heat effects in systems involving gas-liquid reactions and concludes that in the majority of the systems involving chemical reactions temperature effects are not very important. For some systems in which large amounts of heat may be liberated, there are compensating effects which decrease the effect on the rate of absorption. For example, increasing temperatures tend simultaneously to increase the rate of chemical reaction and to decrease the solubility of the reactant at the solvent interface. Systems in which compensating effects can occur include absorption of CO_2 in amine solutions and absorption of CO_2 in NaOH solutions.

There are, however, a number of well-known systems in which heat effects definitely cannot be ignored. Examples include absorption of ammonia in water, dehumidification of air with concentrated H_2SO_4 , absorption of HCl in water, and absorption of SO_3 in H_2SO_4 . Another interesting example is the absorption of acetone in water, in which the heat effects are mild but not negligible.

Some very thorough and knowledgeable discussions of the problems involved in gas absorption with large heat effects have been presented by Coggan and Bourne [*Trans. Inst. Chem. Eng.*, **47**, T96, T160 (1969)], by Bourne, von Stockar, and Coggan [*Ind. Eng. Chem. Process Des. Dev.*, **13**, 115, 124 (1974)], and also by von Stockar and Wilke [*Ind. Eng. Chem. Fundam.*, **16**, 89 (1977)]. The first two of these references discuss plate-tower absorbers and include interesting experimental studies of the absorption of ammonia in water. The third reference discusses the design of packed-tower gas absorbers and includes a shortcut design method based on a semitheoretical correlation of rigorous calculation results. All these authors clearly demonstrate both theoretically and experimentally that when the solvent is volatile, the temperature inside an absorber can go through a maximum. They note that the least expensive of the solvents, water, is capable of exhibiting this unusual "hot-spot" behavior.

From a designer's point of view there are a number of different approaches to be considered in dealing with heat effects, depending on the requirements of the job at hand. For example, one can (1) add internal or external heat-transfer surface to remove heat from the absorber; (2) treat the process as if it were isothermal by arbitrarily assuming that the temperature of the liquid phase is everywhere the same and then add a design safety factor; (3) employ the classical adiabatic model, which assumes that the heat of solution manifests itself only as sensible heat in the liquid phase and that solvent vaporization is negligible; (4) use semitheoretical shortcut methods derived from rigorous calculations; and (5) employ rigorous design procedures requiring the use of a digital computer.

For preliminary-screening work the simpler methods may be adequate, but for final designs one should seriously consider using a more rigorous approach.

Effects of Operating Variables Conditions that can give rise to significant heat effects are (1) an appreciable heat of solution and (2) absorption of large amounts of solute in the liquid phase. The second of these conditions can arise when the solute concentration in the inlet gas is large, when the liquid flow rate is relatively low (small L_M/G_M), when the solubility of the solute in the liquid phase is high, and/or when the operating pressure is high.

When the solute is absorbed very rapidly, the rate of heat liberation often is largest near the bottom of the tower. This has the effect of causing the equilibrium line to curve upward near the solute-rich end, although it may remain relatively straight near the lean end, corresponding to the temperature of the lean solvent.

If the solute-rich gas entering the bottom of an absorption tower is cold, the liquid phase may be cooled somewhat by transfer of sensible heat to the gas. A much stronger cooling effect can occur when the solvent is volatile and the entering rich gas is not saturated with respect to the solvent. It is possible to experience a condition in which

solvent is being evaporated near the bottom of the tower and condensed near the top. Under these conditions there may develop a pinch point in which the operating and equilibrium curves approach each other at a point inside the tower.

In the references cited previously, the authors discuss the influence of operating variables upon the performance of plate towers when large heat effects are involved. Some general observations are as follows:

Operating Pressure Raising the pressure may increase the separation efficiency considerably. Calculations involving the absorption of methanol from water-saturated air showed that doubling the pressure doubled the concentration of methanol which could be tolerated in the feed gas while still achieving a preset concentration specification in the off gas.

Temperature of Fresh Solvent The temperature of the entering solvent has surprisingly little influence upon the degree of absorption or upon the internal-temperature profiles in an absorber when the heat effects are due primarily to heat of solution or to solvent vaporization. In these cases the temperature profile in the liquid phase apparently is dictated solely by the internal-heat effects.

Temperature and Humidity of Rich Gas Cooling and consequent dehumidification of the feed gas to an absorption tower can be very beneficial. A high humidity (or relative saturation with solvent) limits the capacity of the gas phase to take up latent heat and therefore is unfavorable to absorption. Thus, dehumidification of the inlet gas prior to introducing it into the tower is worth considering in the design of gas absorbers with large heat effects.

Liquid-to-Gas Ratio The L/G ratio can have a significant influence on the development of temperature profiles in gas absorbers. High L/G ratios tend to result in less strongly developed temperature profiles owing to the high heat capacity of the liquid phase. As the L/G is increased, the operating line moves away from the equilibrium line and there is a tendency for more solute to be absorbed per stage. However, there is a compensating effect in that as more heat is liberated at each stage, the plate temperatures will tend to rise, causing an upward shifting of the equilibrium line.

As the L/G is decreased, the concentration of solute tends to build up in the upper parts of the absorber, and the point of highest temperature tends to move upward in the tower until finally the maximum temperature develops only on the topmost plate. Of course, the capacity of the liquid phase to absorb solute falls progressively as the L/G is reduced.

Number of Stages When the heat effects combine to produce an extended zone within the tower where little absorption is taking place (i.e., a pinch zone), the addition of plates to the tower will have no useful effect on separation efficiency. Solutions to these difficulties must be sought by increasing the solvent flow, introducing strategically placed coolers, cooling and dehumidifying the inlet gas, and/or raising the tower operating pressure.

Equipment Considerations When the solute has a large heat of solution and the feed gas contains a large percentage of solute, as in the absorption of HCl in water, the effects of heat release during absorption may be so pronounced that the installation of heat-transfer surface to remove the heat of absorption may be as important as providing sufficient interfacial area for the mass-transfer process itself. The added heat-transfer surface may consist of internal cooling coils on the plates, or else the solvent may be withdrawn from a point intermediate in the tower and passed through an external heat exchanger (intercooler) for cooling.

In many cases the rate of heat liberation is largest near the bottom of the tower, where solute absorption is more rapid, so that cooling surfaces or intercoolers are required only on the first few trays at the bottom of the column. Coggan and Bourne [*Trans. Inst. Chem. Eng.*, **47**, T96, T160 (1969)] found, however, that the optimal position for a single interstage cooler does not necessarily coincide with the position of the maximum temperature or with the center of a pinch. They found that in a 12-plate tower, two strategically placed interstage coolers tripled the allowable ammonia feed concentration for a given off-gas specification. For a case involving methanol absorption, it was found that more separation was possible in a 12-stage column with two intercoolers than in a simple column with 100 stages and no intercoolers.

In the case of HCl absorption, a shell-and-tube heat exchanger often is employed as a cooled wetted-wall vertical-column absorber so that the exothermic heat of reaction can be removed continuously as it is released into the liquid film.

Installation of heat-exchange equipment to precool and dehumidify the feed gas to an absorber also deserves consideration in order to take advantage of the cooling effects created by vaporization of solvent in the lower sections of the tower.

Classical Isothermal Design Method When the feed gas is sufficiently dilute, the exact design solution may be approximated by the isothermal one over a broad range of L/G ratios, since heat effects generally are less important when washing dilute-gas mixtures. The problem, however, is one of defining the term "sufficiently dilute" for each specific case. For a new absorption duty, the assumption of isothermal operation must be subjected to verification by the use of a rigorous design procedure.

When heat-exchange surface is being provided in the design of an absorber, the isothermal design procedure can be rendered valid by virtue of the exchanger design specifications. With ample surface area and a close approach, isothermal operation can be guaranteed.

For preliminary screening and feasibility studies or for rough cost estimates, one may wish to employ a version of the isothermal method which assumes that the liquid temperatures in the tower are everywhere equal to the inlet-liquid temperature. In their analysis of packed-tower designs, von Stockar and Wilke [Ind. Eng. Chem. Fundam. 16, 89 (1977)] showed that the isothermal method tended to underestimate the required depth of packing by a factor of as much as 1.5 to 2. Thus, for rough estimates one may wish to employ the assumption that the temperature is equal to the inlet-liquid temperature and then apply a design factor to the result.

Another instance in which the constant-temperature method is used involves the direct application of experimental K_{GA} values obtained at the desired conditions of inlet temperatures, operating pressure, flow rates, and feed-stream compositions. The assumption here is that, regardless of any temperature profiles that may exist within the actual tower, the procedure of "working the problem in reverse" will yield a correct result. One should be cautious about extrapolating such data very far from the original basis and be careful to use compatible equilibrium data.

Classical Adiabatic Design Method The classical adiabatic method assumes that the heat of solution serves only to heat up the liquid stream and that there is no vaporization of solvent. This assumption makes it feasible to relate increases in the liquid-phase temperature to the solute concentration x by a simple enthalpy balance. The equilibrium curve can then be adjusted to account for the corresponding temperature rise on an xy diagram. The adjusted equilibrium curve will become more concave upward as the concentration increases, tending to decrease the driving forces near the bottom of the tower, as illustrated in Fig. 14-8 in Example 6.

Colburn [Trans. Am. Inst. Chem. Eng., 35, 211 (1939)] has shown that when the equilibrium line is straight near the origin but curved slightly at its upper end, N_{OC} can be computed approximately by assuming that the equilibrium curve is a parabolic arc of slope m_2 near the origin and passing through the point x_1, K_1x_1 at the upper end. The Colburn equation for this case is

$$N_{OC} = \frac{1}{1 - m_2 G_M / L_M} \times \ln \left[\frac{(1 - m_2 G_M / L_M)^2}{1 - K_1 G_M / L_M} \left(\frac{y_1 - m_2 x_2}{y_2 - m_2 x_2} \right) + \frac{m_2 G_M}{L_M} \right] \quad (14-46)$$

Comparisons by von Stockar and Wilke [Ind. Eng. Chem. Fundam., 16, 89 (1977)] between the rigorous and the classical adiabatic design methods for packed towers indicate that the simple adiabatic method underestimates the packing depths by as much as a factor of 1.25 to 1.5. Thus, when using the classical adiabatic method, one should consider the possible need to apply a design safety factor.

A slight variation of the above method accounts for increases in the solvent content of the gas stream between the inlet and the outlet of the tower and assumes that the evaporation of solvent tends to cool the liquid. This procedure offsets a part of the temperature rise that

would have been predicted with no solvent evaporation and leads to the prediction of a shorter tower.

Rigorous Design Methods A detailed discussion of rigorous methods for the design of packed and plate absorbers when large heat effects are involved is beyond the scope of this section. In principle, material and energy balances may be executed under the same constraints as for rigorous distillation calculations (see Sec. 13). The MESH equations are solved, but for absorption or stripping, convergence may be quite sensitive to the relatively large heat effects compared with distillation. Absorption-stripping programs are included in the software packages for process simulation. The paper of von Stockar and Wilke [Ind. Eng. Chem. Fundam. 16, 89 (1977)] presents an interesting shortcut method for the design of packed absorbers which closely approximates rigorous results.

Direct Comparison of Design Methods The following problem, originally solved by Sherwood, Pigford, and Wilke (*Mass Transfer*, McGraw-Hill, New York, 1975, p. 616), was employed by von Stockar and Wilke as the basis for a direct comparison between the isothermal, adiabatic, semitheoretical shortcut, and rigorous design methods for estimating the height of packed towers.

Example 5: Packed Absorber, Acetone into Water Inlet gas to an absorber consists of a mixture of 6 mole percent acetone in air saturated with water vapor at 15°C and 101.3 kPa (1 atm). The scrubbing liquor is pure water at 15°C, and the inlet gas and liquid rates are given as 0.080 and 0.190 kmol/s respectively. The liquid rate corresponds to 20 percent over the theoretical minimum as calculated by assuming a value of x_1 corresponding to complete equilibrium between the exit liquor and the incoming gas. H_C and H_L are given as 0.42 and 0.30 m respectively, and the acetone equilibrium data at 15°C are $p_A^0 = 19.7$ kPa (147.4 torr), $\gamma_A = 6.46$, and $m_A = 6.46 \times 19.7/101.3 = 1.26$. The heat of solution of acetone is 7656 cal/gmol (32.05 kJ/gmol), and the heat of vaporization of solvent (water) is 10,755 cal/gmol (45.03 kJ/gmol). The problem calls for determining the height of packing required to achieve a 90 percent recovery of the acetone.

The following table compares the results obtained by von Stockar and Wilke (op. cit.) for the various design methods:

Design method used	N_{OC}	Packed height, m	Design safety factor
Rigorous	5.56	3.63	1.00
Shortcut rigorous	5.56	3.73	0.97
Classical adiabatic	4.01	2.38	1.53
Classical isothermal	3.30	1.96	1.85

It should be clear from this example that there is considerable room for error when approximate design methods are employed in situations involving large heat effects, even for a case in which the solute concentration in the inlet gas was only 6 mole percent.

Example 6: Solvent Rate for Absorption Let us consider the absorption of acetone from air at atmospheric pressure into a stream of pure water fed to the top of a packed absorber at 25°C. The inlet gas at 35°C contains 2 percent by volume of acetone and is 70 percent saturated with water vapor (4 percent H_2O by volume). The mole-fraction acetone in the exit gas is to be reduced to 1/400 of the inlet value, or 50 ppmv. For 100 kmol of feed-gas mixture, how many kilomoles of fresh water should be fed to provide a positive-driving force throughout the packing? How many transfer units will be needed according to the classical adiabatic method? What is the estimated height of packing required if $H_{OC} = 0.70$ m?

The latent heats at 25°C are 7656 kcal/kmol for acetone and 10,490 kcal/kmol for water, and the differential heat of solution of acetone vapor in pure water is given as 2500 kcal/kmol. The specific heat of air is 7.0 kcal/(kmol·K).

Acetone solubilities are defined by the equation

$$K = y^0/x = \gamma_A p_a / p_T \quad (14-47)$$

where the vapor pressure of pure acetone in mmHg (torr) is given by (Sherwood et al., *Mass Transfer*, McGraw-Hill, New York, 1975, p. 537):

$$p_A^0 = \exp(18.1594 - 3794.06/T) \quad (14-48)$$

and the liquid-phase-activity coefficient may be approximated for low concentrations ($x \leq 0.01$) by the equation

$$\gamma_a = 6.5 \exp(2.0803 - 601.2/T) \quad (14-49)$$

Typical values of acetone solubility as a function of temperature at a total pressure of 760 mmHg are shown in the following table:

$t, ^\circ\text{C}$	25	30	35	40
γ_a	6.92	7.16	7.40	7.63
$p_a, \text{ mmHg}$	229	283	346	422
$K = \gamma_a p_a^0 / 760$	2.09	2.66	3.37	4.23

For dry gas and liquid water at 25°C, the following enthalpies are computed for the inlet- and exit-gas streams (basis, 100 kmol of gas entering):

Entering gas:	
Acetone	$(2(2500 + 7656) = 20,312 \text{ kcal})$
Water vapor	$4(10,490) = 41,960$
Sensible heat	$(100)(7.0)(35 - 25) = 7,000$
	$69,272 \text{ kcal}$

Exit gas (assumed saturated with water at 25°C):

Acetone	$(2/400)(94/100)(2500) = 12 \text{ kcal}$
Water vapor	$94 \left(\frac{23.7}{760 - 23.7} \right) (10,490) = 31,600$
	$31,612 \text{ kcal}$

Enthalpy change of liquid = 69,272 – 31,612 = 37,660 kcal/100 kmol gas. Thus, $\Delta t = t_1 - t_2 = 37,660/18L_M$, and the relation between L_M/G_M and the liquid-phase temperature rise is

$$L_M/G_M = (37,660)/(18)(100) \Delta t = 20.92/\Delta t$$

The following table summarizes the critical values for various assumed temperature rises:

$\Delta t, ^\circ\text{C}$	L_M/G_M	K_1	$K_1 G_M/L_M$	$m_2 G_M/L_M$
0		2.09	0.	0.
2	10.46	2.31	0.221	0.200
3	6.97	2.42	0.347	0.300
4	5.23	2.54	0.486	0.400
5	4.18	2.66	0.636	0.500
6	3.49	2.79	0.799	0.599
7	2.99	2.93	0.980	0.699

Evidently a temperature rise of 7°C would not be a safe design because the equilibrium line nearly touches the operating line near the bottom of the tower, creating a pinch. A temperature rise of 6°C appears to give an operable design, and for this case $L_M = 349$ kmol per 100 kmol of feed gas.

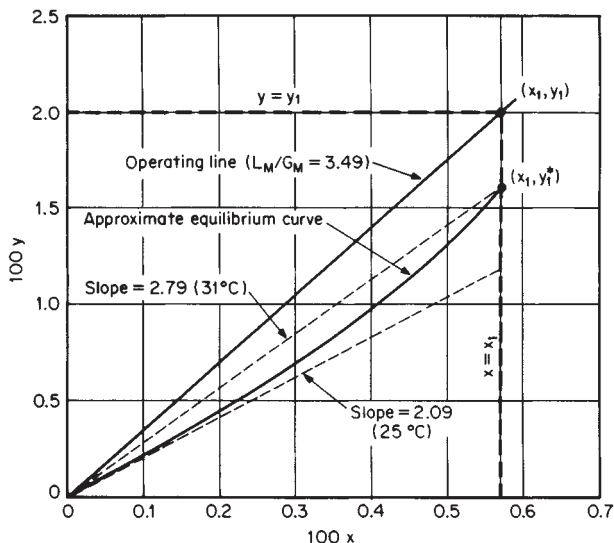


FIG. 14-8 Design diagram for adiabatic absorption of acetone in water, Example 6.

The design diagram for this case is shown in Fig. 14-8, in which the equilibrium curve is drawn with a French curve so that the slope at the origin m_2 is equal to 2.09 and passes through the point $x_1 = 0.02/3.49 = 0.00573$ at $y^* = 0.00573 \times 2.79 = 0.0160$.

The number of transfer units can be calculated from the adiabatic design equation, Eq. (14-46):

$$N_{OC} = \frac{1}{1 - 0.599} \ln \left[\frac{(1 - 0.599)^2}{(1 - 0.799)} (400) + 0.599 \right] = 14.4$$

The estimated height of tower packing by assuming $H_{OC} = 0.70$ m and a design safety factor of 1.5 is

$$h_T = (14.4)(0.7)(1.5) = 15.1 \text{ m (49.6 ft)}$$

For this tower, one should consider the use of two or more shorter packed sections instead of one long section.

MULTICOMPONENT SYSTEMS

When no chemical reactions are involved in the absorption of more than one soluble component from an insoluble gas, the design conditions (pressure, temperature, and liquid-to-gas ratio) normally are determined by the volatility or the physical solubility of the least soluble component for which complete recovery is economical. Components of lower volatility (higher solubility) also will be recovered completely.

The more volatile (i.e., less soluble) components will be only partially absorbed even though the effluent liquid becomes completely saturated with respect to these lighter substances. When a condition of saturation exists, the value of y_1/y_2 will remain finite even for an infinite number of plates or transfer units. This can be seen in Fig. 14-9, in which the asymptotes become vertical for values of mG_M/L_M greater than unity. If the amount of volatile component in the incoming fresh solvent is negligible, then the limiting value of y_1/y_2 for each of the highly volatile components is

$$y_1/y_2 = S/(S - 1) \quad (14-50)$$

where $S = mG_M/L_M$ and the subscripts 1 and 2 refer to the bottom and top of the tower respectively.

When the gas stream is dilute, absorption of each constituent can be considered separately as if the other components were absent. The following example illustrates the use of this principle.

Example 7: Multicomponent Absorption, Dilute Case Air entering a tower contains 1 percent acetaldehyde and 2 percent acetone. The liquid-to-gas ratio for optimum acetone recovery is $L_M/G_M = 3.1$ mol/mol when the fresh-solvent temperature is 31.5°C. The value of y^*/x for acetaldehyde has been measured as 50 at the boiling point of a dilute solution, 93.5°C. What will be the percentage recovery of acetaldehyde be under conditions of optimal acetone recovery?

Solution. If the heat of solution is neglected, y^*/x at 31.5°C is equal to $50(1200/7300) = 8.2$, where the factor in parentheses is the ratio of pure-acetaldehyde vapor pressures at 31.5 and 93.5°C respectively. Since L_M/G_M is equal to 3.1, the value of S for the aldehyde is $S = mG_M/L_M = 8.2/3.1 = 2.64$, and $y_1/y_2 = S/(S - 1) = 2.64/1.64 = 1.61$. The acetaldehyde recovery is therefore equal to $100 \times 0.61/1.61 = 38$ percent recovery.

In concentrated systems the change in gas and liquid flow rates within the tower and the heat effects accompanying the absorption of all the components must be considered. A trial-and-error calculation from one theoretical stage to the next usually is required if accurate results are to be obtained, and in such cases calculation procedures similar to those described in Sec. 13 normally are employed. A computer procedure for multicomponent adiabatic absorber design has been described by Feintuch and Treybal [Ind. Eng. Chem. Process Des. Dev., 17, 505 (1978)]. Also see Holland, *Fundamentals and Modeling of Separation Processes*, Prentice Hall, Englewood Cliffs, N.J., 1975.

14-16 GAS ABSORPTION AND GAS-LIQUID SYSTEM DESIGN

When two or more gases are absorbed in systems involving chemical reactions, the situation is much more complex. This topic is discussed later in the subsection "Absorption with Chemical Reaction."

Graphical Design Method for Dilute Systems The following notation for multicomponent absorption calculations has been adapted from Sherwood, Pigford, and Wilke (*Mass Transfer*, McGraw-Hill, New York 1975, p. 415):

$$L_M^s = \text{moles of solvent per unit time}$$

$$G_M^0 = \text{moles of rich feed gas to be treated per unit time}$$

$$X = \text{moles of one solute per mole of solute-free solvent fed to the top of the tower}$$

$$Y = \text{moles of one solute in the gas phase per mole of rich feed gas to be treated}$$

Subscripts 1 and 2 refer to the bottom and top of the tower respectively, and the material balance for any one component may be written as

$$L_M^s(X - X_2) = G_M^0(Y - Y_2) \quad (14-51)$$

or else as

$$L_M^s(X_1 - X) = G_M^0(Y_1 - Y) \quad (14-52)$$

For the special case of absorption from lean gases with relatively large amounts of solvent, the equilibrium lines are defined for each component by the relation

$$Y^0 = K'X \quad (14-53)$$

Thus, the equilibrium line for each component passes through the origin with slope K' , where

$$K' = K(G_M^0/L_M^s)/(L_M^s/L_M^s) \quad (14-54)$$

and $K = y^0/x$. When the system is sufficiently dilute, $K' \approx K$.

The liquid-to-gas ratio L_M^s/G_M^0 is chosen on the basis of the solubility of the least soluble substance in the feed gas that must be absorbed completely. Each individual component will then have its own operating line with slope equal to L_M^s/G_M^0 (i.e., the operating lines for all the various components will be parallel to each other).

A typical diagram for the complete absorption of pentane and heavier components from a lean gas mixture is shown in Fig. 14-9. The oil used as solvent for this case was assumed to be solute-free (i.e., $X_2 = 0$), and the "key component," butane, was identified as that component absorbed in appreciable amounts whose equilibrium line is most

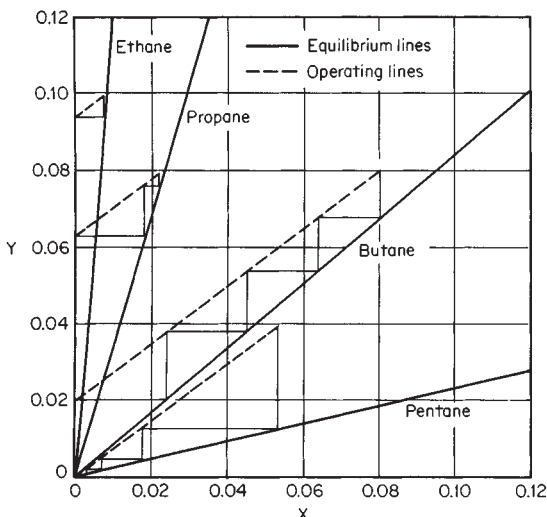


FIG. 14-9 Graphical design method for multicomponent systems; absorption of butane and heavier components in a solute-free lean oil.

nearly parallel to the operating lines (i.e., the K value for butane is approximately equal to L_M^s/G_M^0).

In Fig. 14-9, the composition of the gas with respect to components more volatile than butane will approach equilibrium with the liquid phase at the bottom of the tower. The gas composition with respect to components less volatile (heavier) than butane will approach equilibrium with the oil entering the tower, and since $X_2 = 0$, the components heavier than butane will be completely absorbed.

Four theoretical plates have been stepped off for the key component (butane) on Fig. 14-9 and are sufficient to give a 75 percent recovery of butane. The operating lines for the other components were drawn in with the same slope and were placed so as to give the same number of theoretical plates insofar as possible.

The diagram of Fig. 14-9 shows that for the light components equilibrium is achieved easily in fewer than four theoretical plates and that for the heavier components nearly complete recovery is obtained in four theoretical plates. The diagram also shows that absorption of the light components takes place in the upper part of the tower and absorption of the heavier components takes place in the lower section of the tower.

Algebraic Design Method for Dilute Systems The design method described above can be performed algebraically by employing the following modified version of the Kremser formula:

$$\frac{Y_1 - Y_2}{Y_1 - mX_2} = \frac{(A^0)^{N+1} - A^0}{(A^0)^{N+1} - 1} \quad (14-55)$$

where for dilute gas absorption $A^0 = L_M^s/mG_M^0$ and $m \doteq K = y^0/x$.

The left-hand side of Eq. (14-55) represents the efficiency of absorption of any one component of the feed-gas mixture. If the solvent oil is denuded of solute so that $X_2 = 0$, the left-hand side is equal to the fractional absorption of the component from the rich feed gas. When the number of theoretical plates N and the liquid and gas rates L_M^s and G_M^0 have been fixed, the fractional absorption of each component may be computed directly and the operating lines need not be placed by trial and error as in the graphical approach described earlier.

According to Eq. (14-55), when A^0 is less than unity and N is large,

$$(Y_1 - Y_2)/(Y_1 - mX_2) \doteq A^0 \quad (14-56)$$

This equation can be employed for estimating the fractional absorption of the more volatile components whenever the value of A^0 for the component is smaller than the value of A^0 for the key component by a factor of 3 or more.

When A^0 is very much larger than unity and when N is large, the right-hand side of Eq. (14-55) becomes equal to unity. This signifies that the gas will leave the top of the tower in equilibrium with the incoming oil, and when $X_2 = 0$, it corresponds to complete absorption of the component in question. Thus, the least volatile components may be assumed to be at equilibrium with the lean oil at the top of the tower.

When $A^0 = 1$, the right-hand side of Eq. (14-55) becomes indeterminate. The solution for this case is

$$(Y_1 - Y_2)/(Y_1 - mX_2) = N/(N + 1) \quad (14-57)$$

For systems in which the absorption factor A^0 for each component is not constant throughout the tower, an effective absorption factor for use in the equations just presented can be estimated by the Edmister formula

$$A_e^0 = \sqrt{A_1^0(A_2^0 + 1) + 0.25} - 0.5 \quad (14-58)$$

This procedure is a reasonable approximation only when no pinch points exist within the tower and when the absorption factors vary in a regular manner between the bottom and the top of the tower.

Example 8: Multicomponent Absorption, Concentrated Case

A hydrocarbon feed gas is to be treated in an existing four-theoretical-tray absorber to remove butane and heavier components. The recovery specification for the key component, butane, is 75 percent. The composition of the exit gas from the absorber and the required liquid-to-gas ratio are to be estimated. The feed-gas composition and the equilibrium K values for each component at the temperature of the (solute-free) lean oil are presented in the following table:

Component	Mole %	K value
Methane	68.0	74.137
Ethane	10.0	12.000
Propane	8.0	3.429
Butane	8.0	0.833
Pentane	4.0	0.233
C ₆ plus	2.0	0.065

For $N = 4$ and $Y_2/Y_1 = 0.25$, the value of A^0 for butane is found to be equal to 0.89 from Eq. (14-55) by using a trial-and-error method. The values of A^0 for the other components are then proportional to the ratios of their K values to that of butane. For example, $A^0 = 0.89/(0.833/12.0) = 0.062$ for ethane. The values of A^0 for each of the other components and the exit-gas composition as computed from Eq. (14-55) are shown in the following table:

Component	A^0	Y_2 , mol/mol feed	Exit gas, mole %
Methane	0.010	67.3	79.1
Ethane	0.062	9.4	11.1
Propane	0.216	6.3	7.4
Butane	0.890	2.0	2.4
Pentane	3.182	0.027	0.03
C ₆ plus	11.406	0.0012	0.0014

The molar liquid-to-gas ratio required for this separation is computed as $L_M/G_M^0 = A^0 \times K = 0.89 \times 0.833 = 0.74$.

We note that this example is the analytical solution to the graphical design problem shown in Fig. 14-9, which therefore is the design diagram for this system.

ABSORPTION WITH CHEMICAL REACTION

Introduction Many present-day commercial gas absorption processes involve systems in which chemical reactions take place in the liquid phase. These reactions generally enhance the rate of absorption and increase the capacity of the liquid solution to dissolve the solute, when compared with physical absorption systems.

A necessary prerequisite to understanding the subject of absorption with chemical reaction is the development of a thorough understanding of the principles involved in physical absorption, as discussed earlier in this section and in Section 5. There are a number of excellent references on the subject, such as the book by Danckwerts (*Gas-Liquid Reactions*, McGraw-Hill, New York, 1970) and Astarita et al. (*Gas Treating with Chemical Solvents*, Wiley, New York, 1983).

Recommended Overall Design Strategy When considering the design of a gas-absorption system involving chemical reactions, the following procedure is recommended:

1. Consider the possibility that the physical design methods described earlier in this section may be applicable.
2. Determine whether commercial design overall \hat{K}_{GA} values are available for use in conjunction with the traditional design method, being careful to note whether or not the conditions under which the \hat{K}_{GA} data were obtained are essentially the same as for the new design. Contact the various tower-packing vendors for information as to whether \hat{K}_{GA} data are available for your system and conditions.
3. Consider the possibility of scaling up the design of a new system from experimental data obtained in a laboratory-bench scale or a small pilot-plant unit.
4. Consider the possibility of developing for the new system a rigorous, theoretically based design procedure which will be valid over a wide range of design conditions.

These topics are discussed in the subsections that follow.

Applicability of Physical Design Methods Physical design methods such as the classical isothermal design method or the classical adiabatic design method may be applicable for systems in which chemical reactions are either extremely fast or extremely slow or when chemical equilibrium is achieved between the gas and liquid phases.

If the liquid-phase reaction is extremely fast and irreversible, the rate of absorption may in some cases be completely governed by the gas-phase resistance. For practical design purposes one may assume (for example) that this gas-phase mass-transfer limited condition will exist when the ratio y_i/y is less than 0.05 everywhere in the apparatus.

From the basic mass-transfer flux relationship for species A (Sec. 5),

$$N_A = k_G(y - y_i) = k_L(x_i - x) \quad (14-59)$$

one can readily show that this condition on y_i/y requires that the ratio x_i/x be negligibly small (i.e., a fast reaction) and that the ratio $mk_G/k_L = mk_G/k_L^0\phi$ be less than 0.05 everywhere in the apparatus. The ratio $mk_G/k_L^0\phi$ will be small if the equilibrium back pressure of the solute over the liquid solution is small (i.e., small m ; high reactant sol-

ubility), or the reaction-enhancement factor $\phi = k_L/k_L^0$ is very large, or both.

As discussed later, the reaction-enhancement factor ϕ will be large for all extremely fast pseudo-first-order reactions and will be large for extremely fast second-order irreversible reaction systems in which there is a sufficiently large excess of liquid-phase reagent. When the rate of an extremely fast second-order irreversible reaction system $A + vB \rightarrow$ products is limited by the availability of the liquid-phase reagent B , then the reaction-enhancement factor may be estimated by the formula $\phi = 1 + B^0/vc_i$. In systems for which this formula is applicable, it can be shown that the interface concentration y_i will be equal to zero whenever the ratio $k_G y v / k_L^0 B^0$ is less than or equal to unity.

Figure 14-10 illustrates the gas-film and liquid-film concentration profiles one might find in an extremely fast (gas-phase mass-transfer limited) second-order irreversible reaction system. The solid curve for reagent B represents the case in which there is a large excess of bulk-liquid reagent B^0 . The dashed curve in Fig. 14-10 represents the case in which the bulk concentration B^0 is not sufficiently large to prevent the depletion of B near the liquid interface and for which the equation $\phi = 1 + B^0/vc_i$ is applicable.

Whenever these conditions on the ratio y_i/y apply, the design can be based upon the physical rate coefficient \hat{k}_G or upon the height of one gas-phase mass-transfer unit H_G . The gas-phase mass-transfer limited condition is approximately valid, for instance, in the following systems: absorption of NH_3 into water or acidic solutions, vaporization of water into air, absorption of H_2O into concentrated sulfuric acid solutions, absorption of SO_2 into alkali solutions, absorption of H_2S from a dilute-

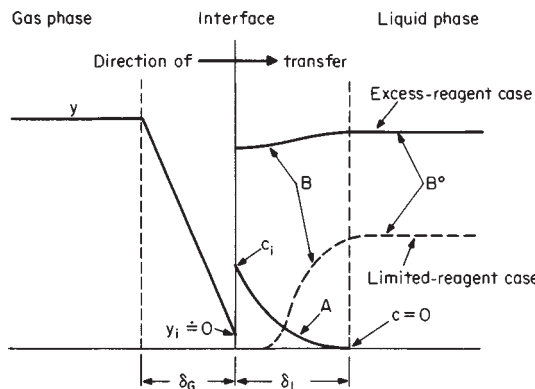


FIG. 14-10 Gas-phase and liquid-phase solute-concentration profiles for an extremely fast (gas-phase mass-transfer limited) irreversible reaction system $A + vB \rightarrow$ products.

14-18 GAS ABSORPTION AND GAS-LIQUID SYSTEM DESIGN

gas stream into a strong alkali solution, absorption of HCl into water or alkaline solutions, or absorption of Cl₂ into strong alkali.

When liquid-phase chemical reactions are **extremely slow**, the gas-phase resistance can be neglected and one can assume that the rate of reaction has a predominant effect upon the rate of absorption. In this case the differential rate of transfer is given by the equation

$$dn_A = R_A f_H S dh = (k_L^0 a / \rho_L) (c_i - c) S dh \quad (14-60)$$

where n_A = rate of solute transfer, R_A = volumetric reaction rate, a function of c and T , f_H = fractional liquid volume holdup in tower or apparatus, S = tower cross-sectional area, h = vertical distance, k_L^0 = liquid-phase mass-transfer coefficient for pure physical absorption, a = effective interfacial mass-transfer area per unit volume of tower or apparatus, ρ_L = average molar density of liquid phase, c_i = solute concentration in liquid at gas-liquid interface, and c = solute concentration in bulk liquid.

Although the right-hand side of Eq. (14-60) remains valid even when chemical reactions are extremely slow, the mass-transfer driving force may become increasingly small, until finally $c \approx c_i$. For extremely slow first-order irreversible reactions, the following rate expression can be derived from Eq. (14-60):

$$R_A = k_1 c = k_1 c_i / (1 + k_1 \rho_L f_H / k_L^0 a) \quad (14-61)$$

where k_1 = first-order reaction rate coefficient.

For **dilute systems** in countercurrent absorption towers in which the equilibrium curve is a straight line (i.e., $y_i = mx_i$) the differential relation of Eq. (14-60) is formulated as

$$dn_A = -G_M S dy = k_1 c f_H S dh \quad (14-62)$$

where G_M = molar gas-phase mass velocity and y = gas-phase solute mole fraction.

Substitution of Eq. (14-61) into Eq. (14-62) and integration lead to the following relation for an **extremely slow first-order reaction** in an absorption tower:

$$y_2 = y_1 \exp(-\gamma) \quad (14-63)$$

$$\text{where } \gamma = \frac{k_1 \rho_L f_H h_T / m G_M}{(1 + k_1 \rho_L f_H / k_L^0 a)} \quad (14-64)$$

In Eq. (14-63) the subscripts 1 and 2 refer to the bottom and the top of the tower respectively.

The Hatta number N_{Ha} usually is employed as the criterion for determining whether or not a reaction can be considered extremely slow. For extremely slow reactions a reasonable criterion is

$$N_{Ha} = \sqrt{k_1 D_A / k_L^0} \leq 0.3 \quad (14-65)$$

where D_A = liquid-phase diffusion coefficient of the solute in the sol-

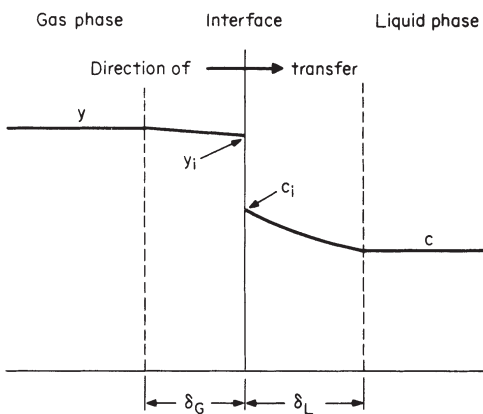


FIG. 14-11 Gas-phase and liquid-phase solute-concentration profiles for an extremely slow (kinetically limited) reaction system for which N_{Ha} is less than 0.3.

vent. Figure 14-11 illustrates the concentration profiles in the gas and liquid films for the case of an extremely slow chemical reaction.

We note that when the second term in the denominator of Eq. (14-64) is small, the liquid holdup in the tower can have a significant influence upon the rate of absorption if an extremely slow chemical reaction is involved.

When **chemical equilibrium** is achieved quickly throughout the liquid phase (or can be assumed to exist), the problem becomes one of properly defining the physical and chemical equilibria for the system. It sometimes is possible to design a plate-type absorber by assuming chemical-equilibrium relationships in conjunction with a stage efficiency factor as is done in distillation calculations. Rivas and Prausnitz [Am. Inst. Chem. Eng. J., 25, 975 (1979)] have presented an excellent discussion and example of the correct procedures to be followed for systems involving chemical equilibria.

Traditional Design Method The traditionally employed conventional procedure for designing packed-tower gas-absorption systems involving chemical reactions makes use of overall volumetric mass-transfer coefficients as defined by the equation

$$K'_C a = n_A / (h_T S p_T \Delta y_{1m}^\circ) \quad (14-66)$$

where $K'_C a$ = overall volumetric mass-transfer coefficient, n_A = rate of solute transfer from the gas to the liquid phase, h_T = total height of tower packing, S = tower cross-sectional area, p_T = total system pressure, and Δy_{1m}° is defined by the equation

$$\Delta y_{1m}^\circ = \frac{(y_1 - y^\circ)_1 - (y_1 - y^\circ)_2}{\ln [(y_1 - y^\circ)_1 / (y_1 - y^\circ)_2]} \quad (14-67)$$

in which subscripts 1 and 2 refer to the bottom and top of the absorption tower respectively, y = mole-fraction solute in the gas phase, and y° = gas-phase solute mole fraction in equilibrium with bulk-liquid-phase solute concentration x . When the equilibrium line is straight, $y^\circ = mx$.

The traditional design method normally makes use of overall $K'_C a$ values even when resistance to transfer lies predominantly in the liquid phase. For example, the CO₂-NaOH system most commonly used for comparing the $K'_C a$ values of various tower packings is a liquid-phase-controlled system. When the liquid phase is controlling, extrapolation to different concentration ranges or operating conditions is not recommended since changes in the reaction mechanism can cause k_L to vary unexpectedly and the overall $K'_C a$ values do not explicitly show such effects.

Overall $K'_C a$ data may be obtained from tower-packing vendors for many of the established commercial gas-absorption processes. Such data often are based either upon tests in large-diameter test units or upon actual commercial operating data. Since extrapolation to untried operating conditions is not recommended, the preferred procedure for applying the traditional design method is equivalent to duplicating a previously successful commercial installation. When this is not possible, then a commercial demonstration at the new operating conditions may be required, or else one could consider using some of the more rigorous methods described later.

Aside from the lack of an explicitly defined liquid-phase-resistance term, the limitations on the use of Eq. (14-66) are related to the fact that its derivation implicitly assumes that the system is dilute ($y_{BM} \approx 1$) and that the operating and equilibrium curves are straight lines over the range of tower operation. Also, Eq. (14-66) is strictly valid only for the temperature and pressure at which the original test was run even though the total pressure p_T appears in the denominator.

The ambiguity of the total pressure effect can be seen by a comparison of the gas-phase- and liquid-phase-controlled cases: when the gas phase controls, the liquid-phase resistance is negligible and $K'_C a = K'_C a p_T$ is independent of the total pressure. For this case the coefficient $K'_C a$ is inversely proportional to the total system pressure as shown in Eq. (14-66). On the other hand, when the liquid phase controls, the correct equation is

$$K'_C a = K_C a / p_T = k_L a / H \quad (14-68)$$

where H is the Henry's-law constant defined as $H = p_i / x_i$. This equation indicates that $K'_C a$ will be independent of the total system pressure as long as the Henry's-law constant H does not depend on the

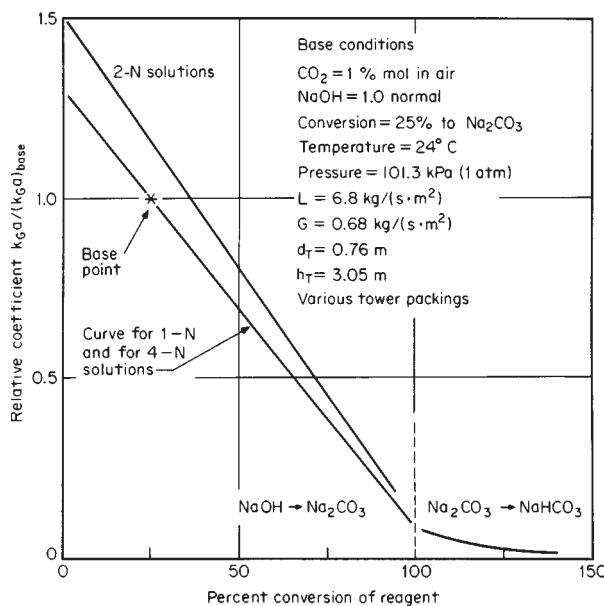


FIG. 14-12 Effects of reagent-concentration and reagent-conversion level upon the relative values of $\hat{K}_{G'a}$ in the $\text{CO}_2\text{-NaOH}\text{-H}_2\text{O}$ system. [Adapted from Eckert *et al.*, Ind. Eng. Chem., 59(2), 41 (1967).]

total pressure (this will be true only for relatively low pressures). On the basis of this comparison it should be clear that the effects of total system pressure upon $K'_c a$ are not properly defined by Eq. (14-66), especially in cases in which the liquid-phase resistance cannot be neglected.

In using Eq. (14-66), therefore, it should be understood that the numerical values of $K'_c a$ will be a complex function of the pressure, the temperature, the type and size of tower packing employed, the liquid and gas mass flow rates, and the system composition (for example, the degree of conversion of the liquid-phase reactant).

Figure 14-12 illustrates the influence of system composition and **degree of reactant conversion** upon the numerical values of $K'_c a$ for the absorption of CO_2 into sodium hydroxide solutions at constant conditions of temperature, pressure, and type of packing. An excellent experimental study of the influence of operating variables upon overall $K'_c a$ values is that of Field *et al.* (*Pilot-Plant Studies of the Hot Carbonate Process for Removing Carbon Dioxide and Hydrogen Sulfide*, U.S. Bureau of Mines Bulletin 597, 1962).

Table 14-2 illustrates the observed variations in $\hat{K}_{G'a}$ values for different packing types and sizes for the $\text{CO}_2\text{-NaOH}$ system at a 25 percent reactant-conversion level for two different liquid flow rates. The lower rate of $2.7 \text{ kg}/(\text{s} \cdot \text{m}^2)$ or $2000 \text{ lb}/(\text{h} \cdot \text{ft}^2)$ is equivalent to $4 (\text{U.S. gal}/\text{min})/\text{ft}^2$ and is typical of the liquid rates employed in fume scrubbers. The higher rate of $13.6 \text{ kg}/(\text{s} \cdot \text{m}^2)$ or $10,000 \text{ lb}/(\text{h} \cdot \text{ft}^2)$ is equivalent to $20 (\text{U.S. gal}/\text{min})/\text{ft}^2$ and is more typical of absorption towers such as are used in CO_2 removal systems, for example. We note also that two different gas velocities are represented in the table, corresponding to superficial velocities of 0.59 and 1.05 m/s (1.94 and 3.44 ft/s).

Table 14-3 presents a typical range of $\hat{K}_{G'a}$ values for chemically reacting systems. The first two entries in the table represent systems that can be designed by the use of purely physical design methods, for they are completely gas-phase mass-transfer limited. To ensure a negligible liquid-phase resistance in these two tests, the HCl was absorbed into a solution maintained at less than 8 percent weight HCl and the NH_3 was absorbed into a water solution maintained below pH 7 by the addition of acid. The last two entries in Table 14-3 represent liquid-phase mass-transfer limited systems.

The effects of system pressure on these $\hat{K}_{G'a}$ values can be estimated as in Eq. (14-68) by noting that $\hat{K}_{G'a} = K'_c a y_{BM}^\circ = K'_c a y_{BM}^\circ p_T$ and recalling that (1) in gas-phase mass-transfer limited systems $\hat{K}_{G'a} = k_{Ga}$ and is independent of system pressure, and (2) for liquid-phase mass-transfer limited systems in which H is constant the $\hat{K}_{G'a}$ values can be corrected to other pressures by the relation $\hat{K}_{G'a}$ at $p_2 = (\hat{K}_{G'a}$ at $p_1)) \times p_2/p_1$. When both resistances are significant, it is advisable to employ experimentally derived corrections. In any case it is inadvisable to make large pressure corrections by these procedures without experimental verification.

Scaling Up from Laboratory or Pilot-Plant Data For many years it has been thought by practitioners of the art of gas absorption that it would be impossible to carry out an absorption process in a laboratory apparatus or small-scale pilot plant in such a way that the data could be of use in the design of a commercial absorption unit. Indeed, even today most commercial gas-absorption units are designed primarily on the basis of prior commercial experience by using the traditional design methods described previously. Although duplication of a previous commercial design is by far the preferred method, this approach is of little value in developing a completely new process or in attempting to extrapolate an existing design to widely different operating conditions.

Since the early 1960s there have been developed some excellent laboratory experimental techniques, which unfortunately have largely been ignored by the industry. A noteworthy exception was described by Ouwerkerk (*Hydrocarbon Process.*, April 1978, pp. 89–94), in which it was revealed that both laboratory and small-scale pilot-plant data were employed as the basis for the design of an 8.5-m- (28-ft-) diameter commercial Shell Claus off-gas treating (SCOT) plate-type absorber. It is claimed that the cost of developing comprehensive design procedures can be kept to a minimum, especially in the development of a new process, by the use of these modern techniques.

TABLE 14-2 Typical Effects of Packing Type, Size, and Liquid Rate on $\hat{K}_{G'a}$ in a Chemically Reacting System, $\hat{K}_{G'a}$, $\text{kmol}/(\text{h} \cdot \text{m}^3)$

Packing size, mm	$L = 2.7 \text{ kg}/(\text{s} \cdot \text{m}^2)$				$L = 13.6 \text{ kg}/(\text{s} \cdot \text{m}^2)$			
	25	38	50	75–90	25	38	50	75–90
Berl-saddle ceramic	30	24	21		45	38	32	
Raschig-ring ceramic	27	24	21		42	34	30	
Raschig-ring metal	29	24	19		45	35	27	
Pall-ring plastic	29	27	26*	16	45	42	38*	24
Pall-ring metal	37	32	27	21*	56	51	43	27*
Intalox-saddle ceramic	34	27	22	16*	56	43	34	26*
Super-Intalox ceramic	37*		26*		59*		40*	
Intalox-saddle plastic	40*		24*	16*	56*		37*	26*
Intalox-saddle metal	43*	35*	30*	24*	66*	58*	48*	37*
Hy-Pak metal	35	32*	27*	18*	54	50*	42*	27*

Data courtesy of the Norton Company.

Operating conditions: CO_2 , 1 percent mole in air; NaOH , 4 percent weight (1 normal); 25 percent conversion to sodium carbonate; temperature, 24°C (75°F); pressure, 98.6 kPa (0.97 atm); gas rate = $0.68 \text{ kg}/(\text{s} \cdot \text{m}^2) = 0.59 \text{ m/s} = 500 \text{ lb}/(\text{h} \cdot \text{ft}^2) = 1.92 \text{ ft/s}$ except for values with asterisks, which were run at $1.22 \text{ kg}/(\text{s} \cdot \text{m}^2) = 1.05 \text{ m/s} = 900 \text{ lb}/(\text{h} \cdot \text{ft}^2) = 3.46 \text{ ft/s}$ superficial velocity; packed height, 3.05 m (10 ft); tower diameter, 0.76 m (2.5 ft). To convert table values to units of $(\text{lb-mol})/(\text{h} \cdot \text{ft}^3)$, multiply by 0.0624.

TABLE 14-3 Typical \hat{K}_{GA} Values for Various Chemically Reacting Systems, kmol/(h·m³)

Gas-phase reactant	Liquid-phase reactant	\hat{K}_{GA}	Special conditions
HCl	H ₂ O	353	Gas-phase limited
NH ₃	H ₂ O	337	Gas-phase limited
Cl ₂	NaOH	272	8% weight solution
SO ₂	Na ₂ CO ₃	224	11% weight solution
HF	H ₂ O	152	
Br ₂	NaOH	131	5% weight solution
HCN	H ₂ O	114	
HCHO	H ₂ O	114	Physical absorption
HBr	H ₂ O	98	
H ₂ S	NaOH	96	4% weight solution
SO ₂	H ₂ O	59	
CO ₂	NaOH	38	4% weight solution
Cl ₂	H ₂ O	8	Liquid-phase limited

Data courtesy of the Norton Company.

Operating conditions (see text): 38-mm ceramic Intalox saddles; solute gases, 0.5–1.0 percent mole; reagent conversions = 33 percent; pressure, 101 kPa (1 atm); temperature, 16–24°C; gas rate = 1.3 kg/(s·m²) = 1.1 m/s; liquid rates = 3.4 to 6.8 kg/(s·m²); packed height, 3.05 m; tower diameter, 0.76 m. Multiply table values by 0.0624 to convert to (lb·mol)/(h·ft³).

In 1966, in a paper that now is considered a classic, Danckwerts and Gillham [*Trans. Inst. Chem. Eng.*, **44**, T42 (1966)] showed that data taken in a small stirred-cell laboratory apparatus could be used in the design of a packed-tower absorber when chemical reactions are involved. They showed that if the packed-tower mass-transfer coefficient in the absence of reaction (k_L^0) can be reproduced in the laboratory unit, then the rate of absorption in the laboratory apparatus will respond to chemical reactions in the same way as in the packed column even though the means of agitating the liquid in the two systems might be quite different.

According to this method, it is not necessary to investigate the kinetics of the chemical reactions in detail, nor is it necessary to determine the solubilities or the diffusivities of the various reactants in their unreacted forms. To use the method for scaling up, it is necessary independently to obtain data on the values of the interfacial area per unit volume a and the physical mass-transfer coefficient k_L^0 for the commercial packed tower. Once these data have been measured and tabulated, they can be used directly for scaling up the experimental laboratory data for any new chemically reacting system.

Danckwerts and Gillham did not investigate the influence of the gas-phase resistance in their study (for some processes gas-phase resistance may be neglected). However, in 1975 Danckwerts and Alper [*Trans. Inst. Chem. Eng.*, **53**, 34 (1975)] showed that by placing a stirrer in the gas space of the stirred-cell laboratory absorber, the gas-phase mass-transfer coefficient \hat{k}_G in the laboratory unit could be made identical to that in a packed-tower absorber. When this was done, laboratory data obtained for chemically reacting systems having a significant gas-side resistance could successfully be scaled up to predict the performance of a commercial packed-tower absorber.

If it is assumed that the values of \hat{k}_G , k_L^0 , and a have been measured for the commercial tower packing to be employed, the procedure for using the laboratory stirred-cell reactor is as follows:

1. The gas-phase and liquid-phase stirring rates are adjusted so as to produce the same values of \hat{k}_G and k_L^0 as will exist in the commercial tower.

2. For the reaction system under consideration, experiments are made at a series of bulk-liquid and bulk-gas compositions representing the compositions to be expected at different levels in the commercial absorber (on the basis of a material balance).

3. The rates of absorption $r_A(c_i, B^0)$ are measured at each pair of gas and liquid compositions.

For dilute-gas systems one form of the equation to be solved in conjunction with these experimental data is

$$h_T = \frac{G_M}{a} \int_{y_2}^{y_1} \frac{dy}{r_A} \quad (14-69)$$

where h_T = height of commercial tower packing, G_M = molar gas-phase mass velocity, a = effective interfacial area for mass transfer per unit

volume in the commercial tower, y = mole-fraction solute in the gas phase, and r_A = experimentally determined rate of absorption per unit of exposed interfacial area.

By using the series of experimentally measured rates of absorption, Eq. (14-69) can be integrated numerically to determine the height of packing required in the commercial tower.

There are a number of different types of experimental laboratory units that could be used to develop design data for chemically reacting systems. Charpentier [*ACS Symp. Ser.*, **72**, 223–261 (1978)] has summarized the state of the art with respect to methods of scaling up laboratory data and tabulated typical values of the mass-transfer coefficients, interfacial areas, and contact times to be found in various commercial gas absorbers as well as in currently available laboratory units.

The laboratory units that have been employed to date for these experiments were designed to operate at a total system pressure of about 100 kPa (1 atm) and at near-ambient temperatures. In practical situations, it may become necessary to design a laboratory absorption unit that can be operated either under vacuum or at elevated pressures and over a reasonable range of temperatures in order to apply the Danckwerts method.

It would be desirable to reinterpret existing data for commercial tower packings to extract the individual values of the interfacial area a and the mass-transfer coefficients \hat{k}_G and k_L^0 in order to facilitate a more general usage of methods for scaling up from laboratory experiments. Some progress in this direction has already been made, as discussed later in this section. In the absence of such data, it is necessary to operate a pilot plant or a commercial absorber to obtain \hat{k}_G , k_L^0 , and a as described by Ouwerkerk (op. cit.).

Principles of Rigorous Absorber Design Danckwerts and Alper [*Trans. Inst. Chem. Eng.*, **53**, 34 (1975)] have shown that when adequate data are available for the kinetic-reaction-rate coefficients, the mass-transfer coefficients \hat{k}_G and k_L^0 , the effective interfacial area per unit volume a , the physical solubility or Henry's law constants, and the effective diffusivities of the various reactants, then the design of a packed tower can be calculated from first principles with considerable precision.

For example, the packed-tower design equation for a dilute system in which gas-phase reactant A is being absorbed and reacted with liquid-phase reagent B is

$$r_A a dh = \frac{L_M}{v \rho_L} dB_h^0 = -G_M dy_h \quad (14-70)$$

where r_A = specific rate of absorption per unit interfacial area, a = interfacial area per unit volume of packing, h = height of packing, L_M = molar liquid mass velocity, v = number of moles of B reacting with 1 mol of A; ρ_L = average molar density of liquid phase, B_h^0 = bulk-liquid-phase reagent concentration (a function of h), G_M = molar gas-phase mass velocity, and y_h = mole fraction A in gas phase (a function of h).

For dilute systems it can be assumed that G_M , L_M , and ρ_L are constant, and it normally is assumed that the interfacial area a of the packing is constant and is equal to the value that would exist without reaction. This last assumption needs careful consideration, since different methods for measuring a may give different results. Sharma and Danckwerts [*Br. Chem. Eng.*, **15**(4), 522 (1970)] have reviewed various techniques for measuring interfacial areas.

Under the above assumptions for dilute systems Eq. (14-70) can be integrated as follows:

$$h_T = \frac{L_M}{v \rho_L a} \int_{B_1^0}^{B_2^0} \frac{dB_h^0}{r_A} = \frac{G_M}{a} \int_{y_2}^{y_1} \frac{dy_h}{r_A} \quad (14-71)$$

where h_T = total height of packing and the subscripts 1 and 2 refer to the bottom and the top of the tower packing respectively.

The specific absorption rate $r_A = r_A(c_i, B^0)$ is a function of h and may be computed by combining the rate equation

$$r_A = k_L(x_i - x) = (k_L/\rho_L)(c_i - c) \quad (14-72)$$

with the material-balance, or operating-curve, equation

$$G_M(y - y_2) = (L_M/v \rho_L)(B_2^0 - B^0) \quad (14-73)$$

and with the appropriate relation for computing the interfacial concentration x_i of reactant A. In Eq. (14-72) the mass-transfer coefficient k_L is the coefficient with chemical reaction; i.e., $k_L = \phi k_L^0$.

The interfacial concentration x_i is computed by combining the equilibrium relation $y_i = mx_i$ with the equation $k_G(y - y_i) = k_L(x_i - x)$ to obtain

$$x_i = \frac{y/m + (k_L/mk_G)x}{(1 + k_L/mk_G)} \quad (14-74)$$

According to Eq. (14-74), when k_L is very large and the ratio k_L/mk_G is much larger than unity, $x_i - x = yk_G/k_L$ and the specific absorption rate is defined by the equation

$$r_A = k_L(x_i - x) = k_G y \quad (14-75)$$

This is the **gas-phase mass-transfer limited condition**, which can be substituted into Eq. (14-71) to obtain the following equation for calculating the height of packing for a dilute system:

$$h_T = (G_M/k_{GA}) \ln(y_1/y_2) = H_C \ln(y_1/y_2) \quad (14-76)$$

At the other extreme, when the ratio k_L/mk_G is much smaller than unity, the interfacial concentration of reactant A may be approximated by the equilibrium relation $x_i = y/m$, and the specific absorption rate expression is

$$r_A = k_L(x_i - x) = k_L(y/m - x) \quad (14-77)$$

For **fast chemical reactions** the reactant A is *by definition* completely consumed in the thin film near the liquid interface. Thus, $x = 0$, and

$$r_A = k_L y/m = (k_L/\rho_L) c_i \quad (14-78)$$

This is known as the **liquid-phase mass-transfer limited condition**, as illustrated in Fig. 14-13.

Inspection of Eqs. (14-71) and (14-78) reveals that for fast chemical reactions which are liquid-phase mass-transfer limited the only unknown quantity is the mass-transfer coefficient k_L . The problem of rigorous absorber design therefore is reduced to one of defining the influence of chemical reactions upon k_L . Since the physical mass-transfer coefficient k_L^0 is already known for many tower packings, it

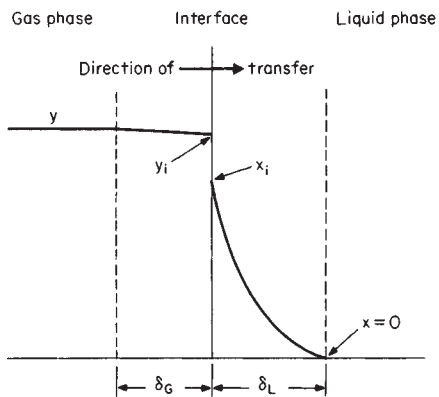


FIG. 14-13 Gas-phase and liquid-phase solute-concentration profiles for a liquid-phase mass-transfer limited reaction system in which N_{Ha} is larger than 3.

often is convenient to work in terms of the ratio k_L/k_L^0 as discussed in the following paragraphs.

Estimation of k_L for Irreversible Reactions Figure 14-14 illustrates the influence of either first- or second-order irreversible chemical reactions on the mass-transfer coefficient k_L as developed by Van Krevelen and Hoflyzer [Rec. Trav. Chim., 67, 563 (1948)] and as later refined by Perry and Pigford and by Brian et al. [Am. Inst. Chem. Eng. J., 7, 226 (1961)].

First-order and pseudo-first-order reactions are represented by the upper curve in Fig. 14-14. We note that for first-order reactions when the Hatta number N_{Ha} is larger than about 3, the rate coefficient k_L can be computed by the formula

$$k_L = \sqrt{k_1 D_A} = \sqrt{(k_2 B^0) D_A} \quad (14-79)$$

where k_L = liquid-phase mass-transfer coefficient, k_1 = first-order-reaction-rate coefficient, $k_2 B^0$ = pseudo-first-order-reaction-rate coef-

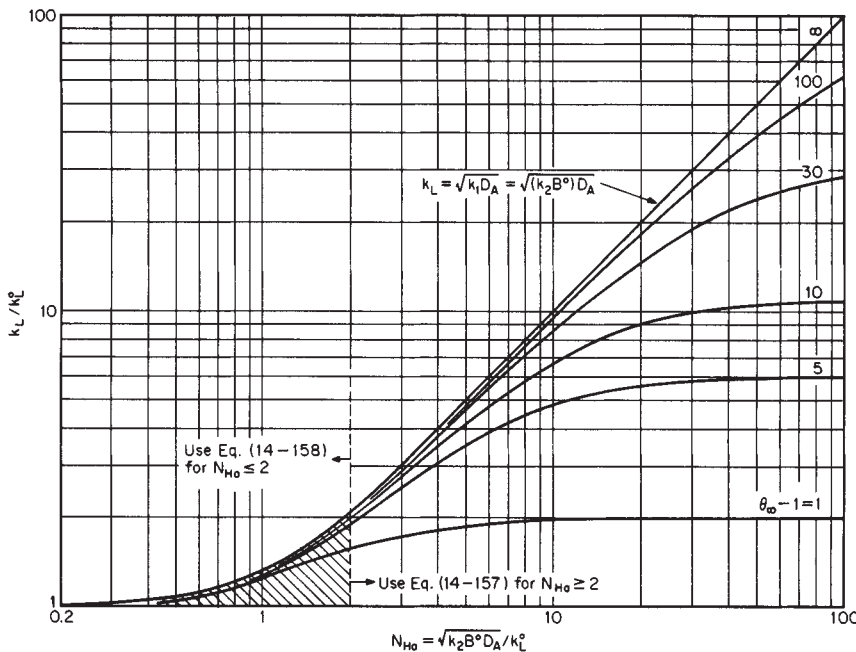


FIG. 14-14 Influence of irreversible chemical reactions on the liquid-phase mass-transfer coefficient k_L . [Adapted from Van Krevelen and Hoflyzer, Rec. Trav. Chim., 67, 563 (1948).]

ficient, and D_A = diffusion coefficient of gaseous reactant A in the liquid phase.

The parameter values for the curves of Fig. 14-14 originally were defined from film theory as $(D_B/D_A)(B^0/vc_i)$ but later were refined by the results of penetration theory to the definition $(\phi_\infty - 1)$, where

$$\phi_\infty = \sqrt{D_A/D_B} + \sqrt{D_B/D_A}(B^0/vc_i) \quad (14-80)$$

in which D_B = diffusion coefficient of the liquid-phase reactant B and ϕ_∞ = value of k_L/k_L^0 for large values of N_{Ha} approaching infinity.

For design purposes the entire graph of Fig. 14-14 can be represented by the following pair of equations:

For $N_{Ha} \geq 2$:

$$k_L/k_L^0 = 1 + (\phi_\infty - 1)\{1 - \exp[-(N_{Ha} - 1)/(\phi_\infty - 1)]\} \quad (14-81)$$

For $N_{Ha} \leq 2$:

$$k_L/k_L^0 = 1 + (\phi_\infty - 1)\{1 - \exp[-(\phi_\infty - 1)^{-1}]\} \exp[1 - 2/N_{Ha}] \quad (14-82)$$

where the Hatta number N_{Ha} is defined as

$$N_{Ha} = \sqrt{k_2 B^0 D_A} / k_L^0 \quad (14-83)$$

Equation (14-81) originally was reported by Porter [*Trans. Inst. Chem. Eng.*, **44**(1), T25 (1966)]. Equation (14-82) was derived by the author.

The Van Krevelen-Hoftyzer relationship was tested experimentally for the second-order system in which CO_2 reacts with either NaOH or KOH solutions by Nijsing et al. [*Chem. Eng. Sci.*, **10**, 88 (1959)]. Nijsing's results for the NaOH system are shown in Fig. 14-15 and are in excellent agreement with the second-order-reaction theory. Indeed, these experimental results can be described very well by Eqs. (14-80) and (14-81) when values of $v = 2$ and $D_A/D_B = 0.64$ are employed in the equations.

For fast irreversible chemical reactions, therefore, the principles of rigorous absorber design can be applied by first establishing the effects of the chemical reaction on k_L and then employing the appropriate material-balance and rate equations in Eq. (14-71) to perform the integration to compute the required height of packing.

For an isothermal absorber involving a dilute system in which a **liquid-phase mass-transfer limited** first-order irreversible chemical reaction is occurring, the packed-tower design equation is derived as

$$h_T = (mG_M/\sqrt{k_1 D_A} a) \ln(y_1/y_2) \quad (14-84)$$

For a dilute system in which the **liquid-phase mass-transfer limited** condition is valid, in which a very fast second-order reaction is involved, and for which N_{Ha} is very large, the equation

$$k_L/k_L^0 = \phi_\infty = \sqrt{D_A/D_B} + \sqrt{D_B/D_A} B^0/vc_i \quad (14-85)$$

is valid and results in the following equation for computing the height of packing in a packed tower:

$$h_T = \frac{mG_M}{k_L^0 a} \sqrt{\frac{D_B}{D_A}} \int_{y_2}^{y_1} \frac{dy}{\frac{mb^0 D_B}{v p_L D_A} + y} \quad (14-86)$$

Evaluation of the integral in Eq. (14-86) requires a knowledge of the liquid-phase bulk concentration of B as a function of y. This relationship is obtained by means of a material balance around the tower, as shown in Eq. (14-73). Numerical integration by a quadrature method such as Simpson's rule normally will be required for this calculation.

Estimation of k_L for Reversible Reactions When the reaction is of the form $A \rightleftharpoons B$, where B is a nonvolatile product and the equilibrium constant is defined by $K_{eq} = K_{eq} c_A$, the expressions for computing k_L become extremely complex. A good discussion of this situation is given in *Mass Transfer* by Sherwood, Pigford, and Wilke (McGraw-Hill, New York, 1975, p. 317). Three limiting cases are listed below:

1. For very slow reactions,

$$\lim_{k_1 \rightarrow 0} k_L = k_L^0 \quad (14-87)$$

2. For extremely fast reactions where K_{eq} is very large,

$$\lim_{K_{eq} \rightarrow \infty} k_L = \sqrt{k_1 D_A} \quad (14-88)$$

3. For extremely fast reactions where K_{eq} is finite,

$$\lim_{K_{eq} \text{ finite}} k_L = (1 + K_{eq}) k_L^0 \quad (14-89)$$

When one of these three conditions is applicable, the appropriate design equation can be obtained by substitution into Eq. (14-71), followed by integration of the resulting relationship.

Some more complex situations involving reversible reactions are discussed in *Mass Transfer* (*ibid.*, pp. 336–343).

Simultaneous Absorption of Two Reacting Gases In multi-component physical absorption the presence of one gas often does not affect the rates of absorption of the other gases. When chemical reactions in which two or more gases are competing for the same liquid-phase reagent are involved, selectivity of absorption can be affected by

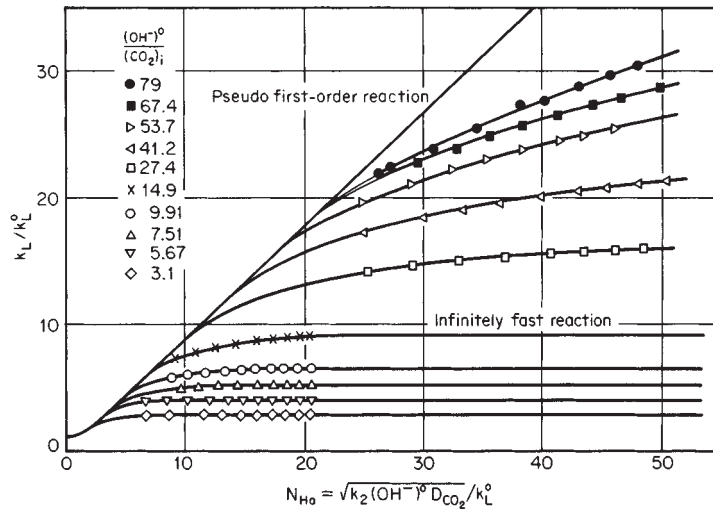


FIG. 14-15 Experimental values of k_L/k_L^0 for absorption of CO_2 into NaOH solutions at 20°C. [Data of Nijsing et al., *Chem. Eng. Sci.*, **10**, 88 (1959).]

the choice of design conditions, and the situation may become extremely complex from a designer's point of view.

The classic work on this subject is that of Ramachandran and Sharma [*Trans. Inst. Chem. Eng.*, **49**, 253 (1971)] and is recommended to those needing further details. The following references also are offered as a sampling of the literature on the subject:

- CO_2 and H_2S . Danckwerts and Sharma, *Chem. Eng. (London)*, CE244-280 (October 1966); Onda, et al., *J. Chem. Eng. Japan*, **5**, 27 (1972); Rivas and Prausnitz, *Am. Inst. Chem. Eng. J.*, **25**, 975 (1979).
- CO_2 and SO_2 . Goettler and Pigford, *Inst. Chem. Eng. Symp. Ser.*, **28**, 1 (1968); Teramoto et al., *Int. Chem. Eng.*, **18**, 250 (1978).
- SO_2 and NO_2 . Takeuchi and Yamanaka, *Ind. Eng. Chem. Process Des. Dev.*, **17**, 389 (1978).

Desorption with Chemical Reaction When chemical reactions are involved in a stripping operation, the design problem can become extremely complex. In fact, much less is known about this very important process than is known about absorption. A classic work on this subject is that of Shah and Sharma [*Trans. Inst. Chem. Eng.*, **54**, 1 (1976)], which is recommended to those in need of more details.

In the subsection "Design of Gas-Absorption Systems" it was stated that more often than not the liquid-phase residence time and, hence, the liquid holdup are considered to be the most important design parameters for stripping towers. If Eq. (14-60) is redefined to represent the stripping process for an extremely slow liquid-phase reaction for which $R_A = k_1 c$, then one finds that the liquid holdup will be a factor only when the ratio $k_1 p_L f_H / k_1' a$ is less than unity. Thus, one can ensure that the liquid-phase reaction rate is not limiting by increasing the temperature and the liquid holdup until this ratio is equal to or greater than unity. The preferred method at present is to base the design on prior commercial experience.

Use of Literature for Specific Systems A large body of experimental data obtained in bench-scale laboratory units and in small-diameter packed towers has been published since the early 1940s. One might wish to consider using such data for a particular chemically

reacting system as the basis for scaling up to a commercial design. Extreme caution is recommended in interpreting such data for the purpose of developing commercial designs, as extrapolations of this kind of information can lead to serious errors. Extrapolation to temperatures, pressures, or liquid-phase reagent conversions different from those that were employed by the original investigator definitely should be regarded with caution.

Bibliographies presented in the general references listed at the beginning of this section are an excellent source of information on specific chemically reacting systems. *Gas-Liquid Reactions* by Danckwerts (McGraw-Hill, New York, 1970) contains a tabulation of references to specific chemically reacting systems. *Gas Treating with Chemical Solvents* by Astarita et al. (Wiley, New York, 1983) deals with the absorption of acid gases, and includes an extensive listing of patents. *Gas Purification* by Kohl and Riesenfeld (Gulf Publishing, Houston, 1985) presents data and references for many chemically reacting systems of current commercial interest.

In searching for data on a particular system, a computerized search of *Chemical Abstracts*, *Engineering Index*, and National Technical Information Service (NTIS) data bases should seriously be considered. Although the NTIS computer contains only information published after 1970, one normally can assume that most pre-1970 publications of merit likely will be referenced in the bibliographies of current articles on the subject.

The experimental data for the system $\text{CO}_2\text{-NaOH-Na}_2\text{CO}_3$ are unusually well known as the result of the work of many experimenters. A serious study of the data and theory for this system therefore is recommended as the basis for developing a good understanding of the kind and quality of experimental information that is needed for design purposes.

In addition to data on CO_2 , information can readily be found in the literature for the following systems: O_2 , Cl_2 , NH_3 , NO_2 , NO , SO_2 , SO_3 , H_2S , COS , CS_2 , HCl , HBr , HCN , H_2 , COCl_2 , PCl_3 , olefins, dienes, and water vapor.

GAS-LIQUID CONTACTING SYSTEMS

Gas-liquid contacting systems are utilized for transferring mass, heat, and momentum between the phases, subject to constraints of physical and chemical equilibrium. Process equipment for such systems is designed to achieve the appropriate transfer operations with a minimum expenditure of energy and capital investment.

In this section emphasis is placed on the transfer of mass. Typical gas-liquid mass-transfer systems are:

Distillation	Evaporation
Flashing	Humidification
Rectification	Dehumidification
Absorption	Dephlegmation
Stripping	Spray drying

Distillation is the separation of the constituents of a liquid mixture via partial vaporization of the mixture and separate recovery of vapor and residue. The process of vaporization is generally of a differential nature.

Flashing is a distillation process in which the total vapor removed approaches phase equilibrium with the residue liquid.

Rectification is the separation of the constituents of a liquid mixture by successive distillations (partial vaporizations and condensations) and is obtained via the use of an integral or differential process. Separations into effectively pure components may be obtained through this procedure.

Stripping or desorption is the transfer of gas, dissolved in a liquid, into a gas stream. The term is also applied to that section of a fractionating column below the feed plate.

Absorption is the transfer of a soluble component in a gas-phase mixture into a liquid absorbent whose volatility is low under process conditions.

Evaporation generally refers to the removal of water, by vaporization, from aqueous solutions of nonvolatile substances.

Humidification and dehumidification refer to the transfer of water between a gas stream and a water stream.

Dephlegmation, or partial condensation, refers to the process in which a vapor stream is cooled to a desired temperature such that a portion of the less volatile components of the stream is removed from the vapor by condensation.

Spray drying is an extension of the evaporative process in which almost all the liquid is removed from a solution of a nonvolatile solid in the liquid.

All these processes are, in common, liquid-gas mass-transfer operations and thus require similar treatment from the aspects of phase equilibrium and kinetics of mass transfer. The fluid-dynamic analysis of the equipment utilized for the transfer also is similar for many types of liquid-gas process systems.

Process equipment utilized for liquid-gas contacting is based on a combination of operating principles of the three categories:

Mode of flow of streams
Countercurrent
Cocurrent
Cross-flow
Gross mechanism of transfer
Differential
Integral
Continuous phase
Gas°
Liquid

[°] In this section the terms "gas" and "vapor" are used interchangeably. The latter is often used in distillation, in which the gas phase is represented by an equilibrium vapor.

14-24 GAS ABSORPTION AND GAS-LIQUID SYSTEM DESIGN

TABLE 14-4 Characteristics of Liquid-Gas Systems

Equipment designation	Mode of flow	Gross mechanism	Continuous phase	Primary process applications
Plate column	Cross-flow, countercurrent	Integral	Liquid and/or gas	Absorption, rectification, stripping
Packed column	Countercurrent, cocurrent	Differential	Liquid and/or gas	Absorption, rectification, stripping, humidification, dehumidification
Wetted-wall (falling-film) column	Countercurrent, cocurrent	Differential	Liquid and/or gas	Absorption, rectification, stripping, evaporation
Spray chamber	Cocurrent, cross-flow, countercurrent	Differential	Gas	Absorption, stripping, humidification, dehumidification
Heat exchanger	Cocurrent, countercurrent	Differential	Gas	Evaporation, dephlegmation
Agitated vessel	Complete mixing	Integral	Liquid	Absorption
Line mixer	Cocurrent	Differential	Liquid or gas	Absorption, stripping

The combination of these characteristics utilized in the various types of process equipment is indicated in Table 14-4.

PLATE COLUMNS

Plate Types Plate columns utilized for liquid-gas contacting may be classified according to mode of flow in their internal contacting devices:

1. Cross-flow plates
2. Counterflow plates

The cross-flow plate (Fig. 14-16a) utilizes a liquid downcomer and is more generally used than the counterflow plate (Fig. 14-16b) because of transfer-efficiency advantages and greater operating range. The liquid-flow pattern on a cross-flow plate can be controlled by placement

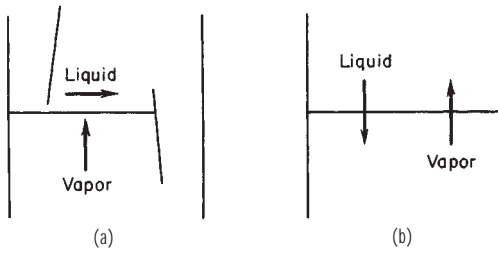


FIG. 14-16 (a) Cross-flow plate (side view). (b) Countercurrent plate (side view).

of downcomers in order to achieve desired stability and transfer efficiency. Commonly used flow arrangements are shown in Fig. 14-17. A guide for the tentative selection of flow pattern is given in Table 14-5.

It should be noted that the fraction of column cross-sectional area available for gas dispersers (perforations, bubble caps) decreases when more than one downcomer is used. Thus, optimum design of the plate involves a balance between liquid-flow accommodation and effective use of cross section for gas flow.

Most new designs of cross-flow plates employ perforations for dispersing gas into liquid on the plate. These perforations may be simple

TABLE 14-5 Selection of Cross-Flow-Plate Flow Pattern*

Estimated tower diam., ft	Range of liquid capacity, gal/min			
	Reverse flow	Cross-flow	Double pass	Cascade double pass
3	0-30	30-200		
4	0-40	40-300		
6	0-50	50-400	400-700	
8	0-50	50-500	500-800	
10	0-50	50-500	500-900	900-1400
12	0-50	50-500	500-1000	1000-1600
15	0-50	50-500	500-1100	1100-1800
20	0-50	50-500	500-1100	1100-2000

*Bolles, chap. 14 in Smith, *Design of Equilibrium Stage Processes*, McGraw-Hill, New York, 1963. To convert feet to meters, multiply by 0.3048; to convert gallons per minute to decimeters per second (liters per second), multiply by 0.06309; and to convert gallons per minute to cubic meters per second, multiply by 6.309×10^{-5} .

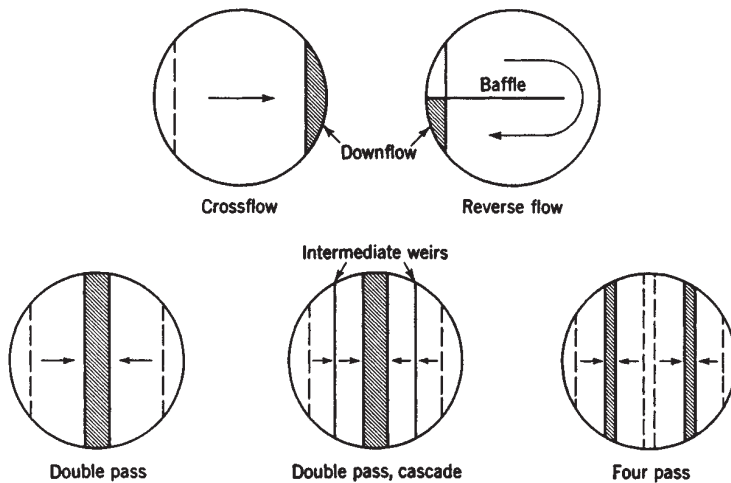


FIG. 14-17 Common liquid-flow patterns, cross-flow plates. (Smith, *Design of Equilibrium Stage Processes*, McGraw-Hill, New York, 1963.)

round orifices, or they may contain movable "valves" that provide variable orifices of noncircular shape. These perforated plates are called sieve plates (Fig. 14-18) or valve plates (Fig. 14-19). For sieve plates, liquid is prevented from flowing through the perforations by the flowing action of the gas; thus, when the gas flow is low, it is possible for some or all of the liquid to drain through the perforations and in effect bypass portions of the contacting zone. The valve plate is designed to minimize this drainage, or "weeping," since the valve tends to close as the gas flow becomes lower, the total orifice area varying to maintain a dynamic-pressure balance across the plate.

Historically the most common gas disperser for cross-flow plates has been the bubble cap. This device has a built-in seal which prevents liquid drainage at low gas-flow rates. Typical bubble caps are shown in Fig. 14-20. Gas flows up through a center riser, reverses flow under the cap, passes downward through the annulus between riser and cap, and finally passes into the liquid through a series of openings, or "slots," in the lower side of the cap.

Bubble caps were used almost exclusively as cross-flow-plate dispersers until about 1950, when they were largely displaced by simple or valve-type perforations. Many varieties of bubble-cap design were used (and therefore are extant in many operating columns), but in most cases bell caps of 75- to 150-mm (3- to 6-in) diameter were utilized.

In counterflow plates, liquid and gas utilize the same openings for flow. Thus, there are no downcomers. Openings are usually simple round perforations in the 3- to 13-mm ($\frac{1}{4}$ - to $\frac{1}{2}$ -in) range (dual-flow plate) or long slots with widths of 6 to 13 mm ($\frac{1}{4}$ to $\frac{1}{2}$ in) (Turbogrid tray). The plate material can be corrugated (Ripple tray) to segregate partially gas and liquid flow. In general, gas and liquid flow in a pulsating fashion with a particular opening passing both gas and liquid in an intermittent fashion.

A counterflow plate often used for contacting gases with liquids containing solids is the baffle plate, or "shower deck" (Fig. 14-21).

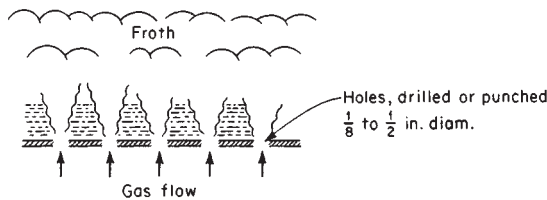


FIG. 14-18 Sieve-plate dispersers. To convert inches to millimeters, multiply by 25.4.

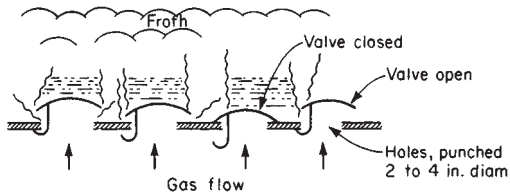


FIG. 14-19 Valve-plate dispersers. To convert inches to millimeters, multiply by 25.4.

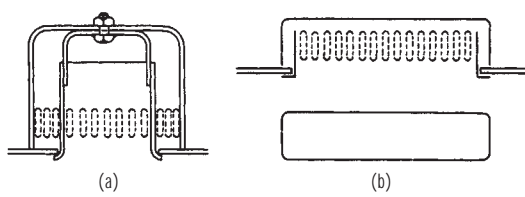


FIG. 14-20 (a) Circular or bell cap. (b) Tunnel cap.

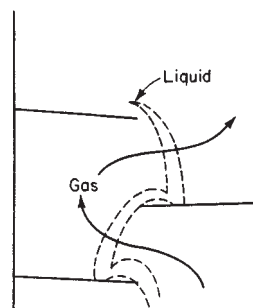


FIG. 14-21 Baffle plate (shower deck).

Typically the plate is half-moon in shape and is sloped slightly in the direction of liquid flow. Gas contacts the liquid as it showers from the plate, and a serrated lip or weir at the edge of the plate can be used to improve the distribution of liquid in the shower.

The baffle plate operates with liquid dispersed and gas as the continuous phase and is used primarily in heat-transfer applications.

In summary, the perforated plate with liquid cross-flow (the "sieve plate") is the most common type specified for new designs. Schematic diagrams of such a plate are shown in Fig. 14-22. Nomenclature items are shown, with heights h_{lb} , h_f , h_{lo} , and h_t referring to liquid entering, froth, liquid + froth leaving, and equivalent clear liquid averaged across the plate. For the plan view, area terms are as follows: A_t = tower total cross section; A_a = active area; A_d = area of one downcomer; A_n = net area for vapor flow (usually total cross section minus blocking downcomers); and A_h = area of holes or perforations. For the single cross-flow plate shown,

$$A_t = A_a + 2A_d$$

$$A_n = A_a + A_d = A_t - A_d$$

When downcomers are sloped or when perforations do not occupy essentially all the area between the downcomers, these simple relations do not apply. However, their adaptation should be obvious from the geometry involved.

The term "froth" in Fig. 14-22 suggests aeration in which the liquid phase is continuous. Under certain conditions there can be an inversion to a gas-continuous regime, or "spray." The spray has its phase boundaries equivalent to the boundaries for froth shown in Fig. 14-22.

Plate-Column Capacity The maximum allowable capacity of a plate for handling gas and liquid flow is of primary importance because it fixes the minimum possible diameter of the column. For a constant liquid rate, increasing the gas rate results eventually in excessive entrainment and flooding. At the flood point it is difficult to obtain net downward flow of liquid, and any liquid fed to the column is carried out with the overhead gas. Furthermore, the column inventory of liquid increases, pressure drop across the column becomes quite large, and control becomes difficult. Rational design calls for operation at a safe margin below this maximum allowable condition.

Flooding may also be brought on by increasing the liquid rate while holding the gas rate constant. Excessive liquid flow can overtax the capacity of downcomers or other passages, with the ultimate result of increased liquid inventory, increased pressure drop, and the other characteristics of a flooded column.

These two types of flooding are usually considered separately when a plate column is being rated for capacity. For identification purposes they are called entrainment flooding (or "priming") and downflow flooding. When counterflow action is destroyed by either type, transfer efficiency is lost and reasonable design limits have been exceeded.

Minimum allowable capacity of a column is determined by the need for effective dispersion and contacting of the phases. The types of plates differ in their ability to permit low flows of gas and liquid. A cross-flow sieve plate can operate at reduced gas flow down to a point where liquid drains through the perforations and gas dispersion is inadequate for good efficiency. Valve plates can be operated at very

14-26 GAS ABSORPTION AND GAS-LIQUID SYSTEM DESIGN

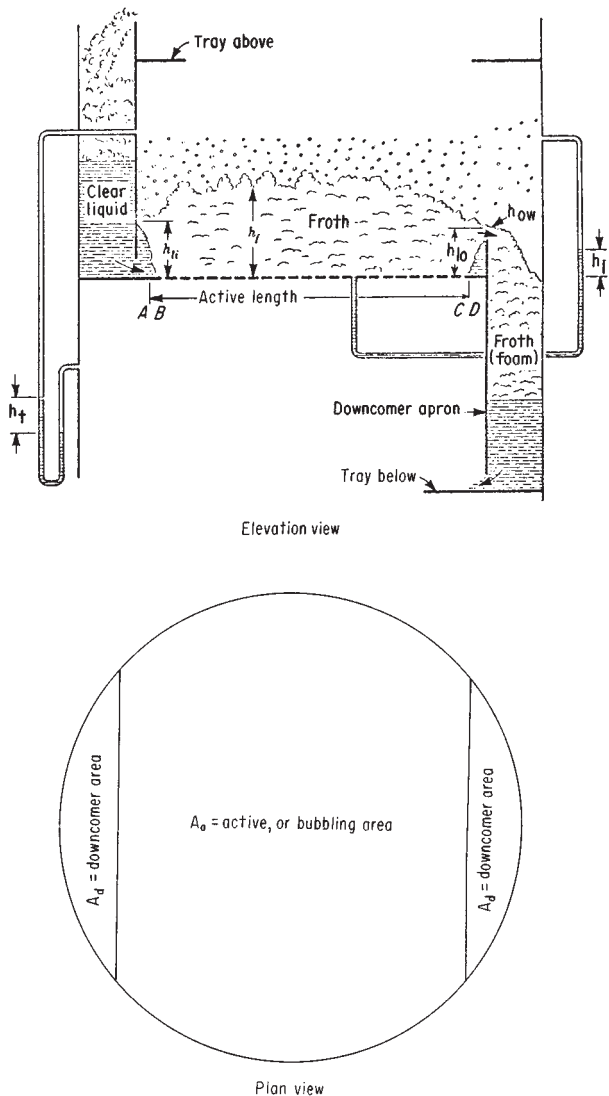


FIG. 14-22 Sieve-plate diagram. (*Smith, Design of Equilibrium Stage Processes. McGraw-Hill, New York, 1963.*)

low gas rates because of valve closing. Bubble-cap plates can be operated at very low gas rates because of their seal arrangement. All devices have a definite minimum gas rate below which there is inadequate dispersion for intimate contacting. Similarly, there are minimum liquid flows below which good distribution is not possible, although the reverse-flow plate (Fig. 14-17) can accommodate extremely low liquid flows.

For all plate devices a qualitative capacity diagram is shown in Fig. 14-23. The shape and extent of the satisfactory operating zone in Fig. 14-23 vary according to type of plate device. As a specific example, Fig. 14-24 shows actual test data for two cross-flow plates in distillation service at total reflux. The abscissa parameter is called the *F*-factor and is a vapor kinetic energy term. The decline in efficiency of the sieve plate at low *F*-factors is evident and is the result of liquid falling through some of the holes ("weeping"). The decline in efficiency of both devices at high *F*-factors results from liquid entrainment. For new designs, it is the objective of the designer to predict the likely location of performance curves such as those shown.

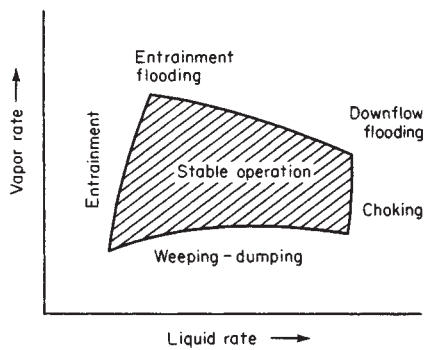


FIG. 14-23 Stable operating region, plates. (*Smith, Design of Equilibrium Stage Processes. McGraw-Hill, New York, 1963.*)

Entrainment Flooding The early work of Souders and Brown [*Ind. Eng. Chem.*, **26**, 98 (1934)] based on a force balance on an average suspended droplet of liquid led to the definition of a capacity parameter C_{sbf} :

$$C_{sbf} = U_n \sqrt{\rho_L / (\rho_t - \rho_g)} \quad (14-90)$$

where U_n = linear gas velocity based on net area A_n , m/s
 ρ_g = gas density, kg/m³
 ρ_L = liquid density, kg/m³

For cross-flow plates, net area is the column cross section less than area blocked by the downcomer or downcomers (Fig. 14-22). The vapor velocity in the net area represents an approach velocity and thus controls the level of liquid entrainment. For counterflow plates, net area is the same as the column cross section, since no downcomers are involved.

Maximum allowable values of the capacity parameter are for a flooding condition and are designated C_{sbf} . Experimental values have been correlated against a dimensionless flow parameter F_{LG} as shown in Fig. 14-25. The flow parameter represents a ratio of liquid to vapor kinetic energies:

$$F_{LG} = \frac{L}{G} \left(\frac{\rho_G}{\rho_L} \right)^{0.5} \quad (14-91)$$

Low values of F_{LG} indicate vacuum operation, high values indicate operation at higher pressures or at high liquid/vapor loadings as in gas absorption. The liquid/gas ratio L/G is based on mass flow rates. The parameter serves as a criterion for two-phase flow characteristics on the plate, as discussed by Hofhuis and Zuideweg [*Inst. Chem. Engrs. Symp. No. 56*, 2.2-1 (1979)]. Notations on Fig. 14-25 are from this source. The correlation in Fig. 14-25 is intended to cover the full range of flow parameters, with the low values of C_{sbf} to the right likely to result from downcomer flow restrictions rather than excessive entrainment. The curves may be expressed in equation form as [Lygeros and Magoulas, *Hydrocarbon Proc.* **65**(12), 43 (1986)]:

$$C_{sbf} = 0.0105 + 8.127 (10^{-4}) (TS^{0.755}) \exp[-1.463 F_{LG}^{0.842}] \quad (14-92)$$

where TS = plate spacing, mm.

Figure 14-25 or Eq. (14-92) may be used for sieve plates, valve plates, or bubble-cap plates. The value of the flooding vapor velocity must be considered as approximate, and prudent designs call for approaches to flooding of 75 to 85 percent. The value of the capacity parameter (ordinate term in Fig. 14-25) may be used to calculate the maximum allowable vapor velocity through the net area of the plate:

$$U_{nf} = C_{sbf,flood} \left(\frac{\sigma}{20} \right)^{0.2} \left(\frac{\rho_L - \rho_g}{\rho_g} \right)^{0.5} \quad (14-93)$$

where U_{nf} = gas velocity through net area at flood, m/s

C_{sbf} = capacity parameter, m/s

σ = liquid surface tension, mN/m (dyn/cm)

ρ_L = liquid density, kg/m³

ρ_g = gas density, kg/m³

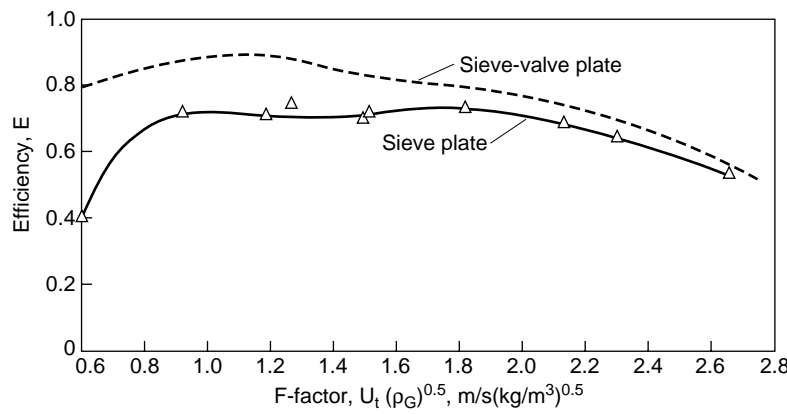


FIG. 14-24 Performance of two crossflow plates operating at 0.13 bar pressure and total reflux. Test mixture: ethylbenzene/styrene. Spacing between plates is 0.50 m, and outlet weir height is 38 mm. U_t = superficial vapor velocity, ρ_G = vapor density. [Billet, Conrad, and Grubb, I. Chem. E. Symp. Ser. No. 32, 5, 111 (1969).]

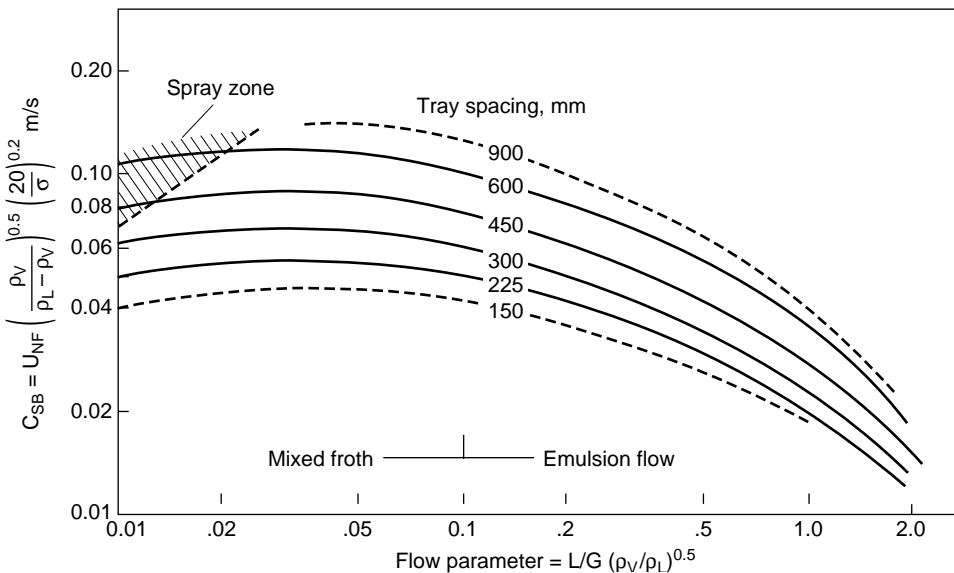


FIG. 14-25 Flooding correlation for columns with crossflow plates (sieve, valve, bubble-cap). [Fair, Pet/Chem Eng 33(10), 45 (September 1961).]

Figure 14-25 gives flooding-gas velocities to ± 10 percent subject to the following restrictions:

1. System is low or non-foaming
2. Weir height is less than 15 percent of plate spacing
3. Sieve-plate perforations are 13 mm ($\frac{1}{2}$ in) or less in diameter
4. Ratio of slot (bubble cap), perforation (sieve), or full valve opening (valve plate) area A_h to active area A_a is 0.1 or greater. Otherwise the value of U_{nf} obtained from Fig. 14-25 should be corrected:

A_h/A_a	$U_{nf}/U_{nf, \text{Fig. 14-25}}$
0.10	1.00
0.08	0.90
0.06	0.80

where A_h = total slot, perforated, or open-valve area on plate.

For counterflow plates, the curves of Fig. 14-25 may be used for open areas of 20 percent or greater. Plates with 15 percent open areas have about 85 percent of the curve values, and open areas of less than 15 percent are not recommended. For counterflow-plate columns of the segmental-baffle type, 50 percent cut, allowable C_{sbf} values are about 15 percent greater than those shown in Fig. 14-25, when vertical spacings of the baffles are equal to the tray spacings shown.

An alternate method for predicting the flood point of sieve and valve plates has been reported by Kister and Haas [Chem. Eng. Progr., 86(9), 63 (1990)] and is said to reproduce a large data base of measured flood points to within ± 30 percent. It applies to entrainment flooding only (values of F_{LG} less than about 0.5). The general predictive equation is

$$C_{sbf} = 0.0277(d_h^2\sigma/\rho_L)^{0.125}(\rho_C/\rho_L)^{0.1}(TS/h_{cl})^{0.5} \quad (14-94)$$

where d_h = hole diameter, mm

σ = surface tension, mN/m (dyn/cm)
 ρ_C, ρ_L = vapor and liquid densities, kg/m³

TS = plate spacing, mm

h_{cl} = clear liquid height at the froth-to-spray transition, mm; obtained from:

$$h_{cl} = h_{cl,H_2O} (996/\rho_t)^{0.5(1-n)} \quad (14-95)$$

$$h_{cl,H_2O} = \frac{0.497 A_f^{0.791} d_h^{0.833}}{1 + 0.013 L^{-0.59} A_f^{1.79}} \quad (14-96)$$

$$n = 0.00091 d_h/A_f \quad (14-97)$$

In Eq. 14-96, $L = m^3$ liquid downflow/(hr-m weir length) and A_f = fractional hole area based on active ("bubbling") area; for instance, $A_f = A_h/A_a$.

For valve trays, adaptations of Eqs. (14-94) to (14-97) are required:

$$d_h = \frac{4 \times (\text{area of opening of one fully open valve})}{\text{wetted perimeter of opening of one fully open valve}} \quad (14-98)$$

$$A_f = \frac{\text{no. valves} \times (\text{area of opening of one fully open valve})}{\text{active (bubbling) area}} \quad (14-99)$$

Example 9: Loading/Flooding of a Distillation Plate An available sieve plate column of 2.5-m diameter is being considered for an ethylbenzene/styrene separation. An evaluation of loading at the top plate will be made. Key dimensions of the single-crossflow plate are:

Column cross section, m^2	4.91
Downcomer area, m^2	0.25
Net area, m^2	4.66
Active area, m^2	4.41
Hole area, m^2	0.617
Hole diameter, mm	4.76
Weir length, m	1.50
Weir height, mm	38
Plate spacing, mm	500

Conditions and properties at the top plate are:

Temperature, °C	78
Pressure, torr	100
Vapor flow, kg/h	25,500
Vapor density, kg/m³	0.481
Liquid flow, kg/h	22,000
Liquid density, kg/m³	841
Surface tension, mN/m	25

The dimensions and flow rates are scaled to represent the conditions shown in Fig. 14-24.

Solution. The flow parameter $F_{LG} = 0.021$ (Eq. 14-73). From Fig. 14-25, $C_{sbf} = 0.095$ m/s. Then,

$$U_{nf} = \frac{0.095}{(0.481/841)^{0.5} (20/25)^{0.2}} = 4.15 \text{ m/s}$$

This gives a superficial F -factor at flood = $U_f \rho_G^{0.5} = 4.15 (4.66/4.91)(.481)^{0.5} = 2.73 \text{ m/s}(\text{kg}/\text{m}^3)^{0.5}$, or about 90 percent of a value extrapolated from Fig. 14-24.

The alternate method of Kister and Haas may be applied to the same problem:

$$L = \frac{22,000}{841 \times 1.50} = 17.44 \text{ m}^3/\text{hr-m weir}$$

$$A_f = \frac{0.617}{4.41} = 0.14$$

By Eq. 14-96, $h_{cl,H_2O} = 7.98 \text{ mm}$

$$\text{Eq. 14-97: } n = 0.0309$$

$$\text{Eq. 14-95: } h_{cl} = 8.66 \text{ mm}$$

Finally, by Eq. 14-94,

$$C_{sbf} = 0.0277 [(4.76)(25/841)]^{0.125} \times (0.481/841)^{0.1} (500/8.66)^{0.5} \\ = 0.0947 \text{ m/s}$$

about the same as the answer obtained from Fig. 14-25.

For the design condition, F -factor is $2.08 \text{ m/s}(\text{kg}/\text{m}^3)^{0.5}$, or about 76 percent of flood. The proposed column is entirely adequate for the service required.

Entrainment Entrainment in a plate column is that liquid which is carried with the vapor from a plate to the plate above. It is detrimental in that the effective plate efficiency is lowered because liquid from a plate of lower volatility is carried to a plate of higher volatility, thereby diluting distillation or absorption effects. Entrainment is also detrimental when nonvolatile impurities are carried upward to contaminate the overhead product from the column.

Many experimental studies of entrainment have been made, but few of them have been made under actual distillation conditions. The studies are often questionable because they are limited to the air-water system, and they do not use a realistic method for collecting and measuring the amount of entrainment. It is clear that the dominant variable affecting entrainment is gas velocity through the two-phase zone on the plate. Mechanisms of entrainment generation are discussed in the subsection "Liquid-in-Gas Dispersions."

For distillations, it is often of more interest to ascertain the effect of entrainment on efficiency than to predict the quantitative amount of liquid entrained. For this purpose, the correlation shown in Fig. 14-26 is useful. The parametric curves in the figure represent approach to the entrainment flood point as measured or as predicted by Fig. 14-25 or some other flood correlation. The abscissa values are those of the flow parameter discussed earlier. The ordinate values ψ are fractions of gross liquid downflow, defined as follows:

$$\psi = \frac{e}{L + e} \quad (14-100)$$

where e = absolute entrainment of liquid, moles/time

L = liquid downflow rate without entrainment, moles/time

Figure 14-26 also accepts the validity of the Colburn equation [Ind. Eng. Chem., 28, 526 (1936)] for the effect of entrainment on efficiency:

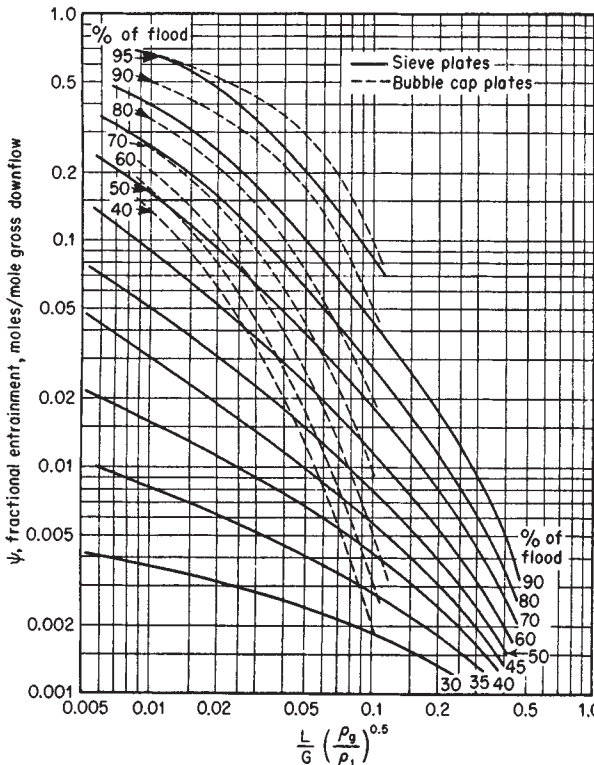


FIG. 14-26 Entrainment correlation. L/G = liquid-gass mass ratio; and ρ_l and ρ_g = liquid and gas densities. [Fair, Pet./Chem. Eng., 33(10), 45 (September 1961).]

$$\frac{E_a}{E_{mc}} = \frac{1}{1 + E_{mc} [\psi/(1 - \psi)]} \quad (14-101)$$

where E_{mc} = Murphree vapor efficiency [see Eq. (14-28)]

E_a = Murphree vapor efficiency, corrected for recycle of liquid entrainment

The Colburn equation is based on complete mixing on the plate. For incomplete mixing, e.g., liquid approaching plug flow on the plate, Rahman and Lockett [*I. Chem. E. Symp. Ser. No. 61*, 111 (1981)] and Lockett et al. [*Chem. Eng. Sci.*, **38**, 661 (1983)] have provided corrections for Eq. 14-44. Figure 14-26 and Eq. 14-94 may be used to evaluate the effects of entrainment on efficiency.

Example 10: Entrainment Effect on Plate Efficiency For the data shown in Fig. 14-24, estimate the efficiency of the sieve plate at a superficial F -factor of $2.6 \text{ m/s}(\text{kg/m}^3)$.

The data show a midrange dry efficiency of 0.7 (70 percent). They indicate a flood F -factor value of about 3.0. Thus, the approach to flood is $2.6/3.0 = 0.87$ (87 percent). The data were taken at total reflux, and thus $F_{LG} = (0.481/841)0.5 = 0.024$ (densities taken from Example 9). From Fig. 14-26, $\psi = 0.19$, and from Eq. (14-76):

$$\frac{E_a}{E_{mc}} = \frac{1}{1 + 0.70[0.19/(1 - 0.19)]} = 0.87$$

Thus, the wet efficiency $E_a = 0.87(0.70) = 0.61$ (61 percent). Figure 14-24 shows that for $F = 2.6$, the measured efficiency is 0.55 (55 percent).

Weeping Liquid flow through sieve-plate perforations occurs when the gas pressure drop through the perforations is not sufficient to create bubble surface and support the static head of froth above the perforations. Weeping can be deleterious in that liquid tends to short-circuit the primary contacting zones. On the other hand, some mass transfer to and from the weeping liquid occurs. Usual practice is to design so that deleterious weeping does not occur, based on a correlation such as that shown in Fig. 14-27.

In Fig. 14-27, h_d = head loss to gas flow through perforations, mm liquid [see Eq. (14-107)], and h_e = head loss due to bubble formation, mm liquid. The latter loss is based on the energy required for bubble formation:

$$h_b = \frac{4\sigma}{d_h} \quad (14-102)$$

with a convenient dimensional form for use in Fig. 14-27 being:

$$h_\sigma = 409 \left(\frac{\sigma}{\rho_L d_h} \right) \quad (14-103)$$

where σ = surface tension, mN/m

ρ_L = liquid density, kg/m^3

d_h = diameter of a perforation, mm

h_e = head loss due to bubble formation, mm liquid

If design shows a condition *above* the appropriate curve of Fig. 14-27, weeping will not be deleterious to plate performance as measured by a drop in plate efficiency (as in Fig. 14-24 for the sieve plate).

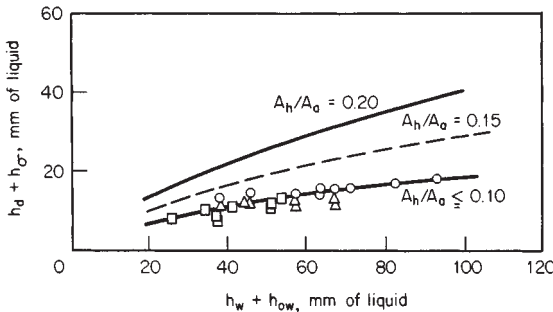


FIG. 14-27 Weeping, sieve plates. To convert millimeters to inches, multiply by 0.0394. (*Smith, Design of Equilibrium Stage Processes, McGraw-Hill, New York, 1963.*)

Downflow Flooding Columns can flood because of their inability to handle large quantities of liquid. For crossbow plates this limit on liquid rate is evidenced by downcomer backup to the plate above. To avoid downflow flooding one must size the column downcomers such that excessive backup does not occur.

Downcomer backup is calculated from the pressure-balance equation

$$h_{dc} = h_t + h_w + h_{ow} + h_{da} + h_{hg} \quad (14-104)$$

where h_{dc} = height in downcomer, mm liquid

h_t = total pressure drop across the plate, mm liquid

h_w = height of weir at plate outlet, mm liquid

h_{ow} = height of crest over weir, mm liquid

h_{da} = head loss due to liquid flow under downcomer apron, mm liquid

h_{hg} = liquid gradient across plate, mm liquid

The heights of head losses in Eq. (14-104) should be in consistent units, e.g., millimeters or inches of liquid under operating conditions on the plate.

As noted, h_{dc} is calculated in terms of equivalent clear liquid. Actually, the liquid in the downcomer may be aerated and actual backup is

$$h'_{dc} = \frac{h_{dc}}{\phi_{dc}} \quad (14-105)$$

where ϕ_{dc} is an average relative froth density (ratio of froth density to liquid density) in the downcomer. Design must not permit h'_{dc} to exceed the value of plate spacing; otherwise, flooding can be precipitated. In fact, plate spacing may be determined by some safe approach to the calculated value of h'_{dc} .

The value of ϕ_{dc} depends upon the tendency for gas and liquid to disengage (froth to collapse) in the downcomer. For cases favoring rapid bubble rise (low gas density, low liquid viscosity, low system foamability) collapse is rapid, and clear liquid fills the bottom of the downcomer (Fig. 14-22). For such cases, it is usual practice to employ a value of $\phi_{dc} = 0.5$. For cases favoring slow bubble rise (high gas density, high liquid viscosity, high system foamability), values of $\phi_{dc} = 0.2$ to 0.3 should be used. As the critical point is approached in high-pressure distillations and absorptions, special precautions with downcomer sizing are mandatory, and sloping of the downcomer apron may be used to provide additional disengaging surface (but at the expense of cross-sectional area for perforations). Even so, some gas can be expected to recycle under the downcomer apron.

Plate Layouts Cross-flow plates, whether bubble-cap, sieve, or valve, are similar in layout (Fig. 14-28). Possible zones on each plate are:

Active vapor-dispersion

Peripheral stiffening and support

Disengaging

Distributing

Downcomer

The downcomer zones generally occupy 10 to 30 percent of the total cross section. For segmental downcomers, weir length ranges from 60 to 80 percent of the column diameter, so that the downcomer zone on each end of the plate occupies from 5 to 15 percent of the total cross section.

The fraction of plate area occupied by disengaging and distributing zones ranges from 5 to 20 percent of the cross section. For most sieve-plate designs, these zones are eliminated completely.

The peripheral stiffening zone (tray ring) is generally 25 to 50 mm (1 to 2 in) wide and occupies 2 to 5 percent of the cross section, the fraction decreasing with increase in plate diameter. Periphery waste (Fig. 14-28) occurs primarily with bubble-cap trays and results from the inability to fit the cap layout to the circular form of the plate. Valves and perforations can be located close to the wall and little dead area results. Typical values of the fraction of the total cross-sectional area available for vapor dispersion and contact with the liquid for cross-flow plates with a chord weir equal to 75 percent of the column diameter are given in Table 14-6.

The plate thickness of bubble-cap and sieve plates is generally established by mechanical design factors and has little effect on pressure drop. For a sieve plate, however, the plate is an integral component of the vapor-dispersion system, and its thickness is important.

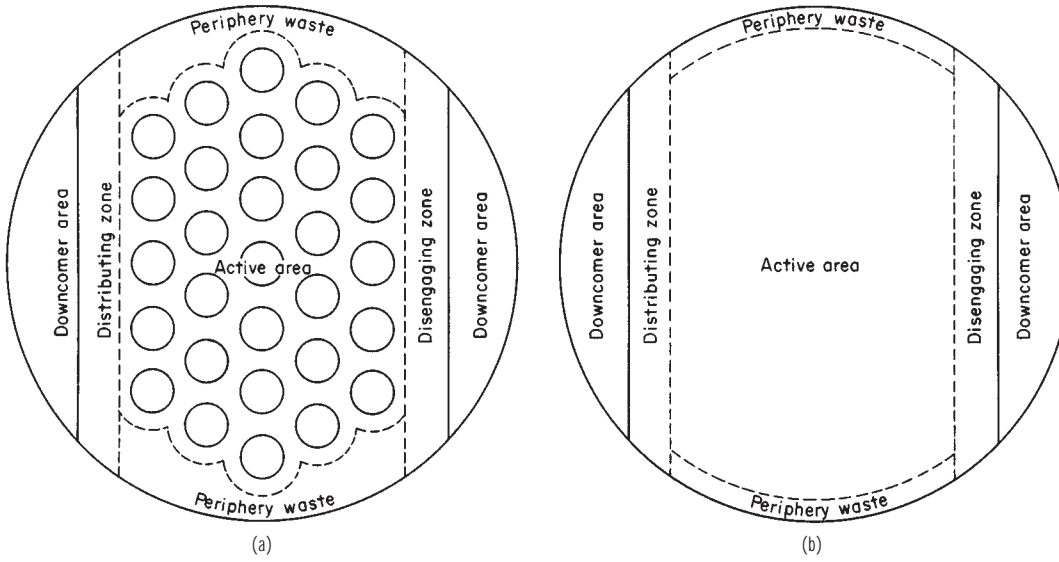


FIG. 14-28 Zone distribution. (a) Bubble-cap plate. (b) Sieve or valve plate.

For sieve plates, thickness is usually in the 10-to-14 U.S. standard gauge range of 3.58 to 1.98 mm, or 0.141 to 0.078 in. Hardness of metal, size of die, and limits on hole size (for process reasons) lead to the following thickness criterion:

$$0.4 < \frac{\text{plate thickness}}{\text{hole diameter}} < 0.7$$

Bubble caps and valves are generally arranged on an equilateral-triangle layout. Center-to-center spacing should be great enough to minimize impact of vapor streams from adjacent units. Weights of valves on the same plate can be varied to control available flow area at different vapor loadings. Hole sizes for sieve plates range from 1 mm to 25 mm (0.04 to 1 in) diameter, with sizes in the 4- to 12-mm (0.16- to 0.50-in) range being popular. Small holes have less entrainment but may present fouling problems. The smaller hole sizes may lead to punching problems, however, although 1-2 mm holes can be punched from aluminum plate materials. The spacing of the holes, usually on an equilateral-triangle basis, ranges from 2½ to four diameters. Closer

spacings lead to excessive weeping, and greater spacings lead to excessive pressure drop and to entrainment because of high hole velocities.

Countercurrent plates are of perforated or slotted construction and require no downcomers. The vapor and the liquid use the same openings, alternating on an intermittent basis. Layout of such plates is extremely simple. Types of such plates used commercially are

Perforated (dual-flow)

Slotted (Turbogrid)

Perforated-corrugated (Ripple)

The open area for these plates ranges from 15 to 30 percent of the total cross section compared with 5 to 15 percent for sieve plates and 8 to 15 percent for bubble-cap plates. Hole sizes range from 6 to 25 mm (¼ to 1 in), and slot widths from 6 to 12 mm (¼ to ½ in). The Turbogrid and Ripple plates are proprietary devices.

Pressure Drop Methods for estimating fluid-dynamic behavior of crossflow plates are analogous, whether the plates be bubble-cap, sieve, or valve. The total pressure drop across a plate is defined by the general equation (see Fig. 14-29)

$$h_t = h_d + h'_L \quad (14-106)$$

where h_t = total pressure drop, mm liquid

h_d = pressure drop across the dispersion unit (dry hole for sieve plates; dry valve for valve plates; dry cap, riser, and slot drop for bubble caps, mm liquid)

h'_L = pressure drop through aerated mass over and around the disperser, mm liquid

It is convenient and consistent to relate all of these pressure-drop terms to height of equivalent clear liquid (de aerated basis) on the plate, in either millimeters or inches of liquid.

Pressure drop across the disperser is calculated by variations of the standard orifice equation:

$$h_d = K_1 + K_2 \left(\frac{\rho_G}{\rho_L} \right) U_h^2 \quad (14-107)$$

where U_h = linear gas velocity through risers (bubble caps) or perforations (sieve plate), m/s.

For bubble caps, K_1 is the drop through the slots and K_2 is the drop through the riser, reversal, and annular areas. Equations for evaluating these terms for various bubble-cap designs are given by Bolles (in chap. 14 of Smith, *Equilibrium Stage Processes*, McGraw-Hill, New York, 1963), or may be found in previous editions of this handbook.

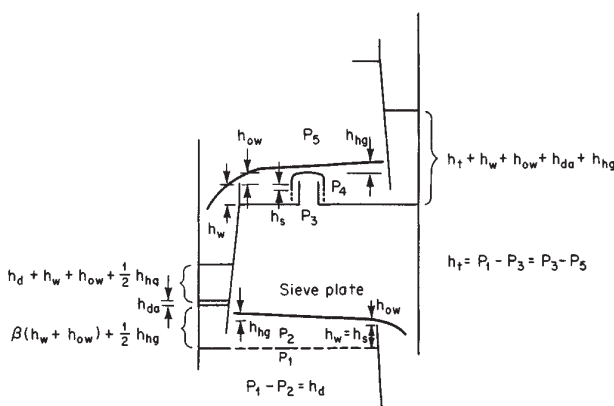
FIG. 14-29 Pressure-drop contributions for cross-flow plates. h_d = pressure drop through cap or sieve, equivalent height of plate liquid; h_w = height of weir; h_{ow} = weir crest; h_s = static liquid seal; h_{hg} = hydraulic gradient; and h_{da} = loss under downcomer.

TABLE 14-6 Representative Plate Efficiencies

Disperser	System	Column diameter, ft	Tray spacing, in	Pressure, psia	Static submergence, in	Efficiency, %		Remarks	Ref.
						E_{mv}^*	$E_{oc}^†$		
Bubble-cap	Ethanol-water	1.31	10.6	14.7	1.18	83–87			1
		1.31	16.3	14.7	1.18	84–97			2
	Methanol-water	2.5	14	14.7	1.2	80–85			3
		3.2	15.7	14.7	1.0	90–95			4
	Ethyl benzene-styrene	2.6	19.7	1.9	0.2	55–68			5
		4.0	24	14.7	0.25	65–90			
	Cyclohexane- <i>n</i> -heptane				24	65–90			
					50	65–90			
	Cyclohexane- <i>n</i> -heptane	4.0	24	5	0.6	65–85		Tunnel caps	6
				24		75–100			
Sieve	Benzene-toluene	1.5	15.7	14.7	1.5	70–80			7
	Toluene-isoctane	5.0	24	14.7	0.4		60–80		8
	Methanol-water	3.2	15.7	14.7		70–90		10.8% open	3
	Ethanol-water	2.5	14	14.7	1.0	75–85		10.4%	2
	Methanol-water	3.2	15.7	14.7	1.57	90–100		4.8% open	3
	Ethyl benzene-styrene	2.6	19.7	1.9	0.75	70		12.3% open	9
	Benzene-toluene	1.5	15.7	14.7	3.0	60–75		8% open	14
	Methyl alcohol- <i>n</i> -propyl alcohol- <i>sec</i> -butyl alcohol	6.0	18	18	1.38		64		10
	Mixed xylenes + C ₈ -C ₁₀ paraffins and naphthenes	13.0	21	25	1.25		86		5
	Cyclohexane- <i>n</i> -heptane	4.0	24	5	2.0	60–70		14% open	13
Valve				24		80		14% open	13
				4.0	2.0	70–80		8% open	12
	Isobutane- <i>n</i> -butane	4.0	24	165	2.0	110		14% open	13
		4.0	24	165	2.0	120		8% open	12
		4.0	24	300	2.0	110		8% open	12
		4.0	24	400	2.0	100		8% open	12
	n-heptane-toluene	1.5	15.7	14.7	3.0	60–75		8% open	14
	methanol-water	2.0	13.6	14.7	2.0	68–72%		10% open	15
	isopropanol-water	2.0	13.6	14.7	2.0	59–63%			15
	toluene-methylcyclohexane	2.0	13.6	14.7	2.0	70–82%			15

References

- Kirschbaum, Z. Ver. Dtsch. Ing. Beih. Verfahrenstechn., (5), 131 (1938); (3), 69 (1940).
- Kirschbaum, *Distillier-Rektifiziertechnik*, 4th ed., Springer-Verlag, Berlin and Heidelberg, 1969.
- Kastanek and Standart, *Sep. Sci.*, **2**, 439 (1967).
- Billet and Raichle, *Chem. Ing. Tech.*, **38**, 825 (1966); **40**, 377 (1968).
- AICHE Research Committee, *Tray Efficiency in Distillation Columns*, final report, University of Delaware, Newark, 1958.
- Raichle and Billet, *Chem. Ing. Tech.*, **35**, 831 (1963).
- Zuiderweg, Verburg, and Gilissen, *Proc. Intn. Symp.*, Brighton, England, 1960.
- Manning, Marple, and Hinds, *Ind. Eng. Chem.*, **49**, 2051 (1957).
- Billet, *Proc. Intn. Symp.*, Brighton, England, 1970.
- Mayfield, Church, Green, Lee, and Rasmussen, *Ind. Eng. Chem.*, **44**, 2238 (1952).
- Fractionation Research, Inc., "Report of Tests of Nutter Type B Float Valve Tray," July 2, 1964 from Nutter Engineering Co.
- Sakata and Yanagi, *Inst. Chem. Eng. Symp. Ser.*, no. 56, 3.2/21 (1979).
- Yanagi and Sakata, *Ind. Eng. Chem. Process Des. Dev.*, **21**, 712 (1982).
- Zuiderweg and Van der Meer, *Chem. Tech. (Leipzig)*, **24**, 10 (1972).
- Korchinsky, *Trans. I. Chem. E.*, **72**, Part A, 472 (1994).

*See Eq. (14-130).

†See Eq. (14-127).

NOTE: To convert feet to meters, multiply by 0.3048; to convert inches to centimeters, multiply by 2.54; and to convert psia to kilopascals, multiply by 6.895.

For sieve plates, $K_1 = 0$ and $K_2 = 50.8/C_v^2$. Values of C_v are taken from Fig. 14-30. Values from Fig. 14-30 may be calculated from

$$C_v = 0.74 (A_h/A_a) + \exp[0.29(t_h/d_h) - 0.56] \quad (14-108)$$

For valve plates, values of K_1 and K_2 depend on whether the valves are fully open. They also depend on the shape and weight of the valves. Vendors of valve plates make K_1 and K_2 data (or their equivalent) readily available. An analysis of valve plate pressure drop has been reported by Bolles [*Chem. Eng. Progr.* **72**(9), 43 (1976)], and typical dry head loss data, shown in Fig. 14-31, are taken from that work.

Pressure drop through the aerated liquid [h'_L , in Eq. (14-106)] is calculated by

$$h'_L = \beta h_{ds} \quad (14-109)$$

where β = aeration factor, dimensionless
 h_{ds} = calculated height of clear liquid over the dispersers, mm
(dynamic seal)

The aeration factor β has been determined for bubble-cap and sieve plates, and a representative correlation of its values is shown in Fig. 14-32. Values of β in the figure may be calculated from

$$\beta = 0.0825 \ln \left(\frac{q}{L_w} \right) - 0.269 \ln F_{ch} + 1.679 \quad (14-110)$$

where L_w = weir length, m
 F_{ch} = F-factor for flow through holes, $F_{ch} = U_h \rho_C^{0.5}$, m/s (kg/m^3)^{0.5}

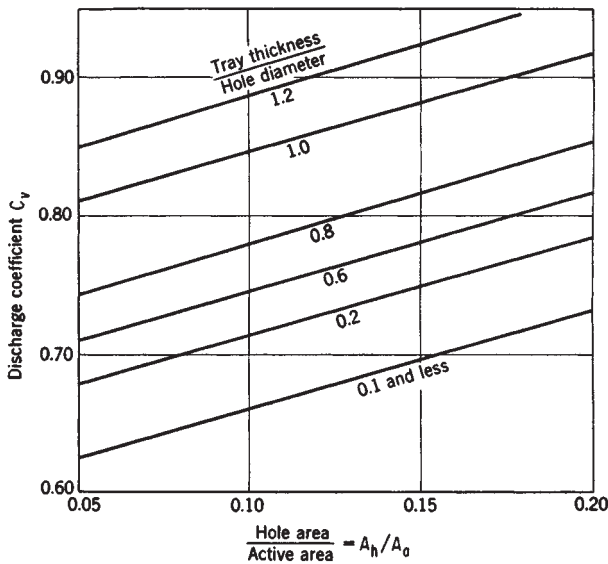


FIG. 14-30 Discharge coefficients for gas flow, sieve plates. [Liebson, Kelley, and Bullington, Pet. Refiner, 36(3), 288 (1957).]

For sieve and valve plates,

$$h_{ds} = h_w + h_{ow} + 0.5h_{hg} \quad (14-111)$$

where h_w = weir height, mm

h_{ow} = height of crest over weir equivalent clear liquid, mm

h_{hg} = hydraulic gradient across plate height of equivalent clear liquid, mm

The value of weir height crest h_{ow} may be calculated from the Francis weir equation and its modifications for various weir types. For a segmental weir and for height in millimeters of clear liquid,

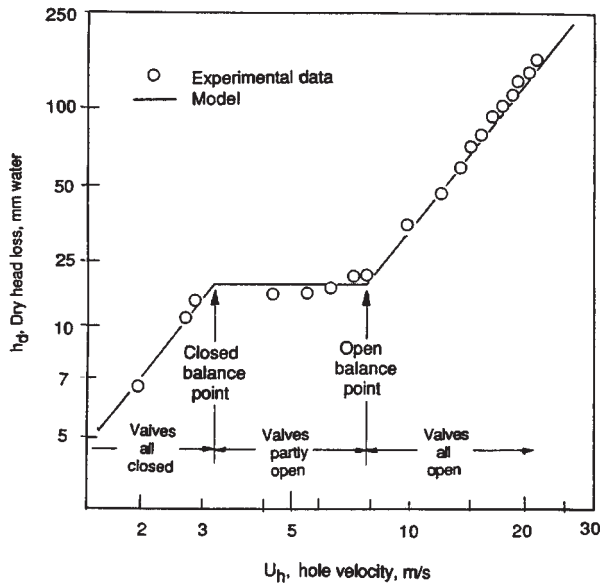


FIG. 14-31 Pressure drop for a valve plate, measured versus model prediction of Bolles [Chem. Eng. Progr. 72(9), 43 (1976)]. Reproduced with permission of the American Institute of Chemical Engineers. Copyright © 1976 AIChE. All rights reserved.

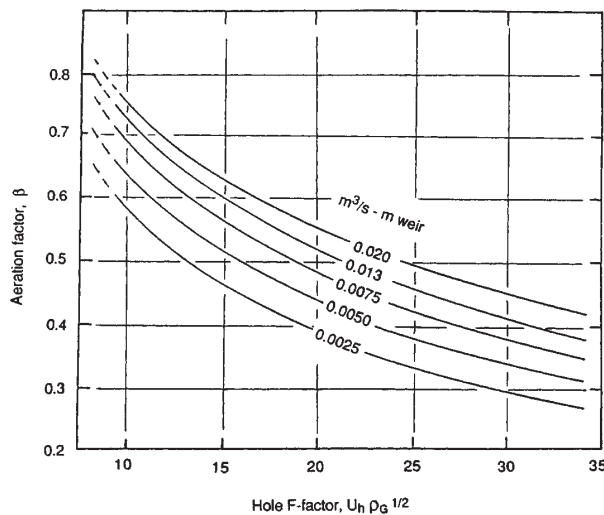


FIG. 14-32 Aeration factor for pressure drop calculation, sieve plates. [Bolles and Fair, Encyclopedia of Chemical Processing and Design, vols. 16, 86. J. M. McKetta (ed.), Marcel Dekker, New York, 1982.]

$$h_{ow} = 664 \left(\frac{q}{L_w} \right)^{2/3} \quad (14-112)$$

where q = liquid flow, m^3/s

L_w = weir length, m

For serrated weirs,

$$h_{ow} = 851 \left(\frac{q'}{\tan \theta/2} \right)^{0.4} \quad (14-113)$$

where q' = liquid flow, m^3/s per serration

θ = angle of serration, degrees

For circular weirs,

$$h_{ow} = 44,300 \left(\frac{q}{d_w} \right)^{0.704} \quad (14-114)$$

where q = liquid flow, m^3/s

d_w = weir diameter, mm

As noted, the weir crest h_{ow} is calculated on an equivalent clear-liquid basis. A more realistic approach is to recognize that in general a froth or spray flows over the outlet weir (settling can occur upstream of the weir if a large "calming zone" with no dispersers is used). Bennett et al. [AIChE J., 29, 434 (1983)] allowed for froth overflow in a comprehensive study of pressure drop across sieve plates; their correlation for residual pressure drop h'_L in Eq. (14-87) is represented by Eqs. (14-115) through (14-120):

$$h'_L = h_L + h'_\sigma \quad (14-115)$$

where h'_L = pressure drop through the aerated liquid ($= h_L - h'_\sigma$), mm

h_L = effective clear-liquid height (liquid holdup), mm

h'_σ = pressure drop for surface generation, mm

$$= \left(\frac{472\sigma}{gp_L} \right) \left(\frac{g(\rho_L - \rho_G)}{d_h \sigma} \right)^{1/3} \quad (14-116)$$

with σ = surface tension, mN/m .

First, an effective froth density ϕ_e (dimensionless) is calculated:

$$\phi_e = \exp(-12.55K_s^{0.91}) \quad (14-117)$$

where $\phi_e = h_L/h_f$

h_f = froth height, mm

$K_s = U_a \cdot [\rho_g / (\rho_L - \rho_G)]^{0.5} = F_{ca} / (\Delta \rho)^{0.5}$

U_a = vapor velocity through the active area, m/s
 F_{ca} = F -factor based on active area, $\text{m/s}(\text{kg/m}^3)^{0.5}$

Then the liquid holdup is calculated:

$$h_L = \phi_e [h_w + 15,330C(q/\phi_e)^{2/3}] \quad (14-119)$$

$$\text{where } C = 0.0327 + 0.0286 \exp[-0.1378h_w]. \quad (14-120)$$

In these equations, the h terms and d_h (perforation diameter) are in mm, densities are in kg/m^3 , surface tension is in mN/m , and flow rate q is in m^3/s . The gravitational constant g is 9.81 m/s^2 . For total pressure drop across the plate, Eq. (14-96) is used in conjunction with Eq. (14-107) and Fig. 14-30.

For a base of 302 data points covering a wide range of systems and conditions, Eqs. (14-115) through (14-120) gave an average error of ± 0.35 percent. For a similar data base, Eqs. (14-106) and (14-109) together with Fig. 14-32 gave an average error of less than 5 percent. Although more difficult to use, the method of Bennett et al. is recommended when determination of pressure drop is of critical importance.

Example 11: Pressure Drop, Sieve Plate For the conditions of Example 10, estimate the pressure drop for flow across one plate. The thickness of the plate metal is 2 mm and the hole diameter is 4.8 mm. The superficial F -factor is $2.08 \text{ m/s}(\text{kg/m}^3)^{1/2}$.

Solution. Method A: Eqs. (14-106, 14-109, 14-110), where $h_t = h_d + \beta(h_w + h_{ow})$. For $F_{ca} = 2.08$, $F_{ch} = 2.32$ and $F_{th} = 16.55$. From Example 9, $L_w = 1.50 \text{ m}$ and $h_w = 38 \text{ mm}$. For a liquid rate of $22,000 \text{ kg/hr}$, $q = 7.27(10^{-3}) \text{ m}^3/\text{s}$, and $q/L_w = 4.8(10^{-3})$. By Eq. (14-110) or Fig. 14-32, $\beta = 0.48$. From Eq. (14-108) or Fig. 14-30, $C_e = 0.78$. Then, by Eq. (14-107), $h_d = 32.6 \text{ mm}$ liquid. Using Eq. (14-112), $h_{ow} = 18.9 \text{ mm}$. Finally, $h_t = h_d + \beta(h_w + h_{ow}) = 32.6 + 0.48(38 + 18.9) = 60.0 \text{ mm}$ liquid.

Method B: Bennett et al. $h_t = h_d + h_L + h'_o$; h_d = same as for Method A.

Eq. (14-116): $h'_o = [(472 \times 25)/(9.81 \times 841)] [(9.81 \times 841)/(5 \times 25)]^{1/3} = 5.47 \text{ mm}$; Eq. (14-118): $K_s = F_{ca}/\Delta\rho^{0.5} = 2.32/(841 - 0.481)^{0.5} = 2.32/(840.5)^{0.5} = 0.080 \text{ m/s}$; Eq. (14-117): $\phi_e = \exp[-12.55(0.080)^{0.91}] = 0.284$ (effective froth density); Eq. (14-120): $C = 0.0327 + 0.0286 \exp[-0.1378(38)] = 0.0329$; and Eq. (14-119): $h_L = 0.284[38 + 15,330(0.0329)(0.007270/0.284)]^{2/3} = 23.23 \text{ mm}$. Finally, $h_t = h_d + h_L + h'_o = 32.6 + 23.23 + 5.47 = 61.3 \text{ mm}$ liquid.

When straight or serrated segmental weirs are used in a column of circular cross section, a correction may be needed for the distorted pattern of flow at the ends of the weirs, depending on liquid flow rate. The correction factor F_w from Fig. 14-33 is used directly in Eq. (14-112) or Eq. (14-119). Even when circular downcomers are utilized, they are often fed by the overflow from a segmental weir. When the weir crest over a straight segmental weir is less than 6 mm ($\frac{1}{4}$ in.), it is desirable to use a serrated (notched) weir to provide good liquid distribution. Inasmuch as fabrication standards permit the tray to be 3 mm ($\frac{1}{8}$ in.) out of level, weir crests less than 6 mm ($\frac{1}{4}$ in.) can result in maldistribution of liquid flow.

Loss under Downcomer The head loss under the downcomer apron, as millimeters of liquid, may be estimated from

$$h_{da} = 165.2 \left(\frac{q}{A_{da}} \right)^2 \quad (14-121)$$

where q = volumetric flow of liquid, m^3/s and A_{da} = minimum area of flow under the downcomer apron, m^2 . Although the loss under the downcomer is small, the clearance is significant from the aspect of tray stability and liquid distribution. The seal between the top of the liquid on the plate and the bottom of the downcomer should range between 13 and 38 mm ($\frac{1}{2}$ and $1\frac{1}{2}$ in.).

Hydraulic Gradient Hydraulic gradient, the head of liquid necessary to overcome the frictional resistance to liquid (froth) passage across the plate, is important for plate stability inasmuch as it is the only liquid head that varies across the length of passage. If the gradient is excessive, the upstream portion of the plate may be rendered inoperative because of increased resistance to gas flow caused by increased liquid head (Fig. 14-34). In general the empirical criterion for stable operation is $h_d > 2.5h_{hg}$.

Sieve plates usually have negligible hydraulic gradient. Bubble-cap plates can have significant gradient because of the blockage by the caps. Valve plates presumably are intermediate, with hydraulic-gradient characteristics approaching those of sieve plates.

For bubble-cap plates, hydraulic-gradient must be given serious consideration. It is a function of cap size, shape, and density on the plate. Methods for analyzing bubble-cap gradient may be found in the chapter by Bolles (Smith, *Design of Equilibrium Stage Processes*, Chap. 14, McGraw-Hill, New York, 1963) or in previous edition of this handbook.

The hydraulic gradient on sieve plates should be checked in cases of long flow path of liquid. Hughmark and O'Connell (*Chem. Eng. Prog.*, **53**(3), 127 (1957)] presented a correlation for determining sieve-plate hydraulic gradient. Although the correlation does not explicitly indicate an effect of gas velocity, the effect is implicit in the choice of friction factor. The gradient is predicted by the relationship

$$h_{hg} = \frac{1000f U_f^2 L_f}{g R_h} \quad (14-122)$$

where f = friction factor correlated against a Reynolds modulus as in pipe flow

$$N_{Reh} = \frac{R_h U_f \rho_L}{\mu_L} \quad (14-123)$$

as shown in Fig. 14-34. In Eqs. (14-122) and (14-123), R_h is the hydraulic radius of the aerated mass, defined as follows:

$$R_h = \frac{\text{cross section}}{\text{wetted perimeter}} = \frac{h_f D_f}{2h_f + 1000D_f} \quad (14-124)$$

where D_f is the arithmetic average between tower diameter and weir

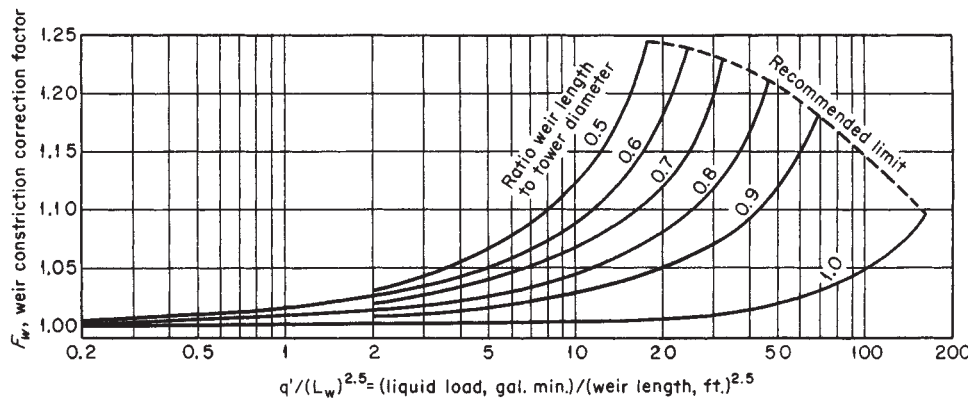


FIG. 14-33 Correction for effective weir length. To convert gallons per minute to cubic meters per second, multiply by 6.309×10^{-5} ; to convert feet to meters, multiply by 0.3048. [Bolles, Pet. Refiner, **25**, 613 (1946).]

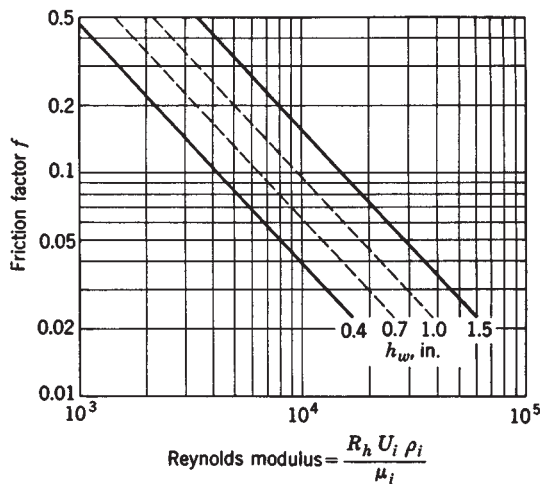


FIG. 14-34 Friction factor for froth crossflow, sieve plates. To convert inches to millimeters, multiply by 25.4. (Smith, Design of Equilibrium Stage Processes, McGraw-Hill, New York, 1963.)

length (average width of flow path), and h_f is froth height. The value of h_f is estimated from Eq. (14-117a). U_f is the velocity of the aerated mass, m/s, and is the same as for the clear liquid:

$$U_f = \frac{1000q}{h_f \phi e D_f} = \frac{1000q}{h_L D_f} \quad (14-125)$$

Other terms in Eqs. (14-122) through (14-125) are:

$$\begin{aligned} g &= \text{acceleration of gravity, m/s}^2 \\ L_f &= \text{length of flow path across plate, m} \\ q &= \text{liquid-flow rate, m}^3/\text{s} \\ \phi e &= \text{froth density on plate, dimensionless} \\ \mu_L &= \text{liquid viscosity, Pa·s or kg/(m·s)} \\ \rho_L &= \text{liquid density, kg/m}^3 \end{aligned}$$

Phase Inversion Normally the two-phase mixture on the plate is in the form of a bubbly, or aerated liquid. This liquid-continuous mixture is called a *froth*. Under high gas rates and low liquid rates, however, the regime can invert to a gas-continuous *spray* comprising a multitude of liquid droplets of varying diameter. Many studies of this froth-to-spray transition have been made, most of them with air and water. The results of one such study, useful for design purposes, are shown in Fig. 14-35. The spray is predicted to prevail above the appropriate curve. Reviews of phase inversion have been provided by Lockett [Distillation Tray Fundamentals, Cambridge Univ. Press, Cambridge, U.K., 1986] and Prado et al. [Chem. Eng. Progr., 83(3), 32 (1987)]. The latter combined experimental observations of inversion with evaluations of plate efficiency, and proposed the following relationship for determining the gas velocity through the active portion of the tray, at the inversion point:

$$U_a^* = C_1 \rho_G^{-0.50} \rho_L^{0.692} \sigma^{0.06} A_f^{0.25} \left(\frac{q}{L_w} \right)^{0.05} d_h^{-0.1} \quad (14-126)$$

where U_a^* = gas velocity through active area at inversion, m/s

ρ_G = gas density, kg/m³

ρ_L = liquid density, kg/m³

σ = surface tension, mN/m

A_f = hole/active area ratio

q/L_w = liquid flow, m³/s·m weir

d_h = hole diameter, mm

$C_1 = 0.0583$ for 25.4-mm overflow weirs

= 0.0568 for 50.4-mm overflow weirs

= 0.0635 for 101.6-mm overflow weirs

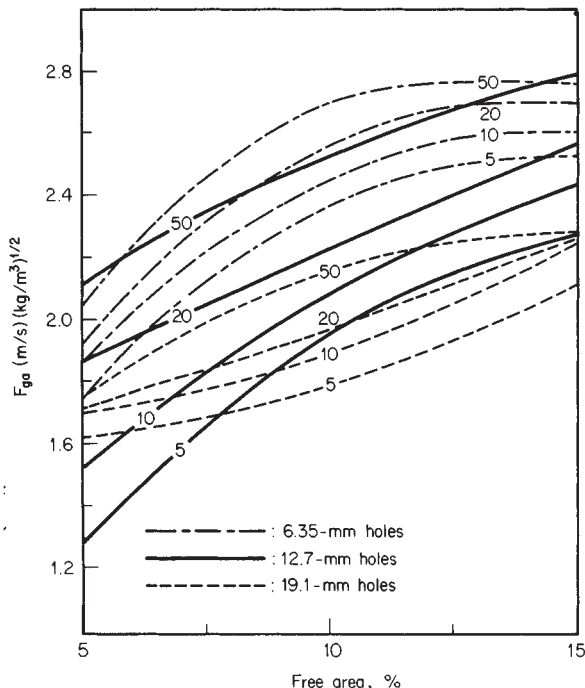


FIG. 14-35 Transition from froth to spray regime for holes of various diameters. Values on curves are liquid loadings, $\text{m}^3/(\text{h}\cdot\text{m} \text{weir length})$. To convert cubic meters per hour-meter to cubic feet per hour-foot, multiply by 10.764; to convert (meters per second) ($\text{kilograms per cubic meter})^{1/2}$ to (feet per second) ($\text{pounds per cubic foot})^{1/2}$, multiply by 0.8197; and to convert millimeters to inches, multiply by 0.0394. [Loon, Pinczewski, and Fell, Trans. Inst. Chem. Eng., 51, 374 (1973).]

Figure 14-35 also provides a means for estimating whether spray or froth might prevail on the tray. As can be seen, low values of the flow parameter F_{LG} , as for vacuum fractionators, can lead to the spray regime.

Plate Efficiency The efficiency of a plate for mass transfer depends upon three sets of design parameters:

1. The system—composition and properties
2. Flow conditions—rates of throughput
3. Geometry—plate type and dimensions

The designer has little control over the first set but can deal effectively with the other two. Ultimate concern is with *overall column efficiency*:

$$E_{oc} = N_t/N_a \quad (14-127)$$

or the ratio of *theoretical plates* to *actual plates* required to make the separation. In arriving at a value of E_{oc} for design, the designer may rely on plant test data or on judicious use of pilot-plant-efficiency measurements. If such direct information is not available, the designer must resort to predictive methods.

Methods for predicting plate efficiency are of three general types:

1. Empirical methods
2. Direct scale-up from laboratory measurements
3. Theoretical or semitheoretical mass-transfer methods

The first of these gives E_{oc} directly. The second gives a point efficiency [Eq. (18-30)]. The third involves the prediction of individual phase efficiencies.

Empirical Predictive Methods Two empirical correlations which have found wide use are the one of Drickamer and Bradford [Trans. Am. Inst. Chem. Eng., 39, 319 (1943)] and a modification of it by O'Connell [Trans. Am. Inst. Chem. Eng., 42, 741 (1946)]. The latter is shown in Fig. 14-36, the Drickamer-Brown data are included in the distillation plot.

A semitheoretical method which gives overall efficiency is that of

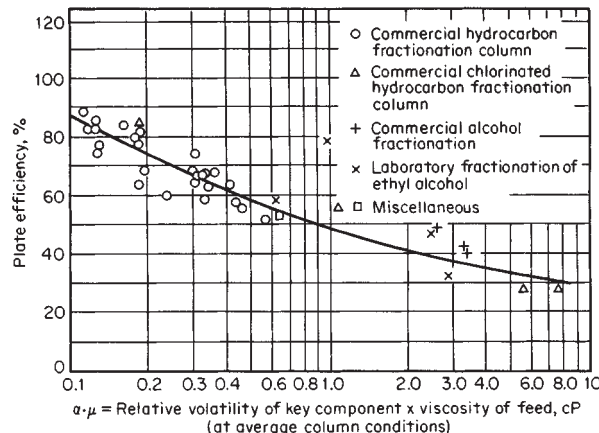


FIG. 14-36 O'Connell correlation for overall column efficiency E_{oc} for distillation. To convert centipoises to pascal-seconds, multiply by 10^{-3} . [O'Connell, Trans. Am. Inst. Chem. Eng., 42, 741 (1946).]

Bakowski [Br. Chem. Eng., 8, 384, 472 (1963); 14, 945 (1969)]. It is based on the assumption that the mass-transfer rate for a component moving to the vapor phase is proportional to the concentration of the component in the liquid and to its vapor pressure. Also, the interfacial area is assumed proportional to liquid depth, and surface renewal rate is assumed proportional to gas velocity. The resulting general equation for binary distillation is

$$E_{oc} = \frac{1}{1 + 3.7(10^4) \frac{KM}{h'p/T}} \quad (14-128)$$

where E_{oc} = overall column efficiency, fractional
 K = vapor-liquid equilibrium ratio, y°/x
 y° = gas-phase concentration at equilibrium, mole fraction
 x = liquid-phase concentration, mole fraction
 M = molecular weight
 h' = effective liquid depth, mm
 ρ_l = liquid density, kg/m³
 T = temperature, K

For sieve or valve plates, $h' = h_w$, outlet weir height. For bubble-cap plates, $h' =$ height of static seal. The original references present validations against laboratory and small-commercial-column data. Modifications of the efficiency equation for absorption-stripping are also included.

Direct Scale-Up of Laboratory Distillation Efficiency Measurements It has been found by Fair, Null, and Bolles [Ind. Eng. Chem. Process Des. Dev., 22, 53 (1983)] that efficiency measurements in 25- and 50-mm- (1- and 2-in-) diameter laboratory Oldershaw columns closely approach the point efficiencies [Eq. (14-129)] measured in large sieve-plate columns. A representative comparison of scales of operation is shown in Fig. 14-37. Note that in order to achieve agreement between efficiencies it is necessary to ensure that (1) the systems being distilled are the same, (2) comparison is made at the same relative approach to the flood point, (3) operation is at total reflux, and (4) a standard Oldershaw device (a small perforated-plate column with downcomers) is used in the laboratory experimentation. Fair et al. made careful comparisons for several systems, utilizing as large-scale information the published efficiency studies of Fractionation Research, Inc.

Theoretical Predictive Methods The approach to equilibrium on a plate may be defined as the ratio of the actual change in gas composition as it passes through the plate to the change that would have occurred if the gas had reached a state of equilibrium with the liquid. If a point on plate n is considered, this definition leads to the **point efficiency**:

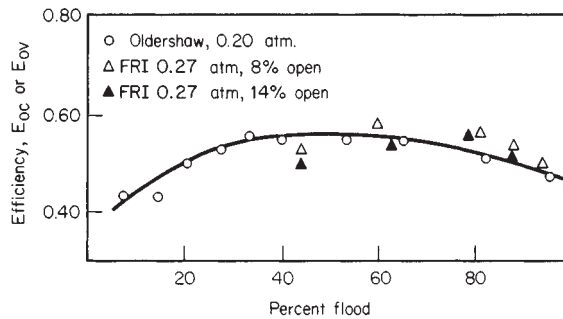


FIG. 14-37 Overall column efficiency of 25-mm Oldershaw column compared with point efficiency of 1.22-m-diameter-sieve-plate column of Fractionation Research, Inc. System = cyclohexane-*n*-heptane. [(Fair, Null, and Bolles, Ind. Eng. Chem. Process Des. Dev., 22, 53 (1982).]

$$E_{og} = \left(\frac{y_n - y_{n-1}}{y_n^\circ - y_{n-1}} \right)_{\text{point}} \quad (14-129)$$

where y_n° is the gas concentration in equilibrium with liquid concentration at the point. This efficiency cannot exceed 1.0 (100 percent). If there are liquid-concentration gradients on the plate (i.e., plate liquid is not completely mixed), then y° will vary and E_{og} may vary from point to point on the plate. It should be noted that an analogous efficiency definition could be expressed on the basis of liquid concentrations. It should be noted also that vaporization efficiency (Holland, *Fundamentals of Multicomponent Distillation*, McGraw-Hill, New York, 1981) could be used:

$$E_v = y_n/y_n^\circ \quad (14-130)$$

For the entire plate and for gas concentrations, the Murphree vapor efficiency is used:

$$E_{mv} = \left(\frac{y_n - y_{n-1}}{y_n^\circ - y_{n-1}} \right)_{\text{plate}} \quad (14-131)$$

where y_n° is gas concentration in equilibrium with the concentration of the liquid leaving the plate (flowing into the downcomer, for a cross-flow plate). Because of concentration gradients in the liquid, E_{mv} can exceed 100 percent.

The best-established theoretical method for predicting E_{oc} is that of the AIChE (*Bubble-Tray Design Manual*, American Institute of Chemical Engineers, New York, 1958). It is based on the sequential prediction of point efficiency, Murphree efficiency, and overall column efficiency:

$$E_{og} \rightarrow E_{mv} \rightarrow E_{oc}$$

with suitable correction of E_{mv} for entrainment. The AIChE model is the basis for the development which follows.

On the basis of the two-film model for mass transfer, and relating all efficiencies to gas-phase concentrations (for convenience only; a similar development can be made on the basis of liquid concentrations), point efficiency can be expressed in terms of transfer units:

$$E_{og} = 1 - e^{-N_{og}} \quad (14-132)$$

where N_{og} = overall transfer units calculated from Eq. (14-133).

$$N_{og} = \frac{1}{1/N_g + \lambda/N_\ell} \quad (14-133)$$

where N_g = gas-phase transfer units
 N_ℓ = liquid-phase transfer units
 $\lambda = mG_m/L_m$ (stripping factor)
 m = slope of equilibrium curve
 G_m = gas rate, mol/s
 L_m = liquid rate, mol/s

Transfer units are dimensionless and are defined further in Sec. 5. According to Eq. (14-133), the evaluation of point efficiencies reduces

14-36 GAS ABSORPTION AND GAS-LIQUID SYSTEM DESIGN

to the prediction of point values of N_g and N_ℓ plus the evaluation of m , G_m , and L_m for the particular conditions under investigation.

Gas-phase transfer units are obtained from Eq. (14-134)

$$N_g = k_g a \theta_g \quad (14-134)$$

where k_g = gas-phase mass-transfer coefficient, $(\text{kg}\cdot\text{mol})/(\text{s}\cdot\text{m}^2)$
($\text{kg}\cdot\text{mol}/\text{m}^3$) or m/s

a = effective interfacial area for mass transfer, m^2/m^3 froth
on plate

θ_g = residence time of gas in froth zone, s

The effect of increasing gas rate is to increase k_g and decrease θ_g , with the result that N_g tends to be constant over a range of gas rates.

For sieve trays, Chan and Fair [Ind. Eng. Chem. Proc. Des. Dev., 23, 814 (1983)] used a data bank of larger-scale distillation column efficiencies to deduce the following expression for the product $k_G a$:

$$k_G a = \frac{316 D_G^{1/2} (1030 f + 867 f^2)}{h_L^{1/2}} \quad (14-135)$$

where k_g = gas-phase mass-transfer coefficient, m/s

a = effective interfacial area, m^2/m^3 froth

D_G = gas-phase diffusion coefficient, m^2/s

f = approach to flood, fractional

h_L = liquid holdup on plate, mm

Note that the product of the mass-transfer coefficient and the interfacial area is a volumetric coefficient and obviates the need for a value of the interfacial area. While areas for mass transfer on plates have been measured, the experimental contacting equipment differed significantly from that used for commercial distillation or gas absorption, and the reported areas are considered unreliable for design purposes.

For evaluating the residence time θ_G of gas in the froth, the volume of the froth is taken as $A_a h_f$, where the height of the froth h_f is obtained by first determining effective froth density [Eq. (14-117)]. The dimensionless froth density is defined by

$$\phi = \frac{h_L}{h_f + \epsilon(\rho_G/\rho_L)} \quad (14-136)$$

When $\rho_L \gg \rho_G$, $\phi \sim h_L/h_f$ and $\epsilon \sim 1 - \phi$ (14-137)

then, residence time(s) may be estimated as

$$\theta_G = \frac{\epsilon h_f A_a}{10^3 Q} = \frac{1 - \phi h_L A_a}{10^3 \phi Q} \quad (14-138)$$

where Q = volumetric flow of vapor through the plate, m^3/s

h_f = froth height, $\text{mm} = h_L/\phi$

Liquid phase transfer units are obtained from

$$N_L = k_L a \theta_L \quad (14-139)$$

where k_L = liquid phase transfer coefficient, $(\text{kg}\cdot\text{mol})/(\text{s}\cdot\text{m}^2)$
($\text{kg}\cdot\text{mol}/\text{m}^3$) = m/s

a = effective interfacial area for mass transfer, m^2/m^3 froth
or spray on the plate

θ_L = residence time of liquid in the froth or spray zone, s

The mass-transfer coefficient of Eq. (14-139) is carried as a product with interfacial area (giving a volumetric mass transfer coefficient):

Sieve plates:

$$k_L a = (3.875 \times 10^8 D_L)^{0.5} (0.40 U_a \rho_G^{0.5} + 0.17) \quad (14-140)$$

Bubble-cap plates:

$$k_L a = (4.127 \times 10^8 D_L)^{0.5} (0.21 U_a \rho_G^{0.5} + 0.15) \quad (14-141)$$

where D_L = liquid-phase diffusion coefficient, m^2/s (see Sec. 3).

The residence time of liquid in the froth is

$$\theta_L = \frac{(1 - \epsilon) h_f A_a}{10^3 q} \quad (14-142)$$

where q = volumetric flow of liquid across the plate, m^3/s .

In summary, the point efficiency E_{og} is computed from Eq. (14-132) using N_{og} from Eq. (14-113), N_G from Eq. (14-134) and m based on the relative volatility of the system. For a binary mixture and a zone of constant relative volatility,

$$m = \frac{\alpha_{ij}}{[1 + (\alpha_{ij} - 1)x_i]^2} \quad (14-143)$$

where α_{ij} = relative volatility, component i (more volatile material) relative to component j , and x_i = mole fraction of i in the liquid.

The method for estimating point efficiency, outlined here, is not the only approach available for sieve plates, and more mechanistic methods are under development. For example, Prado and Fair [Ind. Eng. Chem. Res., 29, 1031 (1990)] have proposed a method whereby bubbling and jetting are taken into account; however the method has not been validated for nonaqueous systems. Chen and Chuang [Ind. Eng. Chem. Res., 32, 701 (1993)] have proposed a more mechanistic model for predicting point efficiency, but it needs evaluation against a commercial scale distillation data bank. One can expect more development in this area of plate efficiency prediction.

Example 12: Estimation of Plate Efficiency For the conditions of Examples 9 and 11, estimate the point efficiency of the tray. Additional property data:

Relative volatility, ethylbenzene/styrene	1.40
Stripping factor, λ	1.17
Gas diffusion coefficient, m^2/s	$2.09 (10^{-5})$
Liquid diffusion coefficient, m^2/s	$3.74 (10^{-9})$

Solution

Gas flow: $25.500/(3600 \times 0.481) = 14.73 \text{ m}^3/\text{s}$
Liquid flow: $22.000/(3600 \times 841) = 0.00727 \text{ m}^3/\text{s}$
Froth density (Example 11), $\phi = 0.284$
Liquid holdup (Example 11), $h_L = 23.23 \text{ mm liquid}$
Approach to flood (Example 9) = $0.74 = 74\%$

Gas residence time in froth [Eq. (14-138)] = $[(1 - 0.284)(23.23)(4.41)]/[10^3 (0.284)(14.73)] = 0.0175 \text{ s}$

Gas volumetric coefficient [Eq. (14-135)] = $k_G a = [316 (2.09 \times 10^{-5})^{0.5} [1030(0.74) - 867(0.74^2)]]/(23.23)^{0.5} = 86.1 \text{ s}^{-1}$

Number of gas-phase transfer units [Eq. (14-134)]: $N_G = k_G a \theta_G = 86.1(0.0175) = 1.51$

Liquid residence time in froth [Eq. (14-142)] = $[(0.284)(81.8)(4.41)]/10^3 (0.00727) = 14.1 \text{ s}$

Liquid volumetric coefficient [Eq. (14-140)] = $[3.875(10^8)(3.74(10^{-9}))^{0.5} [0.40(3.34)(0.481)^{0.5} + 0.17]] = 1.32 \text{ s}^{-1}$

Number of liquid-phase transfer units [Eq. (14-139)]: $N_L = k_L a \theta_L = 1.32 (14.1) = 18.6$

Number of overall transfer units [Eq. (14-133)]: $N_{OG} = 1/[1/1.51 + 1.17/18.6] = 1.37$

Point efficiency [Eq. (14-132)]: $E_{OG} = 1 - \exp(-N_{OG}) = 1 - \exp(-1.37) = 0.75 (75\%)$

This value of efficiency is slightly higher than the measured value (Fig. 14-24).

Effects of Gas and Liquid Mixing As noted previously, it is necessary in most instances to convert point efficiency E_{og} to Murphree plate efficiency E_{mw} . This is true because of incomplete mixing; only in small laboratory or pilot-plant columns, under special conditions, is the assumption $E_{og} = E_{mw}$ likely to be valid. For a crossflow plate with no liquid mixing there is plug flow of liquid. For this condition of liquid flow, Lewis [Ind. Eng. Chem., 28, 399 (1936)] analyzed effects of gas mixing on efficiency. He considered three cases:

1. Gas enters plate at uniform composition (gas completely mixed between plates).

2. Gas unmixed; liquid flows in the same direction on successive plates.

3. Gas unmixed; liquid flows in alternate direction on successive plates.

Case 1 has found the widest application in practice and is represented by the relationship

$$E_{mw} = 1/\lambda [\exp(\lambda E_{og}) - 1] \quad (14-144)$$

λ is defined as for Eq. (14-133). Equation (14-144) assumes the following in addition to the base conditions:

1. L/V is constant.
2. Slope of equilibrium curve m is constant.
3. Point efficiency is constant across the tray.

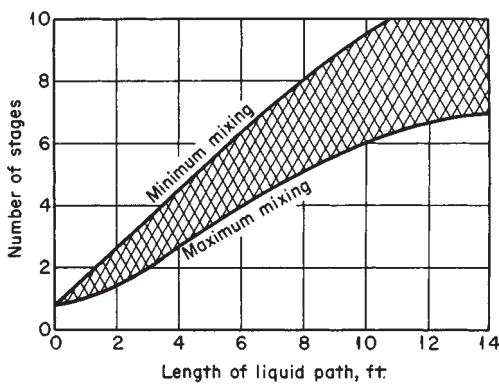


FIG. 14-38 Effect of length of liquid path on number of stages. To convert feet to meters, multiply by 0.3048. [O'Connell and Gautreaux, Chem. Eng. Prog., **51**, 236 (1955).]

Most plate columns operate under conditions such that gas is completely mixed as it flows between the plates, but few operate with pure plug flow of liquid. Departure from plug flow of liquid has been studied by Gautreaux and O'Connell [Chem. Eng. Prog., **51**, 232 (1955)] by assuming that liquid mixing can be represented as occurring in a series of stages of completely mixed liquid. For this model,

$$E_{mv} = \frac{1}{\lambda} \left[\left(1 + \lambda \frac{E_{og}}{n} \right)^n - 1 \right] \quad (14-145)$$

where n = number of stages occurring on the tray.

An approximation of the number of stages can be obtained from Fig. 14-38 using the following criteria:

1. Increased liquid rate favors plug flow.

2. Sieve plates have less back mixing than bubble-cap plates because of less obstruction to flow.
3. Increased gas rate increases turbulence and the degree of back mixing of liquid.

An alternative approach is presented in the AIChE *Bubble-Tray Design Manual* and is based on an eddy-diffusion model. According to this model,

$$\frac{E_{mv}}{E_{og}} = \frac{1 - e^{-(n' + N_{Pe})}}{(n' + N_{Pe}) \{ 1 + [(n' + N_{Pe})/n'] \}} + \frac{e^n - 1}{n' \{ 1 + [n'/(n' + N_{Pe})] \}} \quad (14-146)$$

$$\text{where } n' = \frac{N_{Pe}}{2} \left(\sqrt{1 - 4\lambda \frac{E_{og}}{N_{Pe}}} - 1 \right)$$

$$N_{Pe} = \text{Péclet number (dimensionless)} = \frac{Z_t^2}{D_E \theta_t}$$

$$Z_t = \text{length of liquid travel, m; and} \\ \lambda = \text{stripping factor [see Eq. (14-133)].}$$

The value of θ_t is calculated from Eq. (14-142). The term D_E is an eddy-diffusion coefficient that is obtained from experimental measurements. For sieve plates, Barker and Self [Chem. Eng. Sci., **17**, 541 (1962)] obtained the following correlation:

$$D_E = 6.675(10^{-3})U_a^{1.44} + 0.922(10^{-4})h_t - 0.00562 \quad (14-147)$$

where D_E = eddy-diffusion coefficient, m^2/s

U_a = gas velocity through active area of plate, m/s

h_t = liquid holdup on plate (Eq. 18-16), mm

For bubble-cap plates, the eddy-diffusion correlation in the AIChE *Bubble-Tray Design Manual* should be used.

The graphical representation of Eq. (14-146) is indicated in Fig. 14-39, where as usual $\lambda = mG_m/L_m$.

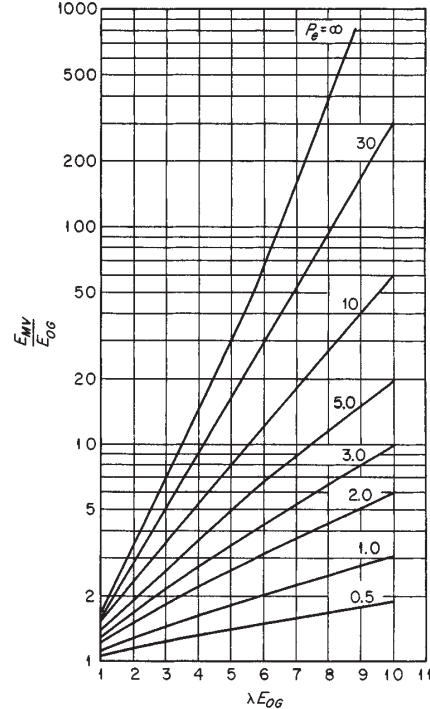
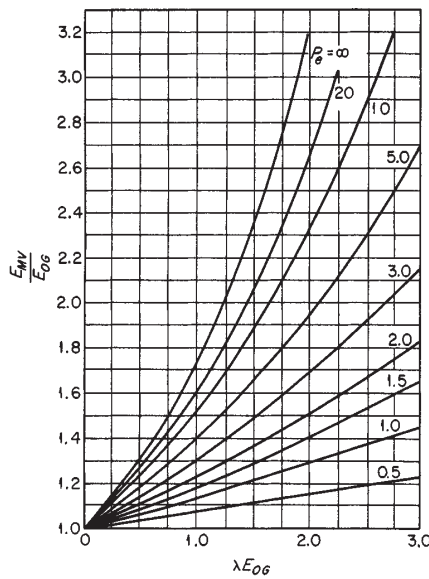


FIG. 14-39 Mixing curves. P_e = Péclet number (N_{Pe}). (Bubble-Tray Design Manual, American Institute of Chemical Engineers, New York, 1958.)

The dimensionless Péclet number in Eq. (14-146) is a key parameter in evaluating departure from plug flow of liquid across the plate. The higher its value, the greater the enhancement of point efficiency, as shown in Fig. 14-39. A long liquid flow path Z_L , a high liquid flow rate (low q_L), and a low amount of diffusive backmixing (low value of D_E) contribute to the plug flow effect. For use in the Gautreaux/O'Connell model [Eq. (14-145), Fig. 14-38], it can be shown that the number of mixing stages n is approximately

$$n = \frac{N_{Pe} + 2}{2} \quad (14-148)$$

Overall Column Efficiency Calculated values of E_{me} must be corrected for entrainment, if any, by the Colburn equation [Eq. (14-101)]. The resulting corrected efficiency E_a is then converted to column efficiency by the relationship of Lewis [*Ind. Eng. Chem.*, **28**, 399 (1936)]:

$$E_{oc} = \frac{N}{N_t} = \frac{\log [1 + E_a(\lambda - 1)]}{\log \lambda} \quad (14-149)$$

Comparison of Efficiency of Various Plates Several studies of various plates have been carried out under conditions such that direct and meaningful comparisons are possible. Required conditions include identical system, same pressure, same column diameter, and equivalent submergence. Standart and coworkers [*Br. Chem. Eng.*, **11** (11), 1370 (1966); *Sep. Sci.*, **2**, 439 (1967)] used the methanol-water system at atmospheric pressure in a 1.0-m (3.3-ft) column. For a plate spacing of 0.4 m (15.7 in) they studied the following:

1. Bubble-cap plate—70-mm (2.75-in) round caps, 25.4-mm (1.0-in) submergence
 2. Sieve plate—4.0-mm ($\frac{5}{32}$ in) holes, hole-active area = 0.048, 40-mm (1.57-in) outlet weir
 3. Turbogrid plate—4.6-mm (0.18-in) slot width, 14.7 percent open area
 4. Ripple plate—2.85-mm ($\frac{7}{64}$ in) holes, 10.8 percent open area
- Efficiency data from the work are summarized in Fig. 14-40.

Kirschbaum (*Distillier-Rektifiziertechnik*, 4th ed., Springer-Verlag, Berlin and Heidelberg, 1969) reported on studies of the ethanol-water system at atmospheric pressure, using several columns. For a 0.75-m (2.46-ft) column and 0.35-m (14-in) plate spacing, the following were covered:

1. Bubble-cap plate—90-mm (3.5-in) round caps, 30-mm (1.2-in) static submergence
2. Sieve plate—10-mm ($\frac{25}{64}$ -in) holes, hole/active area = 0.104, 25.4-mm (1.0-in) outlet weir
3. Valve plate—40-mm (1.57-in) holes, 45 valves per plate, 25.4-mm (1.0-in) outlet weir.

Efficiency data are given in Fig. 14-41.

Billet and coworkers [*Chem. Ing. Tech.*, **38**, 825 (1966); *Instn. Chem. Engrs. Symp. Ser. No. 32, 5*, 111 (1969)] used the ethylbenzene/styrene system at 100 torr and a 0.8-m column with 500-mm plate spacing. Two weir heights were used, 19 and 38 mm. Operation was at

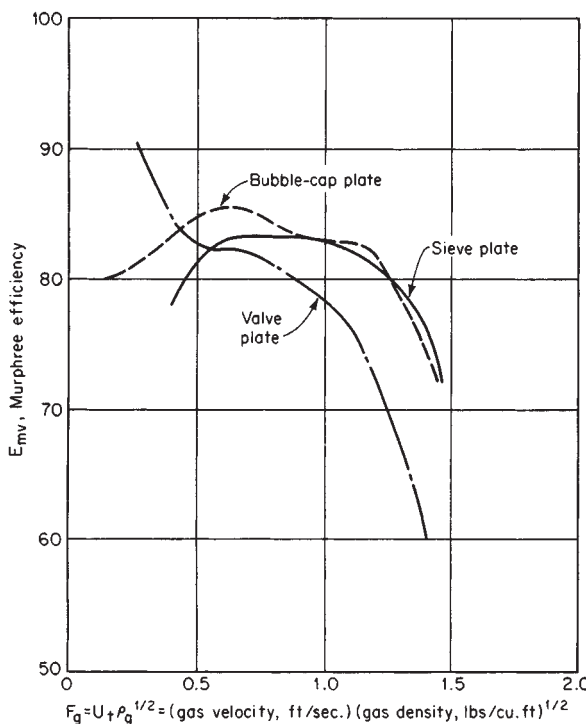


FIG. 14-41 Plate efficiencies, ethanol-water. To convert (feet per second) (pounds per cubic foot)^{1/2} to (meters per second) (kilograms per cubic meter)^{1/2}, multiply by 1.2199. (Kirschbaum, *Destillier-Rektifiziertechnik*, 4th ed., Springer-Verlag, Berlin and Heidelberg, 1969.)

total reflux. A variety of plate devices were tested, and Fig. 14-42 shows typical results for the following:

Curve 1	Bubble-cap plate, 35-mm weir
Curve 2	Valve plate with 64 V-1 valves
Curve 3	Sieve plate, 38-mm weir
Curve 4	Sieve-valve plate, 38-mm weir, 49 valves, 140 holes

Testing of plates and other devices is carried out by Fractionation Research, Inc. for industrial sponsors. Some of the test data for sieve plates have been published for the cyclohexane/n-heptane and isobutane/n-butane systems. Representative data are shown in Fig. 14-43. These are taken from Sakata and Yanagi [*Instn. Chem. Engrs. Symp. Ser. No. 56*, 3.2/21 (1979)] and Yanagi and Sakata [*Ind. Eng. Chem. Proc. Des. Devel.*, **21**, 712 (1982)]. The column diameter was 1.2 m, tray spacing was 600 mm, and weir height was 50 mm.

Work at the University of Manchester Institute of Science and Technology (UMIST) has resulted in several papers reporting efficiency data taken in a 0.6-m-diameter column. The systems methanol/water, isopropanol/water, and toluene methylcyclohexane have been used. The results may be found in Lockett and Ahmed [*Chem. Eng. Res. Des.*, **61**, 110 (1983)], Korchinsky et al. [*Trans. Chem. E.*, **72**, 406 (1994)], and Korchinsky [ibid., 472].

All the foregoing test programs involve distillation of well-defined mixtures under total reflux conditions. The primary value of the results is in the comparative data, but it should be emphasized that the design of each device was not necessarily optimized for the test conditions.

Additional plate-efficiency data are listed in Table 14-6.

PACKED COLUMNS

Introduction Packed columns for gas-liquid contacting are used extensively for absorption, stripping, and distillation operations. Usually the columns are filled with a randomly oriented packing material, but for an increasing number of applications the packing is very care-

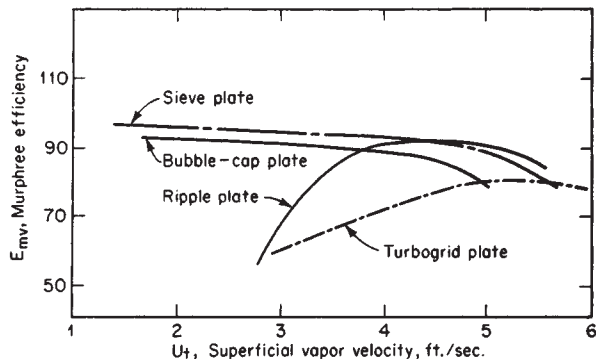


FIG. 14-40 Plate efficiencies, methanol-water. To convert feet per second to meters per second, multiply by 0.3048. [Standart et al., *Br. Chem. Eng.*, **11**, 1370 (1966); *Sep. Sci.*, **2**, 439 (1967).]

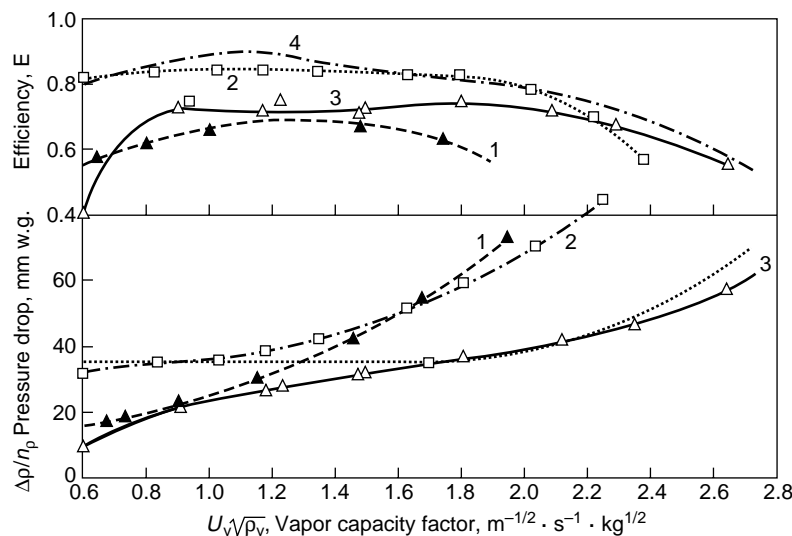


FIG. 14-42 Overall (Murphree) efficiency and pressure drop data for several devices using the same test mixture (ethylbenzene/styrene). See text for details. [Billet, Conrad, and Grubb, *Instn. Chem. Engrs. Symp. Ser.* No. 32, 5, 111 (1979).]

fully positioned in the column. The packed column is characteristically operated with counterflow of the phases.

The packed column is a simple device compared with the plate column (Fig. 14-44). A typical column consists of a cylindrical shell containing a support plate for the packing material and a liquid distributing device designed to provide effective irrigation of the packing. Devices may be added to the packed bed to provide redistribution of liquid that might channel down the wall or otherwise become maldistributed. Several beds, each with liquid distributor and support device, may be used within the same column shell. For example, a distillation column with rectifying and stripping zones, requires a minimum of two beds.

The key issue in packed column design is the selection of the packing material. Such material should provide effective contacting of the phases without excessive pressure drop. Many packings are commercially available, each possessing specific advantages with respect to cost, surface availability, interface regeneration, pressure drop, weight, and corrosion resistance. Packed beds may be divided into two categories: Those containing packing elements that are placed in the column in a random arrangement, usually by dumping; and those containing carefully installed elements designed specifically to fit the column dimensions. The former elements are called random, or dumped, packings. The latter are called ordered, or structured, packings. Typical random and structured packings are shown in Fig. 14-45.

Packed Columns versus Plate Columns Packed columns are usually specified when plate devices would not be feasible because of undesirable fluid characteristics or some special design requirement. Conditions favoring packed columns are:

1. For columns less than 0.6-m (2.0-ft) diameter, packings are usually cheaper than plates unless alloy-metal packings are required.
2. Acids and many other corrosive materials can be handled in

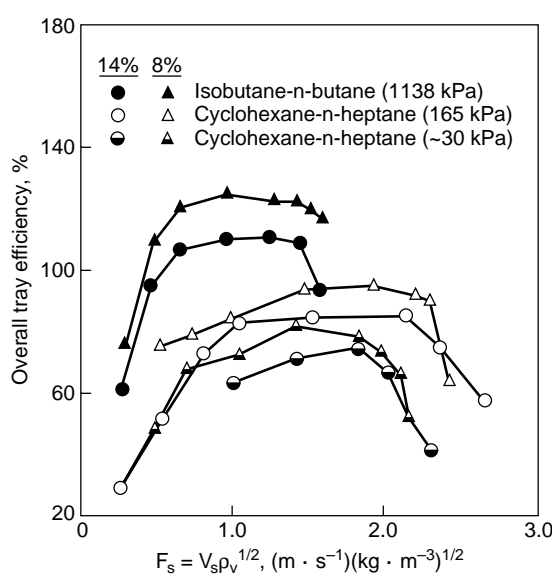


FIG. 14-43 Overall (Murphree) efficiencies of sieve plates with hole/active area ratios of 0.08 and 0.14. Efficiency values greater than 1.0 (100%) result from crossflow effects (Figs. 14-38, 14-39). [Yanagi and Sakata, *Ind. Eng. Chem., Proc. Des. Devel.*, **21**, 712 (1982).] Reproduced with permission, copyright © 1982 American Chemical Society.

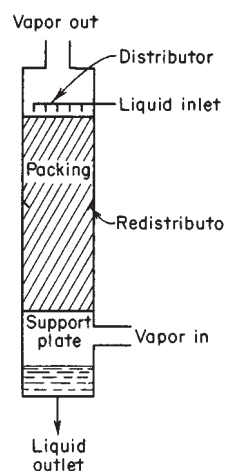


FIG. 14-44 Packed column (schematic).

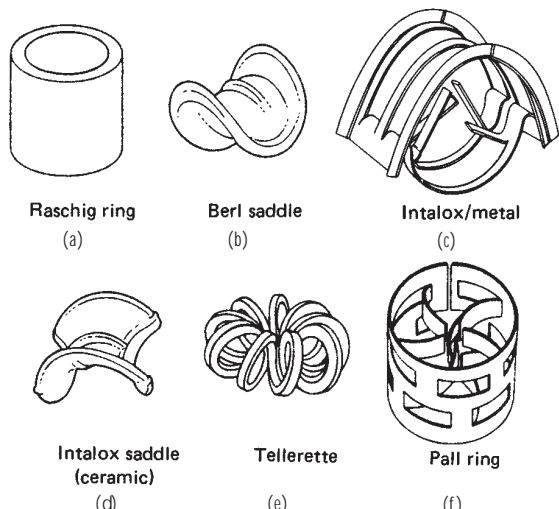


FIG. 14-45a Representative random packings. Types (c), (e) and (f) are the through-flow variety.

packed columns because construction can be of ceramic, carbon, or other resistant materials.

3. Packings often exhibit desirable efficiency-pressure-drop characteristics for critical vacuum distillations.

4. Liquids tending to foam may be handled more readily in packed columns because of the relatively low degree of liquid agitation by the gas.

5. Holdup of liquid can be quite low in packed columns, an advantage when the liquid is thermally sensitive.

Conditions unfavorable to packed columns are:

1. If solids are present in the liquid or gas, plate columns can be designed to permit easier cleaning.

2. Some packing materials are subject to easy breakage during insertion into the column or resulting from thermal expansion and contraction.

3. High liquid rates can often be handled more economically in plate columns than in packed columns.

4. Cooling coils can be incorporated more readily into plate devices.

5. Low liquid rates lead to incomplete wetting of column packings, thus decreasing contacting efficiency.

Packed-Column Hydraulics Pressure drop of a gas flowing upward through a packing countercurrently to liquid flow, is characterized graphically in Fig. 14-46. At very low liquid rates, the effective open cross section of the packing is not appreciably different from that of dry packing, and pressure drop is due to flow through a series of variable openings in the bed. Thus, pressure drop is proportional approximately to the square of the gas velocity, as indicated in the region AB.

At higher liquid rates the effective open cross section is smaller because of the presence of liquid, and a portion of the energy of the gas stream is used to support an increasing quantity of liquid in the column (region A'B'). For all liquid rates, a zone is reached where pressure drop is proportional to a gas-flow-rate power distinctly higher than 2; this zone is called the **loading zone**, as indicated in Fig. 14-46. The increase in pressure drop is due to the rapid accumulation of liquid in the packing-void volume.

As the liquid holdup increases, one of two changes may occur. If the packing is composed essentially of extended surfaces, the effective orifice diameter becomes so small that the liquid surface becomes continuous across the cross section of the column, generally at the top of the packing. Column instability occurs concomitantly with a rising continuous-phase liquid body in the column. The change in pressure drop is quite great with only a slight change in gas rate (condition C or C'). The phenomenon is called *flooding* and is analogous to entrainment flooding in a plate column.

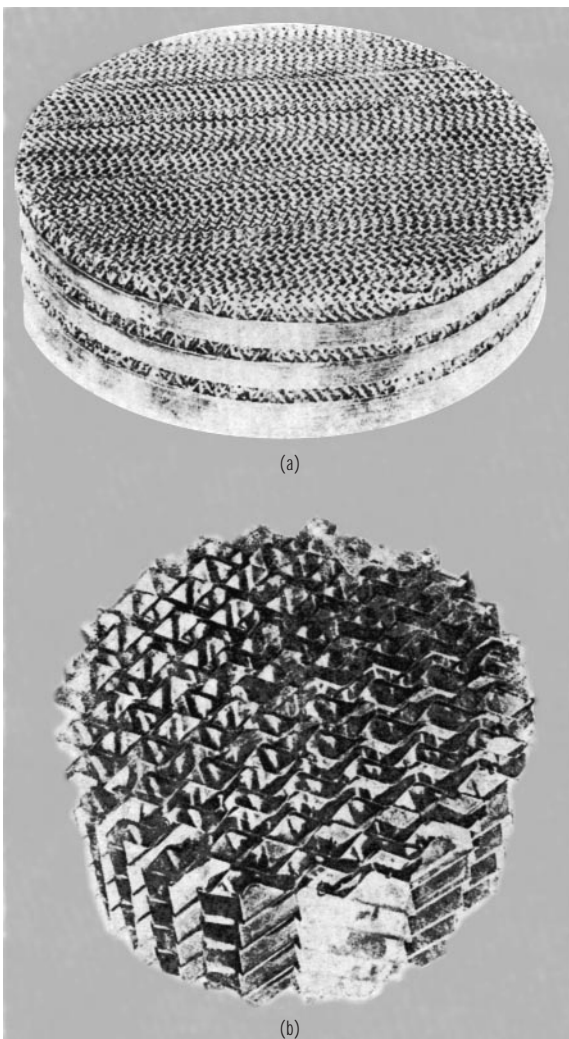


FIG. 14-45b Representative arranged-type packings: (a) Koch Sulzer, (b) Flexipac. (Courtesy Koch Engineering Co., Inc.)

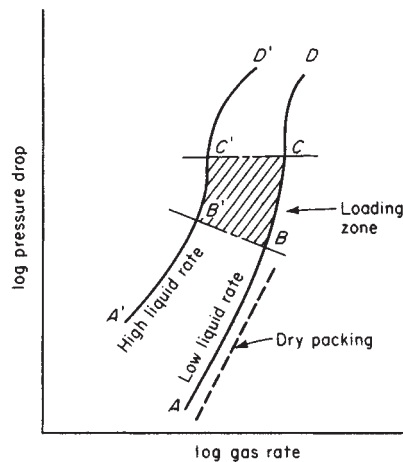


FIG. 14-46 Pressure-drop characteristics of packed columns.

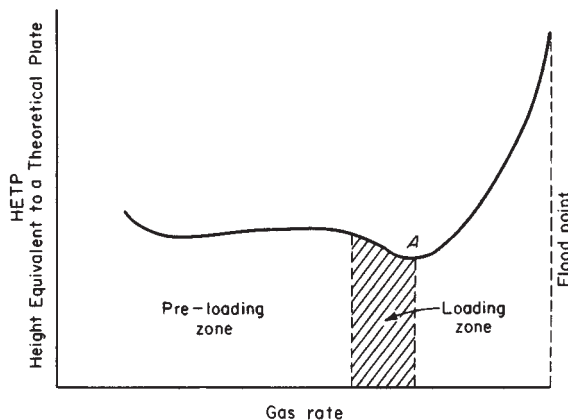


FIG. 14-47 Efficiency characteristics of packed columns (total-reflux distillation.)

If the packing surface is discontinuous in nature, a phase inversion occurs, and gas bubbles through the liquid. The column is not unstable and can be brought back to gas-phase continuous operation by merely reducing the gas rate. Analogously to the flooding condition, the pressure drop rises rapidly as phase inversion occurs.

A stable operating condition beyond "flooding" (region *CD* or *C'D'*) for nonextended surface packing with the liquid as the continuous phase and the gas as the dispersed phase has been reported by Lerner and Grove [*Ind. Eng. Chem.*, **43**, 216 (1951)] and Teller [*Chem. Eng.*, **61**(9), 168 (1954)].

For total-reflux distillations carried out in packed columns, regions of loading and flooding are identified by their effects on mass-transfer efficiency, as shown in Fig. 14-47. Gas and liquid rate increase

together, and a point is reached at which liquid accumulates rapidly (point *A*) and effective surface for mass transfer decreases rapidly.

Flooding and Loading Since flooding or phase inversion normally represents the maximum capacity condition for a packed column, it is desirable to predict its value for new designs. The first generalized correlation of packed-column flood points was developed by Sherwood, Shipley, and Holloway [*Ind. Eng. Chem.*, **30**, 768 (1938)] on the basis of laboratory measurements primarily on the air-water system.

Later work with air and liquids other than water led to modifications of the Sherwood correlation, first by Leva [*Chem. Eng. Prog. Symp. Ser.*, **50**(10), 51 (1954)] and later in a series of papers by Eckert. The generalized flooding-pressure drop chart by Eckert [*Chem. Eng. Progr.*, **66**(3), 39 (1970)], included in the previous edition of this handbook, was modified and simplified by Strigle [*Packed Tower Design and Applications*, Gulf Publ. Co., Houston, 1994] as shown in Fig. 14-48. It includes pressure drop curves, as introduced by Leva [*Chem. Eng. Progr. Symp. Ser.* No. 10, **50**, 51 (1954)], and is often called the generalized pressure drop correlation (GPDC). The ordinate scale term is a capacity parameter related to the Souders-Brown coefficient used for plate columns:

$$C_s = U_t \left[\frac{\rho_G}{(\rho_L - \rho_G)} \right]^{0.5} F_p^{0.5} \nu^{0.05} \quad (14-150)$$

where U_t = superficial gas velocity, ft/s
 ρ_G, ρ_L = gas and liquid densities, lb/ft³ or kg/m³
 F_p = packing factor, ft⁻¹
 ν = kinematic viscosity of liquid, cS

The abscissa scale term is the same flow parameter used for plates (dimensionless):

$$F_{LG} = \frac{L}{G(\rho_G/\rho_L)^{0.5}} \quad (14-151)$$

There is not a specific flood curve; a pressure drop of 1.50 in H₂O/ft is considered to represent an incipient flooding condition, although

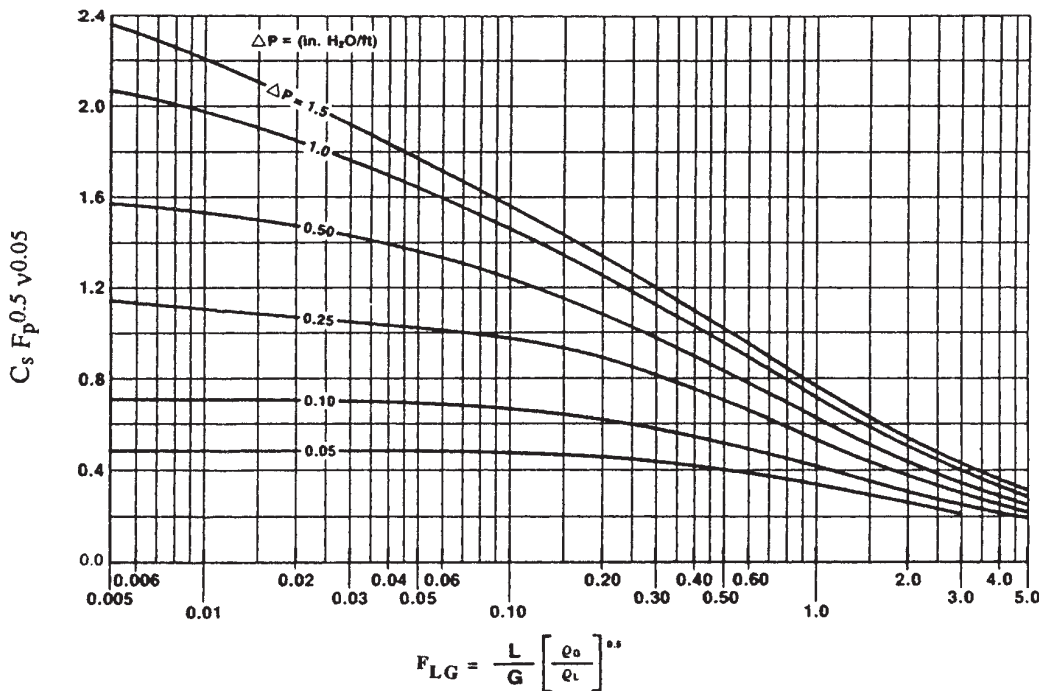


FIG. 14-48 Generalized pressure drop correlation of Eckert/Leva, as modified by Strigle. To convert inches H₂O to mm H₂O/m, multiply by 83.31. From *Packed Tower Design and Applications* by Ralph E. Strigle, Jr., copyright © 1994 by Gulf Publishing Co., Houston, Texas. Used with permission. All rights reserved.

14-42 GAS ABSORPTION AND GAS-LIQUID SYSTEM DESIGN

pressure drops at flooding have been measured in the range of 2.0–2.5 inches H₂O/ft.

The packing factor F_p is empirically determined for each packing type and size. Values of F_p , together with general dimensional data for individual packings, are given in Table 14-7. For pressure drop and flooding estimates, values of F_p should always be used with caution. A detailed analysis of the GPD^C approach (Fig. 14-48) was made by Kister and Gill [Chem. Eng. Progr., 87(2), 32 (1991)] who amassed a large data bank, mostly for random packings. They found it necessary to use separate curves for each packing type and size and also to differentiate between aqueous and nonaqueous systems. An example of their work is shown in Fig. 14-49, for 2-inch (50 mm) metal Pall rings. Note that a packing factor of 27 ft⁻¹ was used for this packing. A complete set of charts for both random and ordered packings is given in Chap. 10 of the book by Kister (*Distillation Design*, McGraw-Hill, New York, 1992).

Pressure Drop Reference to pressure drop has already been made in connection with the GPD^C (Fig. 14-48). For gas flow through dry packings, pressure drop may also be estimated by use of an orifice equation. For irrigated packings, pressure drop increases because of the presence of liquid, which effectively decreases the available cross section for gas flow (Fig. 14-46). In principle, there should be a method for correcting the dry pressure drop for the presence of water. This approach was used by Leva [Chem. Eng. Progr. Symp. Ser. No. 10, 50, 51 (1954)]. A more recent method by Robbins [Chem. Eng. Progr., 87(1), 19 (1990)] utilizes the same approach and is described here. The total pressure drop is

$$\Delta P_t = \Delta P_d + \Delta P_L \quad (14-152)$$

where ΔP_t = total pressure drop, inches H₂O per foot of packing

$$\Delta P_d = \text{dry pressure drop} = C_3 G_f^2 10^{(C_4 L_f)} \quad (14-153)$$

ΔP_L = pressure drop due to liquid presence

$$= 0.4[L_f/20,000]^{0.1} [C_3 G_f^2 10^{(C_4 L_f)}]^4 \quad (14-154)$$

$$G_f = \text{gas loading factor} = 986 F_s (F_{pd}/20)^{0.5} \quad (14-155)$$

$$L_f = \text{liquid loading factor} = L (62.4/\rho_L) (F_{pd}/20)^{0.5} \mu_L^{0.1} \quad (14-156)$$

The term F_{pd} is a dimensionless dry packing factor, specific for a given packing type and size. Values of F_{pd} are given in Table 14-7. For operating pressures above atmospheric, and for certain packing sizes, L_f and G_f are calculated differently:

$$G_f = 986 F_s (F_{pd}/20)^{0.5} 10^{0.3} \rho_g \quad (14-157)$$

$$L_f = L (62.4/\rho_L) (F_{pd}/20)^{0.5} \mu_L^{0.2} \quad F_{pd} > 200 \quad (14-158)$$

$$= L (62.4/\rho_L) (20/F_{pd})^{0.5} \mu_L^{0.1} \quad F_{pd} < 200 \quad (14-159)$$

The Robbins equations require careful attention to dimensions. However, use of the equations has been simplified through the introduction of Fig. 14-50. The terms L_f and G_f are evaluated, and the ΔP_L is obtained directly from the chart. Basic nomenclature for the Robbins method follows:

$$C_3 = 7.4 (10)^{-8}$$

$$C_4 = 2.7 (10)^{-5}$$

F_{pd} = dry packing factor, dimensionless

F_s = superficial F-factor for gas, $U_g \rho_g^{0.5}$, ft/s(lb/ft³)^{0.5}

G = gas mass velocity = lb/hr·ft²

G_f = gas loading factor, lb/hr·ft²

L = liquid mass velocity, lb/hr·ft²

L_f = liquid loading factor, lb/hr·ft²

ΔP = pressure drop, inches H₂O/ft packing ($\times 83.3 = \text{mm H}_2\text{O}/\text{m packing}$)

ρ_g = gas density, lb/ft³

ρ_L = liquid density, lb/ft³

μ_L = liquid viscosity, cP

For ordered, or structured, packings, pressure-drop estimation methods have been reviewed by Fair and Bravo [Chem. Eng. Progr., 86(1), 19 (1990)]. It is not common practice to use the packing factor approach for predicting pressure drop or flooding. For operation below the loading point, the model of Bravo et al. [*Hydrocarbon*

TABLE 14-7a Characteristics of Structured Packings

Name	Material	Nominal size	Surface area, m ² /m ³	% voids	Packing factor, 1/m	Vendor
Flexipac	S	1	558	91	108	Koch
		2	223	93	72	
		3	134	96	52	
Flexiramic	C	28	282	70	131	Koch
		48	157	74	79	
		88	102	85	49	
Gempak	S	4A	446	92	105	Glitsch
		3A	335	93	69	
		2A	223	95	53	
Intalox	S	1T	315	95	66	Norton
		2T	213	97	56	
		3T	177	97	43	
Max-Pak	S	—	229	95	39	Jaeger
Mellapak	S	125Y	125	97	33	Sulzer
		125X°	125	97		
		250Y	250	95	66	
		250X°	250	95	8	
		350Y	350	93	75	
		500X°	500	91	25	
Montz-Pak	S	B1-125	125	97		Julius Montz
		B1-250	250	95	72	
		B1-350	350	93		
Ralupak	S	A3-500	500	91		
		BSH-250	250	95		
Sulzer	G	BSH-500	500	91		
		250YC°	250	95		Raschig
		AX°	250	95		Sulzer
		BX°	492	90	69	
		CY	700	85		

NOTES: *60° corrugation angle (with the horizontal); all others 45°.

Packing factors from Kister and Gill [Chem. Eng. Progr., 87(2), 32 (1991), and Houston AIChE meeting, March 19–23, 1995].

Materials of construction: C = ceramic; E = expanded metal; G = metal gauze; S = sheet metal.

Vendors: Glitsch, Inc., Dallas, Texas; Koch Engineering Co., Wichita, Kansas; Jaeger Products, Inc., Houston, Texas; Julius Montz, Hilden, Germany; Raschig AG, Ludwigshafen, Germany; and Sulzer Bros., Winterthur, Switzerland.

Proc., 65(3), 45 (1986)] is preferred. To use this and alternate models, dimensional characteristics of structured packing must be defined. Figure 14-51 shows nomenclature and definitions of key dimensions. Not shown, but also important, is the angle the corrugations make with the horizontal (usually 45 or 60°). Then the Rocha et al. predictive equation is:

$$\Delta P_t = \left[0.171 + \left(\frac{92.7}{Re_g} \right) \right] \left(\rho_g \frac{U_{ge}^2}{S} \right) \left[\frac{1}{1 - C_o Fr_L^{0.05}} \right]^5 \quad (14-160)$$

$$\text{where } Re_g = \frac{SU_{ge}\rho_g}{\mu_g}$$

$$U_{ge} = \frac{U_g}{(\epsilon \sin \theta)}$$

$$Fr_L = \frac{U_L^2}{(Sg)}$$

and where S = length of corrugation side

U_g = superficial velocity of gas

ϵ = void fraction of packing

θ = corrugation angle (from horizontal), deg.

U_L = superficial liquid velocity

g = gravitational constant

Any consistent set of units may be used.

This model applies in the region below the loading point, and it cannot predict the flood point because it does not include the effects of gas velocity on liquid holdup. The model of Stichlmair et al. [*Gas*

TABLE 14-7b Characteristics of Random Packings

Name	Material	Nominal size		Wall thickness, mm	Bed weight, kg/m ³	Area, m ² /m ³	% voids	Packing factor F _p , m ⁻¹	Dry packing factor F _{pd} , m ⁻¹	Vendor
		mm	Number							
Raschig rings	C	6	—	1.6	960	710	62	—	5250	Various
		13	—	2.4	880	370	64	1900	1705	
		25	—	3.2	670	190	74	587	492	
		50	—	6.4	660	92	74	213	230	
		75	—	9.5	590	62	75	121	—	
Raschig rings	M	19	—	1.6	1500	245	80	984	—	Various
		25	—	1.6	1140	185	86	472	492	
		50	—	1.6	590	95	92	187	223	
		75	—	1.6	400	66	95	105	—	
Pall rings	M	16	—	0.40	—	—	92	256	262	Norton, Koch, Glitsch
		25	—	0.51	480	205	94	183	174	
		38	—	0.64	415	130	95	131	91	
		50	—	0.81	385	115	96	89	79	
		90	—	—	270	92	97	59	46	
Cascade mini rings (CMR)	M	—	1	—	389	250	96	131	102	Glitsch
		—	1.5	—	234	144	97	95	—	
		—	2.5	—	195	123	98	72	79	
		—	3	—	58	103	98	46	43	
	P	—	1A	—	71	185	94	98	92	
	—	—	3A	—	40	74	96	39	33	
Berl saddles	C	6	—	—	900	900	60	—	2950	Koch
		13	—	—	865	465	62	790	900	
		25	—	—	720	250	68	360	308	
		38	—	—	640	150	71	215	154	
		50	—	—	625	105	72	150	102	
Intalox saddles	C	6	—	—	864	984	65	302	2720	Norton
		13	—	—	736	623	71	—	613	
		25	—	—	672	256	73	302	208	
		50	—	—	608	118	76	131	121	
		75	—	—	576	92	79	72	66	
Fleximax	M	—	300	—	—	141	98	85	—	Koch
		—	400	—	—	85	98	56	—	
Metal Intalox (IMTP)	M	25	—	—	352	230	97	134	141	Norton
		40	—	—	237	154	97	79	85	
		50	—	—	150	98	98	59	56	
		70	—	—	130	56	98	39	—	
Nutter rings	M	—	1	0.30	178	168	98	98	89	Nutter
		—	2	0.45	173	96	98	59	56	
		—	2.5	0.45	145	83	66	52	49	
		—	3.0	0.50	133	66	98	43	36	
Pall rings	P	25	—	—	80	206	90	180	180	Norton
		50	—	—	61	102	92	85	82	
		90	—	—	53	85	92	56	39	
	C	25	—	—	—	—	—	351	—	
	—	38	—	—	—	—	—	180	—	
	—	50	—	—	—	—	—	141	—	
Intalox saddles	P	—	1	—	96	207	90	131	131	Norton
		—	2	—	56	108	93	92	85	
Snowflake	P	—	—	—	45	92	95	43	—	Norton
Nor-Pac	P	25	1	—	72	180	92	82	—	NSW
		38	1.5	—	61	144	93	56	—	
		50	2.0	—	53	102	94	39	—	
Tri-Pack	P	25	1	—	72	180	92	82	—	Jaeger
		50	2	—	53	102	94	39	—	
VSP	M	25	1	—	352	206	98	105	—	Jaeger
		50	2	—	296	112	96	69	—	
Tellerettes	P	25	1	—	112	180	87	—	—	Ceilcote
		50	2	—	59	125	93	—	—	

NOTES: M = metal, carbon steel. Other metals available.

P = plastic, polypropylene. Other plastics available.

Packing factor \bar{F}_p from Kister and Gill [Chem. Eng. Progr., 87(2), 32 (1991) and Houston AIChE meeting, March 19–23, 1995]; Strigle, *Packed Tower Design and Applications* [Gulf Publishing Co., Houston, Texas, 1994]; dry packing factor F_{pd} from Robbins [Chem. Eng. Progr., 87(1), 19 (1990)].

Vendors: Ceilcote Co., Berea, Ohio; Glitsch, Inc., Dallas, Texas; Koch Engineering Co., Wichita, Kansas; Jaeger Products, Inc., Houston, Texas; NSW Corp., Roanoke, Virginia; Norton Co., Akron, Ohio; and Nutter Engineering Co., Tulsa, Oklahoma.

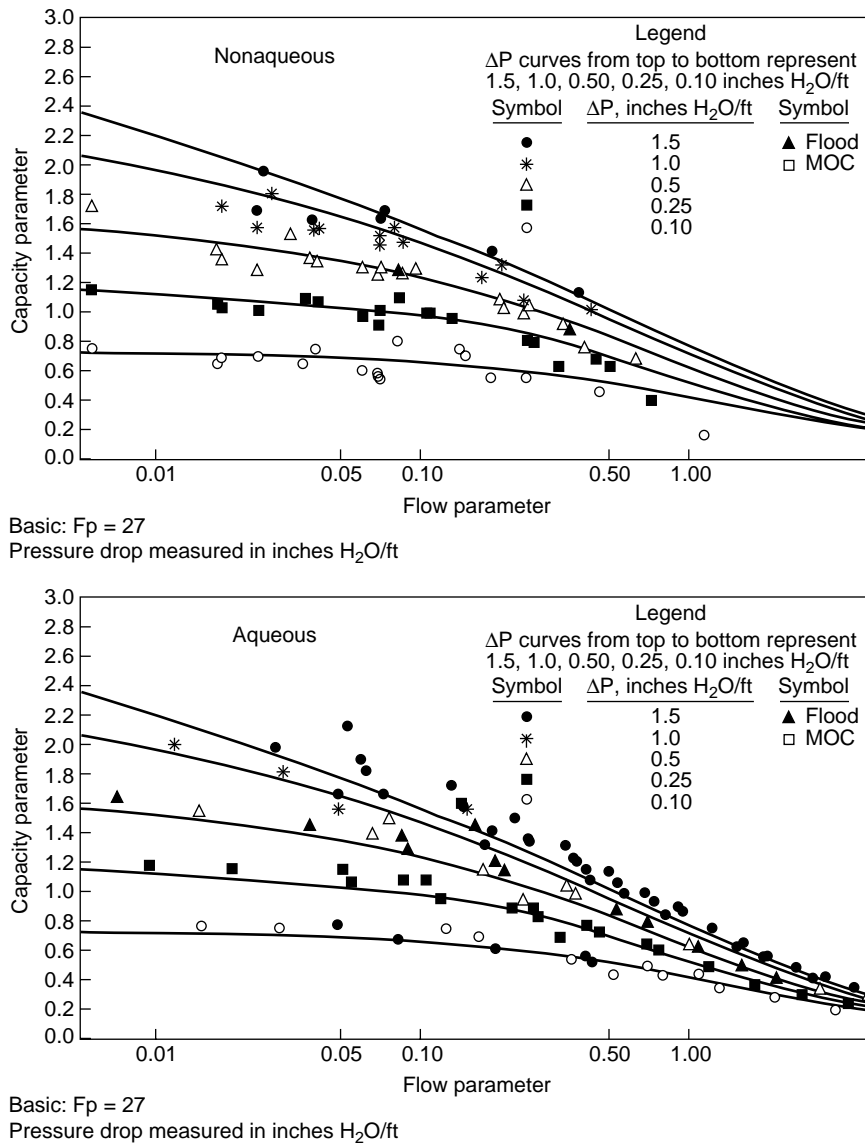


FIG. 14-49 Pressure drop/flooding correlation of Kister and Gill for 2-inch metal Pall rings. The upper chart is for nonaqueous systems, the lower chart for aqueous systems. To convert inches H_2O/ft to mm H_2O/m , multiply by 83.31.

Sepn. Purif., **3**, 19 (1989)] takes holdup into account and applies to random as well as structured packings. It is somewhat cumbersome to use and requires three constants for each packing type and size. Such constants have been evaluated, however, for a number of commonly used packings. A more recent pressure drop and holdup model, suitable for extension to the flood point, has been published by Rocha et al. [*Ind. Eng. Chem. Research*, **35**, 1660 (1996)]. This model takes into account variations in surface texturing of the different brands of packing.

Representative pressure drop data for random and structured packings are given in Figs. 14-52–14-54.

Example 13: Packed Column Pressure Drop Air and water are flowing countercurrently through a bed of 2-inch metal Pall rings. The air mass velocity is 2.03 kg/s-m^2 (1500 lbs/hr-ft^2), and the liquid mass velocity is 12.20 kg/s-m^2 (9000 lbs/hr-ft^2). Calculate the pressure drop by the generalized pres-

sure drop (GPDC, Fig. 14-48) and the Robbins methods. Properties: $\rho_G = 0.074 \text{ lbs/ft}^3$; $\rho_L = 62.4 \text{ lbs/ft}^3$; $\mu_L = 1.0 \text{ cP}$; $v = 1.0 \text{ cS}$. The packing factor $F_p = 27 \text{ ft}^{-1}$. For Robbins, $F_{pd} = 24 \text{ ft}^{-1}$. The flow parameter $F_{LG} = L/G = (\rho_G/\rho_L)^{0.5} = (9000/1500) (0.072/62.4)^{0.5} = 0.207$. The F-factor is $F_s = U_s \rho_G^{0.5} = G/(\rho_G^{0.5} 3600) = 1500/[(0.074)^{0.5} (3600)] = 1.53 \text{ ft/s(lb/ft)}^{0.5}$.

Using the GPDC method, the capacity parameter [by Eq. (14-150)] = $U_t [\rho_G/(\rho_L - \rho_G)]^{0.5} F_p^{0.5} v^{0.05}$, which is roughly equivalent to

$$\frac{F_s}{\rho_L^{0.5}} F_p^{0.5} v^{0.05} = \left(\frac{1.53}{62.4} \right)^{0.5} 27^{0.5} (1.0) = 1.01$$

Referring to Fig. 14-48, the intersection of the capacity parameter and the flow parameter lines gives a pressure drop of 0.38 inches H_2O/ft packing. (The same result is obtained from the Kister/Gill chart, Fig. 14-49.)

Using the Robbins method, $C_f = 986 F_s (F_{pd}/20)^{0.5} = 986(1.53)(24/20)^{0.5} = 1653$. $L_f = L (62.4/\rho_L) (F_{pd}/20)^{0.5} \mu^{0.1} = 9000 (1.0)(1.095)(1.0) = 9859$. $L_f/C_f = 5.96$.

From Fig. 14-50, pressure drop = 0.35 in. H_2O/ft packing.

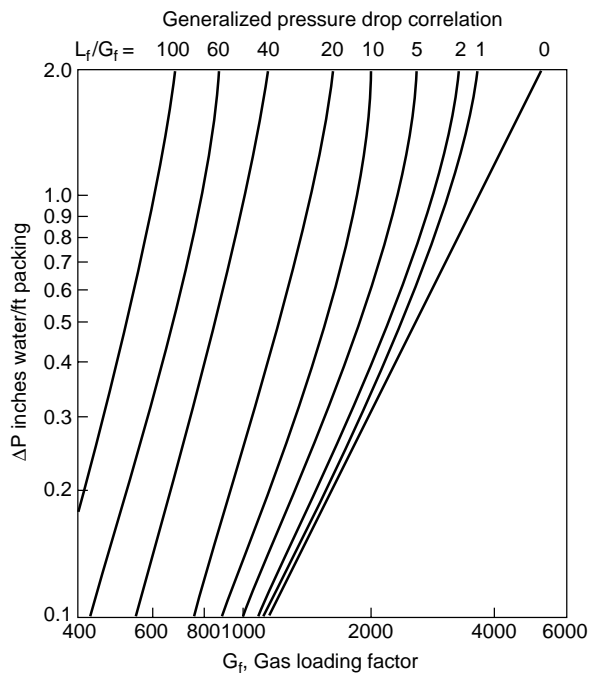
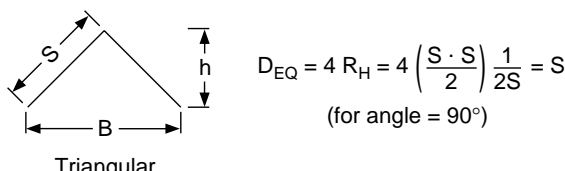
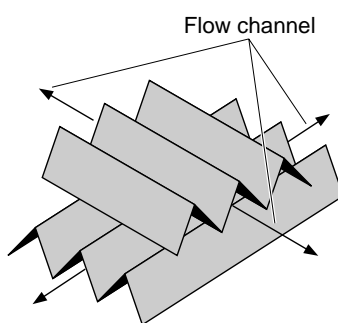


FIG. 14-50 Pressure drop correlation for random packings, as presented by Robbins. [Chem. Eng. Progr., 87(1), 19 (1990). Reproduced with permission of the American Institute of Chemical Engineers. Copyright © 1990 AICHE. All rights reserved.] To convert inches H_2O/ft to mm H_2O/m , multiply by 83.31.



a. Flow channel cross section



b. Flow channel arrangement

FIG. 14-51 Geometric properties of typical structured packings.

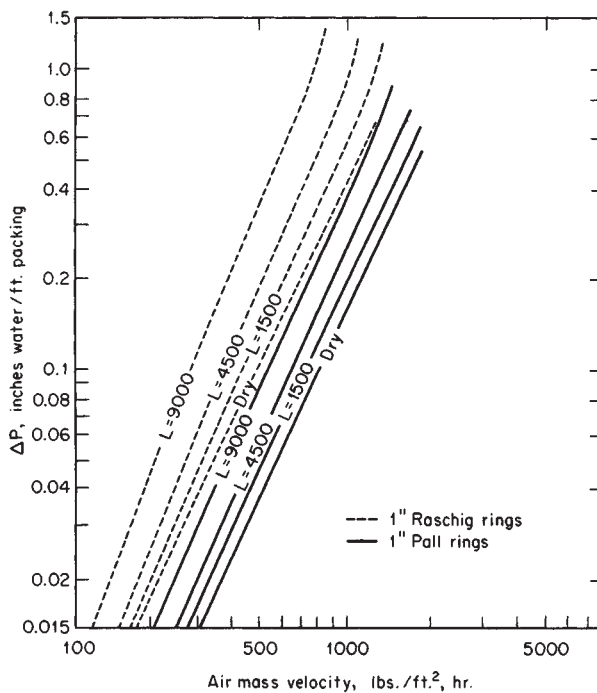
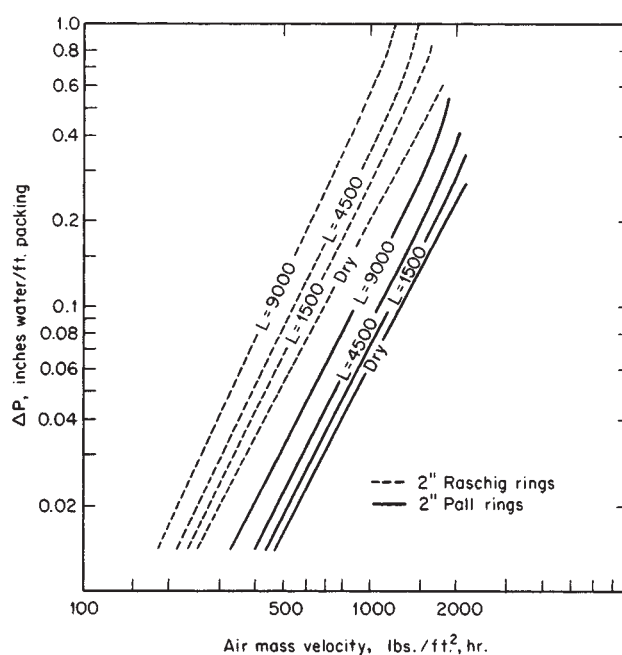


FIG. 14-52 Pressure drop for metal pall rings, 0.024-in wall thickness (1-in size) and 0.036-in wall (2-in size). Metal Raschig rings have $\frac{1}{16}$ -in wall. $L = \text{lb liquid}/(\text{h}\cdot\text{ft}^2)$. To convert inches of water per foot to millimeters of water per meter, multiply by 83.31; to convert inches to millimeters, multiply by 25.4; and to convert pounds per hour-square foot to kilograms per second-square meter, multiply by 0.001356. [Eckert, Foote, and Huntington, Chem. Eng. Progr., 54(1), 70 (1958).]



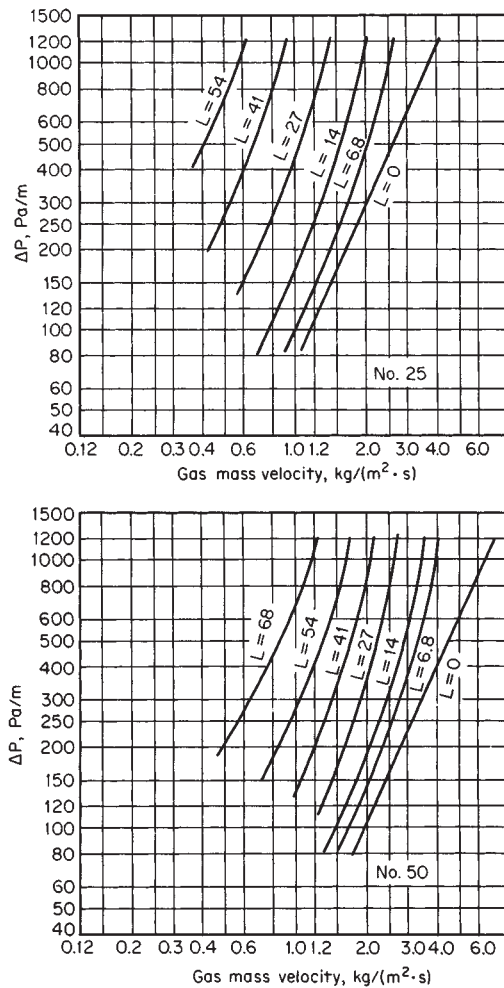


FIG. 14-53 Pressure for metal Intalox saddles, sizes No. 25 (nominal 25 mm) and No. 50 (nominal 50 mm). Air-water system at atmospheric pressure, 760-mm (30-in) column, bed height, 3.05 m (10 ft). L = liquid rate, $\text{kg}/(\text{s} \cdot \text{m}^2)$. To convert kilograms per second-square meter to pounds per hour-square foot, multiply by 151.7; to convert pascals per meter to inches of water per foot, multiply by 0.1225. (Courtesy Norton Company, Akron, Ohio.)

Support Plates While the primary purpose of a packing support is to retain a bed of packing without excessive restriction to gas and liquid flow, it also serves to distribute both streams. Unless carefully designed, the support plate can also cause premature column flooding. Thus, design of the support plate significantly affects column pressure drop and stable operating range.

- Two basic types of support plates may be utilized:
1. Countercurrent
 2. Separate flow passages for liquid and gas

The two types are indicated in Figs. 14-55, 14-56, and 14-57.

The degree of open area on a support plate is the fraction of void inherent in the design of the plate minus that portion of the open area occluded by the packing. To avoid premature flooding, the net open area of the plate must be greater than that of the packing itself. With the countercurrent type of support plate the free area for gas flow can range up to 90 percent of the column cross-sectional area. However, such a plate is easily occluded by the packing pieces resting directly on it.

The separate flow passage devices can be designed for free areas up

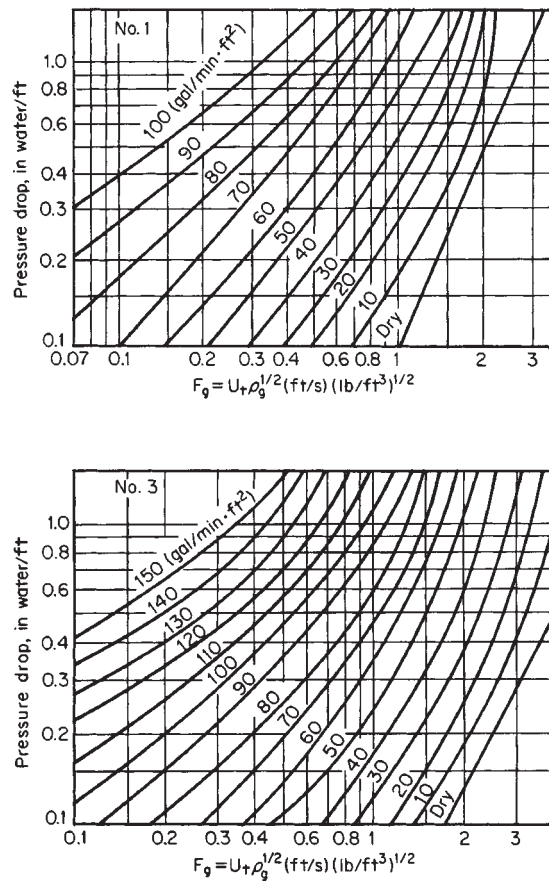


FIG. 14-54 Pressure drop for Flexipac packing, sizes No. 1 and No. 3. Air-water system at atmospheric pressure. Liquid rate in gallons per minute-square foot. To convert (feet per second) (pounds per cubic foot) $^{1/2}$ to (meters per second) (kilograms per cubic meter) $^{1/2}$, multiply by 1.2199; to convert gallons per minute-square foot to pounds per hour-square foot, multiply by 500; to convert inches of water per foot to millimeters of water per meter, multiply by 83.31; and to convert pounds per hour-square foot to kilograms per second-square meter, multiply by 0.001356. (Courtesy Koch Engineering Co., Wichita, Kansas.)

to 90 percent, and because of their geometry they will have very little occlusion by the packing.

Liquid Holdup Three modes of liquid holdup in packed columns are recognized:

1. Static, h_s
2. Total, h_t
3. Operating, h_o

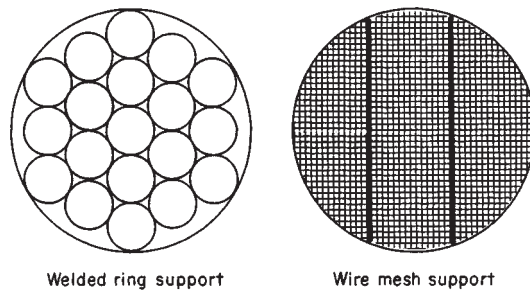


FIG. 14-55 Packing supports (countercurrent).

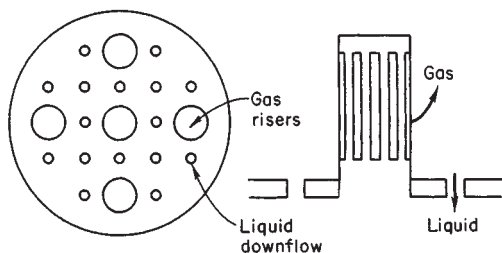


FIG. 14-56 Support plate, cap type (separate flow or "gas-injection" type).

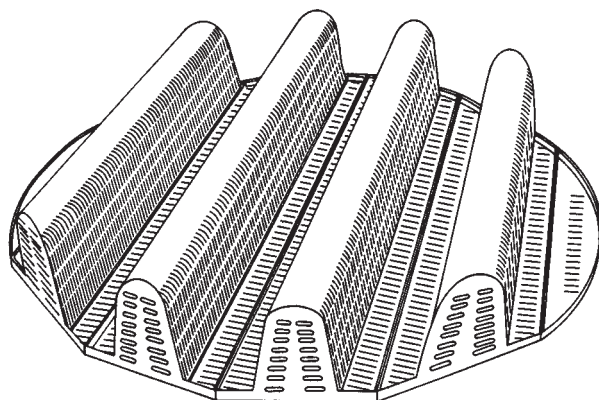


FIG. 14-57 Beam-type "gas-injection" support plate for large columns.

Static holdup is the amount of liquid remaining on packing that has been fully wetted and then drained. Total holdup is the amount of liquid on the packing under dynamic conditions. Operating holdup is the amount of liquid attributed to operation and is measured experimentally as the difference between total and static holdup. Thus,

$$h_t = h_o + h_s \quad (14-161)$$

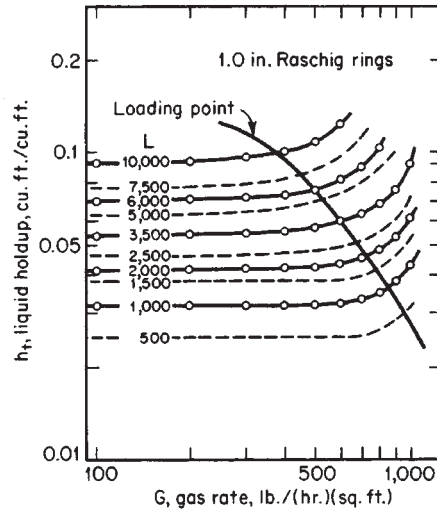


FIG. 14-58 Typical holdup data for random packings and the air-water system. The raschig rings are of ceramic material. To convert pounds per hour per ft^2 to kilograms per second per m^2 , multiply by 0.001356; to convert inches to millimeters, multiply by 25.4. [Shulman et al., *AICHE J.* **1**, 247 (1955).]

where h values are in volumes of liquid per total volume of bed. The effective void fraction under operating conditions is

$$\varepsilon' = \varepsilon - h_t \quad (14-162)$$

Static holdup depends upon the balance between surface-tension forces tending to hold liquid in the bed and gravity or other forces that tend to displace the liquid out of the bed. Estimates of static holdup (for gravity drainage) may be made from the following relationship of Shulman et al. [*Am. Inst. Chem. Eng. J.*, **1**, 259 (1955)]:

$$h_s = 2.79 \frac{C_1 \mu^{C_2} \sigma^{C_3}}{\rho_\ell^{0.37}} \quad (14-163)$$

where μ_ℓ = liquid viscosity, mPa·s
 σ = surface tension, mN/m
 ρ_ℓ = liquid density, kg/m³

and constants are

Packing	C ₁	C ₂	C ₃
1.0-in carbon Raschig rings	0.086	0.02	0.23
1.0-in ceramic Raschig rings	0.00092	0.02	0.99
1.0-in ceramic Berl saddles	0.0055	0.04	0.55

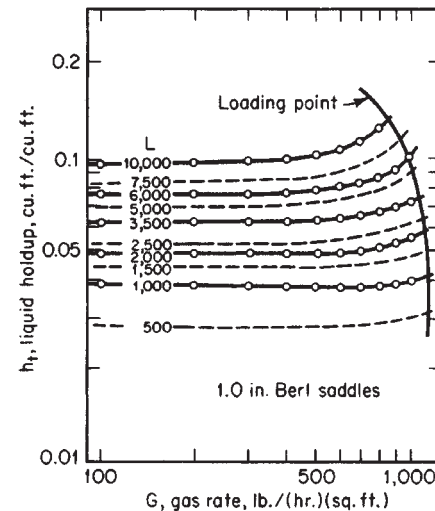
For other packings and for the case in which static holdup is changed by gas flowing through the bed, the method of Dombrowski and Brownell [*Ind. Eng. Chem.*, **46**, 1207 (1954)], which correlates static holdup with a dimensionless capillary number, should be used.

Typical total holdup data for packings are shown in Figs. 14-58 and 14-59. It should be noted that over much of the preloading range gas rate has little effect on holdup.

Operating holdup may be estimated by the dimensionless equation of Buchanan [*Ind. Eng. Chem. Fundam.*, **6**, 400 (1967)]:

$$h_o = 2.2 \left(\frac{\mu'_\ell u_\ell}{g \rho_\ell d_p^2} \right)^{1/3} + 1.8 \left(\frac{u_\ell^2}{gd_p} \right)^{1/2} \quad (14-164)$$

where μ'_ℓ = liquid viscosity, Pa·s
 u_ℓ = liquid superficial velocity, m/s
 g = gravitational constant, m/s²
 ρ_ℓ = liquid density, kg/m³
 d_p = nominal packing size, m



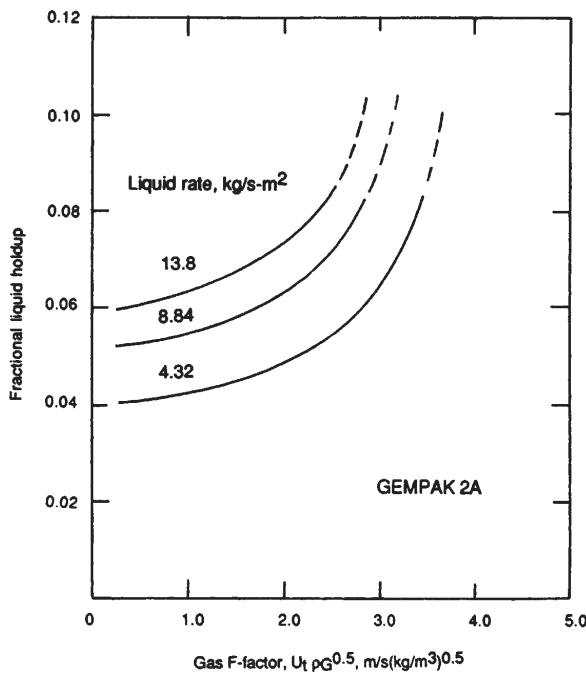


FIG. 14-59 Typical vendor data for liquid holdup of a structured packing, Gempak 2A. [Courtesy Glitsch, Inc., Dallas, Texas.]

The first term is a "film number"; the second is the Froude number. The equation applies to ring packings only operating below the load point and correlates all literature data to about ± 20 percent.

Liquid holdup has been studied by Stichlmair et al. [Gas Sepn. Purif., **3**, 19 (1989)] for both random and structured packings, and by Rocha et al. [Ind. Eng. Chem. Res., **32**, 641 (1993)] for a variety of

structured packings. The holdup model developed by the latter investigators is shown in Fig. 14-60 in a representative case. It is clear that the modern, through-flow random packings and the structured packings have much less operating liquid holdup of liquid than do the older, traditional bluff-body packings.

Operating holdup contributes effectively to mass-transfer rate, since it provides residence time for phase contact and surface regeneration via agglomeration and dispersion. Static holdup is limited in its contribution to mass-transfer rates, as indicated by Thoenes and Kramers [Chem. Eng. Sci., **8**, 271 (1958)]. In laminar regions holdup in general has a negative effect on the efficiency of separation.

Liquid Distribution Uniform initial distribution of liquid at the top of the packed bed is essential for efficient column operation. This is accomplished by a device that spreads the liquid uniformly across the top of the packing. Baker, Chilton, and Vernon [Trans. Am. Inst. Chem. Eng., **31**, 296 (1935)] studied the influence of the bed itself as a distributor and found that a single-point distribution in a 305-mm (12-in) column with 19-mm ($\frac{3}{4}$ -in) packing required 3.05 m (10 ft) of bed before achieving uniform distribution across the bed. They found also a tendency for liquid to migrate toward the column wall (Fig. 14-61), especially for ratios of column diameter to packing size less than 8. For a multipoint distribution, their recommendation was one liquid stream for each 194- cm^2 (30-in 2) column area. Eckert [Chem. Eng. Prog., **57**, 54 (1961)] recommends the following:

Column diameter, m	Streams/ m^2
1.2 or greater	40
0.75	170
0.40	340

Silvey and Keller [*I. Chem. E. Symp. Ser. No. 32*, **4**, 18 (1969)] found that a trough-type distributor with 34 streams/ m^2 gave good liquid distribution in a 1.2-m column, up to a bed height of 10.7 m. Ceramic raschig rings of 38 and 76 mm nominal size were used, and efficiency profiles were measured by means of intermediate bed samples. A plot of their data is shown in Fig. 14-62; for the type of plot, a straight line indicates uniform distribution. The plotting technique is based on the Fenske relationship for theoretical stages (Sec. 13). This

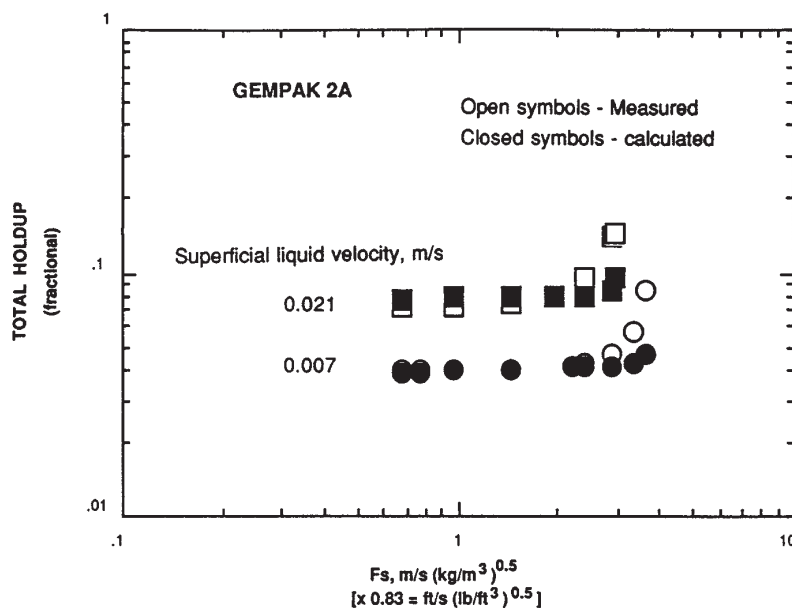


FIG. 14-60 Comparison of measured and calculated values of liquid holdup for Gempak 2A structured packing, air-water system. [Rocha et al., Ind. Eng. Chem., **32**, 641 (1993).] Reproduced with permission. Copyright © 1993 American Chemical Society.

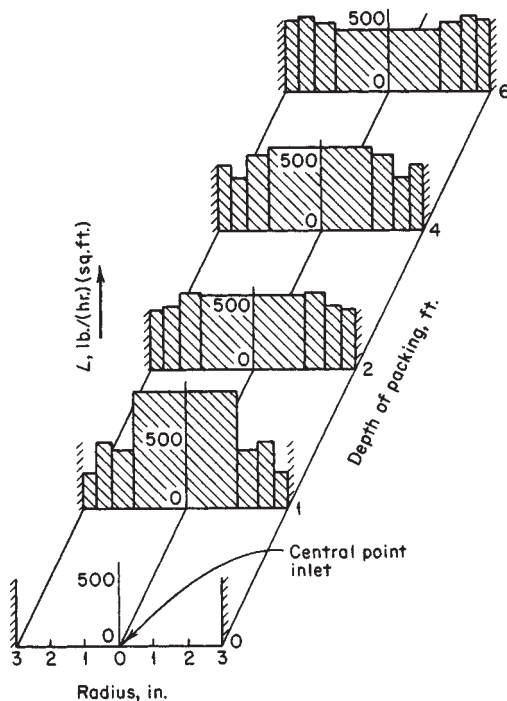


FIG. 14-61 Liquid distribution in a 6-in column packed with $\frac{1}{2}$ -in broken-stone packing. Increments of radius represent equal-annual-area segments of tower cross section. Central-point inlet. Water rate = 500 lb/(h·ft²). Air rate = 810 lb/(h·ft²). To convert pounds per hour-square foot to kilograms per second-square meter, multiply by 0.001356; to convert inches to centimeters, multiply by 2.54. (Data from Baker, Chilton, and Vernon, in Sherwood and Pigford, Absorption and Extraction, 2d ed., McGraw-Hill, New York, 1952.)

same distributor was found to be unsatisfactory by Shariat and Kunesh [Ind. Eng. Chem. Res., **34**, 1273 (1995)] when through-flow pall rings were used. A comparison between the trough distributor and an orifice-riser distributor with 100 streams/m² is shown in Fig. 14-63. In the normal range of operation, 30–70 percent more stages were obtained with the increased number of streams. The column, test mixture (cyclohexane/n-heptane) and operating pressure (1.65 bar) were the same as for the earlier Silvey-Keller tests.

The through-flow random packings and the structured packings require careful attention to liquid distribution. Such packings cannot correct an initial poor distribution. Several of the packing vendors maintain elaborate test stands for conducting special distributor evaluations. In general, practical aspects of design limit the number of streams to 100–120 per m², and these values have proven adequate for the newer packings. Kunesh et al. [Ind. Eng. Chem. Res., **26**, 1845 (1987)] have an in-depth treatment of commercial-scale experiments that support designs of packed column liquid distributors.

Several distributor types are available: trough, orifice-rise, and perforated pipe. Examples of these types are shown in Fig. 14-64. The trough distributor provides good distribution under widely varying flow rates of gas and liquid. The liquid may flow through simple V-notch weirs, or it may flow through tubes that extend from the troughs to near the upper level of the packing. Some deposition of solids can be accommodated.

The orifice-riser distributor is designed to lay the liquid carefully onto the bed, with a minimum of contact with gas during the process. It can be designed to provide a large number of liquid streams, with the limit of sufficient liquid head to provide uniform liquid flow through the orifices. The gas risers must be designed to accommodate the expected variations in flow rate, often with a minimum of pressure drop. For very distribution-sensitive packings, it is necessary to include pour points in the vicinity of the column wall (to within 25 mm).

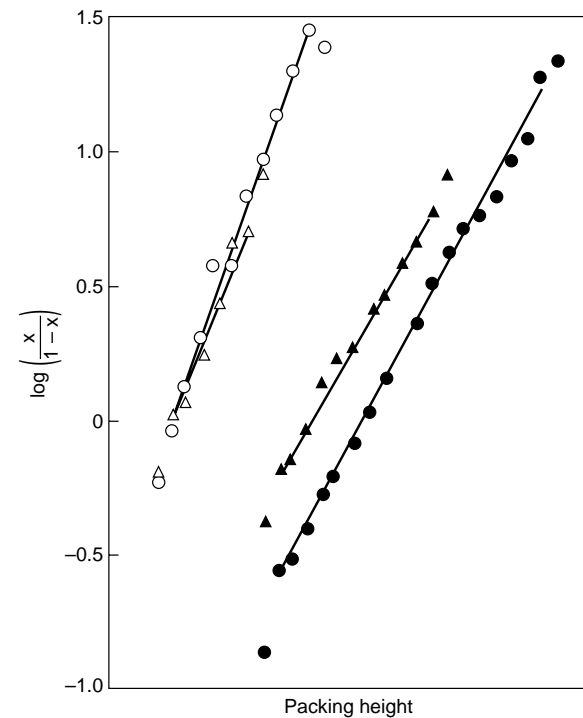


FIG. 14-62 Comparison of composition profiles at different bed heights and two sizes of ceramic raschig rings. Column diameter = 1.2 m, cyclohexane/n-heptane system at 1.65 bar and total reflux. [Silvey and Keller, I. Chem. E. Symp. Ser. No. 32, 1969.]

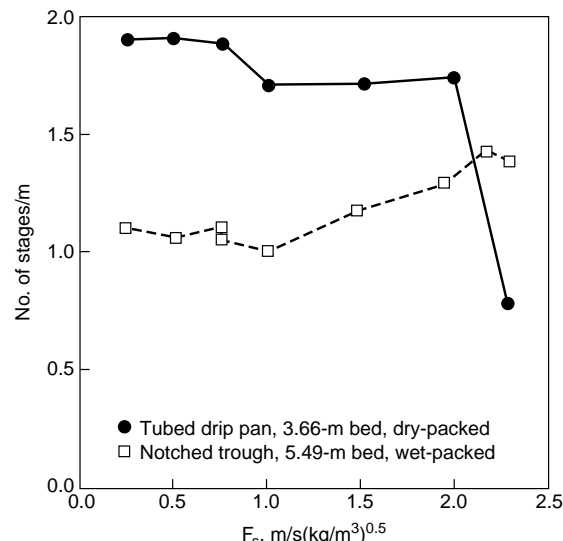


FIG. 14-63 Efficiency of beds of 51 mm Pall rings with two different distributors. Column diameter = 1.2 m, cyclohexane/n-heptane system at 1.65 bar and total reflux. [Shariat and Kunesh, Ind. Eng. Chem. Res., **34**, 1273 (1995).] Reproduced with permission. Copyright © 1995, American Chemical Society.

14-50 GAS ABSORPTION AND GAS-LIQUID SYSTEM DESIGN

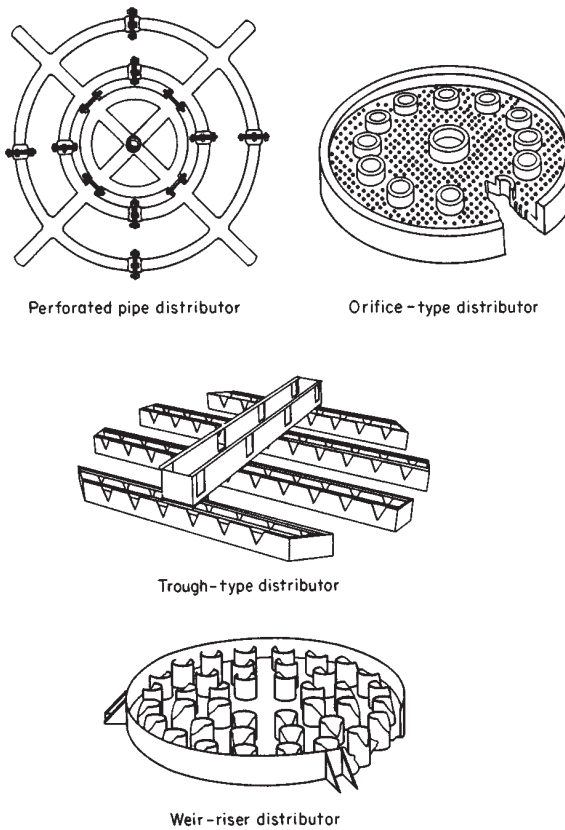


FIG. 14-64 Typical liquid distributors. (Courtesy Norton Company, Akron, Ohio.)

For larger diameter columns, and for low liquid rates, the distributor must be almost exactly level (e.g., within 6 mm for a 3-m diameter) or all pour points will not function. On the other hand, the rises must be high enough to accommodate the backup caused by high liquid rates. The needed head can be estimated from the orifice equation, with a discharge coefficient of 0.5. In some cases the orifices discharge directly into tubes that extend to the packed bed (the "tubed drip-pan distributor").

The perforated pipe distributor comprises a central feed sump and pipes that branch out from the sump to provide the liquid discharge. The level in the sump varies with liquid total flow rate, and the size of the lateral pipes and their perforations must be determined carefully to ensure that the ends of the pipes are not starved for liquid. The orifices are typically 4 to 6 mm diameter, and can be subject to plugging if foreign matter is present. The pipes must be leveled carefully, especially for large diameter columns.

Another type of distributor, not shown in Fig. 14-64, is the spray nozzle. It is usually not recommended for liquid distribution for two reasons. First, except for small columns, it is difficult to obtain a uniform spray pattern for the packing. The full-cone nozzle type is usually used, with the need for a bank of nozzles in larger columns. When there is more than one nozzle, the problem of overlap or underlap arises. A second reason for not using spray nozzles is their tendency toward entrainment by the gas, especially the smaller droplets in the spray size distribution. However, some mass transfer in the spray can be expected.

Maldistribution Departure from uniform distribution of the phases in a packed column can be caused by:

1. The liquid distributor not dividing the liquid evenly over the column cross section.

2. The liquid moving more easily to the wall than vice versa. The resultant channeling along the wall may be accentuated by vapor condensing because of column heat losses.

3. The packing geometry inhibiting lateral distribution.
4. Void variations due to packing being improperly installed.
5. The column being out of vertical alignment.

Cause 1 has been covered in the preceding subsection. Causes 4 and 5 can be handled through careful design and installation. Causes 2 and 3 bear additional discussion at this point.

The effect of channeling on mass-transfer efficiency has been studied theoretically by Manning and Cannon [*Ind. Eng. Chem.*, **49**, 347 (1957)], Huber and Hiltbrunner [*Chem. Eng. Sci.*, **21**, 819 (1966)], and Meier and Huber (*Proc. Intn. Symp. Distill.*, Brighton, England, 1970). Typical results are shown in Fig. 14-65. The effect of maldistribution can be severe, and efforts are being made to relate a maldistribution index to mass-transfer efficiency. Albright [*Hydrocarbon Proc.*, **63**, 173 (Sept. 1984)] developed a computer model to simulate effects of distributor design on bed distribution. Zuiderweg and coworkers [Hoek et al., *Chem. Eng. Res. Des.*, **64**, 431 (1986); Zuiderweg et al., *I. Chem. E. Symp. Ser. No. 104*, B247 (1987); Zuiderweg et al., *Trans. I. Chem. E.*, **71**, Part A, (1993)] have studied the effect of structured and random packed bed designs on maldistribution and, in turn, its effect of packed column efficiency.

Liquid migration to the wall appears to be favored by small-column diameter-packing diameter ratios (for random packings) and can be corrected by the use of side wipers or redistributors. Inhibition of lateral dispersion can be caused by the geometry of certain types of structured packing, according to Huber and Hiltbrunner (op. cit.). With careful attention given to the five causes of maldistribution, it is possible to design commercial packed columns for heights of 8 to 9 m between redistributors.

End Effects Analysis of the mass-transfer efficiency of a packed column should take into account that transfer which takes place outside the bed, i.e., at the ends of the packed sections. Inlet gas may very well contact exit liquid below the bottom support plate, and exit gas can contact liquid from some types of distributors (e.g., spray nozzles). The bottom of the column is the more likely place for transfer, and Silver and Keller [*Chem. Eng. Prog.*, **62**(1), 68 (1966)] found that the

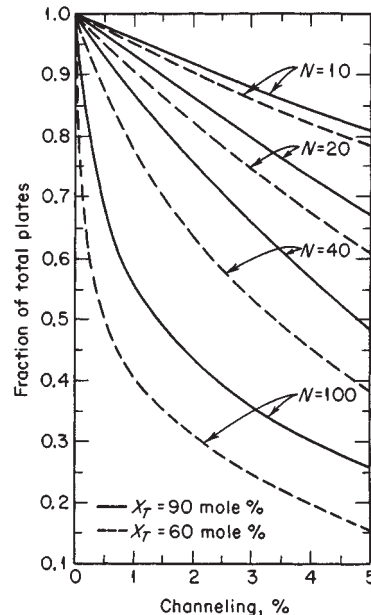


FIG. 14-65 Effect of liquid channeling on column efficiency for a system with a relative volatility of 1.07. Total number of theoretical plates N of 10, 20, 40, and 100 at top liquid composition X of 90 and 60 mole percent. [Manning and Cannon, *Ind. Eng. Chem.*, **49**, 347 (1957).]

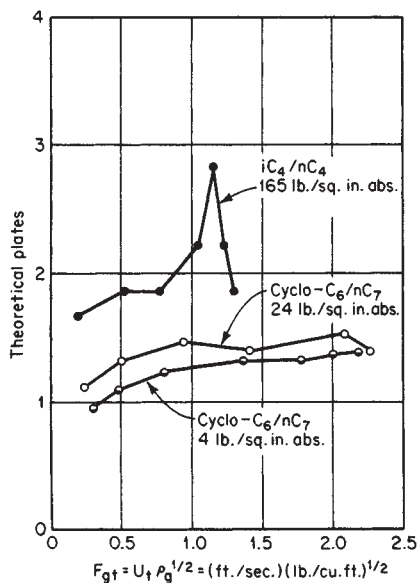


FIG. 14-66 Efficiency of FRI reboiler and space below bottom support plate. To convert pounds per square inch absolute to kilopascals, multiply by 6.8947; to convert (feet per second) (pounds per cubic foot)^{1/2}, to (meters per second) (kilograms per cubic meter)^{1/2}, multiply by 1.2199. [Silvey and Keller, Chem. Eng. Prog., **62**(1), 68 (1966).]

reboiler plus the end effect could give up to two or more theoretical plates (Fig. 14-66).

Interfacial Area The effective area of contact between gas and liquid is that area which participates in the gas-liquid mass-exchange process. This area may be less than the actual interfacial area because of stagnant pools where liquid reaches saturation and no longer participates in the transfer process.

Effective area should not be confused with "wetted area." While film flow of liquid across the packing surface is a contributor, effective area includes also contributions from rivulets, drippings, and gas bubbles. Because of this complex physical picture, effective interfacial area is difficult to measure directly.

Weisman and Bonilla [*Ind. Eng. Chem.*, **42**, 1099 (1950)] determined effective area a_t of 25-mm (1-in) Raschig rings indirectly through the relationship $a_t = (k_g a_t)/k_g$. The k_g data were obtained via evaporation of water from presaturated rings by Taecker and Hougen [*Chem. Eng. Prog.*, **45**, 188 (1949)] and the vaporization $k_g a_t$ data from McAdams et al. [*Chem. Eng. Prog.*, **45**, 241 (1949)] for the air-water irrigated system. The authors proposed that

$$\frac{a_t}{a_t} = 0.54 G^{0.31} L^{0.07} \quad (14-165)$$

for the range of liquid rates from 4 to 17 kg/(s·m²) [2950 to 12,537 lb/(h·ft²)], and where a_t = external surface area of the packing (Table 14-7). In Eq. (14-165), both gas and liquid rates, G and L , are in kg/(s·m²). Areas are in consistent units.

A greater dependency on liquid rate was reported by Shulman et al. [*Am. Inst. Chem. Eng. J.*, **1**, 253 (1955)], who obtained the effective area via vaporization of packing constructed of naphthalene and from calculated ammonia absorption data of Fellinger (Sc.D. thesis, Massachusetts Institute of Technology, 1941), taking account of liquid-phase resistance. On the basis of gross system conditions, the values obtained are indicated in Fig. 14-67 for 25-mm (1-in) Raschig rings and Berl saddles. These packing types in the 12-, 38-, and 50-mm (0.5-, 1.5-, and 2.0-in) sizes were also studied.

Yoshida and Koyanagi [*Am. Inst. Chem. Eng. J.*, **8**, 309 (1962)] used the Weisman-Bonilla approach, accepting the Taecker-Hougen k_g data and making their own $k_g a_t$ measurements under vaporization, absorption, and distillation conditions. They found that the effective

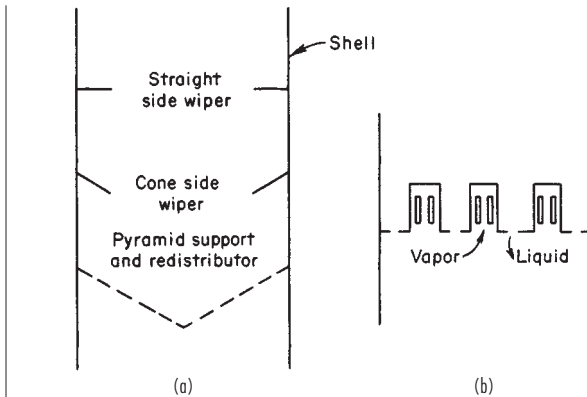


FIG. 14-67 Effective interfacial area based on data of Fellinger. (a) 1-in Raschig rings. (b) 1-in Berl saddles. To convert square feet per cubic foot to square meters per cubic meter, multiply by 3.28; to convert pounds per hour-square foot to kilograms per second-square meter, multiply by 0.001356. [Shulman, Am. Inst. Chem. Eng. J., **1**, 257 (1955).]

area differs between vaporization and absorption, as shown in Fig. 14-68. For distillation, they found effective areas to be different for systems with different surface tensions (Fig. 14-69) but, upon making the surface-tension correction, concluded that areas for distillation are approximately the same as those for absorption.

For structured packings, Rocha et al. [*Ind. Eng. Chem. Res.*, **35**, 1660 (1996)] adapted the model of Shi and Mersmann [*Ger. Chem. Eng.*, **8**, 87 (1985)] to predict effective wetted area:

$$\frac{a_t}{a_t} = F_{SE} \frac{29.12 (We_L Fr_L)^{0.15} S^{0.35}}{Re_L^{0.2} \epsilon^{0.6} (1 - 0.93 \cos \gamma) (\sin \theta)^{0.3}} \quad (14-166)$$

where $We_L = (U_L^2 \rho_L S) / (\sigma g_c)$ = Weber number for liquid
 $Fr_L = U_L^2 / Sg$ = Froude number for liquid
 S = side dimension of corrugation (Fig. 14-51), m
 $Re_L = (U_L S \rho_L) / \mu_L$
 ϵ = void fraction of packing
 γ = contact angle (degrees)
 θ = angle of corrugation channel with horizontal (degrees)
 F_{SE} = factor for surface enhancement

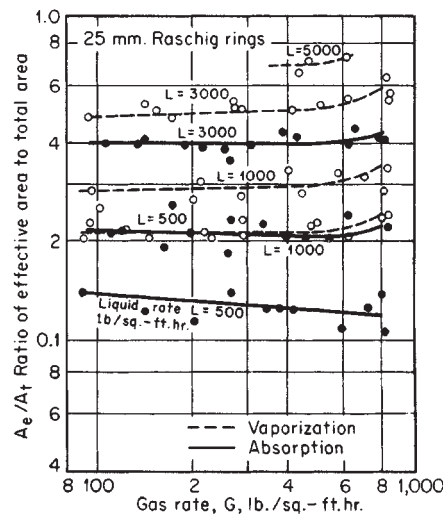


FIG. 14-68 Effective areas for 25-mm Raschig rings. To convert pounds per hour-square foot to kilograms per second-square meter, multiply by 0.001356. [Yoshida and Koyanagi, Am. Inst. Chem. Eng. J., **8**, 309 (1962).]

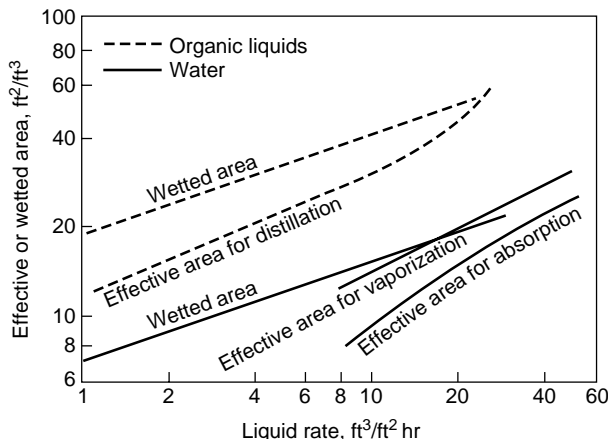


FIG. 14-69 Comparison of effective and wetted areas, 25-mm Raschig rings. To convert cubic feet per square foot-hour to cubic meters per square meter-second, multiply by 8.47×10^{-5} ; to convert square feet per cubic foot to square meters per cubic meter, multiply by 3.28. [Yoshida and Koyanagi, Am. Inst. Chem. Eng. J., 8, 309 (1962).]

Values of F_{SE} range from 0.009 for a smooth metal surface with small perforations, to 0.029 for a pierced metal surface. The contact angle is a key parameter for wettability and was related to the surface tension by Shi and Mersmann. This accounts for the differences in wettability found by Yoshida and Koyanagi (Fig. 14-69). In general, aqueous systems will wet ceramic surfaces better than metal surfaces, unless the latter are oxidized.

Mass Transfer Relationships for calculating rates of mass transfer between gas and liquid in packed absorbers, strippers, and distillation columns may be found in Sec. 5 and are summarized in Table 5-28. The two-resistance approach is used, with rates expressed as transfer units:

$$H_{OG} = H_G + \lambda H_L \quad (14-167)$$

where H_{OG} = height of an overall transfer unit, gas concentration basis, m

H_G = height of a gas-phase transfer unit, m

H_L = height of a liquid-phase transfer unit, m

$\lambda = m/(Lm/Gm)$ = slope of equilibrium line/slope of operating line

The various models for predicting values of H_G and H_L are given in Sec. 5. The important parameters in the models include gas rate, liquid rate, gas and liquid properties (density, viscosity, surface tension, diffusivity), packing type and size, and overall bed dimensions.

In design practice, a less rigorous parameter, HETP, is used as an index of packing efficiency. The HETP is the height of packed bed required to achieve a theoretical stage. The terms H_{OG} and HETP may be related under certain conditions:

$$\text{HETP} = H_{OG} \left[\frac{\ln \lambda}{(\lambda - 1)} \right] \quad (14-168)$$

and since

$$Z_p = (H_{OG})(N_{OG}) = (\text{HETP})(N_t) \quad (14-169)$$

$$N_{OG} = N_t [\ln \lambda / (\lambda - 1)] \quad (14-170)$$

Equations (14-168) and (14-170) have been developed for binary mixture separations and hold for cases where the operating line and equilibrium line are straight. Thus, when there is curvature, the equations should be used for sections of the column where linearity can be assumed. When the equilibrium line and operating line have the same slope, $\text{HETP} = H_{OG}$ and $N_{OG} = N_t$ (theoretical stages).

In practice, the following procedure is normally used:

1. Determine theoretical stages for the separation: binary or multi-component.

2. Convert theoretical stages to transfer units using Eq. (14-170).
3. Determine the height of an overall transfer unit H_{OG} using methods given in Sec. 5, Table 5-28. For a multicomponent mixture, the key components are often used in determining H_{OG} .

4. Calculate the required packed bed height by Eq. (14-169).

Behavior of Various Systems and Packings For orientation purposes, it is helpful to have representative data available for packing performance under a variety of conditions. In the preceding edition of this handbook, extensive data on absorption/stripping systems were given. Emphasis was given to the following systems:

Ammonia-air-water	Liquid and gas phases contributing; chemical reaction contributing
Air-water	Gas phase controlling
Sulfur dioxide-air-water	Liquid and gas-phase controlling
Carbon dioxide-air-water	Liquid phase controlling

The reader may refer to the data in the preceding edition. For the current work, emphasis will be given to one absorption system, carbon dioxide-air-caustic, and to several distillation systems.

Carbon Dioxide-Air-Caustic System The vendors of packings have adopted this system as a "standard" for comparing the performance of different packing types and sizes. For tests, air containing 1.0 mol % CO_2 is passed countercurrently to a circulating stream of sodium hydroxide solution. The initial concentration of NaOH in water is 1.0 N (4.0 wt %), and as the circulating NaOH is converted to sodium carbonate it is necessary to make a mass-transfer correction because of reduced mass-transfer rate in the liquid phase. The procedure has been described by Eckert et al. [Ind. Eng. Chem., 59(2), 41 (1967); Chem. Eng. Progr., 54(1), 790 (1958)]. An overall coefficient is measured using gas-phase (CO_2) concentrations:

$$K_{OGa_e} = \frac{\text{moles CO}_2 \text{ absorbed}}{\text{time-bed volume-partial pressure CO}_2 \text{ driving force}} \quad (14-171)$$

The coefficients are usually corrected to a hydroxide conversion of 25 percent at 24°C. For other conversions, Fig. 14-15 may be used. Reported values of K_{OGa} for representative random packings are given in Table 14-8. The effect of liquid rate on the coefficient is shown in Figs. 14-70 and 14-71.

While the carbon dioxide/caustic test method has become accepted, one should use the results with caution. The chemical reaction masks the effect of physical absorption, and the relative values in the table may not hold for other cases, especially distillation applications where much of the resistance to mass transfer is in the gas phase. Background on this combination of physical and chemical absorption may be found earlier in the present section, under "Absorption with Chemical Reaction."

Distillation Applications Packings are now routinely considered for distillation columns with diameters up to 10 m or more. The pressure drop advantages of the modern, through-flow random pack-

TABLE 14-8 Overall Coefficients for Representative Packings

CO ₂ -air-caustic system		
	Nominal size, mm	Overall coefficient K_{OGa} , kg-moles/(hr·m ³ ·atm)
Ceramic raschig rings	25	37.0
	50	26.1
Ceramic Intalox saddles	25	45.1
	50	30.1
Metal pall rings	25	49.6
	50	34.9
Metal Intalox saddles (IMTP®)	25	54.8
	50	39.1

NOTE: Basis for reported values: CO₂ concentration in inlet gas, 1.0 vol %; 1N NaOH solution in water, 25 percent NaOH conversion; temperature = 24°C; atmospheric pressure: gas rate = 1.264 kg/(s·m³); liquid rate = 6.78 kg/(s·m²).

SOURCE: Strigle, R. L., *Random Packings and Packed Towers*, Gulf Publ. Co., Houston, 1987.

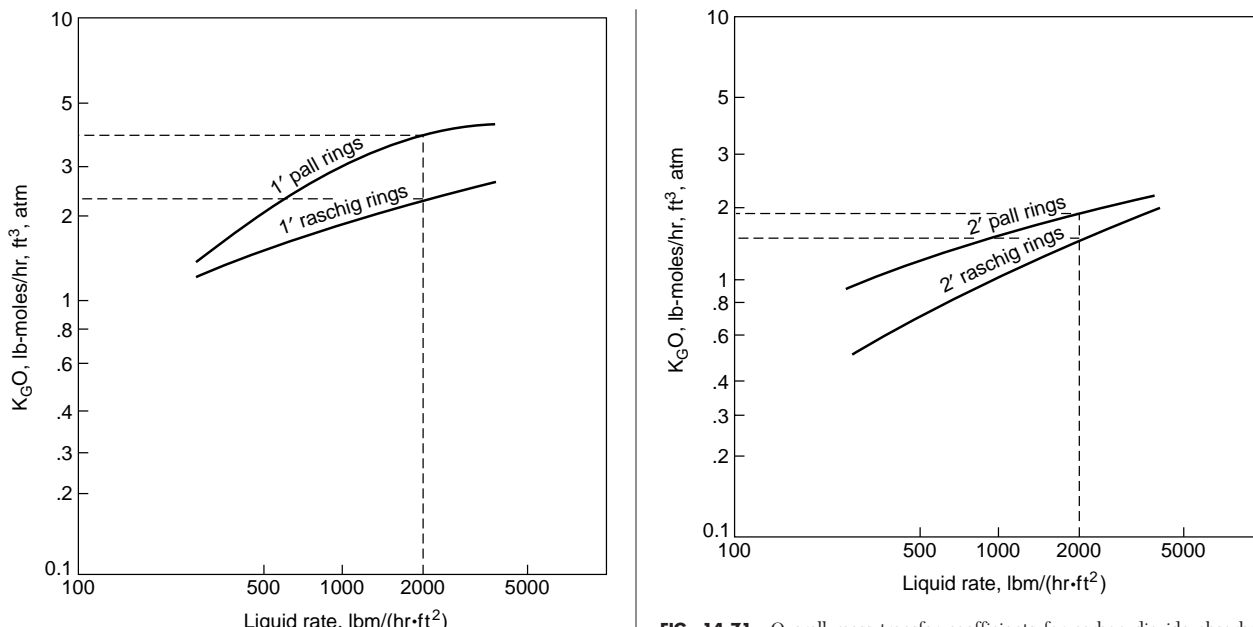


FIG. 14-70 Overall mass transfer coefficients for carbon dioxide absorbed from air by 1N caustic solution. Packing = 1-inch metal raschig and pall rings. Air rate = $0.61 \text{ kg/s} \cdot \text{m}^2$ ($450 \text{ lb/hr} \cdot \text{ft}^2$). To convert $\text{lb/hr} \cdot \text{ft}^2$ to $\text{kg/s} \cdot \text{m}^2$, multiply by 0.00136; to convert $\text{lb-moles/hr} \cdot \text{ft}^3 \text{ atm}$ to $\text{kg-moles/s} \cdot \text{m}^3 \text{ atm}$, multiply by 0.00445. [Eckert *et al.*, Chem. Eng. Progr., 54(1), 70 (1958).]

ings and the ordered, structured packings have made vacuum column applications of particular interest. Test data for total reflux distillations have become available from several sources, such as Fractionation Research, Inc. and The University of Texas at Austin Separations Research Program. Examples of the data from these and other

FIG. 14-71 Overall mass transfer coefficients for carbon dioxide absorbed from air by 1N caustic solution. Packing = 2-inch metal raschig and pall rings. Air rate = $0.61 \text{ kg/s} \cdot \text{m}^2$ ($450 \text{ lb/hr} \cdot \text{ft}^2$). To convert from $\text{lb/hr} \cdot \text{ft}^2$ to $\text{kg/s} \cdot \text{m}^2$, multiply by 0.00136. To convert from $\text{lb-moles/hr} \cdot \text{ft}^3 \text{ atm}$ to $\text{kg-moles/s} \cdot \text{m}^3 \text{ atm}$, multiply by 0.0045. [Eckert *et al.*, Chem. Eng. Progr., 54(1), 70 (1958).]

sources are shown in Figs. 14-72–14-75. The comparative efficiency of different sizes of random packing is shown in Fig. 14-72. As would be expected, the smaller packings have higher mass-transfer efficiency (lower values of HETP). However, their capacity is limited. The equivalent pressure drop data are shown in Fig. 14-73, where the smaller packings are shown to have higher pressure drop.

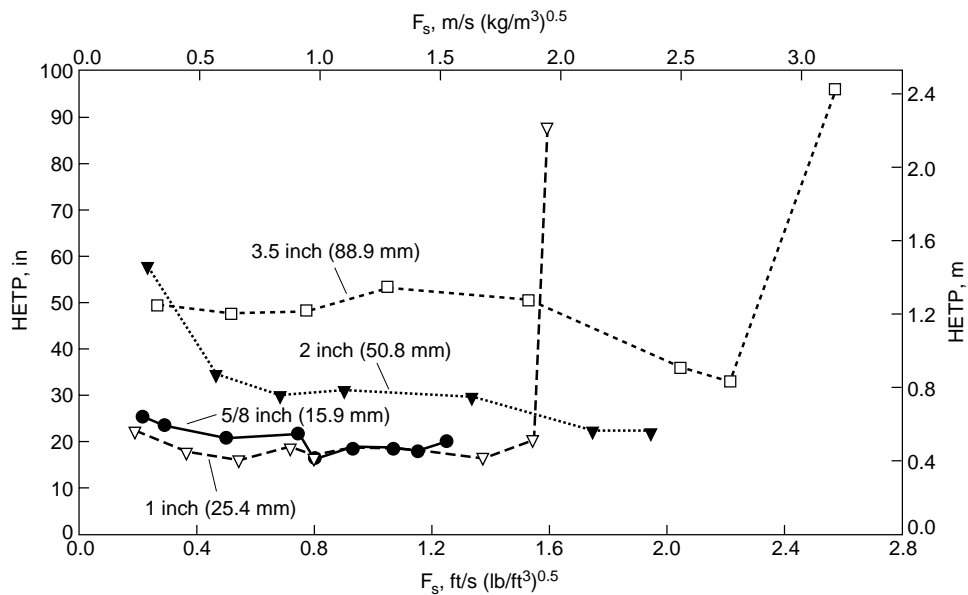


FIG. 14-72 HETP values for four sizes of metal pall rings, vacuum operation. Cyclohexane/n-heptane system, total reflux, 35 kPa (5.0 psia). Column diameter = 1.2 m (4.0 ft). Bed height = 3.7 m (12 ft). Distributor = tubed drip pan, 100 streams/ m^2 . [Adapted from Sharif and Kunesh, Ind. Eng. Chem. Res., 34, 1273 (1995).] Reproduced with permission. Copyright © 1995 American Chemical Society.

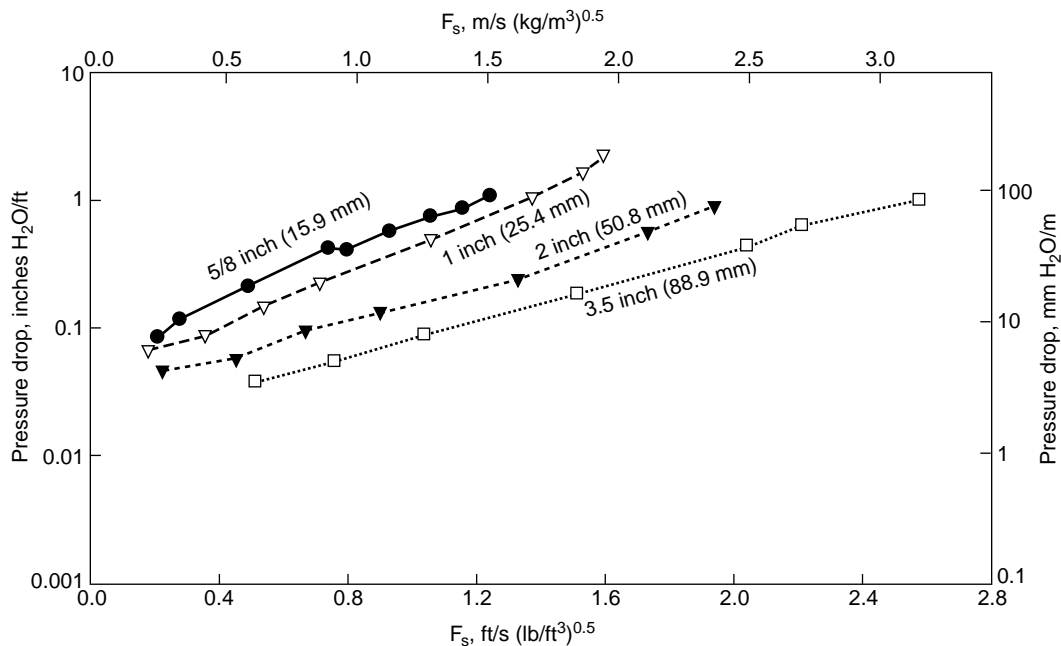


FIG. 14-73 Pressure-drop data for several sizes of pall rings; test conditions same as described for Fig. 14-72. [Shariat and Kunesh, Ind. Eng. Chem. Res., 34, 1273 (1995).] Reproduced with permission. Copyright © 1995 American Chemical Society.

Efficiency data for a representative structured packing at two column diameters are shown in Fig. 14-74. The Max-Pak® packing has a surface area of $246 \text{ m}^2/\text{m}^3$ ($75 \text{ ft}^2/\text{ft}^3$). The same test mixture (cyclohexane/n-heptane) and operating pressure was used for both tests. It would appear that column diameter does not have an influence in this range of values (0.43 to 1.2 m).

Efficiency and pressure drop data for Sulzer BX metal gauze structured packing and for three test mixtures are shown in Fig. 14-75. For the ethyl benzene/styrene test mixture, the effect of operating pressure is shown. The high viscosity mixture, propylene glycol/ethylene

glycol, has a significantly lower efficiency than the other mixtures but does not appear to have a lower capacity.

LIQUID-DISPersed CONTACTORS

Introduction There are two types of gas-liquid contactors where the liquid is deliberately dispersed. In the most common, a spray nozzle is used to generate droplets. A second type is the pipeline contactor, where the entrainment generated by flowing gas generates the droplets.

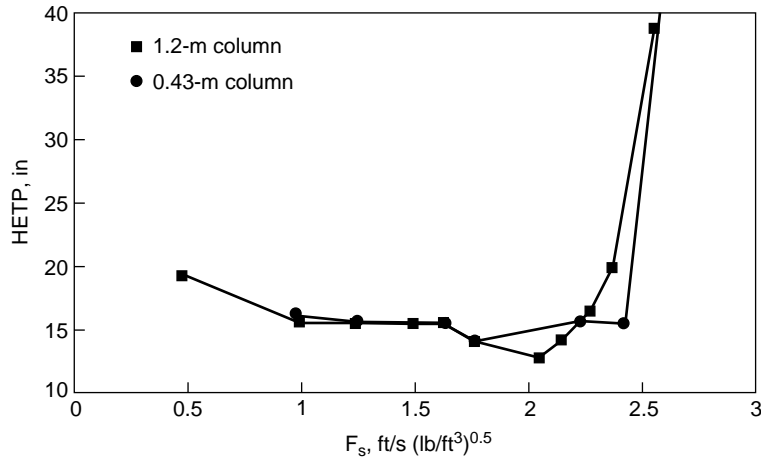


FIG. 14-74 HETP values for Max-Pak structured packing, 35 kPa (5 psia), two column diameters. Cyclohexane/n-heptane system, total reflux. For 0.43 m (1.4 ft) column: perforated pipe distributor, 400 streams/m², 3.05 m (10 ft) bed height. For 1.2 m (4.0 ft) column: tubed drip pan distributor, 100 streams/m², 3.7 m (12 ft) bed height. Smaller column data, University of Texas/Austin; Larger column data, Fractionation Research, Inc. To convert $(\text{ft/s})(\text{lb}/\text{ft}^3)^{0.5}$ to $(\text{m/s})(\text{kg}/\text{m}^3)^{0.5}$, multiply by 1.2199. (Courtesy Jaeger Products, Inc., Houston, Texas.)

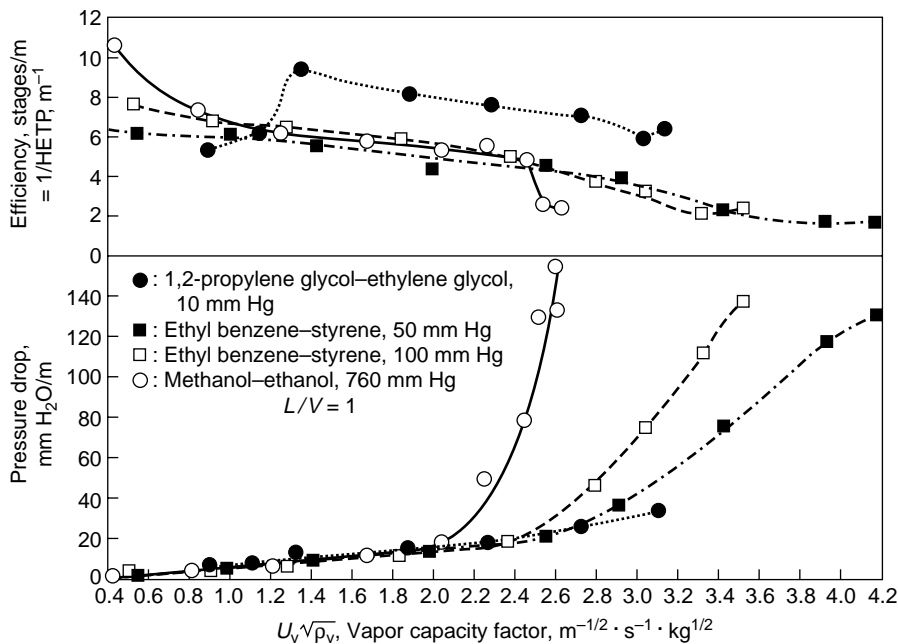


FIG. 14-75 Efficiency and pressure drop data for Sulzer BX structured packing. Test mixtures and operating pressures shown on graph. Total reflux, 0.8 m (2.6 ft) column diameter, ca. 2 m (6.5 ft bed height, perforated pipe distributor, 400 streams/m²). To convert (m/s)(kg/m³)^{0.5} to (ft/s)(lb/ft³)^{0.5}, multiply by 0.8197. [Billet, Conrad, and Grubbs, I. Chem. E. Symp. Serv. 5(32), 111 (1969).]

Because of the minimal internals for solids to grow on, both types of contactors are common in fouling services. The spray nozzle based devices are also inherently low pressure drop.

The disadvantage is that volumetric efficiency is usually much less than conventional trays or packed contactors. Applications are usually limited to cases when only a few transfer units or a single equilibrium stage is required. Since many of these applications tend to be in heat-transfer service, the following discussion will be in terms of thermal properties and thermal measures of performance.

Heat-Transfer Applications Heat-transfer analogs of common mass-transfer terms are:

$$\text{No. of gas-phase transfer units} = \frac{T_{g,\text{out}} - T_{g,\text{in}}}{(T_g - T_i)_{\text{mean}}} = N_g \quad (14-172)$$

$$\text{No. of liquid-phase transfer units} = \frac{T_{\ell,\text{out}} - T_{\ell,\text{in}}}{(T_\ell - T_i)_{\text{mean}}} = N_\ell \quad (14-173)$$

$$\text{Gas-phase volumetric transfer rate} = \frac{Gc_p}{H_g} = h_g a \quad (14-174)$$

$$\text{Diffusivity} = \frac{k}{\rho c_p} = \alpha_T \quad (14-175)$$

where T_g = gas temperature

T_ℓ = liquid temperature

T_i = interface temperature

H_g = height of a gas-phase transfer unit

G = weight gas flow/area

c_p = specific heat

ρ = density

k = thermal conductivity

α_T = thermal diffusivity

Note that the relative performance of a device can be converted from a mass-transfer basis to a heat-transfer basis by introducing these analogies into the rate equations.

The conversion is simplest when $K_g a$ and $K_\ell a$ are defined in terms of mole-fraction driving force:

$$\frac{h_g a}{K_g a} \text{ or } \frac{h_\ell a}{K_\ell a} = \frac{c_p}{M} \left(\frac{\alpha_T}{D} \right)^{0.5} \quad (14-176)$$

where $h_g a, h_\ell a$ = volumetric heat-transfer rate

$K_g a, K_\ell a$ = volumetric mass-transfer rate

c_p = heat capacity

M = molecular weight

α_T/D = ratio of thermal diffusivity to molecular diffusivity, dimensionless

For gases, α_T/D is usually close to 1, since the same basic transfer mechanism exists. For liquids, α_T/D is invariably much greater than 1. A simplified model yields the relation

$$\frac{\alpha_T}{D} = 1.9 \times 10^7 (\mu/T) \quad (14-177)$$

where μ is in Pa·s and T is in K. For a 1-cP (10^{-3} Pa·s) liquid at 310 K, this gives a ratio of 61. This means that a closer approach to equilibrium can be obtained for heat transfer applications that are liquid-limited (such as in condensation of a pure vapor), than can be obtained for mass transfer liquid-limited applications.

Theoretical Transfer Model Transfer from single droplets is theoretically well defined for the gas side. For a droplet moving counter to a gas, interfacial area is (in consistent units)

$$a = \left(\frac{G_\ell}{\rho_\ell (U_\ell - U_g)} \right) \left(\frac{6}{D_d} \right) \quad (14-178)$$

where a = interfacial area/volume

G_ℓ = liquid-flow rate (weight/cross-sectional area)

ρ_ℓ = liquid density

U_ℓ = liquid velocity relative to the gas, often approximately the terminal velocity of droplets (see Sec. 6 for estimation)

U_g = superficial gas velocity

D_d = droplet diameter

14-56 GAS ABSORPTION AND GAS-LIQUID SYSTEM DESIGN

The transfer coefficient is defined by (in inconsistent units)

$$h_g = (k/D_d) (2 + 0.6N_{Re}^{0.5} N_{Pr}^{0.33}) \quad (14-179)$$

where h_g = transfer coefficient

k = thermal conductivity of gas

N_{Re} = Reynolds number = $D_d U_t \rho_g / \mu_g$

N_{Pr} = Prandtl number = $(c_p \mu / k)_g$

The volumetric coefficient $h_g a$ from the combination of Eqs. (14-178) and (14-179) is useful in defining the effect of variable changes but is limited in value because of its dependence on D_d . The product of area and coefficient obtained from a given mass of liquid is proportional to $(1/D_d)^2$ for small diameters. The prime problem is that droplet-size estimating procedures are often no better than ± 50 percent. A secondary problem is that there is no D_d that truly characterizes either the motion or transfer process for the whole spectrum of particle sizes present. See Eqs. (14-193) and (14-194).

The corresponding theory for transfer in the liquid phase is even less certain. If one had static drops, the transfer would be

$$N_t = 0.5 + \frac{4(k/\rho c_p) \pi^2 t}{D_d^2} \text{ (dimensionless)} \quad (14-180)$$

where N_t = liquid-phase transfer units [Eq. (14-173)]

k = liquid thermal conductivity

ρ = liquid density

c_p = liquid specific heat

D_d = droplet diameter

t = time of contact

However, the static-drop assumption is usually extremely conservative. For example, the high interfacial velocity in the spray from nozzles yields a high degree of internal mixing and much higher transfer.

Countercurrent, Cocurrent, or Backmixed Spray-chamber contactors rarely approach countercurrent performance. Backmixing is hard to prevent and often limiting. Backmixing is so severe that many designers simply limit spray-chamber performance to a single equilibrium stage regardless of height. For a direct-contact heat-transfer device, this means that the temperatures of the exiting gas and liquid would be equal. The main cause of the high degree of backmixing is that there is no stabilizing pressure drop caused by packing of plates. Consequently the chief resistance to gas flow is the rain of drops. Anything less than perfect liquid distribution will induce a dodging action in the opposed vapor flow. The result is the development of large eddies and bypass streams. Other sources of deviation from countercurrent flow are large drops falling faster than small ones and liquid striking the walls. About all that can be done is to take special care to obtain a uniform spray pattern with minimum collection at the walls.

Empirical Approach

Sprays Large units generally yield approximately one equilibrium stage even when in nominal counter current flow. See Masters, [*Spray Drying Handbook*, 5th ed., Wiley, New York, (1991)]. For smaller towers, less than one equilibrium stage is typical. Transfer units can be estimated from the data of Pigford and Pyle [*Ind. Eng. Chem.*, **43**, 1949 (1951)]. These data show the height of a gas-limited transfer unit to be 1 to 3 m (3 to 12 ft). Pigford and Pyle show much shorter heights for a liquid-limited transfer unit, in the range of 0.5 to 1 m (1.5 to 3 ft). The high liquid transfer rates result from the high energy dissipation in the liquid and the enhanced transfer at the time of droplet formation. The same behavior is indicated by Simpson and Lynn [*Am. Inst. Chem. Eng. J.*, **23**(5), 666 (1977)], who show a 75 to 95 percent approach to equilibrium stripping in a 1.4-m-tall spray contact in a liquid-limited system.

Pipeline Flow (Quenching) For the case of pipeline quenching, the flows are cocurrent. How closely the gas temperature approaches the liquid depends on e^{-N_g} , where N_g varies with $1/(droplet\ diameter)^2$.

Since the predicted droplet diameter at high velocity pipeline flow varies with $(1/velocity)^{1/2}$, as shown by Eq. (14-201), the volumetric performance is strongly dependent on velocity:

$$N_g = \text{constant} \cdot (\text{velocity})^{2.4} \quad (14-181)$$

An empirical point in support of the strong velocity dependence is the rule of thumb for quenching, requiring a high relative velocity [>60 m/s (200 ft/s)].

Venturi scrubbers are similar in that they need high velocity to achieve small droplets. They are primarily employed for mist and dust collection and are discussed further in the mist-collection portion of this section.

WETTED-WALL COLUMNS

Wetted-wall or falling-film columns have found application in mass-transfer problems when high-heat-transfer-rate requirements are concomitant with the absorption process. Large areas of open surface are available for heat transfer for a given rate of mass transfer in this type of equipment because of the low mass-transfer rate inherent in wetted-wall equipment. In addition, this type of equipment lends itself to annular-type cooling devices.

Gilliland and Sherwood [*Ind. Eng. Chem.*, **26**, 516 (1934)] found that, for vaporization of pure liquids in air streams for streamline flow,

$$\frac{k_g D}{D_g} \frac{P_{BM}}{\pi} = 0.023 N_{Re}^{0.83} N_{Sc}^{0.44} \quad (14-182)$$

where D_g = diffusion coefficient

D = inside diameter of tube

k_g = mass-transfer coefficient, gas phase

Note that the group on the left side of Eq. (14-182) is dimensionless. When turbulence promoters are used at the inlet-gas section, an improvement in gas mass-transfer coefficient for absorption of water vapor by sulfuric acid was observed by Greenewalt [*Ind. Eng. Chem.*, **18**, 1291 (1926)]. A falling off of the rate of mass transfer below that indicated in Eq. (14-182) was observed by Cogan and Cogan (thesis, Massachusetts Institute of Technology, 1932) when a calming zone preceded the gas inlet in ammonia absorption (Fig. 14-76).

In work with the hydrogen chloride-air-water system, Dobratz, Moore, Barnard, and Meyer [*Chem. Eng. Prog.*, **49**, 611 (1953)] using a cocurrent-flow system found that $k_g \propto G^{1.8}$ (Fig. 14-77) instead of the 0.8 power as indicated by the Gilliland equation. Heat-transfer coefficients were also determined in this study. The radical increase in heat-transfer rate in the range of $G = 30 \text{ kg}/(\text{s} \cdot \text{m}^2)$ [20,000 lb/(h-ft²)] was similar to that observed by Tepe and Mueller [*Chem. Eng. Prog.*, **43**, 267 (1947)] in condensation inside tubes.

Gaylord and Miranda [*Chem. Eng. Prog.*, **53**, 139M (1957)] using a multitube cocurrent-flow falling-film hydrochloric acid absorber for hydrogen chloride absorption found

$$K_g = \frac{1.66(10^{-5})}{M_m^{1.75}} \left(\frac{DG}{\mu} \right) \quad (14-183)$$

where K_g = overall mass-transfer coefficient, $(\text{kg} \cdot \text{mol})/(\text{s} \cdot \text{m}^2 \cdot \text{atm})$

M_m = mean molecular weight of gas stream at inlet to tube

D = diameter of tube, m

G = mass velocity of gas at inlet to tube, $\text{kg}/(\text{s} \cdot \text{m}^2)$

μ = viscosity of gas, Pa-s

Note that the group DG/μ is dimensionless. This relationship also satisfied the data obtained for this system, with a single-tube falling-film unit, by Coull, Bishop, and Gaylor [*Chem. Eng. Prog.*, **45**, 506 (1949)].

The rate of mass transfer in the liquid phase in wetted-wall columns is highly dependent on surface conditions. When laminar-flow conditions prevail without the presence of wave formation, the laminar-penetration theory prevails. When, however, ripples form at the surface, and they may occur at a Reynolds number exceeding 4, a significant rate of surface regeneration develops, resulting in an increase in mass-transfer rate.

If no wave formations are present, analysis of behavior of the liquid-film mass transfer as developed by Hatta and Katori [*J. Soc. Chem. Ind.*, **37**, 280B (1934)] indicates that

$$k_\ell = 0.422 \sqrt{\frac{D_F \Gamma}{\rho B_F^2}} \quad (14-184)$$

where $B_F = (3u\Gamma/\rho^2 g)^{1/3}$

D_ℓ = liquid-phase diffusion coefficient, m^2/s

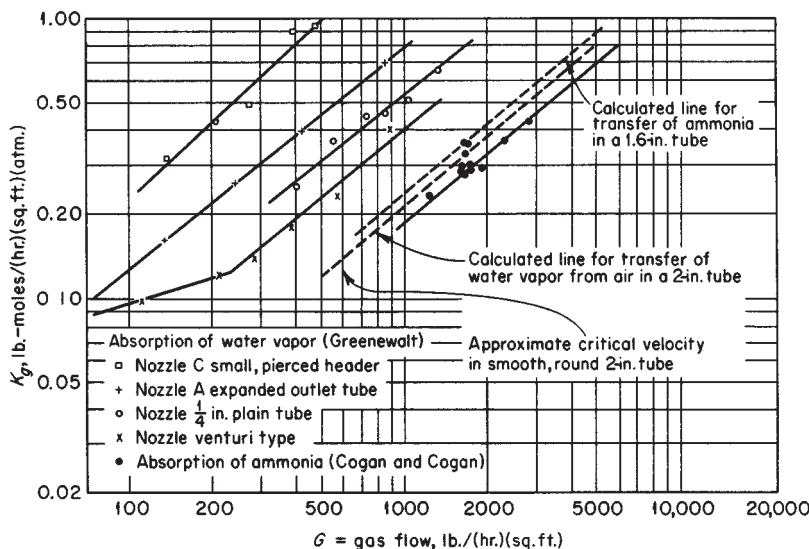


FIG. 14-76 Mass-transfer rates in wetted-wall columns having turbulence promoters. To convert pound-moles per hour-square foot-atmosphere to kilogram-moles per second-square meter-atmosphere, multiply by 0.00136; to convert pounds per hour-square foot to kilograms per second-square meter, multiply by 0.00136; and to convert inches to millimeters, multiply by 25.4. (Data of Greenewalt and Cogan, *Sherwood, and Pigford, Absorption and Extraction, 2d ed.*, McGraw-Hill, New York, 1952.)

ρ = liquid density, kg/m^3

Z = length of surface, m

k_ℓ = liquid-film-transfer coefficient, $(\text{kg}\cdot\text{mol})/[(\text{s}\cdot\text{m}^2)(\text{kg}\cdot\text{mol})/\text{m}^3]$

Γ = liquid-flow rate, $\text{kg}/(\text{s}\cdot\text{m})$ based on wetted perimeter

μ = viscosity of liquid, $\text{Pa}\cdot\text{s}$

g = gravity acceleration, 9.81 m/s^2

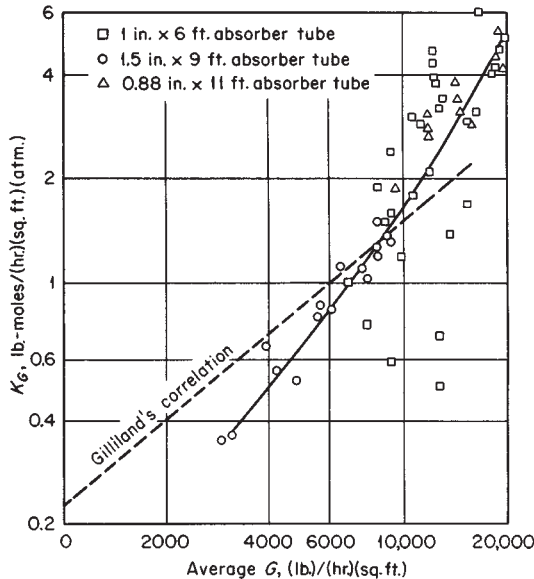


FIG. 14-77 Mass-transfer coefficients versus average gas velocity—HCl absorption, wetted-wall column. To convert pound-moles per hour-square foot-atmosphere to kilogram-moles per second-square meter-atmosphere, multiply by 0.00136; to convert pounds per hour-square foot to kilograms per second-square meter, multiply by 0.00136; to convert feet to meters, multiply by 0.305; and to convert inches to millimeters, multiply by 25.4. [Dobratz *et al.*, Chem. Eng. Prog., **49**, 611 (1953).]

When Z is large or $\Gamma/\rho B_F$ is so small that liquid penetration is complete,

$$k_\ell = 11.800 D_\ell / B_F \quad (14-185)$$

and

$$H_\ell = 0.95 \Gamma B_F / D_\ell \quad (14-186)$$

A comparison of experimental data for carbon dioxide absorption obtained by Hatta and Katori (op. cit.), Grimley [*Trans. Inst. Chem. Eng.*, **23**, 228 (1945)], and Vyazov [*Zh. Tekh. Fiz. (U.S.S.R.)*, **10**, 1519 (1940)] and for absorption of oxygen and hydrogen by Hodgson (S. M. thesis, Massachusetts Institute of Technology, 1949), Henley (B.S. thesis, University of Delaware, 1949), Miller (B.S. thesis, University of Delaware, 1949), and Richards (B.S. thesis, University of Delaware, 1950) was made by Sherwood and Pigford (*Absorption and Extraction*, McGraw-Hill, New York, 1952) and is indicated in Fig. 14-78.

In general, the observed mass-transfer rates are greater than those predicted by theory and may be related to the development of surface rippling, a phenomenon which increases in intensity with increasing liquid path.

Vivian and Peaceman [*Am. Inst. Chem. Eng. J.*, **2**, 437 (1956)] investigated the characteristics of the $\text{CO}_2\text{-H}_2\text{O}$ and $\text{Cl}_2\text{-HCl}$, H_2O system in a wetted-wall column and found that gas rate had no effect on the liquid-phase coefficient at Reynolds numbers below 2200. Beyond this rate, the effect of the resulting rippling was to increase significantly the liquid-phase transfer rate. The authors proposed a behavior relationship based on a dimensional analysis but suggested caution in its application concomitant with the use of this type of relationship. Cognizance was taken by the authors of the effects of column length, one to induce rippling and increase of rate of transfer, one to increase time of exposure which via the penetration theory decreases the average rate of mass transfer in the liquid phase. The equation is

$$\frac{k_\ell h}{D_\ell} = 0.433 \left(\frac{\mu_\ell}{\rho_\ell D_\ell} \right)^{1/2} \left(\frac{\rho_\ell^2 g h^3}{\mu_\ell^2} \right)^{1/6} \left(\frac{4\Gamma}{\mu_\ell} \right)^{0.4} \quad (14-187)$$

where D_ℓ = diffusion coefficient of solute in liquid

g = gravity-acceleration constant

h = length of wetted wall

k_ℓ = mass-transfer coefficient, liquid phase

Γ = mass rate of flow of liquid

μ_ℓ = viscosity of liquid

ρ_ℓ = density of liquid

The equation is dimensionless.

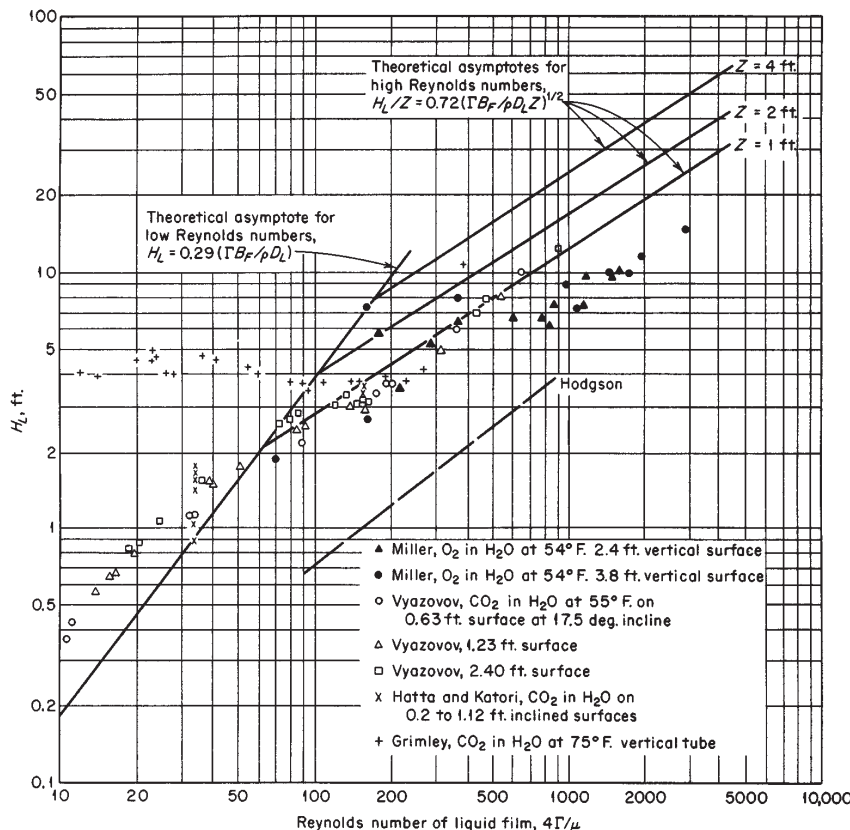


FIG. 14-78 Liquid-film resistance in absorption of gases in wetted-wall columns. Theoretical lines are calculated for oxygen absorption in water at 55°F. To convert feet to meters, multiply by 0.3048; °C = 5/9 (°F - 32). (*Sherwood and Pigford, Absorption and Extraction, 2d ed., McGraw-Hill, New York, 1952.*)

The effect of chemical reaction in reducing the effect of variation of the liquid rate on the rate of absorption in the laminar-flow regime was illustrated by the evaluation of the rate of absorption of chlorine in ferrous chloride solutions in a wetted-wall column by Gilliland, Baddour, and White [*Am. Inst. Chem. Eng. J.*, **4**, 323 (1958)].

Flooding in Wetted-Wall Columns When gas and liquid are in counterflow in wetted-wall columns, flooding can occur at high gas rates. Diehl and Koppany [*Chem. Eng. Prog.*, **65**, Symp. Ser. 42, 77 (1969)] correlated flooding data from a number of sources, including their own work, and developed the following expression:

$$U_f = F_1 F_2 \left(\frac{\sigma}{\rho_g} \right)^{1/2} \quad (14-188)$$

where U_f = flooding gas velocity, m/s

$F_1 = 1.22$ when $3.2 d_i/\sigma > 1.0$

$F_1 = 1.22 (3.2 d_i/\sigma)^{0.4}$ when $3.2 d_i/\sigma < 1.0$

$F_2 = (G/L)^{0.25}$

G/L = gas-liquid mass ratio

d_i = inside diameter of column, mm

σ = surface tension, mN/m (dyn/cm)

ρ_g = gas density, kg/m³

The data covered column sizes up to 50-mm (2-in) diameter; the correlation should be used with caution for larger columns.

GAS-LIQUID-COLUMN ECONOMICS

Estimation of column costs for preliminary process evaluations requires consideration not only of the basic type of internals but also

of their effect on overall system cost. For a distillation system, for example, the overall system can include the vessel (column), attendant structures, supports, and foundations; auxiliaries such as reboiler, condenser, feed heater, and control instruments; and connecting piping. The choice of internals influences all these costs, but other factors influence them as well. A complete optimization of the system requires a full-process simulation model that can cover all pertinent variables influencing economics.

Cost of Internals Installed costs of plates (trays) may be estimated from Fig. 14-79, with corrections for plate material taken from Table 14-9. For two-pass plates the cost is 15 to 20 percent higher. Approximate costs of dumped (random) packing materials may be obtained from Table 14-10, but it should be recognized that, because of competition, there can be significant variations in these costs from vendor to vendor. Also, packings sold in very large quantities carry discounts. In 1995, costs of structured packings, made from sheet metal, averaged \$90–\$110 per cubic foot, but the need for special distributors and redistributors can double the cost of structured packings on a volumetric basis. Note that for Fig. 14-79 and Table 14-9, the effective cost date is January 1990, with the Marshall and Swift cost index being taken as 904.

As indicated above, packed column internals include liquid distributors, packing support plates, redistributors (as needed), and hold-down plates (to prevent movement of packing under flow conditions). Costs of these internals for columns with random packing are given in Fig. 14-80, based on early 1976 prices, and a Marshall and Swift cost index of 460.

Cost of Column The cost of the vessel, including heads, skirt, nozzles, and ladderways, is usually estimated on the basis of weight.

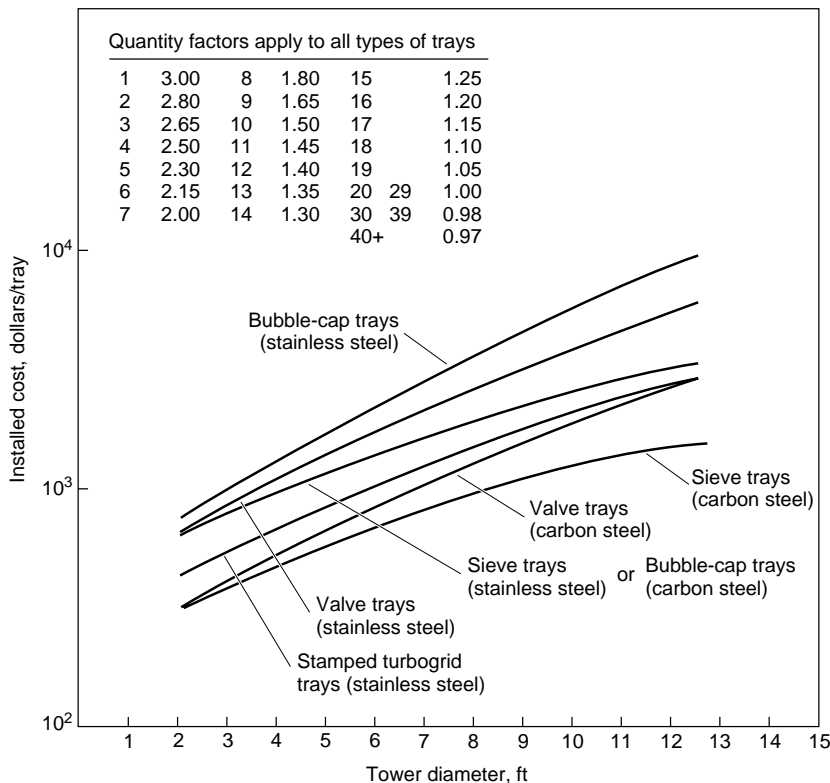


FIG. 14-79 Cost of trays in plate towers. Price includes tray deck, bubble caps, risers, downcomers, and structural-steel parts. The stainless steel designated is type 410 (*Peters and Timmerhaus, Plant Design and Economics for Chemical Engineers, 4th ed.*, McGraw-Hill, New York, 1991).

Figure 14-81 provides early 1990 cost data for the shell and heads, and Fig. 14-82 provides 1990 cost data for connections. For very approximate estimates of complete columns, including internals, Fig. 14-83 may be used. As for Figs. 14-81 and 14-82, the cost index is 904.

Plates versus Packings Bases for using packings instead of plates have been given earlier in this section. In many cases, either type of device may be used. For vacuum fractionations, the low pressure drop characteristics of throughflow random packings and structured packings tend to give them a distinct advantage over plates. On the other hand, structured packings and their many requirements, such as distributors, are more expensive than plates. For atmospheric

and pressure columns, the pressure-drop characteristics of packings are less important, and a decision may be made on installed cost and reliability of design methods. Kister et al. [*Chem. Eng. Progr.*, **90**(2), 23 (1994)] reported a study of the relative capacity and efficiency of plates, modern random packings, and structured packings. They found that, for each device optimally designed for the design require-

TABLE 14-10 Costs of Tower Packings, Uninstalled, January, 1990

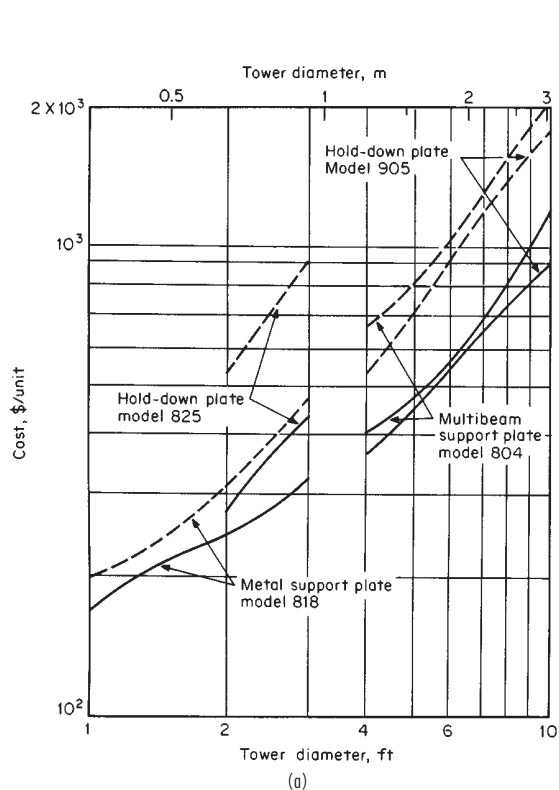
Prices in dollars per ft^3 , 100 ft^3 orders, f.o.b. manufacturing plant

	Size, in, $\$/\text{ft}^3$			
	1	1½	2	3
Raschig rings				
Chemical porcelain	12.8	10.3	9.4	7.8
Carbon steel	36.5	23.9	20.5	16.8
Stainless steel	155	117	87.8	—
Carbon	52	46.2	33.9	31.0
Intalox saddles				
Chemical stoneware	17.6	13.0	11.8	10.7
Chemical porcelain	18.8	14.1	12.9	11.8
Polypropylene	21.2	—	13.1	7.0
Berl saddles				
Chemical stoneware	27.0	21.0	—	—
Chemical porcelain	33.5	21.5	15.6	—
Pall rings				
Carbon steel	29.3	19.9	18.2	—
Stainless steel	131	99.0	86.2	—
Polypropylene	21.2	14.4	13.1	—

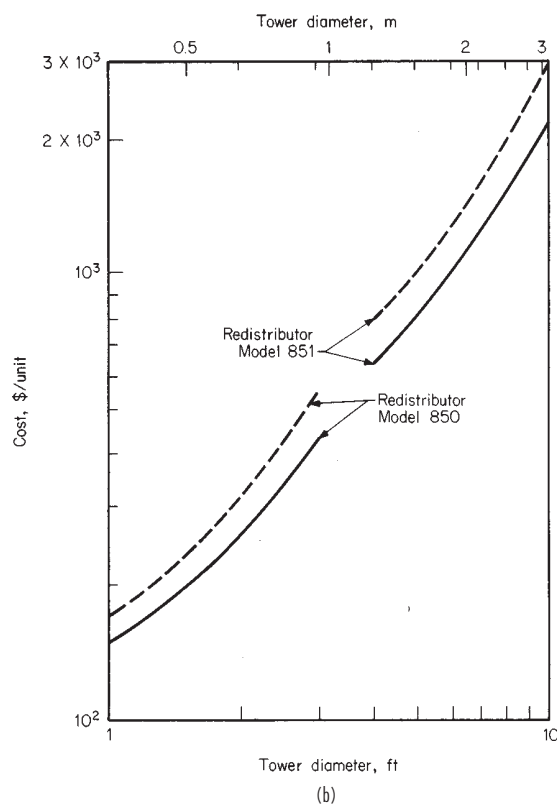
*Peters and Timmerhaus, *Plant Design and Economics for Chemical Engineers, 4th ed.*, McGraw-Hill, New York, 1991. To convert cost per square foot to cost per square meter, multiply by 10.76.

TABLE 14-9 Relative Fabricated Cost for Metals Used in Tray-tower Construction*

Materials of construction	Relative cost per ft^2 of tray area (based on carbon steel = 1)
Sheet-metal trays	
Steel	1
4–6% chrome—½ moly alloy steel	2.1
11–13% chrome type 410 alloy steel	2.6
Red brass	3
Stainless steel type 304	4.2
Stainless steel type 347	5.1
Monel	7.0
Stainless steel type 316	5.5
Inconel	8.2
Cast-iron trays	2.8



(a)



(b)

FIG. 14-80 Cost of internal devices for columns containing dumped packings. (a) Hold-down plates and support plates. (b) Redistributors. (c) Liquid distributors. [Pikulik and Diaz, Chem. Eng., 84(21), 106 (Oct. 10, 1977).]

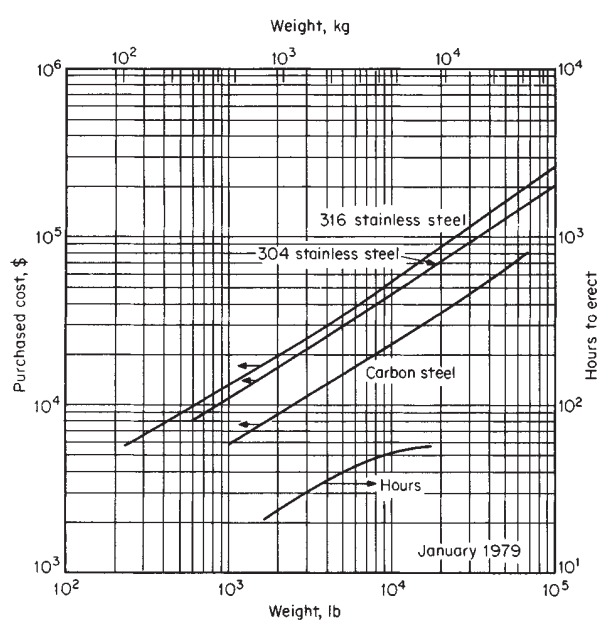


FIG. 14-81 Fabricated costs and installation time of towers. Costs are for shell with two heads and skirt, but without trays, packing, or connections. (Peters and Timmerhaus, Plant Design and Economics for Chemical Engineers, 4th ed., McGraw-Hill, New York, 1991.)

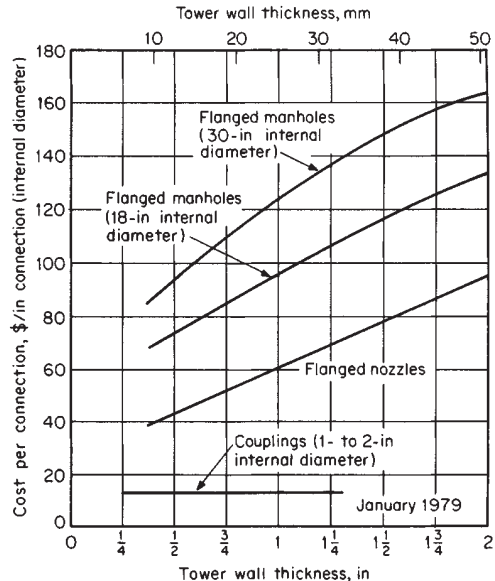


FIG. 14-82 Approximate installed cost of steel-tower connections. Values apply to 2070-kPa connections. Multiply costs by 0.9 for 1035-kPa (150-lb) connections and by 1.2 for 4140-kPa (600-lb) connections. To convert inches to millimeters, multiply by 25.4; to convert dollars per inch to dollars per centimeter, multiply by 0.394. (Peters and Timmerhaus, Plant Design and Economics for Chemical Engineers, 4th ed., New York, McGraw-Hill, 1991.)

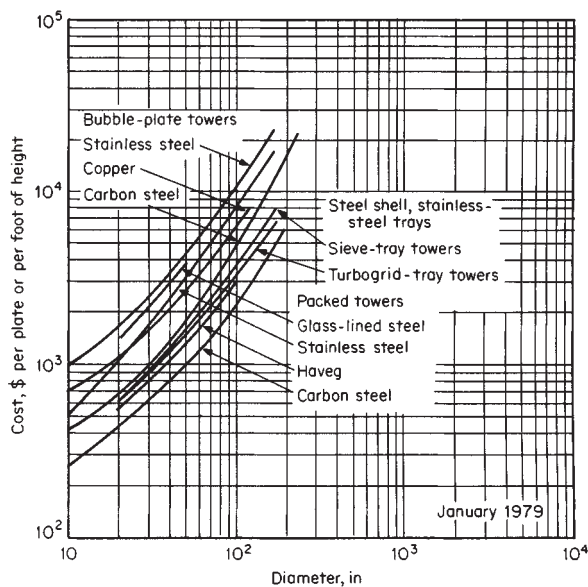


FIG. 14-83 Cost of towers including installation and auxiliaries. To convert inches to millimeters, multiply by 25.4; to convert feet to meters, multiply by 0.305; and to convert dollars per foot to dollars per meter, multiply by 3.28. (*Peters and Timmerhaus, Plant Design and Economics for Chemical Engineers, 4th ed., McGraw-Hill, New York, 1991.*)

ments, a rough guide could be developed on the basis of flow parameter $L/G (\rho_G/\rho_L)^{0.5}$ (ordinate scale in Figs. 14-25 and 14-26) and the following tentative conclusions could be drawn:

Flow Parameter 0.02–0.1

- Plates and random packings have much the same efficiency and capacity.
- Structured packing efficiency is about 1.5 times that of plates or random packing.
- At a parameter of 0.02, the structured packing has a 1.3–1.4 capacity advantage over random packing and plates. This advantage disappears as the parameter approaches 0.1.

Flow Parameter 0.1–0.3

- Plates and random packings have about the same efficiency and capacity.
- Structured packing has about the same capacity as plates and random packings.
- The efficiency advantage of structured packing over random packings and plates decreases from 1.5 to 1.2 as the parameter increases from 0.1 to 0.3.

Flow Parameter 0.3–0.5

- The loss of capacity of structured packing is greatest in this range.
- The random packing appears to have the highest capacity and efficiency, and structured packing the least capacity and efficiency.

Experience indicates that use of structured packings may not have advantages in the higher-pressure (higher-flow-parameter) region. Special considerations for the use of structured packing at higher pressures are detailed by Kurtz et al. [*Chem. Eng. Progr.*, **87**(2), 43 (1991)].

Optimization As stated previously, optimization studies should include the entire system. Such a study was made by Fair and Bolles [*Chem. Eng.*, **75**(9), 156 (1968)], using a light-hydrocarbon system and with the objective of defining optimum reflux ratio. Coolants used were at -87°C , -40°C , and $+30^\circ\text{C}$ (-125°F , -40°F , and $+85^\circ\text{F}$), corresponding to different pressures of operation and associated different condens-

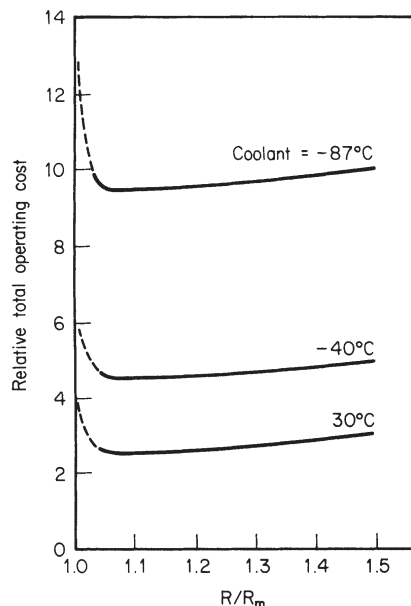


FIG. 14-84 Optimum-reflux-ratio determination. ${}^\circ\text{F} = \frac{9}{5} {}^\circ\text{C} + 32$. [*Fair and Bolles, Chem. Eng.*, **75**(4), 156 (1968).]

ing temperatures. The results are shown in Fig. 14-84; the optimum reflux ratio is quite close to the calculated minimum reflux ratio.

Colburn (chemical engineering lecture notes, University of Delaware, 1943) proposed that the optimum reflux ratio is

$$R_{\text{opt}} = \frac{N + [(C_2/hG_b + C_3)/C_1] + (dN/dR)}{dN/dR} \quad (14-189)$$

where R = external reflux ratio = L/D

N = number of theoretical plates

G_b = allowable vapor velocity in heat exchangers, $(\text{lb-mol})/(\text{h}\cdot\text{ft}^2)$

h = hours of operation

C_1 = amortization rate for tower, dollars/ $(\text{ft}^2\cdot\text{plate}\cdot\text{year})$

C_2 = amortization rate for heat exchangers, dollars/ $(\text{ft}^2\cdot\text{year})$

C_3 = cost of utilities per mole of distillate, dollars/mol

Happel [*Chem. Eng.*, **65**(14), 144 (1958)] using a modification of the Colburn relationship found that the optimum number of trays varies from 2 to 3 times the number at total reflux. Gilliland [*Ind. Eng. Chem.*, **32**, 1220 (1940)] from the establishment of an empirical relationship between reflux ratio and theoretical trays based on a study of existing columns indicated that

$$0.1 < \frac{R_{\text{opt}} - R_{\text{min}}}{R_{\text{min}} + 1} < 0.3$$

and correspondingly

$$0.35 < \frac{N_{\text{opt}} - N_{\text{min}}}{N_{\text{min}} + 1} < 0.52$$

The effect of utilities costs on optimum operation was noted by Kiguchi and Ridgway [*Pet. Refiner*, **35**(12), 179 (1956)], who indicated that in petroleum-distillation columns the optimum reflux ratio varies between 1.1 and 1.5 times the minimum reflux ratio. When refrigeration is involved, $1.1R_{\text{min}} < R_{\text{opt}} < 1.2R_{\text{min}}$, and when cooling-tower water is used in the condensers, $1.2R_{\text{min}} < R_{\text{opt}} < 1.4R_{\text{min}}$.

PHASE DISPERSION

GENERAL REFERENCES: For an overall discussion of gas-liquid breakup processes, see Brodkey, *The Phenomena of Fluid Motions*, Addison-Wesley, Reading, Massachusetts, 1967. For a discussion of atomization devices and how they work, see Masters, *Spray Drying Handbook*, 5th ed., Wiley, New York, 1991; and Lefebvre, *Atomization and Sprays*, Hemisphere, New York, 1989. A beautifully illustrated older source is Dombrowski and Munday, *Biochemical and Biological Engineering Science*, vol. 2, Academic Press, London, 1968, pp. 209–320. Bayvel and Orzechowski, *Liquid Atomization*, Taylor and Francis, Washington DC, 1993, provides additional background into atomizer design. For a survey on fog formation, see Amelin, *Theory of Fog Formation*, Israel Program for Scientific Translations, Jerusalem, 1967.

LIQUID-IN-GAS DISPERSIONS

Liquid Breakup into Droplets There are four basic mechanisms for breakup of liquid into droplets:

- Droplets in a field of high turbulence (i.e., high power dissipation per unit mass)
- Simple jets at low velocity
- Expanding sheets of liquid at relatively low velocity
- Droplets in a steady field of high relative velocity

These mechanisms coexist, and the one that gives the smallest drop size will control. The four mechanisms follow distinctly different velocity dependencies:

1. *Breakup in a highly turbulent field* ($1/\text{velocity}$)^{1.2}. This appears to be the dominant breakup process in distillation trays in the spray regime, pneumatic atomizers, and high-velocity pipeline contactors.

2. *Breakup of a low-velocity liquid jet* ($1/\text{velocity}$)⁰. This governs in special applications like prilling towers and is often an intermediate step in liquid breakup processes.

3. *Breakup of a sheet of liquid* ($1/\text{velocity}$)^{0.67}. This governs drop size in most hydraulic spray nozzles.

4. *Single-droplet breakup at very high velocity* ($1/\text{velocity}$)². This governs drop size in free fall as well as breakup when droplets impinge on solid surfaces.

Droplet Breakup—High Turbulence This is the dominant breakup mechanism for many process applications. Breakup results from local variations in turbulent pressure that distort the droplet shape. Hinze [Am. Inst. Chem. Eng. J., **1**, 289–295 (1953)] applied turbulence theory to obtain the form of Eq. (14-171) and took liquid-liquid data to define the coefficient:

$$D_{\max} = 0.725(\sigma/\rho_G)^{0.6}/E^{0.4} \quad (14-190)$$

where E = (power dissipated)/mass length²/time³
 σ = surface tension mass/time²
 ρ_G = gas density mass/length³

Note that D_{\max} comes out with units of length. Since E typically varies with $(\text{gas velocity})^3$, this results in drop size dependence with $(1/\text{velocity})^{1.2}$.

The theoretical requirement for use of Eq. (14-190) is that the microscale of turbulence $\ll D_{\max}$. This is satisfied in most gas systems. For example, in three cases,

(microscale of turbulence)/ D_{\max}	
distillation tray in spray regime	0.007
pipeline @ 40 m/s and atmospheric pressure	0.012
two-fluid atomizer using 100 m/s air	0.03

For these three applications, Eq. (14-190) gives good prediction of drop size when the design variables are used to calculate E , as illustrated by Eqs. (14-198) and (14-201).

Liquid-Column Breakup Because of increased pressure at points of reduced diameter, the liquid column is inherently unstable. As a result, it breaks into small drops with no external energy input. Ideally, it forms a series of uniform drops with the size of the drops set by the fastest-growing wave. This yields a dominant droplet diameter

about 1.9 times the initial diameter of the jet as shown by Fig. 14-85. As shown, the actual breakup is quite close to prediction, although smaller satellite drops are also formed. The prime advantage of this type of breakup is the greater uniformity of drop size.

For high-viscosity liquids, the drops are larger, as shown by Eq. (14-191):

$$D = 1.9D_j \left[1 + \frac{3\mu_e}{(\sigma\rho_e D_j)^{1/2}} \right] \quad (14-191)$$

where D = diameter of droplet

D_j = diameter of jet

μ_e = viscosity of liquid

ρ_e = density of liquid

σ = surface tension of liquid

These units are dimensionally consistent; any set of consistent units can be used.

As the velocity of the jet is increased, the breakup process changes and ultimately becomes a mix of various competing effects, such as the capture of small drops by bigger ones in the slowing jet and the “turbulent breakup” of the bigger drops. The high-velocity jet is occasionally used in process applications because of the very narrow spray angle (5–20°) and the high penetration into a gas it can give. The focused stream also aids erosion of a surface.

Liquid-Sheet Breakup The basic principle of most hydraulic atomizers is to form a thin sheet that breaks via a variety of mechanisms to form ligaments of liquid which in turn yield chains of droplets. See Fig. 14-86.

For a typical nozzle, the drop size varies with $1/(\text{pressure drop})^{1/3}$. When $(\text{velocity})^2$ is substituted for pressure drop, droplet size is seen to vary with $(\text{velocity})^{-2/3}$.

Isolated Droplet Breakup—in a Velocity Field Much effort has focused on defining the conditions under which an isolated drop will break in a velocity field. The criterion for the largest stable drop

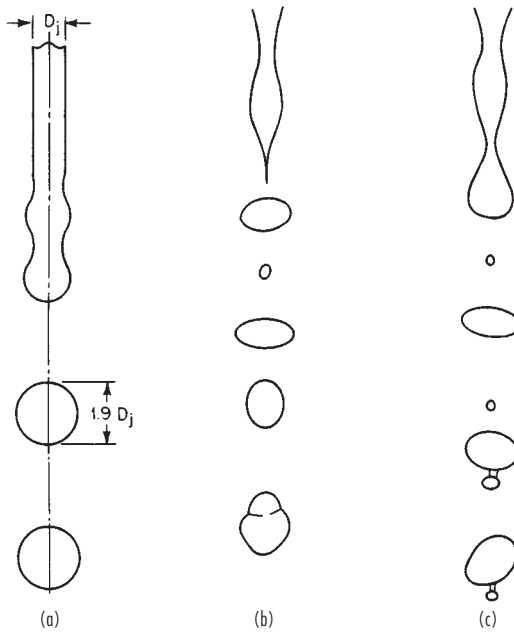


FIG. 14-85 (a) Idealized jet breakup suggesting uniform drop diameter and no satellites. (b) and (c) Actual breakup of a water jet as shown by high-speed photographs. [From W. R. Marshall, “Atomization and Spray Drying,” *Chem. Eng. Prog. Monogr. Ser.*, no. 2 (1954).]

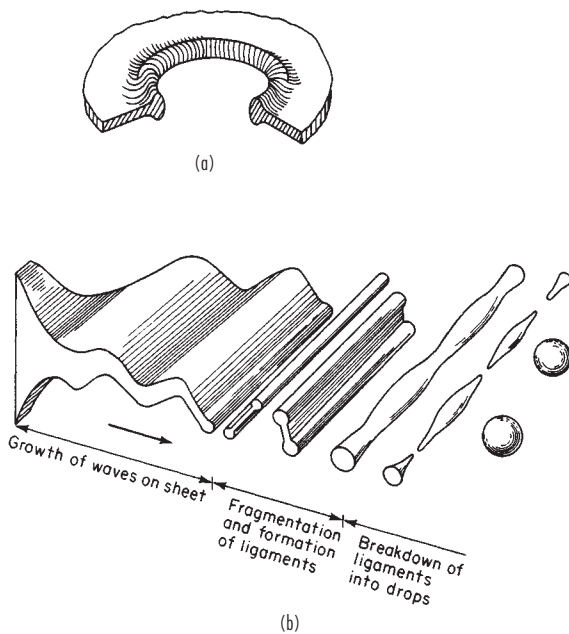


FIG. 14-86 Sheet breakup. (a) By perforation. [After Fraser *et al.*, Am. Inst. Chem. Eng. J., 8(5), 672 (1962).] (b) By sinusoidal wave growth. [After Domrowski and Johns, Chem. Eng. Sci., 18, 203 (1963).]

size is the ratio of aerodynamic forces to surface-tension forces defined by the Weber number, N_{We} (dimensionless):

$$N_{We\ crit} = \text{constant} = [\rho_C (\text{velocity})^2 (D_{max})]/(\sigma) \quad (14-192)$$

$N_{We\ crit}$ for low-viscosity fluids commonly ranges from 10 to 20, with the larger value for a free-fall condition and the smaller for a sudden acceleration. High liquid viscosity also increases $N_{We\ crit}$.

Droplet breakup via impingement appears to follow a similar relationship, but much less data is available. This type of breakup can result from impingement on equipment walls or compressor blades. In general, there is less tendency to shatter on wetted surfaces.

Droplet Size Distribution Instead of the single droplet size implied by the discussion above, a spectrum of droplet sizes is produced. The most common ways to characterize this spectrum are:

- **Volume median (mass median) D_{vm}** . This has no fundamental meaning but is easy to determine since it is at the midpoint of a cumulative-volume plot.
- **Sauter mean D_{32}** . This has the same ratio of surface to volume as the total drop population. It is typically 70 to 90 percent of D_{vm} . It is frequently used in transport processes and is used here to characterize drop size.
- **Maximum D_{max}** . This is the largest-sized particle in the population. It is typically 3 to 4 times D_{32} in turbulent breakup processes, per Walzel [*International Chemical Engineering*, 33, 46, (1993)]. It is the size directly calculated from the power/mass relationship. D_{32} is estimated from D_{max} by

$$D_{32} = 0.3 \cdot D_{max} \quad (14-193)$$

and D_{vm} is estimated from it by

$$D_{vm} = 0.4 \cdot D_{max} \quad (14-194)$$

However, any average drop size is fictitious, and none is completely satisfactory. For example, there is no way in which the high surface and transfer coefficients in small drops can be made available to the larger drops. Hence, a process calculation based on a given droplet size describes only what happens to that size and gives at best an approximation to the total mass.

There are a variety of ways to describe the droplet population. Figures 14-88 and 14-90 illustrate one of the most common methods, the plot of cumulative volume against droplet size on log-normal graph paper. This satisfies the restraint of not extrapolating to a negative drop size. Its other advantages are that it is easy to plot, the results are easy to visualize, and it yields a nearly straight line at lower drop sizes.

Cumulative volume over the range of 1 to 50 percent can also be shown to vary approximately as D^2 . This is equivalent to finding that the number of droplets of a given size is inversely proportional to the droplet area or the surface energy of the droplet.

Atomizers The common need to disperse a liquid into a gas has spawned a large variety of mechanical devices. The different designs emphasize different advantages such as freedom from plugging, pattern of spray, small droplet size, uniformity of spray, high turndown ratio, and low power consumption.

As shown in Table 14-11, most atomizers fall into three categories:

1. Pressure nozzles (hydraulic)
2. Two-fluid nozzles (pneumatic)
3. Rotary devices (spinning cups, disks, or vane wheels)

These share certain features such as relatively low efficiency and low cost relative to most process equipment. The energy required to produce the increase in area is typically less than 0.1 percent of the total energy consumption. This is because atomization is a secondary process resulting from high interfacial shear or turbulence. As droplet sizes decrease, this efficiency drops lower.

Other types are available that use sonic energy (from gas streams), ultrasonic energy (electronic), and electrostatic energy, but they are less commonly used in process industries. See Table 14-11 for a summary of the advantages/disadvantages of the different type units. An expanded discussion is given by Masters [*Spray Drying Handbook*, Wiley, New York, (1991)].

Special requirements such as size uniformity in prilling towers can dictate still other approaches to dispersion. Here plates are drilled with many holes to develop nearly uniform columns.

Commonly, the most important feature of a nozzle is the size of droplet it produces. Since the heat or mass transfer that a given dispersion can produce is often proportional to $(1/D_d)^2$, fine drops are usually favored. On the other extreme, drops that are too fine will not settle, and a concern is the amount of liquid that will be entrained from a given spray operation. For example, if sprays are used to contact atmospheric air flowing at 1.5 m/s, drops smaller than 350 μm [terminal velocity = 1.5 m/s (4.92 ft/s)] will be entrained. Even for the relative coarse spray of the hollow-cone nozzle shown in Fig. 14-88, 7.5 percent of the total liquid mass will be entrained.

Hydraulic (Pressure) Nozzles Manufacturers' data such as shown by Fig. 14-88 are available for most nozzles for the air-water system. In Fig. 14-88, note the much coarser solid-cone spray. The coarseness results from the less uniform discharge.

Effect of Physical Properties on Drop Size Because of the extreme variety of available geometries, no attempt to encompass this variable is made here. The suggested predictive route starts with air-water droplet size data from the manufacturer at the chosen flow rate. This drop size is then corrected by Eq. (14-195) for different viscosity and surface tension:

$$\frac{D_{vm, \text{system}}}{D_{vm, \text{water}}} = \left(\frac{\sigma_{\text{system}}}{73} \right)^{0.25} \left(\frac{\mu_e}{1.0} \right)^{0.25} \quad (14-195)$$

where D_{vm} = volume median droplet diameter

σ = surface tension, mN/m (dyn/cm)

μ_e = liquid viscosity, mPa·s (cP)

The exponential dependencies in Eq. (14-195) represent averages of values reported by a number of studies with particular weight given to Lefebvre ([*Atomization and Sprays*, Hemisphere, New York, (1989)]. Since viscosity can vary over a much broader range than surface tension, it has much more leverage on drop size. For example, it is common to find an oil with 1000 times the viscosity of water, while most liquids fall within a factor of 3 of its surface tension. Liquid density is generally even closer to that of water, and since the data are not clear that a liquid density correction is needed, none is shown in Eq.

14-64 GAS ABSORPTION AND GAS-LIQUID SYSTEM DESIGN

TABLE 14-11 Atomizer Summary

Types of atomizer	Design features	Advantages	Disadvantages
Pressure.	Flow $\alpha(\Delta P/\rho_l)^{1/2}$. Only source of energy is from fluid being atomized.	Simplicity and low cost.	Limited tolerance for solids; uncertain spray with high-viscosity liquids; susceptible to erosion. Need for special designs (e.g., bypass) to achieve turndown. Concentrated spray pattern at cone boundaries.
1. Hollow cone.	Liquid leaves as conical sheet as a result of centrifugal motion of liquid. Air core extends into nozzle. Centrifugal motion developed by tangential inlet in chamber upstream of orifice.	High atomization efficiency.	
a. Whirl chamber (see Fig. 14-87a).	Centrifugal motion developed by inserts in chamber.	Minimum opportunity for plugging.	
b. Grooved core.		Smaller spray angle than 1a and ability to handle flows smaller than 1a.	
2. Solid cone (see Fig. 14-87b).	Similar to hollow cone but with insert to provide even distribution. Liquid leaves as a flat sheet or flattened ellipse.	More uniform spatial pattern than hollow cone. Flat pattern is useful for coating surfaces and for injection into streams.	Coarser drops for comparable flows and pressure drops. Failure to yield same pattern with different fluids. Small clearances.
3. Fan (flat) spray.		Minimal plugging.	Coarser drops.
a. Oval or rectangular orifice (see Fig. 14-87c). Numerous variants on cavity and groove exist.	Combination of cavity and orifice produces two streams that impinge within the nozzle.	Different liquids are isolated until they mix outside of orifice. Can produce a flat circular sheet when jets impinge at 180°.	Extreme care needed to align jets.
b. Deflector (see Fig. 14-87d).	Liquid from plain circular orifice impinges on curved deflector.	Achieves uniform hollow cone atomization pattern with very high turndown (50:1). Simplest control over broad range.	Waste of energy in bypass stream. Added piping for spill flow.
c. Impinging jets (see Fig. 14-87e).	Two jets collide outside nozzle and produce a sheet perpendicular to their plane.		Difficult to maintain proper clearances.
4. Nozzles with wider range of turndown.	A portion of the liquid is recirculated after going through the swirl chamber. Conical sheet is developed by flow between orifice and poppet. Increased pressure causes poppet to move out and increase flow area.		
a. Spill (bypass) (see Fig. 14-87f).			
b. Poppet (see Fig. 14-87g).			
Two-fluid (see Fig. 14-87h).	Gas impinges coaxially and supplies energy for breakup.		Because gas is also accelerated, efficiency is inherently lower than pressure nozzles.
Sonic.	Gas generates an intense sound field into which liquid is directed.		Similar to two-fluid.
Rotary wheels (see Fig. 14-87i) disks, and cups.	Liquid is fed to a rotating surface and spreads in a uniform film. Flat disks, disks with vanes, and bowl-shaped cups are used. Liquid is thrown out at 90° to the axis.		Mechanical complexity of rotating equipment. Radial discharge.
Ultrasound.	Liquid is fed over a surface vibrating at a frequency > 20 kHz.	Fine atomization, small size, and low injection velocity.	Low flow rate and need for ultrasound generator.

(14-195). Vapor density also has an impact on dropsize but the impact is complex, involving conflicts of a number of effects, and vapor density is commonly omitted in atomizer dropsize correlations.

Effect of Pressure Drop and Nozzle Size For a nozzle with a developed pattern, the average drop size can be estimated to fall with rising ΔP (pressure drop) by Eq. (14-196):

$$\frac{D_1}{D_2} = \left(\frac{\Delta P_2}{\Delta P_1} \right)^{1/3} \quad (14-196)$$

For similar nozzles and constant ΔP , the drop size will increase with nozzle size as indicated by Eq. (14-197):

$$\frac{D_1}{D_2} = \left(\frac{\text{orifice diameter}_1}{\text{orifice diameter}_2} \right)^{1/2} \quad (14-197)$$

Once again, these relationships are averages of a number of reported values and are intended as rough guides.

The normal operating regime is well below turbulent breakup velocity. However the data of Kennedy [*J. of Engineering for Gas Turbines and Power*, **108**, 191, (1986)] at very high pressure drop in large nozzles shows a shift to a higher dependence on pressure drop. This data suggests that turbulent droplet breakup can also be governing with hydraulic spray nozzles, although this is unusual.

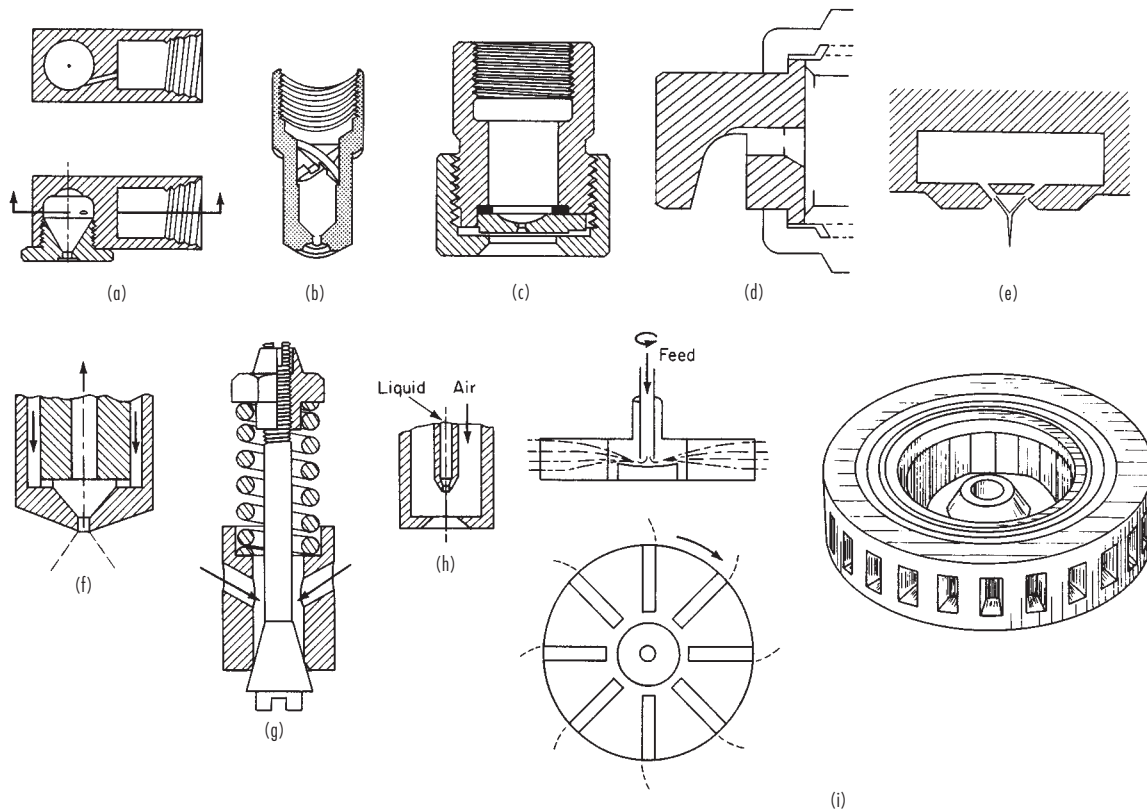


FIG. 14-87 Characteristic spray nozzles. (a) Whirl-chamber hollow cone. (b) Solid cone. (c) Oval-orifice fan. (d) Deflector jet. (e) Impinging jet. (f) Bypass. (g) Poppet. (h) Two-fluid. (i) Vaned rotating wheel.

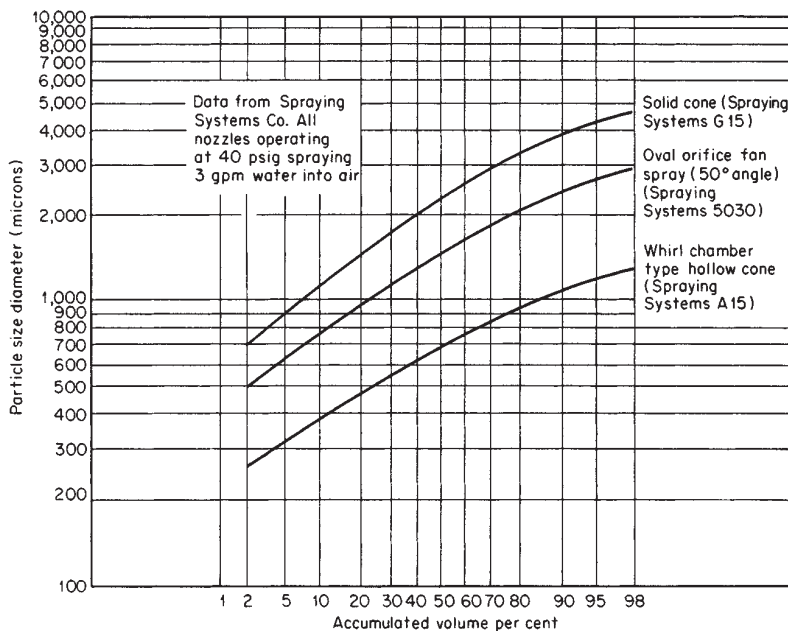


FIG. 14-88 Droplet-size distribution for three different types of nozzles. To convert pounds per square inch gauge to kilopascals, multiply by 6.89; to convert gallons per minute to cubic meters per hour, multiply by 0.227. (*Spraying Systems Inc.*)

14-66 GAS ABSORPTION AND GAS-LIQUID SYSTEM DESIGN

Spray Angle A shift to a smaller-angle nozzle gives slightly larger drops for a given type of nozzle because of the reduced tendency of the sheet to thin. Dietrich [Proc. 1st Int. Conf. Liq. Atomization Spray Systems, Tokyo, (1978)] shows the following:

Angle	25°	50°	65°	80°	95°
D_{em} , μm	1459	1226	988	808	771

In calculating the impact point of spray, one should recognize that the spray angle closes in as the spray moves away from the nozzle. This is caused by loss of momentum of the spray to the gas.

At some low flow, pressure nozzles do not develop their normal pattern but tend to approach solid streams. The required flow to achieve the normal pattern increases with viscosity.

Two-Fluid (Pneumatic) Atomizers This general category includes such diverse applications as venturi atomizers and reactor-effluent quench systems in addition to two-fluid spray nozzles. Depending on the manner in which the two fluids meet, several of the breakup mechanisms may be applicable, but the final one is high-level turbulent rupture.

As shown by Table 14-12, empirical correlations for two-fluid atomization show dependence on high gas velocity to supply atomizing energy, usually to a power dependence close to that for turbulent breakup. In addition, the correlations show a dependence on the ratio of gas to liquid and system dimension.

TABLE 14-12 Exponential Dependence of Drop Size on Different Parameters in Two-Fluid Atomization

	Relative velocity	Surface tension	Gas density	1 + L/G	Atomizer dimension
Jasuja (empirical for small nozzle)	-0.9	0.45	-0.45	0.5	0.55
El-Shanawany and Lefebvre (empirical for small nozzle)	-1.2	0.6	-0.7	1	0.40
Tatterson, Dallman, and Hanratty (pipe flow)	-1	0.5	-0.5		0.5
Hinze (turbulence theory)	-1.2	0.6	-0.6		
Steimmeyer (extension of turbulence theory)	-1.2	0.6	-0.6	0.4	0.4

Further differences from hydraulic nozzles (controlled by sheet and ligament breakup) are the stronger increase in drop size with increasing surface tension and decreasing gas density.

The similarity of these correlations to the dependencies shown by Eq. (14-190) was noted by Steimmeyer [Chem. Eng. Progr., **91**(7), 72 (1995)] who reformulated Hinze's relationship, Eq. (14-190), into Eq. (14-198) by including atomizer variables.

$$D_{32} = 0.29 \left(\frac{\sigma}{\rho_G} \right)^{0.6} (1/\text{velocity})^{1.2} \left(\frac{1+L}{G} \right)^{0.4} \left(D_{\text{nozzle}} \right)^{0.4} \quad (14-198)$$

where σ = surface tension

ρ_G = gas density

L/G = mass ratio of liquid flow to gas flow

D_{nozzle} = diameter of the air discharge

This is remarkably similar to the empirical two-fluid atomizer relationships of El-Shanawany and Lefebvre [*J. Energy*, **4**, 184 (1980)] and Jasuja [*Trans. Am. Soc. Mech. Engr.*, **103**, 514 (1981)]. For example, El-Shanawany and Lefebvre give a relationship for a prefilming atomizer:

$$D_{32} = 0.0711(\sigma/\rho_G)^{0.6}(1/\text{velocity})^{1.2}(1+L/G)(D_{\text{nozzle}})^{0.4}(\rho_L/\rho_G)^{0.1} + 0.015[(\mu_L)^2/(\sigma \times \rho_L)]^{0.5}(D_{\text{nozzle}})^{0.5}(1+L/G) \quad (14-199)$$

where μ_L is liquid viscosity.

According to Jasuja,

$$D_{32} = 0.17(\sigma/\rho_G)^{0.45}(1/\text{velocity})^{0.9}(1+L/G)^{0.5}(D_{\text{nozzle}})^{0.55} + \text{viscosity term} \quad (14-200)$$

(Eqs. 14-198, 14-199, and 14-200 are dimensionally consistent; any set of consistent units on the right-hand side yields the droplet size in units of length on the left-hand side.)

The second, additive term carrying the viscosity impact in Eq. (14-199) is small at viscosities around 1 centipoise but can become controlling as viscosity increases. For example, for air at atmospheric pressure atomizing water, with nozzle conditions.

$$D_{\text{nozzle}} = 0.076 \text{ m (3 inches)}$$

$$\text{velocity} = 100 \text{ m/s (328 ft/s)}$$

$$L/G = 1$$

For this case, Steinmeyer's correlation becomes El-Shanawany, Eq. (14-199) predicts 76 microns with the viscosity term contributing less than 1 percent. With the same system and same L/G , but with an oil with 30 times water viscosity, Eq. (14-199) predicts 91 microns, with the viscosity term contributing 54 percent of the total. The measured values for water and oil cases were 70 and 95 microns, respectively. For comparison, Eq. (14-198) predicts 102 microns for the water case.

Rotary Atomizers For rotating wheels, vaneless disks, and cups, there are three regimes of operation. At low rates, the liquid is shed directly as drops from the rim. At intermediate rates, the liquid leaves the rim as threads; and at the highest rate, the liquid extends from the edge as a thin sheet that breaks down similarly to a fan or hollow-cone spray nozzle. As noted in Table 14-12, rotary devices have many unique advantages such as the ability to handle high viscosity and slurries and produce small droplets without high pressures. The prime applications are in spray drying. See Masters [*Spray Drying Handbook*, Wiley, New York (1991)] for more details.

Pipeline Contactors The power dissipation per unit mass for pipeline flow is similar to that for two-fluid nozzles.

$$D_{32} = 0.79 \left(\frac{\sigma}{\rho_G} \right)^{0.6} \left(\frac{1}{\text{velocity}} \right)^{1.2} (D_{\text{pipe}})^{0.4} \quad (14-201)$$

(The relation is dimensionally consistent; any set of consistent units on the right-hand side yields the droplet size in units of length on the left-hand side.)

The relationship is similar to the empirical correlation of Tatterson, Dallman, and Hanratty [Am. Inst. Chem. Eng. J., **23**(1), 68 (1977)]

$$D_{32} \sim \left(\frac{\sigma}{\rho_G} \right)^{0.5} (1/\text{velocity})^1 (D_{\text{pipe}})^{0.5}$$

Predictions from Eq. (14-201) align well with the Tatterson data. For example, for a velocity of 43 m/s (140 ft/s) in a 0.05-m (1.8-inch) equivalent diameter channel, Eq. (14-201) predicts D_{32} of 490 microns, compared to the measured 460 to 480 microns.

Entrainment Due to Gas Bubbling/Jetting through a Liquid

Entrainment generally limits the capacity of distillation trays and is commonly a concern in vaporizers and evaporators. Fortunately, it is readily controllable by simple inertial entrainment capture devices such as wire mesh pads in gravity separators.

In distillation towers, entrainment lowers the tray efficiency, and 1 pound of entrainment per 10 pounds of liquid is sometimes taken as the limit for acceptable performance. However, the impact of entrainment on distillation efficiency depends on the relative volatility of the component being considered. Entrainment has a minor impact on close separations when the difference between vapor and liquid concentration is small, but this factor can be dominant for systems where the liquid concentration is much higher than the vapor in equilibrium with it (i.e., when a component of the liquid has a very low volatility, as in an absorber).

As shown by Fig. 14-90, entrainment droplet sizes span a broad range. The reason for the much larger drop sizes of the upper curve is the short disengaging space. For this curve, over 99 percent of the entrainment has a terminal velocity greater than the vapor velocity. For contrast, in the lower curve the terminal velocity of the largest particle reported is the same as the vapor velocity. For the settling velocity to limit the maximum drop size entrained, at least 0.8 m (30 in) disengaging space is usually required. Note that even for the lower curve, less than 10 percent of the entrainment is in drops of less than

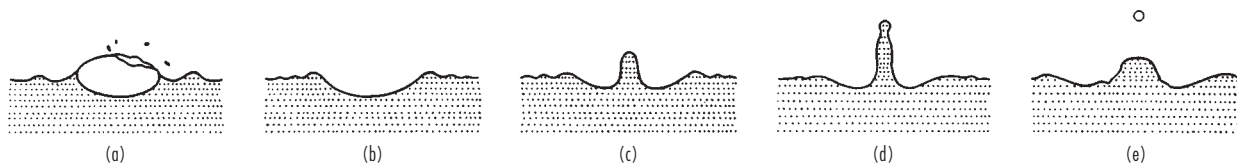


FIG. 14-89 Mechanism of the burst of an air bubble on the surface of water. [Newitt, Dombrowski, and Knellman, Trans. Inst. Chem. Eng., **32**, 244 (1954).]

50 μm . The coarseness results from the relatively low power dissipation per mass on distillation trays. This means that it is relatively easy to remove by a device such as a wire mesh pad. Over 50 percent is typically captured by the underside of the next higher tray or by a turn in the piping leaving an evaporator. Conversely, though small on a mass basis, the smaller drops are extremely numerous. On a number basis, more than one-half of the drops in the lower curve are under 5 μm . These can serve as nuclei for fog condensation in downstream equipment.

Entrainment can stem from a variety of sources.

1. Excessive foaming. This is a case of a gas-in-liquid dispersion (covered in the next subsection).

2. Droplets formed from the collapse of the bubble dome (see Fig. 14-89). These are virtually unavoidable. They are generally under 25 μm , which means that their terminal velocities are low and they are invariably entrained. Fortunately, because of their small size, they contribute little on a weight basis (<0.001 kg liquid/kg vapor), although they dominate on a number basis.

3. Droplets from the jet caused by liquid rushing to fill the cavity left by the bubble (see Fig. 14-89). These droplets range up to 1000 μm , their size depending on bubble size. This is important only at modest loadings. Once foam forms over the surface, drop ejection by this mode decreases sharply.

4. At higher vapor loads, the kinetic energy of the vapor rather than the bubble burst supplies the thrust for jets and sheets of liquid that are thrown up as well as the energy from breakup into "spray." This yields much higher levels of entrainment. In distillation trays it is the most common limit to capacity.

The major variable in setting entrainment (E , weight of liquid entrained per weight of vapor) is vapor velocity. As velocity is increased, the dependence of E on velocity steepens. In the lowest velocity regime, E is proportional to velocity. At values of E of about 0.001 (around 10 percent of flood), there is a shift to a region where the dependence is with $(\text{velocity})^{3-5}$. Near flood, the dependence rises to approximately $(\text{velocity})^8$. In this regime, the kinetic energy of the vapor dominates, and the bulk of the dispersion on the plate is often in the form of a coarse spray.

Pinczewski and Fell [Trans. Inst. Chem. Eng., **55**, 46 (1977)] show that the velocity at which vapor jets onto the tray sets the droplet size, rather than the superficial tray velocity. A maximum superficial velocity formulation that incorporates ϕ , the fractional open area, is logical since the fractional open area sets the jet velocity. Stichlmair and Mersmann [Int. Chem. Eng., **18**(2), 223 (1978)] give such a correlation:

$$U_{\max} = \frac{2.5[\phi g(\rho_l - \rho_g)\sigma]^{1/4}}{\rho_g^{1/2}} \quad (14-202)$$

(The relation is dimensionally consistent; any set of consistent units on the right-hand side yields velocity units for the left-hand side.)

Stichlmair uses the ratio of actual velocity to this maximum velocity together with a term that increases entrainment as the distance gets small between the liquid-vapor layer and the tray deck above. His correlation spans a 10^5 fold range in entrainment. He shows a sharp increase in entrainment at 60 percent of the maximum velocity and attributes the increase to a shift to the spray regime.

Puppich and Goedecke [Chem. Eng. Tech., **10**, 224 (1987)] test this correlation against a wide range of tray types and find generally good agreement. Bubble caps give about twice as much entrainment as the correlation predicts. Sieve trays give about half as much as the correlation predicts.

Steinmeyer [Chem. Eng. Progr., **91**(7), 72 (1995)] derived a corre-

lation for entrainment utilizing predicted drop size from a turbulent power dissipation per unit mass) breakup in the "spray" regime. His predicted drop size matched the data of Pinczewski and Fell. When this prediction is combined with the estimated fraction of the droplet population that is entrained, the entrainment prediction, Eq. (14-203), results. Note that this matches the empirical experience in predicting entrainment varying with (velocity)⁸

$$E = \text{constant } [V]^8 \phi^3 \frac{\rho_g^4}{[g(\rho_l - \rho_g)]^{2.5} \sigma^{1.5}} \quad (14-203)$$

If *flood* is defined as the velocity at which E equals 1, this yields (dimensionless):

$$V_{\text{flood}} = 1.25 \times \frac{[\phi^{0.375}[g(\rho_l - \rho_g)]^{0.3125}\sigma^{0.1875}(Z/Z_{\text{base}})^{0.125}]}{\rho_g^{0.5}} \quad (14-204)$$

where Z is tray spacing in meters and Z/Z_{base} is the ratio of tray spacing to 0.3 m (1 ft).

Fair's empirical correlation for sieve and bubble-cap trays shown in Fig. 14-26 is similar. Note that Fig. 14-26 incorporates a velocity dependence (velocity)⁶⁻⁸ above 90 percent of flood for high-density systems. The correlation implicitly considers the tray design factors such as the open area, tray spacing, and hole diameter through the impact of these factors on percent of flood.

The dependencies of all three correlations are remarkably close, as shown by Table 14-13 and the numeric prediction of flooding velocity is also close.

Correlations can be extended to evaporators at lower velocities by assuming that E declines with (velocity)² between 60 percent and 10 percent of the maximum velocity. At velocities below 10 percent of the maximum velocity, E can be assumed to change directly with velocity.

Fog Condensation This is an entirely different way of forming dispersions. Here, the dispersion results from condensation of a vapor rather than mechanical breakup. The particle sizes are usually much finer (0.1 to 30 μm) and are designated as mist or fog.

Fog particles grow because of excess saturation in the gas. Usually this means that the gas is supersaturated (i.e., it is below its dew point). Sometimes, fog can also grow on soluble foreign nuclei at partial pressures below saturation. Increased saturation can occur through a variety of routes:

1. Mixing of two saturated streams at different temperatures. This is commonly seen in the plume from a stack. Since vapor pressure is an exponential function of temperature, the resultant mixture of two saturated streams will be supersaturated at the mixed temperature. Uneven flow patterns and cooling in heat exchangers make this route to supersaturation difficult to prevent.

2. Increased partial pressure due to reaction. An example is the reaction of SO_3 and H_2O to yield H_2SO_4 , which has much lower vapor pressure than its components.

3. Isoentropic expansion (cooling) of a gas, as in a steam nozzle.

TABLE 14-13 Dependency of Distillation Flood Velocity on Physical Properties and Tray Open Area

	Power/mass	Fair	Stichlmair/Mersmann
ϕ	0.375	0.44	0.5
$\rho_l - \rho_g$	0.3125	0.5	0.25
σ	0.1875	0.2	0.25
ρ_g	0.5	0.5	0.5

14-68 GAS ABSORPTION AND GAS-LIQUID SYSTEM DESIGN

4. Cooling of a gas containing a condensable vapor. Here the problem is that the gas cools faster than condensable vapor can be removed by mass transfer.

These mechanisms can be observed in many common situations. For example, fog via mixing can be seen in the discharge of breath on a cold day. Fog via adiabatic expansion can be seen in the low-pressure area over the wing of an airplane landing on a humid summer day; and fog via condensation can be seen in the exhaust from an automobile air conditioner (if you follow closely enough behind another car to pick up the ions or NO molecules needed for nucleation). All of these occur at a very low supersaturation and appear to be keyed to an abundance of foreign nuclei. All of these fogs also quickly dissipate as heat or unsaturated gas is added.

The supersaturation in condensers arises for two reasons. First, the condensable vapor is generally of higher molecular weight than the noncondensable gas. This means that the molecular diffusivity of the vapor will be much less than the thermal diffusivity of the gas. Restated, the ratio of $N_{\text{sc}}/N_{\text{pr}}$ is greater than 1. The result is that a condenser yields more heat-transfer units $dT_g/(T_g - T_i)$ than mass-transfer units $dY_g/(Y_g - Y_i)$. Second, both transfer processes derive their driving force from the temperature difference between the gas T_g and the interface T_i . Each incremental decrease in interface temperature yields the same relative increase in temperature driving force. However, the interface vapor pressure can only approach the limit of zero. Because of this, for equal molecular and thermal diffusivities a saturated mixture will supersaturate when cooled. The tendency to supersaturate generally increases with increased molecular weight of the condensable, increased temperature differences, and reduced initial superheating. To evaluate whether a given condensing step yields fog requires rigorous treatment of the coupled heat-transfer and mass-transfer processes through the entire condensation. Steinmeyer [*Chem. Eng. Prog.*, **68**(7), 64 (1972)] illustrates this, showing the impact of foreign-nuclei concentration on calculated fog formation. See Table 14-14. Note the relatively large particles generated for cases 1 and 2 for 10,000 foreign nuclei per cm^3 . These are large enough to be fairly easily collected. There have been very few documented problems with industrial condensers despite the fact that most calculate to generate supersaturation along the condensing path. The explanation appears to be a limited supply of foreign nuclei.

Ryan et al. [*Chem. Eng. Progr.*, **90**(8), 83 (1994)] show that separate mass and heat transfer-rate modeling of an HCl absorber predicts 2 percent fog in the vapor. The impact is equivalent to lowering the stage efficiency to 20 percent.

Spontaneous (Homogeneous) Nucleation This process is quite difficult because of the energy barrier associated with creation of the interfacial area. It can be treated as a kinetic process with the

rate a very steep function of the supersaturation ratio ($S = \text{partial pressure of condensable per vapor pressure at gas temperature}$). For water, an increase in S from 3.4 to 3.9 causes a 10,000-fold increase in the nucleation rate. As a result, below a critical supersaturation (S_{crit}), homogeneous nucleation is slow enough to be ignored. Generally, S_{crit} is defined as that which limits nucleation to one particle produced per cubic centimeter per second. It can be estimated roughly by traditional theory (*Theory of Fog Condensation*, Israel Program for Scientific Translations, Jerusalem, 1967) using the following equation:

$$S_{\text{crit}} = \exp \left[0.56 \frac{M}{\rho_l} \left(\frac{\sigma}{T} \right)^{3/2} \right] \quad (14-205)$$

where $\sigma = \text{surface tension, mN/m (dyn/cm)}$

$\rho_l = \text{liquid density, g/cm}^3$

$T = \text{temperature, K}$

$M = \text{molecular weight of condensable}$

Table 14-15 shows typical experimental values of S_{crit} taken from the work of Russel [*J. Chem. Phys.*, **50**, 1809 (1969)].

Since the critical supersaturation ratio for homogeneous nucleation is typically greater than 3, it is not often reached in process equipment.

Growth on Foreign Nuclei As noted above, foreign nuclei are often present in abundance and permit fog formation at much lower supersaturation. For example,

1. **Solids.** Surveys have shown that air contains thousands of particles per cubic centimeter in the 0.1- μm to 1- μm range suitable for nuclei. The sources range from ocean-generated salt spray to combustion processes. The concentration is highest in large cities and industrial regions. When the foreign nuclei are soluble in the fog, nucleation occurs at S values very close to 1.0. This is the mechanism controlling atmospheric water condensation. Even when not soluble, a foreign particle is an effective nucleus if wet by the liquid. Thus, a 1- μm insoluble particle with zero contact angle requires an S of only 1.001 in order to serve as a condensation site for water.

2. **Ions.** Amelin [*Theory of Fog Condensation*, Israel Program for Scientific Translations, Jerusalem, (1967)] reports that ordinary air contains even higher concentrations of ions. These ions also reduce the required critical supersaturation, but by only about 10 to 20 percent, unless multiple charges are present.

3. **Entrained liquids.** Production of small droplets is inherent in the bubbling process, as shown by Fig. 14-90. Values range from near zero to 10,000/ cm^3 of vapor, depending on how the vapor breaks through the liquid and on the opportunity for evaporation of the small drops after entrainment.

As a result of these mechanisms, most process streams contain enough foreign nuclei to cause some fogging. While fogging has been reported in only a relatively low percent of process partial condensers, it is rarely looked for and volunteers its presence only when yield losses or pollution is intolerable.

Dropsize Distribution Monodisperse (nearly uniform droplet size) fogs can be grown by providing a long retention time for growth. However, industrial fogs usually show a broad distribution, as in Fig. 14-91. Note also that for this set of data, the sizes are several orders of magnitude smaller than those shown earlier for entrainment and atomizers.

The result, as discussed in a later subsection, is a demand for different removal devices for the small particles.

While generally fog formation is a nuisance, it can occasionally be useful because of the high surface area generated by the fine drops. An example is insecticide application.

TABLE 14-14 Simulation of Three Heat Exchangers with Varying Foreign Nuclei

	1	2	3
Weight fraction, noncondensable			
Inlet	0.51	0.42	0.02
Outlet	0.80	0.80	0.32
Molecular weight			
Inert	28	29	29
Condensable	86	99	210
Temperature difference between gas and liquid interface, K			
Inlet	14	24	67
Outlet	4	10	4
Percent of liquid that leaves unit as fog			
Nuclei concentration in inlet particles/ cm^3			
100	0.05	1.1	2.2
1,000	0.44	5.6	3.9
10,000	3.2	9.8	4.9
100,000	9.6	11.4	5.1
1,000,000	13.3	11.6	
10,000,000	14.7		
∞	14.7	11.8	5.1
Fog particle size based on 10,000 nuclei/ cm^3 at inlet, μm	28	25	4

TABLE 14-15 Experimental Critical Supersaturation Ratios

	Temperature, K°	S_{crit}
H_2O	264	4.91
$\text{C}_2\text{H}_5\text{OH}$	275	2.13
CH_3OH	264	3.55
C_6H_6	253	5.32
CCl_4	247	6.5
CHCl_3	258	3.73
$\text{C}_6\text{H}_5\text{Cl}$	250	9.5

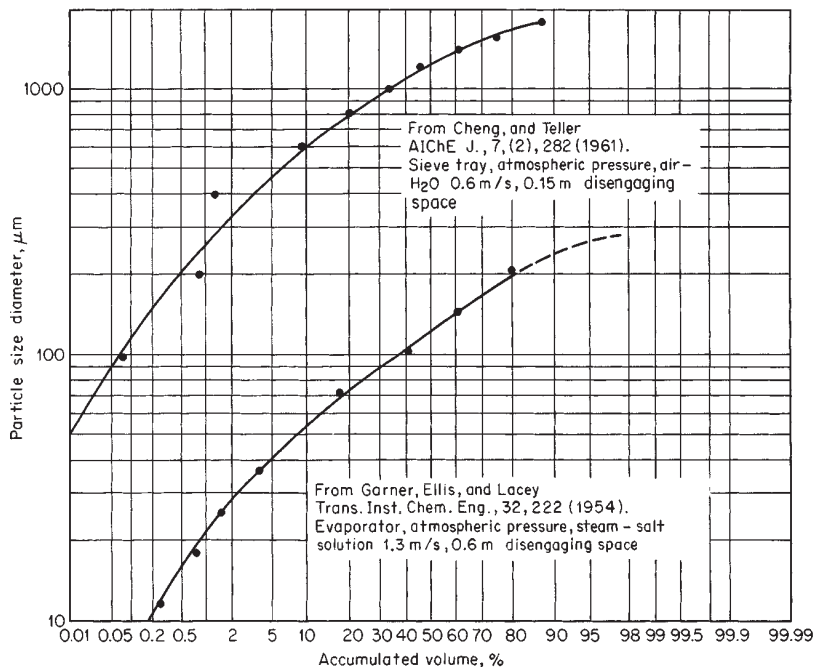


FIG. 14-90 Entrainment droplet-size distribution. To convert meters per second to feet per second, multiply by 3.28, to convert meters to feet multiply by 3.28.

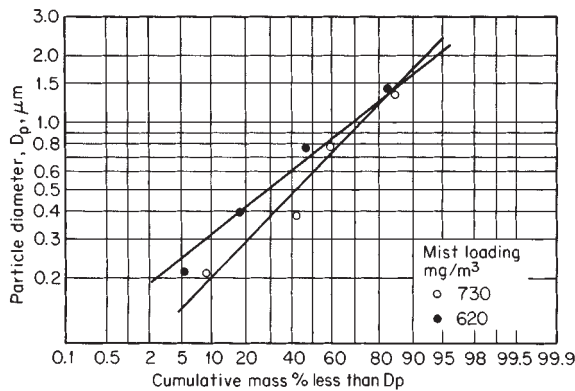


FIG. 14-91 Particle-size distribution and mist loading from absorption tower in a contact H_2SO_4 plant. [Gillespie and Johnstone, Chem. Eng. Prog., 51(2), 74 (1955).]

GAS-IN-LIQUID DISPERSIONS

GENERAL REFERENCES: Comprehensive treatments of bubbles or foams are given by Akers, *Foams: Symposium 1975*, Academic Press, New York, 1973; Bendure, *Tappi*, 58, 83 (1975); Benfratello, *Energ Elettr.*, 30, 80, 486 (1953); Berkman and Egloff, *Emulsions and Foams*, Reinhold, New York, 1941, pp. 1–12–152; Bikerman, *Foams*, Springer-Verlag, New York, 1975; Kirk-Othmer *Encyclopedia of Chemical Technology*, 4th ed., Wiley, New York, 1993, pp. 82–145; Haberman and Morton, *Report 802*, David W. Taylor Model Basin, Washington, 1953; Levich, *Physicochemical Hydrodynamics*, Prentice-Hall, Englewood Cliffs, NJ, 1962; and Soo, *Fluid Dynamics of Multiphase Systems*, Blaisdell, Waltham, Massachusetts, 1967. The formation of bubbles is comprehensively treated by Clift, Grace, and Weber, *Bubbles, Drops and Particles*, Academic, New York, 1978, Kumar and Kuloor, *Adv. Chem. Eng.*, 8, 255–368 (1970) and Wilkinson and Van Dierendonck, *Chem. Eng. Sci.*, 49, 1429–1438 (1994). Design methods for units operation in bubble columns and stirred vessels are

covered by Atika and Yoshida, *Ind. Eng. Chem. Process Des. Dev.*, 13, 84 (1974); Calderbank, *The Chem. Eng. (London)*, CE209 (October, 1967); and Mixing, vol. II, Academic, New York, 1967, pp. 1–111; Fair, *Chem. Eng.*, 74, 67 (July 3, 1967); Jordan, *Chemical Process Dev.*, Interscience, New York, 1968, part 1, pp. 111–175; Mersmann, *Ger. Chem. Eng.*, 1, 1 (1978); Resnick and Gal-Or, *Adv. Chem. Eng.*, 7, 295–395 (1968); Valentini, *Absorption in Gas-Liquid Dispersions*, E. & F. N. Spon, London, 1967; Tatterson, *Fluid Mixing and Gas Dispersion in Agitated Tanks*, McGraw-Hill, 1991; and Deckwer and Schumpe, *Chem. Eng. Sci.*, 48, 889–991 (1993).

The influence of surface-active agents on bubbles and foams is summarized in selected passages from Schwartz and Perry, *Surface Active Agents*, vol. 1, Interscience, New York, 1949; and from Schwartz, Perry, and Berch, *Surface Active Agents and Detergents*, vol. 2, Interscience, New York, 1958. See also Elenkov, *Theor. Found. Chem. Eng.*, 1, 1, 117 (1967); and Rubel, *Antifoaming and Defoaming Agents*, Noyes Data Corp., Park Ridge, NJ, 1972.

A review of foam stability also is given by de Vries, Meded, *Rubber Sticht. Delft*, No. 328, 1957. Foam-separation methodology is discussed by Aguayo and Lemlich, *Ind. Eng. Chem. Process Des. Dev.*, 13, 153 (1974); and Lemlich, *Ind. Eng. Chem.*, 60, 16 (1968). The following reviews of specific applications of gas-to-liquid dispersions are recommended: Industrial fermentations Aiba, Humphrey, and Millis, *Biochemical Engineering*, Academic, New York, 1965. Finn, *Bacteriol. Rev.*, 18, 254 (1954). Oldshue, "Fermentation Mixing Scale-Up Techniques," in *Biotechnology and Bioengineering*, vol. 8, 1966, pp. 3–24. Aerobic oxidation of wastes: Eckenfelder and McCabe, *Advances in Biological Waste Treatment*, Macmillan, New York, 1963. Eckenfelder and O'Connor, *Biological Waste Treatment*, Pergamon, New York, 1961. McCabe and Eckenfelder, *Biological Treatment of Sewage and Industrial Wastes*, vol. 1, Reinhold, New York, 1955. Proceedings of Industrial Waste Treatment Conference, Purdue University, annually. Zlokarnik, *Adv. Biochem. Eng.*, 11, 158–180 (1979). *Cellular elastomers*: Fling, *Natural Rubber Latex and Its Applications: The Preparation of Latex Foam Products*, British Rubber Development Board, London, 1954. Gould, in *Symposium on Application of Synthetic Rubbers*, American Society for Testing and Materials, Philadelphia, 1944, pp. 90–103. *Firefighting foams*: Perri, in Bikerman, op. cit., Chap. 12. Ratzer, *Ind. Eng. Chem.*, 48, 2013 (1956). *Froth-flotation methods and equipment*: Booth, in Bikerman, op. cit., Chap. 13. Gaudin, *Flotation*, McGraw-Hill, New York, 1957. Taggart, *Handbook of Mineral Dressing*, Wiley, New York, 1945, Sec. 12, pp. 52–81. Tatterson, *Fluid Mixing and Gas Dispersion in Agitated Tanks*, McGraw-Hill, New York, 1991.

Objectives of Gas Dispersion The dispersion of gas as bubbles in a liquid or in a plastic mass is effected for one of the following purposes: (1) gas-liquid contacting (to promote absorption or stripping,

with or without chemical reaction), (2) agitation of the liquid phase, or (3) foam or froth production. Gas-in-liquid dispersions also may be produced or encountered inadvertently, sometimes undesirably.

Gas-Liquid Contacting Usually this is accomplished with conventional columns or with spray absorbers (see preceding subsection "Liquid-in-Gas Dispersions"). For systems containing solids or tar likely to plug columns, absorptions accomplished by strongly exothermic reactions, or treatments involving a readily soluble gas or a condensable vapor, however, bubble columns or agitated vessels may be used to your advantage.

Agitation Agitation by a stream of gas bubbles (often air) rising through a liquid is often employed when the extra expense of mechanical agitation is not justified. Gas spargers may be used for simple blending operations involving a liquid of low volatility or for applications where agitator shaft sealing is difficult.

Foam Production This is important in froth-flotation separations; in the manufacture of cellular elastomers, plastics, and glass; and in certain special applications (e.g., food products, fire extinguishers). Unwanted foam can occur in process columns, in agitated vessels, and in reactors in which a gaseous product is formed; it must be avoided, destroyed, or controlled. Berkman and Egloff (*Emulsions and Foams*, Reinhold, New York, 1941, pp. 112–152) have mentioned that foam is produced only in systems possessing the proper combination of interfacial tension, viscosity, volatility, and concentration of solute or suspended solids. From the standpoint of gas comminution, foam production requires the creation of small bubbles in a liquid capable of sustaining foam.

Theory of Bubble and Foam Formation A bubble is a globule of gas or vapor surrounded by a mass or thin film of liquid. By extension, globular voids in a solid are sometimes called bubbles. Foam is a group of bubbles separated from one another by thin films, the aggregation having a finite static life. Although nontechnical dictionaries do not distinguish between foam and froth, a technical distinction is often made. A highly concentrated dispersion of bubbles in a liquid is considered a froth even if its static life is substantially nil (i.e., it must be dynamically maintained). Thus, all foams are also froths, whereas the reverse is not true. The term *lather* implies froth that is worked up on a solid surface by mechanical agitation; it is seldom used in technical discussions. The thin walls of bubbles comprising a foam are called *laminae* or *lamellae*.

Bubbles in a liquid originate from one of three general sources: (1) They may be formed by desupersaturation of a solution of the gas or by the decomposition of a component in the liquid; (2) They may be introduced directly into the liquid by a bubbler or sparger or by mechanical entrainment; and (3) They may result from the disintegration of larger bubbles already in the liquid.

Generation Spontaneous generation of gas bubbles within a homogeneous liquid is theoretically impossible (Bikerman, *Foams: Theory and Industrial Applications*, Reinhold, New York, 1953, p. 10). The appearance of a bubble requires a gas nucleus as a void in the liquid. The nucleus may be in the form of a small bubble or of a solid carrying adsorbed gas, examples of the latter being dust particles, boiling chips, and a solid wall. A void can result from cavitation, mechanically or acoustically induced. Blander and Katz [AIChE J., **21**, 833 (1975)] have thoroughly reviewed bubble nucleation in liquids.

Theory permits the approximation of the maximum size of a bubble that can adhere to a submerged horizontal surface if the contact angle between bubble and solid (angle formed by solid-liquid and liquid-gas interfaces) is known [Wark, *J. Phys. Chem.*, **37**, 623 (1933); Jakob, *Mech. Eng.*, **58**, 643 (1936)]. Because the bubbles that actually rise from a surface are always considerably smaller than those so calculated and inasmuch as the contact angle is seldom known, the theory is not directly useful.

Formation at a Single Orifice The formation of bubbles at an orifice or capillary immersed in a liquid has been the subject of much study, both experimental and theoretical. Bikerman (op. cit., Secs. 3 to 7), Valentin (op. cit., Chap. 2), Jackson (op. cit.), Soo (op. cit., Chap. 3), Fair (op. cit.), Kumer et al. (op. cit.), Clift et al. (op. cit.) and Wilkinson and Van Dierendonck [*Chem. Eng. Sci.*, **49**, 1429 (1994)] have presented reviews and analyses of this subject.

There are three regimes of bubble production (Silberman in *Proceedings of the Fifth Midwestern Conference on Fluid Mechanics*, Univ. of Michigan Press, Ann Arbor, 1957, pp. 263–284): (1) single-bubble, (2) intermediate, and (3) jet.

Single-Bubble Regime Bubbles are produced one at a time, their size being determined primarily by the orifice diameter d_o , the interfacial tension of the gas-liquid film σ , the densities of the liquid ρ_L and gas ρ_G , and the gravitational acceleration g according to the relation

$$d_b = \left(\frac{6\sigma}{d_o^2 (\rho_L - \rho_G)} \right)^{1/3} \quad (14-206)$$

where D_b is the bubble diameter. The bubble size is independent of gas flow rate; the frequency, therefore, is directly proportional to the gas flow rate. Equation (14-206) leads to

$$f = Qg \times \frac{\rho_L - \rho_G}{\pi d_o \sigma} \quad (14-207)$$

where f is the frequency of bubble formation and Q is the volumetric rate of gas flow in consistent units.

Equations (14-206) and (14-207) result from a balance of bubble buoyancy against interfacial tension. They include no inertia or viscosity effects. At low bubbling rates (<1/s), these equations are quite satisfactory. Van Krevelen and Hofstijzer [*Chem. Eng. Prog.*, **46**, 29 (1950)], Guyer and Peterhaus [*Helv. Chim. Acta*, **26**, 1099 (1943)] and Wilkinson (op. cit.) report good agreement with Eq. (14-185) for water, transformer oil, ether, and carbon tetrachloride for vertically oriented orifices with $0.004 < D < 0.95$ cm. If the orifice diameter becomes too large, the bubble diameter will be smaller than the orifice diameter, as predicted by Eq. (14-206), and instability results; consequently, stable, stationary bubbles cannot be produced.

For bubbles formed in water, the orifice diameter that permits bubbles of about its own size is calculated as 0.66 cm. Davidson and Amick [AIChE J., **2**, 337 (1956)] confirmed this estimate in their observation that stable bubbles in water were formed at a 0.64-cm orifice but could not be formed at a 0.79-cm orifice.

For very thin liquids, Eqs. (14-206) and (14-207) are expected to be valid up to a gas-flow Reynolds number of 200 (Valentin, op. cit., p. 8). For liquid viscosities up to 100 cP, Datta, Napier, and Newitt [*Trans. Inst. Chem. Eng.*, **28**, 14 (1950)] and Siems and Kauffman [*Chem. Eng. Sci.*, **5**, 127 (1956)] have shown that liquid viscosity has very little effect on the bubble volume, but Davidson and Schuler [*Trans. Instn. Chem. Eng.*, **38**, 144 (1960)] and Krishnamurthy et al. [*Ind. Eng. Chem. Fundam.*, **7**, 549 (1968)] have shown that bubble size increases considerably over that predicted by Eq. (14-206) for liquid viscosities above 1000 cP. In fact, Davidson et al. (op. cit.) found that their data agreed very well with a theoretical equation obtained by equating the buoyant force to drag based on Stokes' law and the velocity of the bubble equator at break-off:

$$d_b = \left(\frac{6}{\pi} \right) \left(\frac{4\pi}{3} \right)^{1/4} \left(15 \times \frac{vQ}{2g} \right)^{3/4} \quad (14-208)$$

where v is the liquid kinematic viscosity and Q is the gas volumetric flow rate. This equation is dimensionally consistent. The relative effect of liquid viscosity can be obtained by comparing the bubble diameters calculated from Eqs. (14-206) and (14-208). If liquid viscosity appears significant, one might want to use the long and tedious method developed by Krishnamurthy et al. (op. cit.) that considers both surface-tension forces and viscous-drag forces.

Intermediate Regime This regime extends approximately from a Reynolds number of 200 to one of 2100. As the gas flow through a submerged orifice increases beyond the limit of the single-bubble regime, the frequency of bubble formation increases more slowly, and the bubbles begin to grow in size. Between the two regimes there may indeed be a range of gas rates over which the bubble size decreases with increasing rate, owing to the establishment of liquid currents that nip the bubbles off prematurely. The net result can be the occurrence of a minimum bubble diameter at some particular gas rate [Mater, *U.S. Bur. Mines Bull.* 260 (1927) and Bikerman, op. cit., p. 4]. At the upper portion of this region, the frequency becomes very nearly constant with respect to gas rate, and the bubble size correspondingly increases with gas rate. The bubble size is affected primarily by (1) ori-

fice diameter, (2) liquid-inertia effects, (3) liquid viscosity, (4) liquid density, and (5) the relationship between the constancy of gas flow and the constancy of pressure at the orifice.

Kumar et al. have done extensive experimental and theoretical work reported in *Ind. Eng. Chem. Fundam.*, **7**, 549 (1968); *Chem. Eng. Sci.*, **24**, part 1, 731; part 2, 749; part 3, 1711 (1969) and summarized in *Adv. Chem. Eng.*, **8**, 255 (1970). They, along with other investigators—Swope [*Can. J. Chem. Eng.*, **44**, 169 (1972)], Tsuge and Hibino [*J. Chem. Eng. Japan*, **11**, 307 (1972)], Pinczewski [*Chem. Eng. Sci.*, **36**, 405 (1981)], Tsuge and Hibino [*Int. Chem. Eng.*, **21**, 66 (1981)], and Takahashi and Miyahara [ibid., p. 224]—have solved the equations resulting from a force balance on the forming bubble, taking into account buoyancy, surface tension, inertia, and viscous-drag forces for both conditions of constant flow through the orifice and constant pressure in the gas chamber. The design method is complex and tedious and involves the solution of algebraic and differential equations. Although Mersmann [*Ger. Chem. Eng.*, **1**, 1 (1978)] claims that the results of Kumar et al. (loc. cit.) well fit experimental data, Lanauze and Harn [*Chem. Eng. Sci.*, **29**, 1663 (1974)] claim differently:

Further, it has been shown that the mathematical formulation of Kumar's model, including the condition of detachment, does not adequately describe the experimental situation—Kumar's model has several fundamental weaknesses, the computational simplicity being achieved at the expense of physical reality.

In lieu of careful independent checks of predictive accuracy, the results of the comprehensive theoretical work will not be presented here. Simpler, more easily understood predictive methods, for certain important limiting cases, will be presented. As a check on the accuracy of these simpler methods, it will perhaps be prudent to calculate the bubble diameter from the graphical representation by Mersmann (loc. cit.) of the results of Kumar et al. (loc. cit.).

For conditions approaching constant flow through the orifice, a relationship derived by equating the buoyant force to the inertia force of the liquid [Davidson et al., *Trans. Instn. Chem. Engrs.*, **38**, 335 (1960)] (dimensionally consistent),

$$d_b = 1.378 \times \frac{6Q^{6/5}}{\pi g^{3/5}} \quad (14-209)$$

fits experimental data reasonably well. Surface tension and liquid viscosity tend to increase the bubble size—at a low Reynolds number. The effect of surface tension is greater for large orifice diameters. The magnitude of the diameter increase due to high liquid viscosity can be obtained from Eq. (14-208).

For conditions approaching constant pressure at the orifice entrance, which probably simulates most industrial applications, there is no independently verified predictive method. For air at near atmospheric pressure sparged into relatively inviscid liquids (11–100 cP), the correlation of Kumar et al. [*Can. J. Chem. Eng.*, **54**, 503 (1976)] fits experimental data well. Their correlation is presented here as Fig. 14-92.

Wilkinson et al. (op. cit.) make the following observation about the effect of gas density on bubble size: "The fact that the bubble size decreases slightly for higher gas densities can be explained on the basis of a force balance."

Jet Regime With further rate increases, turbulence occurs at the orifice, and the gas stream approaches the appearance of a continuous jet that breaks up 7.6 to 10.2 cm above the orifice. Actually, the stream consists of large, closely spaced, irregular bubbles with a rapid swirling motion. These bubbles disintegrate into a cloud of smaller ones of random size distribution between 0.025 cm or smaller and about 1.25 cm, with a mean size for air and water of about 0.4 cm (Leibson et al., loc. cit.). According to Wilkinson et al. (op. cit.), jetting begins when

$$N_{We,g} = \frac{\rho_g d_o U_o^2}{\sigma} \leq 2 \quad (14-210)$$

There are many contradictory reports about the jet regime, and theory, although helpful (see, for example, Siberman, loc. cit.), is as yet unable to describe the phenomena observed. The correlation of Kumar et al. (Fig. 14-92) is recommended for air-liquid systems.

Formation at Multiple Orifices At high velocities, coalescence of bubbles formed at individual orifices occurs; Helsby and Tuson [Research (London), **8**, 270 (1955)], for example, observed the frequent coalescence of bubbles formed in pairs or in quartets at an orifice. Multiple orifices spaced by the order of magnitude of the orifice diameter increase the probability of coalescence, and when the magnitude is small (as in a sintered plate), there is invariably some. The broken lines of Fig. 14-92 presumably represent zones of increased coalescence and relatively less effective dispersion as the gas rate through porous-carbon tubes is increased. Savitskaya [*Kolloidn. Z.*, **13**, 309 (1951)] found that the average bubble size formed at the surface of a porous plate was such as to maintain constancy of the product of bubble specific surface and interfacial tension as the latter was varied by addition of a surfactant. Konig et al. [*Ger. Chem. Eng.*, **1**, 199 (1978)] produced bubble sizes varying from 0.5 to 4 mm by the use of two porous-plate spargers and one perforated-plate sparger with superficial gas velocities from 1 to 8 cm/s. The small bubble sizes were stabilized by adding up to 0.5 percent of various alcohols to water.

At high-flow rates through perforated plates such as those that occur in distillation columns, Calderbank and Rennie [*Trans. Instn. Chem. Engrs.*, **40**, T3 (1962)]; Porter et al. [ibid., **45**, T265 (1967)]; Rennie and Evans [*Br. Chem. Eng.*, **7**, 498 (1962)]; and Valentini (op. cit., Chap. 3) have investigated and discussed the effect of the flow conditions through the multiple orifices on the froths and foams that occur above perforated plates.

Entrainment and Mechanical Disintegration Gas can be entrained into a liquid by a solid or a stream of liquid falling from the gas phase into the liquid, by surface ripples or waves, and by the vertical swirl of a mass of agitated liquid about the axis of a rotating agita-

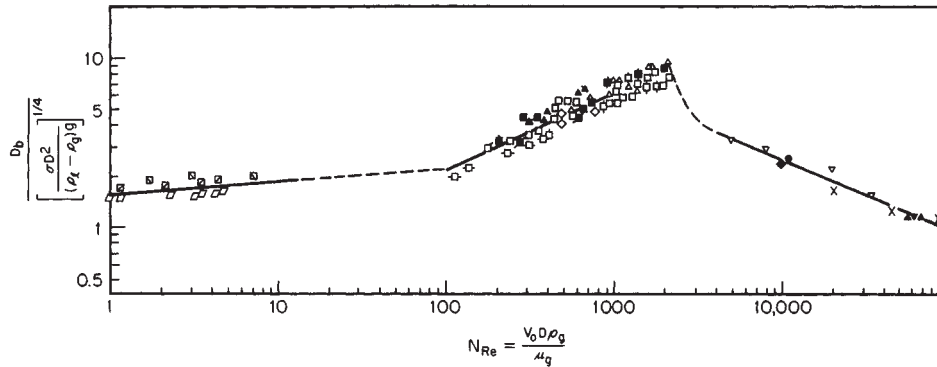


FIG. 14-92 Bubble-diameter correlation for air sparged into relatively inviscid liquids. D_b = bubble diameter, D = orifice diameter, V_o = gas velocity through sparging orifice, P = fluid density, and μ = fluid viscosity. [From Can. J. Chem. Eng., **54**, 503 (1976).]

tor. Small bubbles probably form near the surface of the liquid and are caught into the path of turbulent eddies, whose velocity exceeds the terminal velocity of the bubbles. The disintegration of a submerged mass of gas takes place by the turbulent tearing of smaller bubbles away from the exterior of the larger mass or by the influence of surface tension on the mass when it is attenuated by inertial or shear forces into a cylindrical or disk form. A fluid cylinder that is greater in length than in circumference is unstable and tends to break spontaneously into two or more spheres. These effects account for the action of fluid attrition and of an agitator in the disintegration of suspended gas. Quantitative correlations for gas entrainment by liquid jets and in agitated vessels will be given later.

Foams Two excellent reviews (Shedlovsky, *op. cit.*; Lemlich, *op. cit.*) covering the literature pertinent to foams have been published. A foam is formed when bubbles rise to the surface of a liquid and persist for a while without coalescence with one another or without rupture into the vapor space. The formation of foam, then, consists simply of the formation, rise, and aggregation of bubbles in a liquid in which foam can exist. The life of foams varies over many magnitudes—from seconds to years—but in general is finite. Maintenance of a foam, therefore, is a dynamic phenomenon.

Gravitational force favors the separation of gas from liquid in a dispersive system, causing the bubbles to rise to the liquid surface and the liquid contained in the bubble walls to drain downward to the main body of the liquid. Interfacial tension favors the coalescence and ultimate disappearance of bubbles; indeed, it is the cause of bubble destruction upon the rupture of the laminae.

The viscosity of the liquid in a film opposes the drainage of the film and its displacement by the approach of coalescing bubbles. The higher the viscosity, the slower will be the film-thinning process; furthermore, if viscosity increases as the film grows thinner, the process becomes self-retarding. The viscosity of films appears to be greater than that of the main body of the parent liquid in many cases. Sometimes this is a simple temperature effect, the film being cooler because of evaporation; sometimes it is a concentration effect, with dissolved or fine suspended solids migrating to the interface and producing classical or anomalous increases in viscosity; at yet other times, the effect seems to occur without explanation.

If the liquid laminae of a foam system can be converted to impermeable solid membranes, the film viscosity can be regarded as having become infinite, and the resulting solid foam will be permanent. Likewise, if the laminae are composed of a gingham plastic or a thixotrope, the foam will be permanently stable for bubbles whose buoyancy does not permit exceeding the yield stress. For other nonnewtonian fluids, however, and for all newtonian ones, no matter how viscous, the viscosity can only delay but never prevent foam disappearance. The popular theory, held since the days of Plateau, that foam life is proportional to surface viscosity and inversely proportional to interfacial tension, is not correct, according to Bikerman (*op. cit.*, p. 161), who points out that it is contradicted by experiment.

The idea that foam films drain to a critical thickness at which they spontaneously burst is also rejected by Bikerman. Foam stability, rather, is keyed to the existence of a surface skin of low interfacial tension immediately overlying a solution bulk of higher tension, latent until it is exposed by rupture of the superficial layer [Maragoni, *Nuovo Cimento*, **2**(5-6), 239 (1871)]. Such a phenomenon of surface elasticity, resulting from concentration differences between bulk and surface of the liquid, accounts for the ability of bubbles to be penetrated by missiles without damage. It is conceivable that films below a certain thickness no longer carry any bulk of solution and hence have no capacity to close surface ruptures, thus becoming vulnerable to mechanical damage that will destroy them. The Maragoni phenomenon is consistent also with the observation that neither pure liquids nor saturated solutions will sustain a foam, since neither extreme will allow the necessary differences in concentration between surface and bulk of solution.

The specific ability of certain finely divided, insoluble solids to stabilize foam has long been known [Berkman and Egloff, *op. cit.*, p. 133; and Bikerman, *op. cit.*, Chap. 11]. Bartsch [*Kolloidchem. Beih.*, **20**, 1 (1925)] found that the presence of fine galena greatly extended the life of air foam in aqueous isoamyl alcohol, and the finer the solids, the

greater the stability. Particles on the order of 50 μm length extended the life from 17 seconds to several hours. This behavior is consistent with theory, which indicates that a solid particle of medium contact angle with the liquid will prevent the coalescence of two bubbles with which it is in simultaneous contact. Quantitative observations of this phenomenon are scanty.

Berkman and Egloff explain that some additives increase the flexibility or toughness of bubble walls, rather than their viscosity, to render them more durable. They cite as illustrations the addition of small quantities of soap to saponin solutions or of glycerin to soap solution to yield much more stable foam. The increased stability with ionic additives is probably due to electrostatic repulsion between charged, nearly parallel surfaces of the liquid film, which acts to retard draining and hence rupture.

Characteristics of Dispersion

Properties of Component Phases As discussed in the preceding subsection, dispersions of gases in liquids are affected by the viscosity of the liquid, the density of the liquid and of the gas, and the interfacial tension between the two phases. They also may be affected directly by the composition of the liquid phase. Both the formation of bubbles and their behavior during their lifetime are influenced by these quantities as well as by the mechanical aspects of their environment.

Viscosity and density of the component phases can be measured with confidence by conventional methods, as can the interfacial tension between a pure liquid and a gas. The interfacial tension of a system involving a solution or micellar dispersion becomes less satisfactory, because the interfacial free energy depends on the concentration of solute at the interface. Dynamic methods and even some of the so-called static methods involve the creation of new surfaces. Since the establishment of equilibrium between this surface and the solute in the body of the solution requires a finite amount of time, the value measured will be in error if the measurement is made more rapidly than the solute can diffuse to the fresh surface. Eckenfelder and Barnhart (*Am. Inst. Chem. Engrs.*, 42d national meeting, Repr. 30, Atlanta, 1960) found that measurements of the surface tension of sodium lauryl sulfate solutions by maximum bubble pressure were higher than those by DuNoy tensiometer by 40 to 90 percent, the larger factor corresponding to a concentration of about 100 ppm, and the smaller to a concentration of 2500 ppm of sulfate.

Even if the interfacial tension is measured accurately, there may be doubt about its applicability to the surface of bubbles being rapidly formed in a solution of a surface-active agent, for the bubble surface may not have time to become equilibrated with the solution. Coppock and Meiklejohn [*Trans. Instn. Chem. Engrs.*, **29**, 75 (1951)] reported that bubbles formed in the single-bubble regime at an orifice in a solution of a commercial detergent had a diameter larger than that calculated in terms of the measured surface tension of the solution [Eq. (14-206)]. The disparity is probably a reflection of unequilibrated bubble laminae.

One concerned with the measurement of gas-liquid interfacial tension should consult the useful reviews of methods prepared by Harkins [in Chap. 9 of Weissberger, *Techniques of Organic Chemistry*, 2d ed., vol. 1, part 2, Interscience, New York, 1949], Schwartz and coauthors [*Surface Active Agents*, vol. 1, Interscience, New York, 1949, pp. 263-271; *Surface Active Agents and Detergents*, vol. 2, Interscience, New York, 1958, pp. 389-391, 417-418], and by Adamson [*Physical Chemistry of Surfaces*, Interscience, New York, 1960].

Dispersion Characteristics The chief characteristics of gas-in-liquid dispersions, like those of liquid-in-gas suspensions, are heterogeneity and instability. The composition and structure of an unstable dispersion must be observed in the dynamic situation by looking at the mixture, with or without the aid of optical devices, or by photographing it, preferably in nominal steady state; photographs usually are required for quantitative treatment. Stable foams may be examined after the fact of their creation if they are sufficiently robust or if an immobilizing technique such as freezing is employed [Chang et al., *Ind. Eng. Chem.*, **48**, 2035 (1956)].

The rate of rise of bubbles has been discussed in many papers, including two that present good reviews of the subject [Benfratello, *Energ. Elettr.*, **30**, 80 (1953); Haberman and Morton, *Report 802:*

David W. Taylor Model Basin, Washington, September 1953; Jackson, loc. cit.; Valentin, op. cit., Chap. 2; Soo, op. cit., Chap. 3; Calderbank, loc. cit., p. CE220; and Levich, op. cit., Chap. 8). A comprehensive and apparently accurate predictive method has been published [Jamiyahmadi et al., *Trans ICE*, **72**, part A, 119–122 (1994)]. Small bubbles (below 0.2 mm in diameter) are essentially rigid spheres and rise at terminal velocities that place them clearly in the laminar-flow region; hence their rising velocity may be calculated from Stokes' law. As bubble size increases to about 2 mm, the spherical shape is retained, and the Reynolds number is still sufficiently small (<10) that Stokes' law should be nearly obeyed.

As bubble size increases, two effects set in, however, that alter the velocity. At about $N_{Re} = 100$, a wobble begins that can develop into a helical path if the bubbles are not liberated too closely to one another [Houghton, McLean, and Ritchie, *Chem. Eng. Sci.*, **7**, 40 (1957); and Houghton et al., ibid., p. 111]. Furthermore, for bubbles in the range of 1 mm and larger (until distortion becomes serious) internal circulation can set in [Garner and Hammerton, *Chem. Eng. Sci.*, **3**, (1954); and Haberman and Morton, loc. cit.], and according to theoretical analyses by Hadamard and Rybczynski and given by Levich (op. cit.), the drag coefficient for a low-viscosity dispersed phase and a high-viscosity continuous phase will approach two-thirds of the drag coefficient for rigid spheres, namely $C_D = 16/N_{Re}$. The rise velocity of a circulating bubble or drop will thus be 1.5 times that of a rigid sphere. Redfield and Houghton [*Chem. Eng. Sci.*, **20**, 131 (1965)] have found that CO_2 bubbles rising in pure water agree with the theoretical solution for a circulating drop below $N_{Re} = 1$. Many investigators (see Valentin, op. cit.) have found that extremely small quantities of impurities can retard or stop this internal circulation. In this behavior may lie the explanation of the fact that the addition of long-chain fatty acids to water to produce a concentration of 1.5×10^{-4} molar markedly reduces the rate of rise of bubbles [Stuke, *Naturwissenschaften*, **39**, 325 (1952)].

Above diameters of about 2 mm, bubbles begin to change to ellipsoids, and above 1 cm they become lens-shaped, according to Davies and Taylor [*Proc. Roy. Soc. (London)*, **A200**, 379 (1950)]. The rising velocity in thin liquids for the size range $1 \text{ mm} < D_B < 20 \text{ mm}$ has been reported as 20 to 30 cm/s by Haberman and Morton (op. cit.) and Davenport, Richardson, and Bradshaw [*Chem. Eng. Sci.*, **22**, 1221 (1967)]. Schwerdtfeger [ibid., **23**, 937 (1968)] even found the same for argon bubbles rising in mercury. Surface-active agents have no effect on the rise velocity of bubbles larger than 4 mm in thin liquids (Davenport et al., loc. cit.).

Above a Reynolds number of the order of magnitude of 1000, bubbles assume a helmet shape, with a flat bottom (Eckenfelder and Barnhart, loc. cit.; and Leibson et al., loc. cit.). After bubbles become large enough to depart from Stokes' law at their terminal velocity, behavior is generally complicated and erratic, and the reported data scatter considerably. The rise can be slowed, furthermore, by a wall effect if the diameter of the container is not greater than 10 times the diameter of the bubbles, as shown by Uno and Kintner [*AIChE J.*, **2**, 420 (1956); and Collins, *J. Fluid Mech.*, **28**(1), 97 (1967)]. Work has been done to predict the rise velocity of large bubbles [Rippin and Davidson, *Chem. Eng. Sci.*, **22**, 217 (1967); Grace and Harrison, ibid., 1337; Mendelson, *AIChE J.*, **13**, 250 (1967); Cole, ibid., Lehrer, *J. Chem. Eng. Japan*, **9**, 237; (1976) and Lehrer, *AIChE J.*, **26**, 170 (1980)]. The works of Lehrer present correlations that accurately predict rise velocities for a wide range of system properties. An excellent review of the technical literature concerning the rise of single bubbles and drops has been published by Clift, Grace, and Weber (*Bubbles, Drops and Particles*, Academic, New York, 1978). Mendelson has used a wave theory to predict the terminal velocity, and Cole has checked the theory with additional data. The other authors listed solved some simplified form of the Navier-Stokes equations. Jamiyahmadi et al., loc. cit., have developed a single equation predictive method for bubble rise velocity, which covers the entire range of bubble diameters.

When bubbles are produced in clouds, as by a porous disperser, their behavior during rising is further complicated by interaction among themselves. In addition to the tendency for small bubbles to coalesce and large ones to disintegrate, there are two additional

opposing influences on the rate of rise of bubbles of any particular size: (1) A "chimney effect" can develop in which a massive current upward appears at the axis of the bubble stream, leading to increased net bubble velocity; and (2) the proximity of the bubbles to one another can result in a hindered-settling condition, leading to reduced average bubble velocity. Figure 14-93 shows the data of Houghton et al. (op. cit.) for clouds of bubbles compared with their single-bubble data for pure water and seawater and of Peebles and Garber [*Chem. Eng. Progr.*, **49**, 88 (1953)] for acetic acid and ethyl acetate. The bubble clouds were produced with a sintered-glass plate of mean pore size (inferred from air wet-permeability data) of 81 μm .

The difference between the curves for pure water and seawater again illustrates the significance of small concentrations of solute with respect to bubble behavior. In commercial bubble columns and agitated vessels coalescence and breakup are so rapid and violent that the rise velocity of a single bubble is meaningless. The average rise velocity can, however, be readily calculated from holdup correlations that will be given later.

The quantitative examination of bubble systems is aided by the use of proper illumination and photography. The formation of bubbles at single sources often is sufficiently periodic to be stopped by stroboscopic light. Clouds of rising bubbles are more difficult to assess and require careful technique. Satisfactory photographic methods have been developed by Vermenlen, Williams, and Langlois [*Chem. Eng. Progr.*, **51**, 85 (1955)] and by Calderbank [*Trans. Instn. Chem. Engrs.*, **36**, 443 (1958)] and are described by these authors. Calderbank's technique resulted in particularly precise measurements that permitted a good estimation of the surface area of the dispersed bubbles.

Methods of Gas Dispersion The problem of dispersing a gas in a liquid may be attacked in several ways: (1) The gas bubbles of the desired size or which grow to the desired size may be introduced directly into the liquid; (2) a volatile liquid may be vaporized by either decreasing the system pressure or increasing its temperature; (3) a chemical reaction may produce a gas; or (4) a massive bubble or stream of gas is disintegrated by fluid shear and/or turbulence in the liquid.

Spargers: Simple Bubbler The simplest method of dispersing gas in a liquid contained in a tank is to introduce the gas through an open-end standpipe, a horizontal perforated pipe, or a perforated plate at the bottom of the tank. At ordinary gassing rates (corresponding to the jet regime), relatively large bubbles will be produced regardless of the size of the orifices.

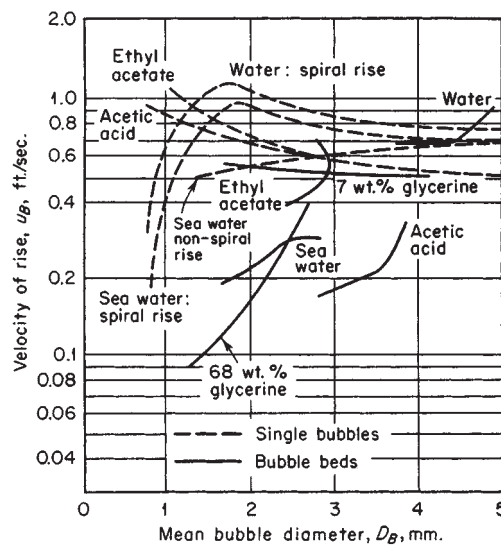


FIG. 14-93 Velocity of rising bubbles, singly and in clouds. To convert feet per second to meters per second, multiply by 0.305. [From *Chem. Eng. Sci.*, **7**, 48 (1957).]

14-74 GAS ABSORPTION AND GAS-LIQUID SYSTEM DESIGN

Perforated-pipe or -plate spargers usually have orifices 3 to 12 mm in diameter. Effective design methods to minimize maldistribution are presented in the fifth edition of this handbook, p. 5-47, 1973, and by Knaebel [*Chem. Eng.*, 116 (Mar. 9, 1981)]. For turbulent flow conditions into the sparger, the following relationship will allow design of a perforated-pipe sparger for a given degree of maldistribution provided $N_h > 5$ and length/diameter < 300.

$$d_p = 0.95(N_h C_v)^{1/2} \times \left(\frac{d_h}{\Delta U_h/U_h} \right)^{1/4} \quad (14-211)$$

where d_p = pipe diameter, d_h = sparging hole diameter, N_h = number of holes in sparger, C_v = orifice coefficient for sparger hole (see *Chemical Engineers' Handbook*, 5th ed., pp. 5-13, 5-34), U_h = average velocity through sparger holes, ΔU_h = difference between maximum and minimum velocities through sparger holes, and $\Delta U_h/U_h$ = fractional maldistribution of flow through sparger holes.

Simple spargers are used as agitators for large tanks, principally in the cement and oil industries. Kauffman [*Chem. Metall. Eng.*, **37**, 178-180 (1930)] reported the following air rates for various degrees of agitation in a tank containing 2.7 m (9 ft) of liquid:

Degree of agitation	Air rate, $m^3/(m^2 \text{ tank cross section}, \text{min})$
Moderate	0.0033
Complete	0.0066
Violent	0.016

For a liquid depth of 0.9 m (3 ft), Kauffman recommended that the listed rates be doubled.

An air lift consisting of a sparger jetting into a draft tube with ports discharging at several heights has been recommended by Heiser [*Chem. Eng.*, **55**(1), 135 (1948)] for maintaining agitation in a heavy, coarse slurry, the level of which varies widely. The design is illustrated in Fig. 14-94.

The ability of a sparger to blend miscible liquids might be described in terms of a fictitious diffusivity. Siemes did so, reporting that the agitation produced by a stream of bubbles rising in a tube with a superficial velocity of about 8.2 cm/s corresponded to an apparent diffusion coefficient as large as 75 cm^2/s [*Chem. Ing. Tech.*, **29**, 727 (1957)]. The blending rate thus is several orders of magnitude higher than it would be by natural diffusive action. These results are

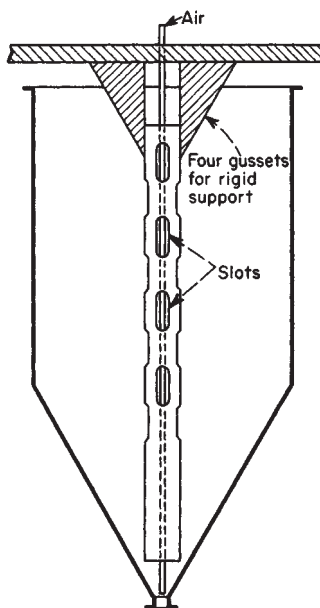


FIG. 14-94 Slotted air lift for agitation of a variable-level charge. [From *Chem. Eng.*, **55**(1), 135 (1948).]

typical of subsequent investigations on back mixing, which will be discussed in more detail later.

Lehrer [*Ind. Eng. Chem. Process Des. Dev.*, **7**, 226 (1968)] conducted liquid-blending tests with air sparging in a 0.61-m-diameter by 0.61-m-tall vessel and found that an air volume equal to about one-half of the vessel volume gave thorough blending of inviscid liquids of equal viscosities. Using an analogy to mechanically agitated vessels in which equal tank turnovers give equal blend times, one would expect this criterion to be applicable to other vessel sizes. Liquids of unequal density would probably require somewhat more air.

Open-end pipes, perforated plates, and ring- or cross-style perforated-pipe spargers are used without mechanical agitation to promote mass transfer, as in chlorinators and biological sewage treatment. In the "quiescent regime" (superficial gas velocity less than 4.57 to 6.1 cm/s [0.15 to 0.2 ft/s]) the previously mentioned spargers are usually operated at orifice Reynolds numbers in excess of 6000 in order to get small bubbles so as to increase the interfacial area and thus increase mass transfer. In the "turbulent regime" (superficial gas velocity greater than 4.57 to 6.1 cm/s), sparger design is not critical because a balance between coalescence and breakup is established very quickly according to Towell et al. [*AIChE Symp. Ser. No. 10*, 97 (1965)]. However, a reasonably uniform orifice distribution over the column cross section is desirable, and according to Fair [*Chem. Eng.*, **74**, 67 (July 3, 1967); 207 (July 17, 1967)] the orifice velocity should be less than 75 to 90 m/s.

Porous Septa In the quiescent regime porous plates, tubes, disks, or other shapes that are made by bonding or sintering together carefully sized particles of carbon, ceramic, polymer, or metal are frequently used for gas dispersion, particularly in foam fractionators. The resulting septa may be used as spargers to produce much smaller bubbles than will result from a simple bubbler. Figure 14-95 shows a com-



FIG. 14-95a Comparison of bubbles from a porous septum and from a perforated-pipe sparger. Air in water at 70°F. Grade 25 porous-carbon diffuser operating under a pressure differential of 13.7 in of water.



FIG. 14-95b Comparison of bubbles from a porous septum and from a perforated-pipe sparger. Air in water at 70°F. Karbate pipe perforated with 1/16-in holes on 1-in centers. (National Carbon Co.) To convert inches to centimeters, multiply by 2.54; °C = $\frac{5}{9}$ (°F - 32).

parison of the bubbles emitted by a perforated-pipe sparger [0.16-cm orifices] and a porous carbon septum (120 μm pores). The gas flux through a porous septum is limited on the lower side by the requirement that, for good performance, the whole sparger surface should bubble more or less uniformly, and on the higher side by the onset of serious coalescence at the surface of the septum, resulting in poor dispersion. In the practical range of fluxes, the size of the bubbles produced depends on both the size of pores in the septum and the pressure drop imposed across it, being a direct function of both.

Table 14-16 lists typical grades of porous carbon, silica, alumina, stainless steel (type 316), and polymers commercially available.

Porous media are also manufactured from porcelain, glass, silicon carbide, and a number of metals: Monel, Inconel, nickel, bronze, Hastelloy C, Stellite L-605, gold, platinum, and many types of stainless steel. The air permeabilities of Table 14-16 indicate the relative flow resistances of the various grades to homogeneous fluid but may not be used in designing a disperser for submerged operation, for the resistance of a septum to the flow of gas increases when it is wet. The air permeabilities for water-submerged porous carbon of some of the grades listed in the table are shown in Fig. 14-96. The data were determined with septa 0.625 inches thick in water at 70°F. Comparable wet-permeability data for 1-in Alundum plates of two grades of fineness are given in Table 14-17.

The gas rate at which coalescence begins to reduce the effectiveness of dispersion appears to depend not only on the pore size and pore structure of the dispersing medium but also on the liquid properties, liquid depth, agitation, and other features of the sparging environment; coalescence is strongly dependent on the concentration of

TABLE 14-16 Characteristics of Porous Septa

Grade	Avg. % porosity	Avg. pore diam.	Air-permeability data		
			Diaphragm thickness, in	Pressure differential, in water	Air flow, cu ft/(sq ft)(min)
Alundum porous alumina*					
P2220		25	1	2	0.35
P2120	36	60	1	2	2
P260	35	164	1	2	15
P236	34	240	1	2	40
P216		720	1	2	110
National porous carbon†					
60	48	33	1	2	
45	48	58	1	2	2
25	48	120	1	2	13
Filtros porous silica‡					
Extra fine	26.0	55	1.5	2	1-3
Fine	28.8	110	1.5	2	4-8
Medium fine	31.1	130	1.5	2	9-12
Medium	33.7	150	1.5	2	13-20
Medium coarse	33.8	200	1.5	2	21-30
Coarse	34.5	250	1.5	2	31-59
Extra coarse	36.5	300	1.5	2	60-100
Porous plastic§					
Teflon		9	0.125	1.38	5
Kel-F		15	0.125	1.38	13
Micro Metallic porous stainless steel¶					
H	45	5	0.125	1.38	1.8
G	50	10	0.125	1.38	3
F	50	20	0.125	1.38	5
E	50	35	0.125	1.38	18
D	50	65	0.125	1.38	60
C	55	165	0.125	27.7	990

*Data by courtesy of Norton Co., Worcester, Mass. A number of other grades between the extremes listed are available.

†Data by courtesy of National Carbon Co., Cleveland, Ohio.

‡Data by courtesy of Filtros Inc., East Rochester, N.Y.

§Data by courtesy of Pall Corp., Glen Cove, N.Y.

¶Similar septa made from other metals are available.

surfactants capable of forming an electrical double layer and thus produce ionic bubbles, long-chain alcohols in water being excellent examples. For porous-carbon media, the manufacturer suggests that the best dispersion performance will result if the broken-line regions of Fig. 14-96 are avoided. For porous stainless-steel spargers, which

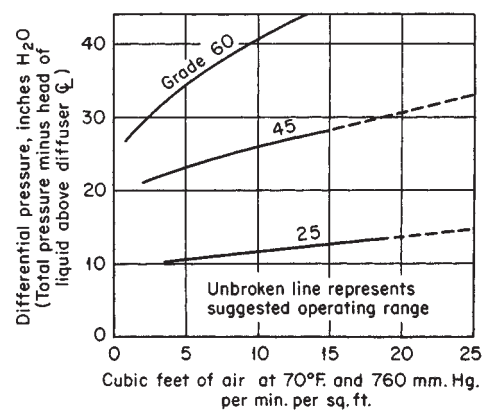


FIG. 14-96 Pressure drop across porous-carbon diffusers submerged in water at 70°F. To convert feet per minute to meters per second, multiply by 0.0051; to convert inches to millimeters, multiply by 25.4; °C = $\frac{5}{9}$ (°F - 32). (National Carbon Co.)

14-76 GAS ABSORPTION AND GAS-LIQUID SYSTEM DESIGN

TABLE 14-17 Wet Permeability of Alundum Porous Plates 1 in Thick*

Dry permeability at 2 in of water differential, cu ft/(min)(sq ft)	Pressure differential across wet plate, in of water	Air flow through wet plate, cu ft/(min)(sq ft)
4.3	20.67	2.0
	21.77	3.0
	22.86	4.0
	23.90	5.0
	4.02	1.0
	4.14	2.0
	4.22	3.0
	4.27	4.0
	4.30	5.0

*Data by courtesy of Norton Company, Worcester, Mass. To convert inches to centimeters, multiply by 2.54; to convert feet per minute to meters per second, multiply by 0.0051.

extend to a lower pore size than carbon, Micro Metallic Division, Pall Corp., recommends (Release 120A, 1959) a working limit of 8 ft/min (0.044 m/s) to avoid serious coalescence. This agrees with the data reported by Konig et al. (loc. cit.), in which 0.08 m/s was used and bubbles as small as 1 mm were produced from a 5-μm porous sparger.

Slabs of porous material are installed by grouting or welding together to form a diaphragm, usually horizontal. Tubes are prone to produce coalesced gas at rates high enough to cause bubbling from their lower faces, but they have the advantage of being demountable for cleaning or replacement (U.S. Patent 2,328,655). Roe [Sewage Works J., 18, 878 (1945)] claimed that silicon carbide tubes are superior to horizontal plates, principally because of the wiping action of the liquid circulating past the tube. He reported respective maximum capacities of 2.5 and 1.5 cm³/s of gas/cm² of sparger for a horizontal tube and a horizontal plate of the same material (unspecified grade). Mounting a flat-plate porous sparger vertically instead of horizontally seriously reduces the effectiveness of the sparger for three reasons: (1) The gas is distributed over a reduced cross section; (2) at normal rates, the lower portion of the sparger may not operate because of difference in hydrostatic head; and (3) there is a marked tendency for bubbles to coalesce along the sparger surface. Bone (M.S. thesis in chemical engineering, University of Kansas, 1948) found that the oxygen sulfite solution coefficient for a 3.2- by 10-cm rectangular porous carbon sparger was 26 to 41 percent lower for vertical than for horizontal operation of the sparger, the greatest reduction occurring when the long dimension was vertical.

Precipitation and Generation Methods For a thorough understanding of the phenomena involved, bubble nucleation should be considered. A discussion of nucleation phenomena is beyond the scope of this Handbook; however, excellent coverages are presented by Blander and Katz.

Boerma and Lankester [Chem. Eng. Sci., 23, 799 (1968)] have measured the surface aeration of a six-bladed disk-type turbine (NOTE: A well-designed pitched-blade turbine will give equal or better perfor-

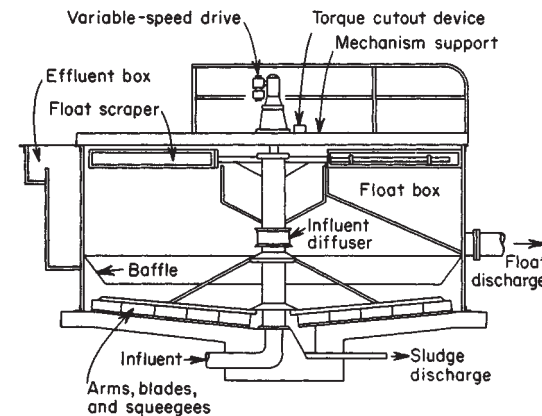


FIG. 14-97 The Flotator dissolved-air flotation thickener. (Process Engineers, Inc., a division of Etmco Corp., now Envirotech Corporation.)

mance). In a fully baffled vessel, the optimum depth to obtain maximum gas dispersion was 15 percent of the liquid depth. In a vessel with baffles extending only halfway to the liquid surface the optimum impeller submergence increased with agitator speed because of the vortex formed. At optimum depth, the following correlation is recommended for larger vessels:

$$Q \left(\text{m}^3/\text{s} \right) = 0.3 \left(\frac{\text{impeller speed, rpm}}{500} \right)^{2.5} \left(\frac{\text{impeller diameter, cm}}{25.4} \right)^{4.5} \quad (14-214)$$

Gas dispersion through the free surface by mechanical aerators is commonplace in aerobic waste-treatment lagoons. Surface aerators are generally of three types: (1) large-diameter flow-speed turbines operating just below the free surface of the liquid, often pontoon-mounted; (2) small-diameter high-speed (normally motor-speed) propellers operating in draft tubes, the units of which are always pontoon-mounted; and (3) hollow-tube turbines (Fig. 14-101). An example of the turbine type is illustrated in Fig. 14-102 and the propeller type is illustrated in Fig. 14-103. There are several other styles of the turbine type; for instance, Mixing Equipment Co., Inc., uses an unshrouded 45° axial-flow turbine [see Dykman and Michel, Chem. Eng., 117 (Mar. 10, 1969)], and Infilco makes a unit that has a large-diameter vaned disk operating just below the free surface with a smaller-diameter submerged-disk turbine for additional solids suspension.

Equipment Selection Ideally, selection of equipment to produce a gas-in-liquid dispersion should be made on the basis of a complete economic analysis. The design engineer and especially the pilot-plant engineer seldom have sufficient information or time to do

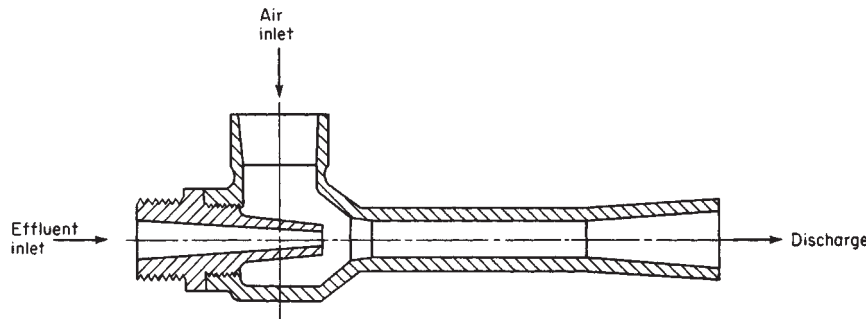


FIG. 14-98 Aeration ejector. (Penberthy, a division of Houdaille Industries, Inc.)

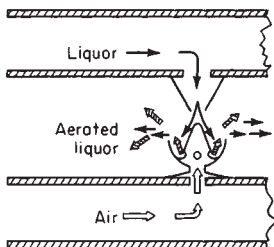


FIG. 14-99 Impingement aerator.

a complete economic analysis. In the following discussion, some guidelines are given as to what equipment might be feasible and what equipment might prove most economical.

For producing foam for foam-separation processes, perforated-plate or porous-plate spargers are normally used. Mechanical agitators are often not effective in the light foams needed in foam fractionation. Dissolved-air flotation, based on the release of a pressurized flow in which oxygen was dissolved, has been shown to be effective some times for particulate removal when sparged air failed because the bubbles formed upon precipitation are smaller—down to 80 μm —than bubbles possible with sparging, typically 1000 μm [Grieves and Ettelt, *AICHE J.*, **13**, 1167 (1967)]. Mechanically agitated surface aerators such as the Wemco-Fagergren flotation unit are used extensively for ore flotation.

To produce foam in batch processes, mechanical agitators are used almost exclusively. The gas can either be introduced through the free surface by the entraining action of the impeller or alternatively sparged beneath the impeller. In such batch operation, the liquid

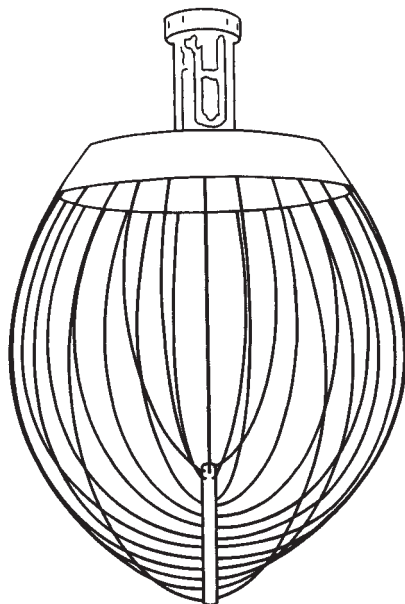


FIG. 14-100 Wire whip.

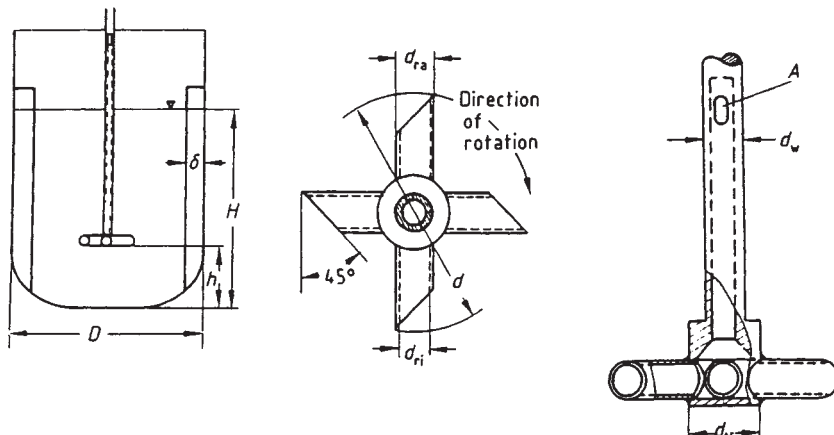


FIG. 14-101 Installation and dimensions of a tube stirrer: $h/d = 1$; $H/D = 1$; $D/\delta = 10$; $A = 1.5 d_w^2$; $D/d_N = 10$; $d/d_N = 3$; $d/d_i = 7.5$; $d/d_m = 6$. [Zlokarnik, Ullman's Encyclopedia of Industrial Chemistry, Sec. 25, VCH, Weinheim, Germany, 1988.]

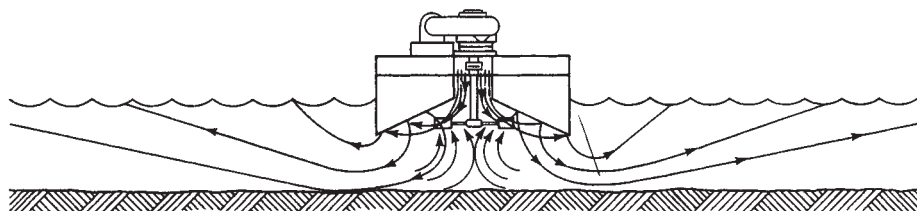


FIG. 14-102 The Cyclox surface aerator. (Cleveland Mixer Co.)

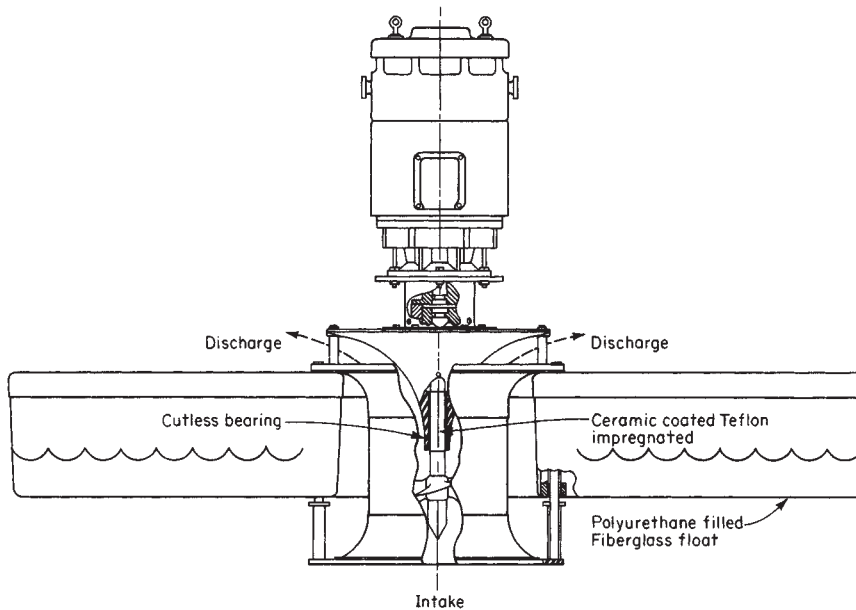


FIG. 14-103 Propeller-type surface aerator. (Ashbrook-Simon-Hartley Corp.)

level gradually rises as the foam is generated; thus, squatly impellers such as turbines are rapidly covered with foam and must almost always be sparged from below. Tall impellers such as the previously mentioned wire whips are especially well suited to entrain gas from the vapor space. For a new application, generally some experimentation with different impellers is necessary in order to get the desired fine final bubble size without getting frothing over initially. For producing foams continually, an aspirating venturi nozzle and restrictions in pipes such as baffles and metal gauzes are generally most economical.

For gas absorption, the equipment possibilities are generally packed columns; plate distillation towers, possibly with mechanical agitation on every plate; deep-bed contactors (bubble columns or sparged lagoons); and mechanically agitated vessels or lagoons. Packed towers and plate distillation columns are discussed elsewhere. Generally these devices are used when a relatively large number of stages (more than two or three) is required to achieve the desired result practically.

The volumetric mass-transfer coefficients and heights of transfer units for bubble columns and packed towers have been compared for absorption of CO_2 into water by Houghton et al. [Chem. Eng. Sci., **7**, 26 (1957)]. The bubble column will tolerate much higher vapor velocities, and in the overlapping region (superficial gas velocities of 0.9 to 1.8 cm/s), the bubble column has about three times higher mass-transfer coefficient and about 3 times greater height of transfer unit. The liquid in a bubble column is, for practical purposes, quite well mixed; thus, chemical reactions and component separations requiring significant plug flow of the liquid cannot be carried out with bubble columns. Bubble columns and agitated vessels are the ideal equipment for processes in which the fraction of gas absorbed need not be great, possibly the gas can be recycled, and the liquid can or should be well mixed. The gas phase in bubble columns is not nearly so well back-mixed as the liquid, and often plug flow of the gas is a logical assumption, but in agitated vessels the gas phase is also well mixed.

The choice of a bubble column or an agitated vessel depends primarily on the solubility of the gas in the liquid, the corrosiveness of the liquid (often a gas compressor can be made of inexpensive material, whereas a mechanical agitator may have to be made of exotic, expensive materials), and the rate of chemical reaction as compared with the mass-transfer rate. Bubble columns and agitated vessels are seldom used for gas absorption except in chemical reactors. As a general rule,

if the overall reaction rate is five times greater than the mass-transfer rate in a simple bubble column, a mechanical agitator will be most economical unless the mechanical agitator would have to be made from considerably more expensive material than the gas compressor.

In bubble columns and simply sparged lagoons, selecting the sparger is a very important consideration. In the turbulent regime (superficial gas velocity greater than 4.6 to 6 cm/s), inexpensive perforated-pipe spargers should be used. Often the holes must be placed on the pipe bottom in order to make the sparger free-draining during operation. In the quiescent regime, porous septa will often give considerably higher overall mass-transfer coefficients than perforated plates or pipes because of the formation of tiny bubbles that do not coalesce. Chain and coworkers (*First International Symposium on Chemical Microbiology*, World Health Organization, Monograph Ser. 10, Geneva, 1952) claimed that porous disks are about twice as effective as open-pipe and ring spargers for the air oxidation of sodium sulfite. Eckenfelder [Chem. Eng. Progr., **52**(7), 290 (1956)] has compared the oxygen-transfer capabilities of various devices on the basis of the operating power required to absorb a given quantity of O_2 . The installed cost of the various pieces of equipment probably would not vary sufficiently to warrant being included in an economic analysis. Surface mechanical aerators are not included in this comparison. Of the units compared, it appears that porous tubes give the most efficient power usage. Kalinske (*Adv. Biol. Waste Treatment*, 1963, p. 157) has compared submerged sparged aerators with mechanical surface aerators. He has summarized this comparison in *Water Sewage Works*, **33** (January 1968). He indicates that surface aerators are significantly more efficient than subsurface aeration, both for oxygen absorption and for gas-stripping operations.

Zlokarnik and Mann (paper at Mixing Conf., Rindge, New Hampshire, August 1975) have found the opposite of Kalinske, i.e., subsurface diffusers, subsurface sparged turbines, and surface aerators compare approximately as 4:2:1 respectively in terms of O_2 transfer efficiency; however, Zlokarnik [*Adv. Biochem. Eng.*, **11**, 157 (1979)] later indicates that the scale-up correlation used earlier might be somewhat inaccurate. When all available information is considered, it appears that with near-optimum design any of the aeration systems (diffusers, submerged turbines, or surface impellers) should give a transfer efficiency of at least 2.25 kg O_2 /kWh. Thus, the final selection should probably be made primarily on the basis of operational reliability, maintenance, and capital costs.

Mass Transfer Mass transfer in plate and packed gas-liquid contactors has been covered earlier in this subsection. Attention here will be limited to deep-bed contactors (bubble columns and agitated vessels). Theory underlying mass transfer between phases is discussed in Sec. 5 of this handbook.

To design deep-bed contactors for mass-transfer operations, one must have, in general, predictive methods for the following design parameters:

- Flooding (for both columns and agitator impellers)
- Holdup of gas phase
- Agitator power requirements
- Gas-phase and liquid-phase mass-transfer coefficients interfacial area
- Interfacial resistance
- Mean driving force for transfer

In most cases, available methods are incomplete or unreliable, and some supporting experimental work is necessary. The methods given here should allow theoretical feasibility studies, help minimize experimentation, and permit a measure of optimization in final design.

Flooding of Agitator Impellers A review of impeller flooding has been done by Sensel et al. [AICHE Symp. Series No. 283, **89** (1993)] and they have offered the following flooding correlation for a six-bladed disk-type turbine.

$$\frac{Q}{ND^3} = 0.0675(ND)T^{-0.4} \quad \text{for } (ND)T^{-0.4} \leq 1.6 \quad (14-215a)$$

$$\frac{Q}{ND^3} = 0.0231[(ND)T^{-0.4}]^{3.75} \quad \text{for } (ND)T^{-0.4} \geq 1.6 \quad (14-215b)$$

Where Q = volumetric flow of gas, ft³/s; N = impeller speed, rev/s; D = impeller diameter, ft; and T = tank diameter, ft.

Gassed Impeller Power Sensel et al. (op. cit.) have developed the following correlation for six-bladed disk impellers.

$$\frac{P_g}{P_o} = 1 - (-0.000715 \mu_L + 0.723)\tanh\left(\frac{24.54Q}{ND^3}\right)\left(\frac{N^2D}{g}\right)^{0.25} \quad (14-216)$$

where P_g = gassed power, P_o = ungassed power, g = gravitational acceleration, and μ_L = liquid viscosity.

Gas Holdup in Agitated Vessels Sensel et al. (op. cit.) have also developed the following correlation for six-bladed disk-type impellers:

$$\epsilon = 0.105 \left(\frac{Q}{ND^3}\right) \left(\frac{N^2D}{g}\right)^{0.5} \left(\frac{ND^2\mu_L}{\rho_L}\right)^{0.1} \quad (14-217)$$

Gas-Phase Mass-Transfer Coefficient This term is quite high in deep-bed contactors, normally leading to negligible gas-phase resistance.

Interfacial Area This consideration in agitated vessels has been reviewed and summarized by Tatterson (op. cit.). Predictive methods for interfacial area are not presented here because correlations are given for the overall volumetric mass transfer coefficient liquid phase controlling mass transfer.

Overall Mass-Transfer Coefficient Tatterson (op. cit.) and Zlokarnik (op. cit.) have summarized the literature covering overall mass-transfer coefficients. There is much scatter in the experimental data because the presence of surface-active agents and electrolytes have a significant effect on the mass transfer. The correlation of Van't Riet [Ind. Eng. Chem. Process Des. Dev., **18**(3), 357 (1979)] is recommended:

$$k_{L,a} = 0.026 \left(\frac{P}{V}\right)^{0.4} U_s^{0.5} \quad \text{for water} \quad (14-218)$$

$$\text{and} \quad k_{L,a} = 0.002 \left(\frac{P}{V}\right)^{0.7} U_s^{0.2} \quad \text{for ionic mixtures} \quad (14-219)$$

where P/V = power/volume, W/m³; U_s = superficial gas velocity, m/s; $k_{L,a}$ = volumetric mass-transfer coefficient, s⁻¹

Interfacial Phenomena These can significantly affect overall mass transfer. In fermentation reactors, small quantities of surface-active agents (especially antifoaming agents) can drastically reduce overall oxygen transfer (Aiba et al., op. cit., pp. 153, 154), and in aerobic

mechanically aerated waste-treatment lagoons, overall oxygen transfer has been found to be from 0.5 to 3 times that for pure water from tests with typical sewage streams (Eckenfelder et al., op. cit., p. 105).

One cannot quantitatively predict the effect of the various interfacial phenomena; thus, these phenomena will not be covered in detail here. The following literature gives a good general review of the effects of interfacial phenomena on mass transfer: Goodridge and Robb, *Ind. Eng. Chem. Fund.*, **4**, 49 (1965); Calderbank, *Chem. Eng. (London)*, CE 205 (1967); Gal-Or et al., *Ind. Eng. Chem.*, **61**(2), 22 (1969); Kintner, *Adv. Chem. Eng.*, **4** (1963); Resnick and Gal-Or, op. cit., p. 295; Valentin, loc. cit.; and Elenkov, loc. cit., and *Ind. Eng. Chem. Ann. Rev. Mass Transfer*, **60**(1), 67 (1968), **60**(12), 53 (1968), **62**(2), 41 (1970). In the following outline, the effects of the various interfacial phenomena on the factors that influence overall mass transfer are given. Possible effects of interfacial phenomena are tabulated below:

1. Effect on continuous-phase mass-transfer coefficient
 - a. Impurities concentrate at interface. Bubble motion produces circumferential surface-tension gradients that act to retard circulation and vibration, thereby decreasing the mass-transfer coefficient.
 - b. Large concentration gradients and large heat effects (very soluble gases) can cause interfacial turbulence (the Marangoni effect), which increases the mass-transfer coefficient.
2. Effect on interfacial area
 - a. Impurities will lower static surface tension and give smaller bubbles.
 - b. Surfactants can electrically charge the bubble surface (produce ionic bubbles) and retard coalescence (soap stabilization of an oil-water emulsion is an excellent example of this phenomenon), thereby increasing the interfacial area.
 - c. Large concentration gradients and large heat effects can cause bubble breakup.
3. Effect on mean mass-transfer driving force
 - a. Relatively insoluble impurities concentrate at the interface, giving an interfacial resistance. This phenomenon has been used in retarding evaporation from water reservoirs.
 - b. The axial concentration variation can be changed by changes in coalescence. The mean driving force for mass transfer is therefore changed.

Gas Holdup (ϵ) in Bubble Columns With coalescing systems, holdup may be estimated from a correlation by Hughmark [*Ind. Eng. Chem. Process Des. Dev.*, **6**, 218–220 (1967)] reproduced here as Fig. 14-104. For noncoalescing systems, with considerably smaller bub-

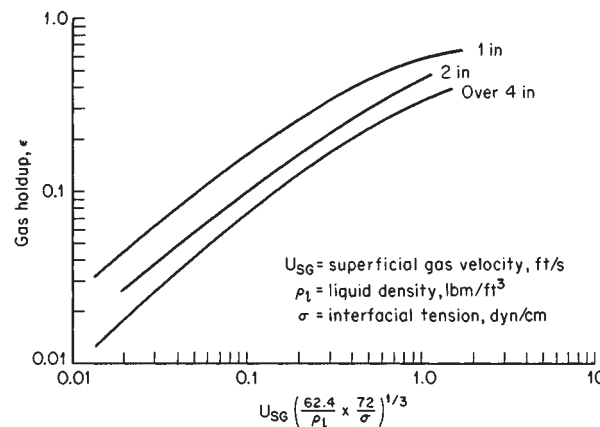


FIG. 14-104 Gas holdup correlation. [Ind. Eng. Chem. Process Des. Dev., **6**, 218 (1967).]

bles, ϵ can be as great as 0.6 at $U_{sg} = 0.05$ m/s, according to Mersmann [Ger. Chem. Eng., **1**, 1 (1978)].

It is often helpful to use the relationship between ϵ and superficial gas velocity (U_{sg}) and the rise velocity of a gas bubble relative to the liquid velocity ($U_r + U_L$, with U_L defined as positive upward):

$$\epsilon = \frac{U_{sg}}{U_r + U_L} \quad (14-220)$$

Rise velocities of bubbles through liquids have been discussed previously.

For a better understanding of the interactions between parameters, it is often helpful to calculate the effective bubble rise velocity U_r from measured values of ϵ ; for example, the data of Mersmann (loc. cit.) indicated $\epsilon = 0.6$ for $U_{sg} = 0.05$ m/s, giving $U_r = 0.083$ m/s, which agrees with the data reported in Fig. 14-43 for the rise velocity of bubble clouds. The rise velocity of single bubbles, for $d_b \sim 2$ mm, is about 0.3 m/s, for liquids with viscosities not too different from water. Using this value in Eq. (14-220) and comparing with Fig. 14-104, one finds that at low values of U_{sg} , the rise velocity of the bubbles is less than the rise velocity of a single bubble, especially for small-diameter tubes, but that the opposite occurs for large values of U_{sg} .

More recent literature regarding generalized correlational efforts for gas holdup is adequately reviewed by Tsuchiya and Nakanishi [Chem. Eng. Sci., **47**(13/14), 3347 (1992)] and Sotelo *et al.* [Int. Chem. Eng., **34**(1), 82–90 (1994)]. Sotelo *et al.* (op. cit.) have developed a dimensionless correlation for gas holdup that includes the effect of gas and liquid viscosity and density, interfacial tension, and diffuser pore diameter. For systems that deviate significantly from the waterlike liquids for which Fig. 14-104 is applicable, their correlation (the fourth numbered equation in the paper) should be used to obtain a more accurate estimate of gas holdup. Mersmann (op. cit.) and Deckwer *et al.* (op. cit.) should also be consulted.

Liquid-phase mass-transfer coefficients in bubble columns have been reviewed by Calderbank ("Mixing," loc. cit.), Fair (Chem. Eng., loc. cit.), Mersmann [Ger. Chem. Eng., **1**, 1 (1978), Int. Chem. Eng., **32**(3) 397–405 (1991)], Deckwer *et al.* [Can. J. Chem. Eng., **58**, 190 (1980)], Hikita *et al.* [Chem. Eng. J., **22**, 61 (1981)] and Deckwer and Schumpe [Chem. Eng. Sci., **48**(5), 889–911 (1993)]. The correlation of Ozturk, Schumpe, and Deckwer [AIChE J., **33**, 1473–1480 (1987)] is recommended. Deckwer *et al.* (op. cit.) have documented the case for using the correlation:

$$\left(\frac{k_{L,a} d_b}{D_L} \right) = 0.62 \left[\frac{\mu_L}{(\rho_L D_L)} \right]^{0.5} \left(\frac{g \rho_L d_b^2}{\sigma} \right)^{0.33} \left(\frac{g \rho_L^2 d_b}{\mu_L^2} \right)^{0.29} \times \left[\frac{U_G}{(g d_b)^{0.5}} \right]^{0.68} \left(\frac{\rho_G}{\rho_L} \right)^{0.04} \quad (14-221)$$

where $k_{L,a}$ = overall mass-transfer coefficient, d_b = bubble diameter = 0.003 m, D_L = diffusivity of gas in liquid, ρ = density, μ = viscosity, σ = interfacial tension, g = gravitational acceleration.

As mentioned earlier, surfactants and ionic solutions significantly affect mass transfer. Normally, surface affects act to retard coalescence and thus increase the mass transfer. For example, Hikita *et al.* [Chem. Eng. J., **22**, 61–69 (1981)] have studied the effect of KCl on mass transfer in water. As KCl concentration increased, the mass transfer increased up to about 35 percent at an ionic strength of 6 g/ml. Other investigators have found similar increases for liquid mixtures.

Axial Dispersion Backmixing in bubble columns has been extensively studied. An excellent review article by Shah *et al.* [AIChE

J., **24**, 369 (1978)] has summarized the literature prior to 1978. Works by Konig *et al.* [Ger. Chem. Eng., **1**, 199 (1978)], Lucke *et al.* [Trans. Inst. Chem. Eng., **58**, 228 (1980)], Riquarts [Ger. Chem. Eng., **4**, 18 (1981)], Mersmann (op. cit.), Deckwer (op. cit.), Yang *et al.* [Chem. Eng. Sci., **47**(9–11), 2859 (1992)], and Garcia-Calvo and Leton [Chem. Eng. Sci., **49**(21), 3643 (1994)] are particularly useful references.

Axial dispersion occurs in both the liquid and the gas phases. The degree of axial dispersion is affected by vessel diameter, vessel internals, gas superficial velocity, and surface-active agents that retard coalescence. For systems with coalescence-retarding surfactants the initial bubble size produced by the gas sparger is also significant. The gas and liquid physical properties have only a slight effect on the degree of axial dispersion, except that liquid viscosity becomes important as the flow regime becomes laminar. With pure liquids, in the absence of coalescence-inhibiting surface-active agents, the nature of the sparger has little effect on the axial dispersion, and experimental results are reasonably well correlated by the dispersion model. For the liquid phase the correlation recommended by Deckwer *et al.* (op. cit.), after the original work by Baird and Rice [Chem. Eng. J., **9**, 171 (1975)] is as follows:

$$\frac{E_L}{(DU_G)} = 0.35 \left(\frac{gD}{U_G^2} \right)^{1/3} \quad (14-222)$$

where E_L = liquid-phase axial dispersion coefficient, U_G = superficial velocity of the gas phase, D = vessel diameter, and g = gravitational acceleration.

The recommended correlation for the gas-phase axial-dispersion coefficient is given by Field and Davidson (loc. cit.):

$$E_G = 56.4 D^{1.33} \left(\frac{U_G}{\epsilon} \right)^{3.56} \quad (14-223)$$

where E_G = gas-phase axial-dispersion coefficient, m^2/s ; D = vessel diameter, m ; U_G = superficial gas velocity, m/s ; and ϵ = fractional gas holdup, volume fraction.

The correlations given in the preceding paragraphs are applicable to vertical cylindrical vessels with pure liquids without coalescence inhibitors. For other vessel geometries such as columns of rectangular cross section, packed columns, and coiled tubes, the work of Shah *et al.* (loc. cit.) should be consulted. For systems containing coalescence-inhibiting surfactants, axial dispersion can be vastly different from that in systems in which coalescence is negligible. Konig *et al.* (loc. cit.) have well demonstrated the effects of surfactants and sparger type by conducting tests with weak alcohol solutions using three different porous spargers. With pure water, the sparger—and, consequently, initial bubble size—had little effect on back mixing because coalescence produced a dynamic-equilibrium bubble size not far above the sparger. With surfactants, the average bubble size was smaller than the dynamic-equilibrium bubble size. Small bubbles produced minimal back mixing up to $\epsilon \approx 0.40$; however, above $\epsilon \approx 0.40$ backmixing increased very rapidly as U_G increased. The rapid increase in back mixing as ϵ exceeds 0.40 was postulated to occur indirectly because a bubble carries upward with it a volume of liquid equal to about 70 percent of the bubble volume, and, for $\epsilon \approx 0.40$, the bubbles carry so much liquid upward that steady, uniform bubble rise can no longer be maintained and an oscillating, slugging flow develops, which produces fluctuating pressure at the gas distributor and the formation of large eddies. The large eddies greatly increase backmixing. For the air–alcohol–water system, the minimum bubble size to prevent unsteady conditions was about 1, 1.5, and 2 mm for $U_G = 1, 3$, and 5 cm/s, respectively. Any smaller bubble size produced increased backmixing. The results of Konig *et al.* (loc. cit.) clearly indicate that the interaction of surfactants and sparger can be very complex; thus, one should proceed very cautiously in designing systems for which surfactants significantly retard coalescence. Caution is particularly important because surfactants can produce either much more or much less backmixing than surfactant-free systems, depending on the bubble size, which, in turn, depends on the sparger utilized.

PHASE SEPARATION

Gases and liquids may be intentionally contacted as in absorption and distillation, or a mixture of phases may occur unintentionally as in vapor condensation from inadvertent cooling or liquid entrainment from a film. Regardless of the origin, it is usually desirable or necessary ultimately to separate gas-liquid dispersions. While separation will usually occur naturally, the rate is often economically intolerable and separation processes are employed to accelerate the step.

GAS-PHASE CONTINUOUS SYSTEMS

Practical separation techniques for liquid particles in gases are discussed. Since gas-borne particulates include both liquid and solid particles, many devices used for dry-dust collection (discussed in Sec. 17 under "Gas-Solids Separation") can be adapted to liquid-particle separation. Also, the basic subject of particle mechanics is covered in Sec. 6. Separation of liquid particulates is frequently desirable in chemical processes such as in countercurrent-stage contacting because liquid entrainment with the gas partially reduces true countercurrentity. Separation before entering another process step may be needed to prevent corrosion, to prevent yield loss, or to prevent equipment damage or malfunction. Separation before the atmospheric release of gases may be necessary to prevent environmental problems and for regulatory compliance.

GENERAL REFERENCES

- G-1. Buonicore and Davis, eds., *Air Pollution Engineering Manual*, Van Nostrand Reinhold, New York, 1992.
- G-2. Calvert and Englund, eds., *Handbook of Air Pollution Technology*, Wiley, New York, 1984.
- G-3. Chermisinoff, ed., *Encyclopedia of Environmental Control Technology*, vol. 2, Gulf Pub., Houston, 1989.
- G-4. McKetta, *Unit Operations Handbook*, vol. 1–2, Dekker, New York, 1992.
- G-5. Wark and Warner, *Air Pollution: Its Origin and Control*, 2d ed., Harper & Row, New York, 1981.
- G-6. Hesketh, *Air Pollution Control*, 1979; *Fine Particles in Gaseous Media*, Ann Arbor Science Pubs., Ann Arbor, MI, 1977.
- G-7. Stern, *Air Pollution*, 3d ed., vols. 3–5, Academic, Orlando, FL, 1976–77.
- G-8. Strauss, *Industrial Gas Cleaning*, 2d ed., Pergamon, New York, 1975.
- G-9. Theodore and Buonicore, *Air Pollution Control Equipment: Selection, Design, Operation and Maintenance*, Prentice Hall, Englewood Cliffs, NJ, 1982.
- G-10. Wang and Pereira, eds., *Handbook of Environmental Engineering*, vol. 1, Humana, Clifton, NJ, 1979.
- G-11. Chermisinoff and Young, *Air Pollution Control and Design Handbook*, parts 1–2, Dekker, New York, 1977.
- G-12. Nonhebel, *Gas Purification Processes for Air Pollution Control*, Newnes-Butterworth, London, 1972.

Sampling

- R-1. *Code of Federal Regulations*, 40 (CFR 40), subchapter C—Air Programs, parts 50–99, Office of the Federal Register, Washington.
- R-2. Ref. G-11, part 1, pp. 65–121.
- R-3. Cooper and Rossano, *Source Testing for Air Pollution Control*, Environmental Science Services, Wilton, Connecticut, 1970.
- R-4. Ref. G-7, vol. 3, pp. 525–587.
- R-5. *Methods of Air Sampling and Analysis*, 2d Ed., American Public Health Assoc., Washington, 1977.
- R-6. Stockham and Fochtman, *Particle Size Analysis*, Ann Arbor Science Pubs., Ann Arbor, Michigan, 1977.
- R-7. Ref. G-2, Ch. 31, pp. 785–832.
- R-8. Ref. G-8, Ch. 2, pp. 39–79.

Specific

- R-9. Calvert, Goldchmid, Leith, and Mehta, NTIS Publ. PB-213016, 213017, 1972.
- R-10. Calvert, *J. Air Pollut. Control Assoc.*, **24**, 929 (1974).
- R-11. Calvert, *Chem. Eng.*, **84**(18), 54 (1977).
- R-12. Calvert, Yung, and Leung, NTIS Publ. PB-248050, 1975.
- R-13. Calvert and Lundgren, *J. Air Pollut. Control Assoc.*, **18**, 677 (1968).
- R-14. Calvert, Lundgren, and Mehta, *J. Air Pollut. Control Assoc.*, **22**, 529 (1972).
- R-15. Yung, Barbarika, and Calvert, *J. Air Pollut. Control Assoc.*, **27**, 348, (1977).
- R-16. Katz, M.S. thesis, Pennsylvania State University, 1958.

- R-17. York and Popple, *Chem. Eng. Prog.*, **59**(6), 45 (1963).
- R-18. York, *Chem. Eng. Prog.*, **50**, 421 (1954).
- R-19. Ref. G-2, Ch. 10, pp. 215–248.

References with the notation (R-) are cited in the text.

Definitions: Mist and Spray Little standardization has been adopted in defining gas-borne liquid particles, and this frequently leads to confusion in the selection, design, and operation of collection equipment. Aerosol applies to suspended particulate, either solid or liquid, which is slow to settle by gravity and to particles from the submicrometer range up to 10 to 20 μm. Mists are fine suspended liquid dispersions usually resulting from condensation and ranging upward in particle size from around 0.1 μm. Spray refers to entrained liquid droplets. The droplets may be entrained from atomizing processes previously discussed under "Liquid-in-Gas Dispersions" in this section. In such instances, size will range from the finest particles produced up to a particle whose terminal settling velocity is equal to the entraining gas velocity if some settling volume is provided. Process spray is often created unintentionally, such as by the condensation of vapors on cold duct walls and its subsequent reentrainment, or from two-phase flow in pipes, gas bubbling through liquids, and entrainment from boiling liquids. Entrainment size distribution from sieve trays has been given by Cheng and Teller [*Am. Inst. Chem. Eng. J.*, **7**(2), 282 (1961)] and evaporator spray by Garner et al. [*Trans. Inst. Chem. Eng.*, **32**, 222 (1954)]. In general, spray can range downward in particle size from 5000 μm. There can be overlapping in size between the coarsest mist particles and the finest spray particles, but some authorities have found it convenient arbitrarily to set a boundary of 10 μm between the two. Actually, considerable overlap exists in the region of 5 to 40 μm. Table 14-18 lists typical ranges of particle size created by different mechanisms. The sizes actually entrained can be influenced by the local gas velocity. Figure 14-105 compares the approximate size range of liquid particles with other particulate material and the approximate applicable size range of collection devices. Figure 17-34 gives an expanded chart by Lapple for solid particles. Mist and fog formation has been discussed previously.

Gas Sampling The sampling of gases containing mists and sprays may be necessary to obtain data for collection-device design, in which case particle-size distribution, total mass loading, and gas volume, temperature, pressure, and composition may all be needed. Other reasons for sampling may be to determine equipment performance, measure yield loss, or determine compliance with regulations.

Location of a sample probe in the process stream is critical especially when larger particles must be sampled. Mass loading in one portion of a duct may be severalfold greater than in another portion as affected by flow patterns. Therefore, the stream should be sampled at a number of points. The U.S. Environmental Protection Agency (R-1) has specified 8 points for ducts between 0.3 and 0.6 m (12 and 24 in) and 12 points for larger ducts, provided there are no flow disturbances for eight pipe diameters upstream and two downstream from the sampling point. When only particles smaller than 3 μm are to be sampled, location and number of sample points are less critical since such particles remain reasonably well dispersed by brownian motion. However, some gravity settling of such particles and even gases of high density have been observed in long horizontal breeching. Isokinetic sampling (velocity at the probe inlet is equal to local duct velocity) is required to get a representative sample of particles larger than 3 μm (error is small for 4- to 5-μm particles). Sampling methods and procedures for mass loading have been developed (R-1 through R-8).

TABLE 14-18 Particle Sizes Produced by Various Mechanisms

Mechanism or process	Particle-size range, μm
Liquid pressure spray nozzle	100–5000
Gas-atomizing spray nozzle	1–100
Gas bubbling through liquid or boiling liquid	20–1000
Condensation processes with fogging	0.1–30
Annular two-phase flow in pipe or duct	10–2000

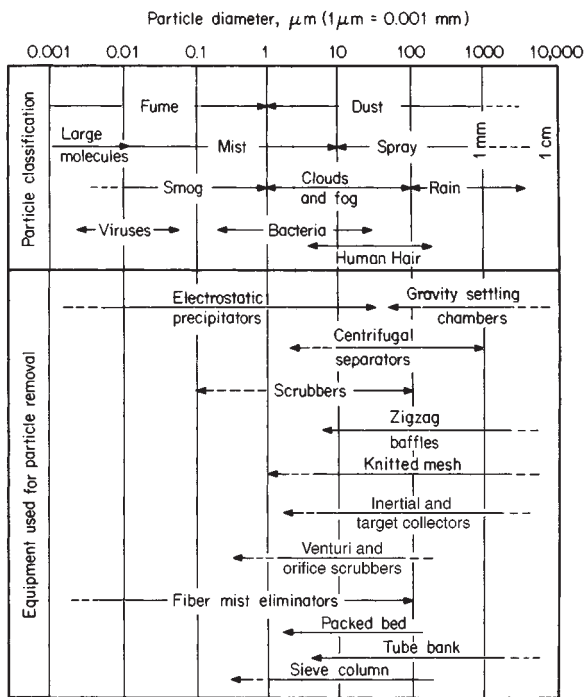


FIG. 14-105 Particle classification and useful collection equipment versus particle size.

Particle-Size Analysis Many particle-size-analysis methods suitable for dry-dust measurement are unsuitable for liquids because of coalescence and drainage after collection. Measurement of particle sizes in the flowing aerosol stream by using a cascade impactor is one of the better means. The impacting principle has been described by Ranz and Wong [Ind. Eng. Chem., **44**, 1371 (1952)] and Gillespie and Johnstone [Chem. Eng. Prog., **51**, 75F (1955)]. The Andersen, Sierra, and University of Washington impactors may be used if the sampling period is kept short so as not to saturate the collection substrate. An impactor designed specifically for collecting liquids has been described by Brink, Kennedy, and Yu [Am. Inst. Chem. Eng. Symp. Ser., **70**(137), 333 (1974)].

Collection Mechanisms Mechanisms which may be used for separating liquid particles from gases are (1) gravity settling, (2) inertial (including centrifugal) impaction, (3) flow-line interception, (4) diffusional (brownian) deposition, (5) electrostatic attraction, (6) thermal precipitation, (7) flux forces (thermophoresis, diffusiophoresis, Stefan flow), and (8) particle agglomeration (nucleation) techniques. Equations and parameters for these mechanisms are given in Table 17-2. Most collection devices rarely operate solely with a single mechanism, although one mechanism may so predominate that it may be referred to, for instance, as an inertial-impaction device.

After collection, liquid particles coalesce and must be drained from the unit, preferably without reentrainment. Calvert (R-12) has studied the mechanism of reentrainment in a number of liquid-particle collectors. Four types of reentrainment were typically observed: (1) transition from separated flow of gas and liquid to a two-phase region of separated-entrained flow, (2) rupture of bubbles, (3) liquid creep on the separator surface, and (4) shattering of liquid droplets and splashing. Generally, reentrainment increased with increasing gas velocity. Unfortunately, in devices collecting primarily by centrifugal and inertial impaction, primary collection efficiency increases with gas velocity; thus overall efficiency may go through a maximum as reentrainment overtakes the incremental increase in efficiency. Prediction of collection efficiency must consider both primary collection and reentrainment.

Procedures for Design and Selection of Collection Devices

Calvert and coworkers (R-9 to R-12 and R-19) have suggested useful design and selection procedures for particulate-collection devices in which direct impingement and inertial impaction are the most significant mechanisms. The concept is based on the premise that the mass median aerodynamic particle diameter D_{pa50} is a significant measure of the difficulty of collection of the liquid particles and that the collection device cut size d_{pe} (defined as the aerodynamic particle diameter collected with 50 percent efficiency) is a significant measure of the capability of the collection device. The aerodynamic diameter for a particle is the diameter of a spherical particle (with an arbitrarily assigned density of 1 g/cm^3) which behaves in an air stream in the same fashion as the actual particle. For real spherical particles of diameter d_p , the equivalent aerodynamic diameter d_{pa} can be obtained from the equation $d_{pa} = d_p (\rho_p C')^{1/2}$, where ρ_p is the apparent particle density (mass/volume) and C' is the Stokes-Cunningham correction factor for the particle size, all in consistent units. If particle diameters are expressed in micrometers, ρ_p can be in grams per cubic centimeter and C' can be approximated by $C' = 1 + A_c (2\lambda/D_p)$, where A_c is a constant dependent upon gas composition, temperature, and pressure ($A_c = 0.88$ for atmospheric air at 20°C) and λ is the mean free path of the gas molecules ($\lambda = 0.10 \mu\text{m}$ for 20°C atmospheric air). For other temperatures or pressures, or gases other than air, calculations using these more precise equations may be made: $A_c = 1.257 + 0.4 \exp[-1.1(d_p/2\lambda)]$ and $\lambda = \mu_g/0.499p_g \times u_m$ (where μ_g is the gas viscosity, $\text{kg}\cdot\text{m}/\text{s}$; p_g is gas density, g/cm^3 ; and u_m is the mean molecular speed, m/s . $u_m = [8R_u T/\pi M]^{1/2}$, where R_u is the universal gas constant, $8.315 \text{ kJ/kg}\cdot\text{mol}\cdot\text{K}$; T is the gas absolute temperature, K ; and M is the molar mass or equivalent molecular weight of the gas. (π is the usual geometric constant.) For test purposes (air at 25°C and 1 atm), $p_g = 1.183 \text{ kg/m}$, $\mu_g = 0.0666 \text{ kg/m}\cdot\text{h}$, $\lambda = 0.067 \mu\text{m}$, and $u_m = 467 \text{ m/s}$. For airborne liquid particles, the assumption of spherical shape is reasonably accurate, and ρ_p is approximately unity for dilute aqueous particles at ambient temperatures. C' is approximately unity at ambient conditions for such particles larger than 1 to 5 μm , so that often the actual liquid particle diameter and the equivalent aerodynamic diameter are identical.

When a distribution of particle sizes which must be collected is present, the actual size distribution must be converted to a mass distribution by aerodynamic size. Frequently the distribution can be represented or approximated by a log-normal distribution (a straight line on a log-log plot of cumulative mass percent of particles versus diameter) which can be characterized by the mass median particle diameter d_{pa50} and the standard statistical deviation of particles from the median σ_g . σ_g can be obtained from the log-log plot by $\sigma_g = D_{pa50}/D_{pe}$ at 15.87 percent = D_{pe} at 84.13 percent/ D_{pa50} .

The grade efficiency η of most collectors can be expressed as a function of the aerodynamic particle size in the form of an exponential equation. It is simpler to write the equation in terms of the particle penetration P_t (those particles not collected), where the fractional penetration $P_t = 1 - \eta$, when η is the fractional efficiency. The typical collection equation is

$$P_t = e^{(-A_a D_{pa} B)} \quad (14-224)$$

where A_a and B are functions of the collection device. Calvert (R-12) has determined that for many devices in which the primary collection mechanism is direct interception and inertial impaction, such as packed beds, knitted-mesh collectors, zigzag baffles, target collectors such as tube banks, sieve-plate columns, and venturi scrubbers, the value of B is approximately 2.0. For cyclonic collectors, the value of B is approximately 0.67. The overall integrated penetration \bar{P}_t for a device handling a distribution of particle sizes can be obtained by

$$\bar{P}_t = \int_0^W \left(\frac{dW}{W} \right) P_t \quad (14-225)$$

where (dW/W) is the mass of particles in a given narrow size distribution and P_t is the average penetration for that size range. When the particles to be collected are log-normally distributed and the collection device efficiency can be expressed by Eq. (14-224), the required overall integrated collection efficiency \bar{P}_t can be related to the ratio of the device aerodynamic cut size D_{pe} to the mass median aerodynamic particle size D_{pa50} . This required ratio for a given distribution and

collection is designated R_{rl} and these relationships are illustrated graphically in Fig. 14-106. For the many devices for which B is approximately 2.0, a simplified plot (Fig. 14-107) is obtained. From these figures, by knowing the desired overall collection efficiency and particle distribution, the value of R_{rl} can be read. Substituting the mass median particle diameter gives the aerodynamic cut size required from the collection device being considered. Therefore, an experimental plot of aerodynamic cut size for each collection device versus operating parameters can be used to determine the device suitability.

Collection Equipment

Gravity Settlers Gravity can act to remove larger droplets. Settling or disengaging space above aerated or boiling liquids in a tank or spray zone in a tower can be very useful. If gas velocity is kept low, all particles with terminal settling velocities (see Sec. 6) above the gas

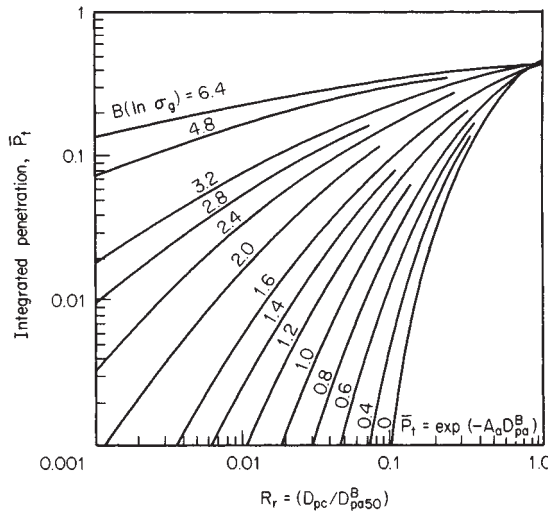


FIG. 14-106 Overall integrated penetration as a function of particle-size distribution and collector parameters. (Calvert, Yung, and Leung, NTIS Publ. PB-248050, 1975.)

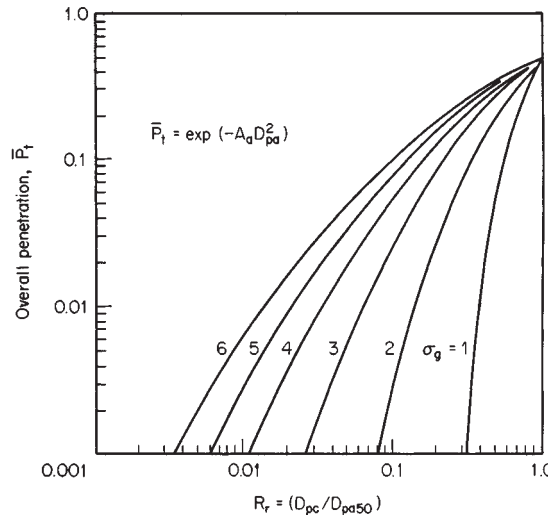


FIG. 14-107 Overall integrated penetration as a function of particle-size distribution and collector cut diameter when $B = 2$ in Eq. (14-224). (Calvert, Goldshmid, Leith, and Mehta, NTIS Publ. PB-213016, 213017, 1972.)

velocity will eventually settle. Increasing vessel cross section in the settling zone is helpful. Terminal velocities for particles smaller than 50 μm are very low and generally not attractive for particle removal. Laminar flow of gas in long horizontal paths between trays or shelves on which the droplets settle is another effective means of employing gravity. Design equations are given in Sec. 17 under "Gas-Solids Separations." Settler pressure drop is very low, usually being limited to entrance and exit losses.

Centrifugal Separation Centrifugal force can be utilized to enhance particle collection to several hundredfold that of gravity. The design of cyclone separators for dust removal is treated in detail in Sec. 17 under "Gas-Solids Separations," and typical cyclone designs are shown in Fig. 17-43. Dimension ratios for one family of cyclones are given in Fig. 17-36. Cyclones, if carefully designed, can be more efficient on liquids than on solids since liquids coalesce on capture and are easy to drain from the unit. However, some precautions not needed for solid cyclones are necessary to prevent reentrainment.

Tests by Calvert (R-12) show high primary collection efficiency on droplets down to 10 μm and in accordance with the efficiency equations of Leith and Licht [Am. Inst. Chem. Eng. Symp. Ser., 68(126), 196–206 (1972)] for the specific cyclone geometry tested if entrainment is avoided. Typical entrainment points are (1) creep along the gas outlet pipe, (2) entrainment by shearing of the liquid film from the walls, and (3) vortex pickup from accumulated liquid in the bottom (Fig. 14-108a). Reentrainment from creep of liquid along the top of the cyclone and down the outlet pipe can be prevented by providing the outlet pipe with a flared conical skirt (Fig. 14-108b), which provides a point from which the liquid can drip without being caught in the outlet gas. The skirt should be slightly shorter than the gas outlet pipe but extend below the bottom of the gas inlet. The cyclone inlet gas should not impinge on this skirt. Often the bottom edge of the skirt is V-notched or serrated.

Reentrainment is generally reduced by lower inlet gas velocities. Calvert (R-12) reviewed the literature on predicting the onset of entrainment and found that of Chien and Ibele (ASME Pap. 62-WA170) to be the most reliable. Calvert applies their correlation to a liquid Reynolds number on the wall of the cyclone, $N_{Re,L} = 4Q_L/h_i v_L$, where Q_L is the volumetric liquid flow rate, cm^3/s ; h_i is the cyclone inlet height, cm ; and v_L is the kinematic liquid viscosity, cm^2/s . He finds that the onset of entrainment occurs at a cyclone inlet gas velocity V_{ci} , m/s , in accordance with the relationship in $V_{ci} = 6.516 - 0.2865 \ln N_{Re,L}$.

Reentrainment from the bottom of the cyclone can be prevented in several ways. If a typical long-cone dry cyclone is used and liquid is kept continually drained, vortex entrainment is unlikely. However, a vortex breaker baffle in the outlet is desirable, and perhaps a flat disk on top extending to within 2 to 5 cm (0.8 to 2 in) of the walls may be

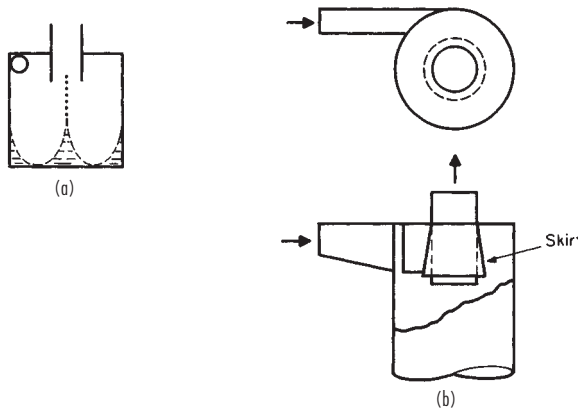


FIG. 14-108 (a) Liquid entrainment from the bottom of a vessel by centrifugal flow. (Rietema and Verver, Cyclones in Industry, Elsevier, Amsterdam, 1961.) (b) Gas-outlet skirt for liquid cyclones. (Stern et al., Cyclone Dust Collectors, American Petroleum Institute, New York, 1955.)

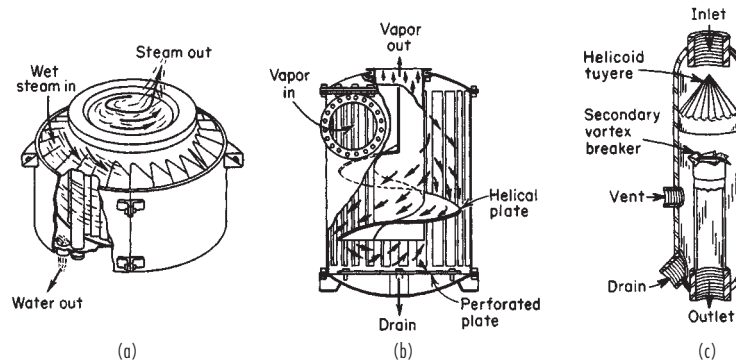


FIG. 14-109 Typical separators using impingement in addition to centrifugal force. (a) Hi-purifier. (V. D. Anderson Co.) (b) Flick separator. (Wurster & Sanger, Inc.) (c) Type RA line separator. (Centrifix Corp., Bull. 220.)

beneficial. Often liquid cyclones are built without cones and have dished bottoms. The modifications described earlier are definitely needed in such situations. Stern, Caplan, and Bush (*Cyclone Dust Collectors*, American Petroleum Institute, New York, 1955) and Rietema and Verver (in Tengbergen, *Cyclones in Industry*, Elsevier, Amsterdam, 1961, chap. 7) have discussed liquid-collecting cyclones.

As with dust cyclones, no reliable pressure-drop equations exist (see Sec. 17), although many have been published. A part of the problem is that there is no standard cyclone geometry. Calvert (R-12) experimentally obtained $\Delta P = 0.000513 \rho_g (\dot{Q}_g / h_i W_i)^2 (2.8 h_i w_i / d_o^2)$, where ΔP is in cm of water; ρ_g is the gas density, g/cm³; \dot{Q}_g is the gas volumetric flow rate, cm³/s; h_i and w_i are cyclone inlet height and width respectively, cm; and d_o is the gas outlet diameter, cm. This equation is in the same form as that proposed by Shepherd and Lapple [*Ind. Eng. Chem.*, **31**, 1246 (1940)] but gives only 37 percent as much pressure drop.

Liquid cyclone efficiency can be improved somewhat by introducing a coarse spray of liquid in the cyclone inlet. Large droplets which are easily collected collide with finer particles as they sweep the gas stream in their travel to the wall. (See subsection "Wet Scrubbers" regarding optimum spray size.) Cyclones may also be operated wet to improve their operation on dry dust. Efficiency can be improved through reduction in entrainment losses since the dust particles become trapped in the water film. Collision between droplets and dust particles aids collection, and adequate irrigation can eliminate problems of wall buildup and fouling. The most effective operation is obtained by spraying countercurrently to the gas flow in the cyclone inlet duct at liquid rates of 0.7 to 2.0 L/m³ of gas. There are also many proprietary designs of liquid separators using centrifugal force, some of which are illustrated in Fig. 14-109. Many of these were originally developed as steam separators to remove entrained condensate. In some designs, impingement on swirl baffles aids separation.

Impingement Separation Impingement separation employs direct impact and inertial forces between particles, the gas streamlines, and target bodies to provide capture. The mechanism is discussed in Sec. 17 under "Gas-Solids Separations." With liquids, droplet coalescence occurs on the target surface, and provision must be made for drainage without reentrainment. Calvert (R-12) has studied droplet collection by impingement on targets consisting of banks of tubes, zigzag baffles, and packed and mesh beds. Figure 14-110 illustrates some other types of impingement-separator designs.

In its simplest form, an impingement separator may be nothing more than a target placed in front of a flow channel such as a disk at the end of a tube. To improve collection efficiency, the gas velocity may be increased by forming the end into a nozzle (Fig. 14-110a). Particle collection as a function of size may be estimated by using the target-efficiency correlation in Fig. 17-39. Since target efficiency will be low for systems with separation numbers below 5 to 10 (small particles, low gas velocities), the mist will frequently be subjected to a number of targets in series as in Fig. 14-110c, d, and g.

The overall droplet penetration is the product of penetration for

each set of targets in series. Obviously, for a distribution of particle sizes, an integration procedure is required to give overall collection efficiency. This target-efficiency method is suitable for predicting efficiency when the design effectively prevents the bypassing or short-circuiting of targets by the gas stream and provides adequate time to accelerate the liquid droplets to gas velocity. Katz (R-16) investigated a jet and target-plate entrainment separator design and found the pressure drop less than would be expected to supply the kinetic energy both for droplet acceleration and gas friction. An estimate based on his results indicates that the liquid particles on the average were being accelerated to only about 60 percent of the gas velocity. The largest droplets, which are the easiest to collect, will be accelerated less than the smaller particles. This factor has a leveling effect on collection efficiency as a function of particle size so that experimental results on such devices may not show as sharp a decrease in efficiency with particle size as predicted by calculation. Such results indicate that in many cases our lack of predicting ability results, not from imperfections in the theoretical treatment, but from our lack of knowledge of velocity distributions within the system.

Katz (R-16) also studied *wave-plate impingement separators* (Fig. 14-110b) made up of 90° formed arcs with an 11.1-mm (0.44-in) radius and a 3.8-mm (0.15-in) clearance between sheets. The pressure drop is a function of system geometry. The pressure drop for Katz's system and collection efficiency for seven waves are shown in Fig. 14-111. Katz used the Souders-Brown expression to define a design velocity for the gas between the waves:

$$U = K \sqrt{\rho_l - \rho_g} / \rho_g \quad (14-226)$$

K is 0.12 to give U in ms⁻¹ (0.4 for ft/s), and ρ_l and ρ_g are liquid and gas densities in any consistent set of units. Katz found no change in efficiency at gas velocities from one-half to 3 times that given by the equation.

Calvert (R-12) investigated *zigzag baffles* of a design more like Fig. 14-110e. The baffles may have spaces between the changes in direction or be connected as shown. He found close to 100 per collection for water droplets of 10 µm and larger. Some designs had high efficiencies down to 5 or 8 µm. Desirable gas velocities were 2 to 3.5 m/s (6.6 to 11.5 ft/s), with a pressure drop for a six-pass baffle of 2 to 2.5 cm (0.8 to 1.0 in) of water. On the basis of turbulent mixing, an equation was developed for predicting primary collection efficiency as a function of particle size and collector geometry:

$$\eta = 1 - \exp \left[- \frac{u_{te} n W \theta}{57.3 U_g b \tan \theta} \right] \quad (14-227)$$

where η is the fractional primary collection efficiency; u_{te} is the drop terminal centrifugal velocity in the normal direction, cm/s; U_g is the superficial gas velocity, cm/s; n is the number of rows of baffles or bends; θ is the angle of inclination of the baffle to the flow path, °; W is the width of the baffle, cm; and b is the spacing between baffles in the same row, cm. For conditions of low Reynolds number ($N_{Re,D} <$

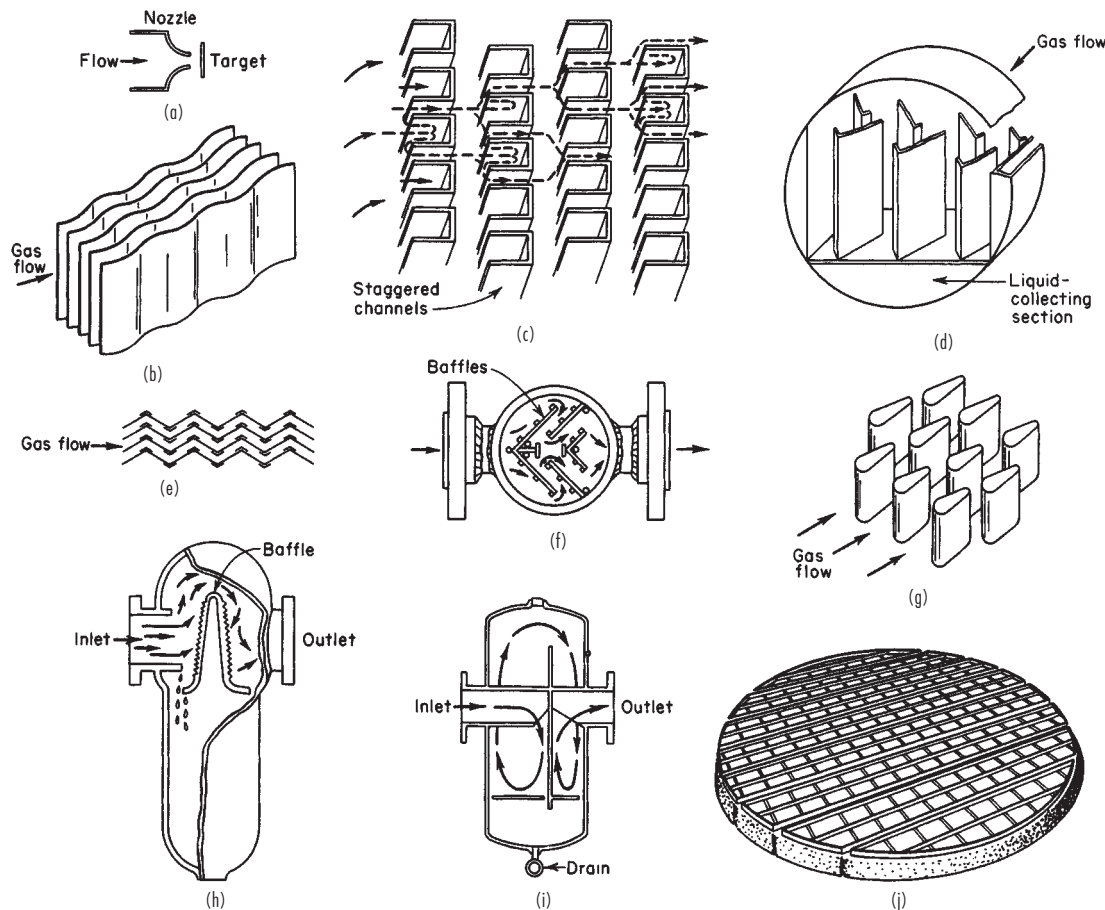


FIG. 14-110 Typical impingement separators. (a) Jet impactor. (b) Wave plate. (c) Staggered channels. (Blaw-Knox Food & Chemical Equipment, Inc.) (d) Vane-type mist extractor. (Maloney-Crawford Tank and Mfg. Co.) (e) Peerless line separator. (Peerless Mfg. Co.) (f) Strong separator. (Strong Carlisle and Hammond.) (g) Karbate line separator. (Union Carbide Corporation) (h) Type E horizontal separator. (Wright-Austin Co.) (i) PL separator. (Ingersoll Rand.) (j) Wire-mesh demister. (Otto H. York Co.)

0.1) where Stokes' law applies, Calvert obtains the value for drop terminal centrifugal velocity of $U_{tc} = d_p^2 \rho_p a / 18 \mu_g$, where d_p and ρ_p are the drop particle diameter, cm, and particle density, g/cm³, respectively; μ_g is the gas viscosity, P; and a is the acceleration due to centrifugal force. It is defined by the equation $a = 2U_g^2 \sin \theta / W \cos^3 \theta$. For situations in which Stokes' law does not apply, Calvert recommends substitution in the derivation of Eq. (14-227) for u of drag coefficients from

drag-coefficient data of Foust et al. (*Principles of Unit Operations*, Tappan Co., Tokyo, 1959).

Calvert found that reentrainment from the baffles was affected by the gas velocity, the liquid-to-gas ratio, and the orientation of the baffles. Horizontal gas flow past vertical baffles provided the best drainage and lowest reentrainment. Safe operating regions with vertical baffles are shown in Fig. 14-112. Horizontal baffles gave the poorest drainage

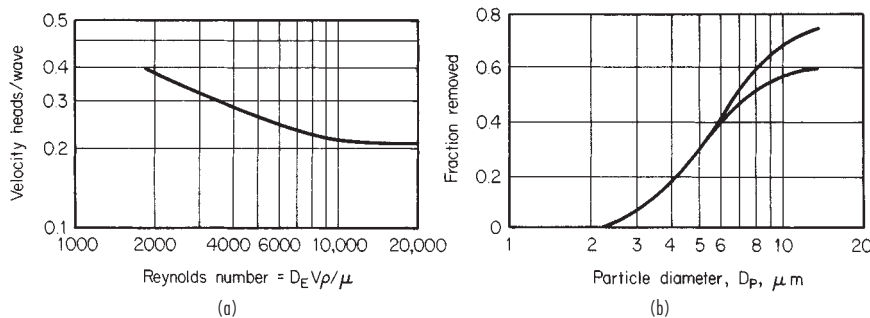


FIG. 14-111 Pressure drop and collection efficiency of a wave-plate separator. (a) Pressure drop. (b) Efficiency D_E = clearance between sheets. (Katz, M.S. thesis, Pennsylvania State University, 1958.)

14-86 GAS ABSORPTION AND GAS-LIQUID SYSTEM DESIGN

and the highest reentrainment, with inclined baffles intermediate in performance. Equation (14-228), developed by Calvert, predicts pressure drop across zigzag baffles. The indicated summation must be made over the number of rows of baffles present.

$$\Delta P = \sum_{i=1}^{i=n} 1.02 \times 10^{-3} f_D \rho_g \frac{U'_g A_p}{2 A_t} \quad (14-228)$$

ΔP is the pressure drop, cm of water; ρ_g is the gas density, g/cm³; A_p is the total projected area of an entire row of baffles in the direction of inlet gas flow, cm²; and A_t is the duct cross-sectional area, cm². The value f_D is a drag coefficient for gas flow past inclined flat plates taken from Fig. 14-113, while U'_g is the actual gas velocity, cm/s, which is related to the superficial gas velocity U_g by $U'_g = U_g / \cos \theta$. It must be noted that the angle of incidence θ for the second and successive rows of baffles is twice the angle of incidence for the first row. Most of Calvert's work was with 30° baffles, but the method correlates well with other data on 45° baffles.

The Karbate line separator (Fig. 14-110g) is composed of several layers of teardrop-shaped target rods of Karbate. A design flow constant K in Eq. (14-226) of 0.035 m/s (1.0 ft/s) is recommended by the manufacturer. Pressure drop is said to be 5½ velocity heads on the basis of the superficial gas velocity. This value would probably increase at high liquid loads. Figure 14-114 gives the manufacturer's reported grade efficiency curve at the design air velocity.

The use of multiple tube banks as a droplet collector has also been studied by Calvert (R-12). He reports that collection efficiency for

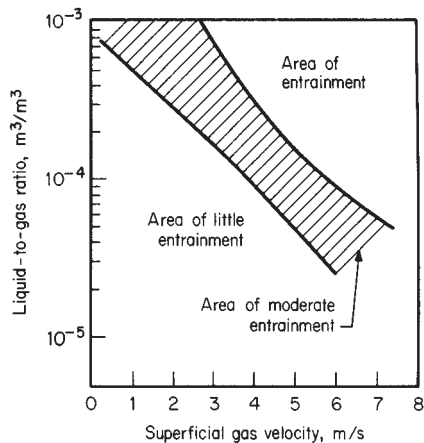


FIG. 14-112 Safe operating region to prevent reentrainment from vertical zigzag baffles with horizontal gas flow. (Calvert, Yung, and Leung, NTIS Publ. PB-248050, 1975.)

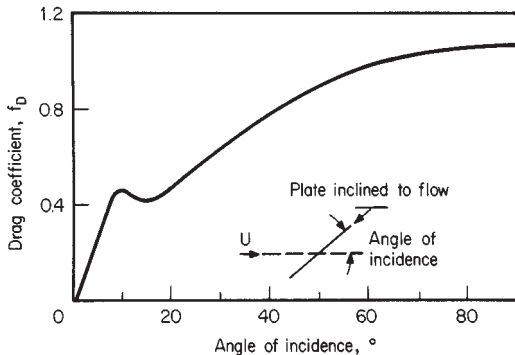


FIG. 14-113 Drag coefficient for flow past inclined flat plates for use in Eq. (14-228). (Calvert, Yung, and Leung, NTIS Publ. PB-248050; based on Fage and Johansen, Proc. R. Soc. (London), 116A, 170 (1927).)

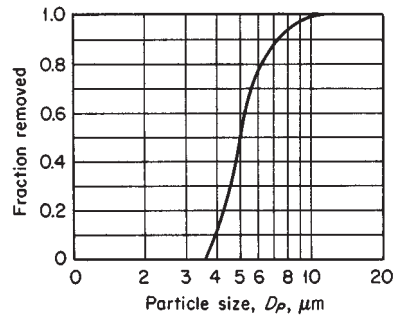


FIG. 14-114 Collection efficiency of Karbate line separator, based on particles with a specific gravity of 1.0 suspended in atmospheric air with a pressure drop of 2.5 cm water gauge. (Union Carbide Corporation Cat. Sec. S-6900, 1960.)

closely packed tubes follows equations for rectangular jet impaction which can be obtained graphically from Fig. 14-115 by using a dimensional parameter β which is based on the tube geometry; $\beta = 2l_i/b$, where b is the open distance between adjacent tubes in the row (orifice width) and l_i is the impaction length (distance between orifice and impingement plane), or approximately the distance between center-lines of successive tube rows. Note that the impaction parameter K_p is plotted to the one-half power in Fig. 14-115 and that the radius of the droplet is used rather than the diameter. Collection efficiency overall for a given size of particle is predicted for the entire tube bank by

$$\eta = 1 - (1 - \eta_b)^N \quad (14-229)$$

where η_b is the collection efficiency for a given size of particle in one stage of a rectangular jet impactor (Fig. 14-115) and N is the number of stages in the tube bank (equal to one less than the number of rows). For widely spaced tubes, the target efficiency η_b can be calculated from Fig. 17-39 or from the impaction data of Golovin and Putnam [Ind. Eng. Chem. Fundam., 1, 264 (1962)]. The efficiency of the overall tube banks for a specific particle size can then be calculated from the equation $\eta = 1 - (1 - \eta_b a'/A)^n$, where a' is the cross-sectional area of all tubes in one row, A is the total flow area, and n is the number of rows of tubes.

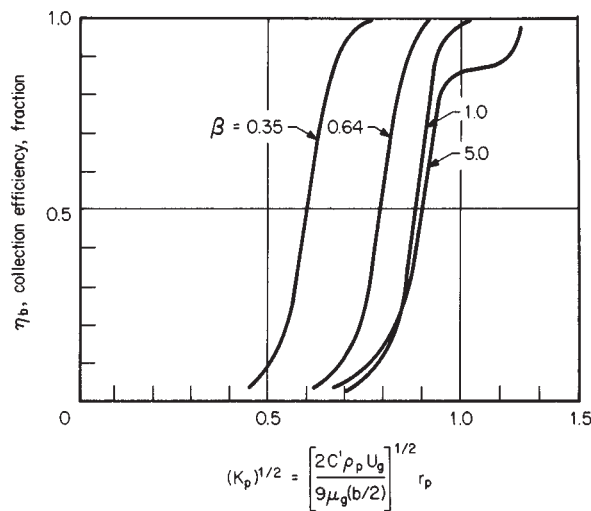


FIG. 14-115 Experimental collection efficiencies of rectangular impactors. C' is the Stokes-Cunningham correction factor; ρ_p , particle density, g/cm³; U_g , superficial gas velocity, approaching the impactor openings, cm/s; and μ_g , gas viscosity, P. [Calvert, Yung, and Leung, NTIS Publ. PB-248050; based on Mercer and Chow, J. Coll. Interface Sci., 27, 75 (1968).]

Calvert reports pressure drop through tube banks to be largely unaffected by liquid loading and indicates that Grimison's correlations in Sec. 6 ("Tube Banks") for gas flow normal to tube banks or data for gas flow through heat-exchanger bundles can be used. However, the following equation is suggested:

$$\Delta P = 8.48 \times 10^{-3} n \rho_g U_g'^2 \quad (14-230)$$

where ΔP is cm of water; n is the number of rows of tubes; ρ_g is the gas density, g/cm³; and U_g' is the actual gas velocity between tubes in a row, cm/s. Calvert did find an increase in pressure drop of about 80 to 85 percent above that predicted by Eq. (14-230) in vertical upflow of gas through tube banks due to liquid holdup at gas velocities above 4 m/s. The onset of liquid reentrainment from tube banks can be predicted from Fig. 14-116. Reentrainment occurred at much lower velocities in vertical upflow than in horizontal gas flow through vertical tube banks. While the top of the cross-hatched line of Fig. 14-116a predicts reentrainment above gas velocities of 3 m/s (9.8 ft/s) at high liquid loading, most of the entrainment settled to the bottom of the duct in 1 to 2 m (3.3 to 6.6 ft), and entrainment did not carry significant distances until the gas velocity exceeded 7 m/s (23 ft/s).

Packed-Bed Collectors Many different materials, including coal, coke, broken solids of various types such as brick, tile, rock, and stone, as well as normal types of tower-packing rings, saddles, and special plastic shapes, have been used over the years in packed beds to remove entrained liquids through impaction and filtration. Separators using natural materials are not available as standard commercial units but are designed for specific applications. Coke boxes were used extensively in the years 1920 to 1940 as sulfuric acid entrainment separators (see *Chemical Engineers' Handbook*, 5th ed., p. 18-87) but have now been largely superseded by more sophisticated and efficient devices.

Jackson and Calvert [Am. Inst. Chem. Eng. J., **12**, 1075 (1966)] studied the collection of fine fuel-oil-mist particles in beds of ½-in glass spheres, Raschig rings, and Berl and Intalox saddles. The mist had a mass median particle diameter of 6 µm and a standard deviation of 2.0. The collection efficiency as a function of particle size and gas

velocity in a 355-mm-(14-in-) diameter by 152-mm-(6-in-) thick bed of Intalox saddles is given in Fig. 14-117. This and additional work have been generalized by Calvert (R-12) to predict collection efficiencies of liquid particles in any packed bed. Assumptions in the theoretical development are that the drag force on the drop is given by Stokes' law and that the number of semicircular bends to which the gas is subjected, η_1 , is related to the length of the bed, Z (cm), in the direction of gas flow, the packing diameter, d_c (cm), and the gas-flow channel width, b (cm), such that $\eta_1 = Z/(d_c + b)$. The gas velocity through the channels, U_{gb} (cm/s), is inversely proportional to the bed free volume for gas flow such that $U_{gb} = U_g [1/(\varepsilon - h_b)]$, where U_g is the gas superficial velocity, cm/s, approaching the bed, ε is the bed void fraction, and h_b is the fraction of the total bed volume taken up with liquid which can be obtained from data on liquid holdup in packed beds. The width of the semicircular channels b can be expressed as a fraction j of the diameter of the packing elements, such that $b = jd_c$. These assumptions (as modified by G. E. Goltz, personal communication) lead to an equation for predicting the penetration of a given size of liquid particle through a packed bed:

$$P_t = \exp \left[\frac{-\pi}{2(j+j^2)(\varepsilon - h_b)} \left(\frac{Z}{d_c} \right) K_p \right] \quad (14-231)$$

$$\text{where } K_p = \frac{\rho_p d_p^2 U_g}{9\mu_g d_c} \quad (14-232)$$

Values of ρ_p and d_p are droplet density, g/cm³, and droplet diameter, cm; μ_g is the gas viscosity, P. All other terms were defined previously. Table 14-19 gives values of j calculated from experimental data of Jackson and Calvert. Values of j for most manufactured packing appear to fall in the range from 0.16 to 0.19. The low value of 0.03 for coke may be due to the porosity of the coke itself.

Calvert (R-12) has tested the correlation in cross-flow packed beds, which tend to give better drainage than countercurrent beds, and has found the effect of gas-flow orientation insignificant. However, the onset of reentrainment was somewhat lower in a bed of 2.5-cm

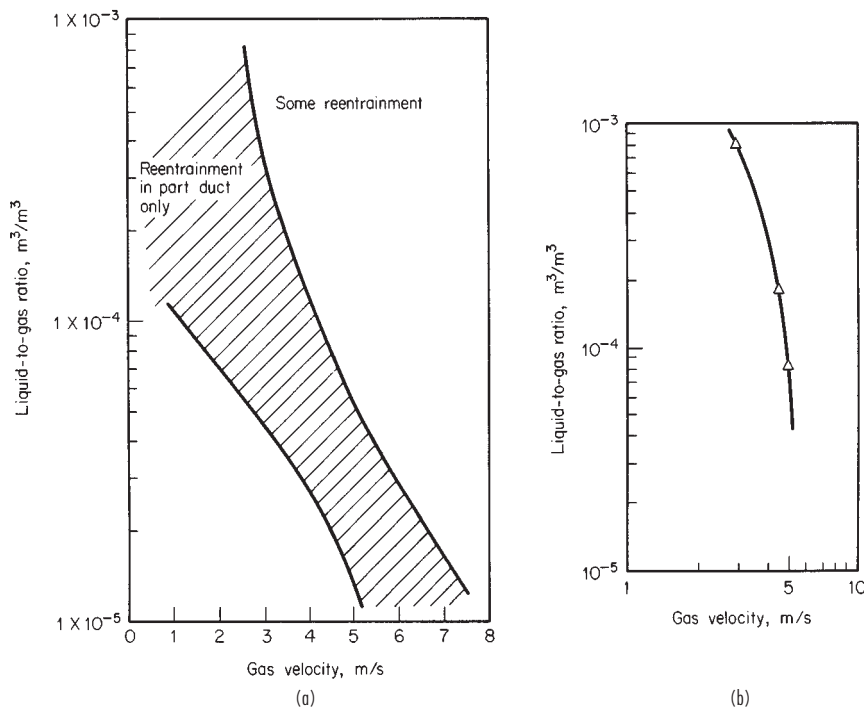


FIG. 14-116 Experimental results showing effect of gas velocity and liquid load on entrainment from (a) vertical tube banks with horizontal gas flow and (b) horizontal tube banks with upflow. To convert meters per second to feet per second, multiply by 3.281. (Calvert, Yung, and Leung, NTIS Publ. PB-248050.)

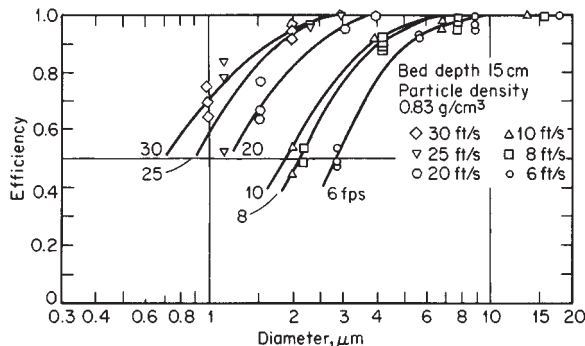


FIG. 14-117 Experimental collection efficiency, ½-in Intalox saddles. To convert feet per second to meters per second, multiply by 0.3048; to convert centimeters to inches, multiply by 0.394; and to convert grams per cubic centimeter to pounds per cubic foot, multiply by 62.43. [Jackson and Calvert, Am. Inst. Chem. Eng. J., **12**, 1975 (1968).]

(1.0-in) pall rings with gas upflow [6 m/s (20 ft/s)] than with horizontal cross-flow of gas. The onset of reentrainment was independent of liquid loading (all beds were nonirrigated), and entrainment occurred at values somewhat above the flood point for packed beds as predicted by conventional correlations. In beds with more than 3 cm (1.2 in) of water pressure drop, the experimental drop with both vertical and horizontal gas flow was somewhat less than predicted by generalized packed-bed pressure-drop correlations. However, Calvert recommends these correlations for design as conservative.

Calvert's data indicate that packed beds irrigated only with the collected liquid can have collection efficiencies of 80 to 90 percent on mist particles down to 3 μm but have low efficiency on finer mist particles. Frequently, irrigated packed towers and towers with internals will be used with liquid having a wetting capability for the fine mist which must be collected. Tennessee Valley Authority (TVA) experiments with the collection of 1.0-μm mass median phosphoric acid mist in packed towers have shown that the strength of the circulating phosphoric acid is highly important [see Baskerville, *Am. Inst. Chem. Eng. J.*, **37**, 79 (1941); and p. 18–87, 5th ed. of the *Handbook*]. Hesketh (*J. Air Pollut. Control Assoc.*, **24**, 942 (1974)) has reported up to 50 percent improvement in collection efficiency in venturi scrubbers on fine particles with the addition of only 0.10 percent of a low-foaming nonionic surfactant to the scrubbing liquid, and others have experienced similar results in other gas-liquid-contacting devices. Calvert (R-9 and R-10) has reported on the efficiency of various gas-liquid-contacting devices for fine particles. Figure 14-118 gives the particle aerodynamic cut size for a single-sieve-plate gas scrubber as a function of sieve hole size d_h , cm; hole gas velocity u_h , m/s; and froth or foam density on the plate F , g/cm³. This curve is based on standard air and water properties and wettable (hydrophilic) particles. The cut diameter decreases with an increase in froth density, which must be predicted from correlations for sieve-plate behavior (see Fig. 14-32). Equation (14-231) can be used to calculate generalized design curves for collection in packed columns in the same fashion by finding parameters of packing size, bed length, and gas velocity which give collection efficiencies of 50 percent for various size particles. Figure 14-119 illustrates such a plot for three gas velocities and two sizes of packing.

TABLE 14-19 Experimental Values for j , Channel Width in Packing as a Fraction of Packing Diameter

Packing size cm	Type of packing	j
in		
1.27	Berl and Intalox saddles, marbles, Raschig rings	0.192
2.54	Berl and Intalox saddles, pall rings	0.190
3.8	Berl and Intalox saddles, pall rings	0.165
7.6–12.7	Coke	0.03

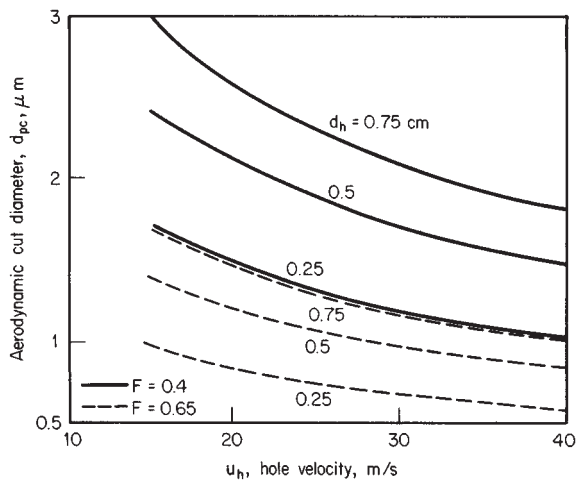


FIG. 14-118 Aerodynamic cut diameter for a single-sieve-plate scrubber as a function of hole size, hole-gas velocity, and froth density, F , g/cm³. To convert meters per second to feet per second, multiply by 3.281; to convert grams per cubic centimeter to pounds per cubic foot, multiply by 62.43. [Calvert, *J. Air Pollut. Control Assoc.*, **24**, 929 (1974).]

Wire-Mesh Mist Collectors Knitted mesh of varying density and voidage is widely used for entrainment separators. Its advantage is close to 100 percent removal of drops larger than 5 μm at superficial gas velocities from about 0.2 m/s (0.6 ft/s) to 5 m/s (16.4 ft/s), depending somewhat on the design of the mesh. Pressure drop is usually no more than 2.5 cm (1 in) of water. A major disadvantage is the ease with which tars and insoluble solids plug the mesh. The separator can be made to fit vessels of any shape and can be made of any material which can be drawn into a wire. Stainless-steel and plastic fibers are most common, but other metals are sometimes used. Generally three basic types of mesh are used: (1) layers with a crimp in the same direction (each layer is actually a nested double layer); (2) layers with a crimp in

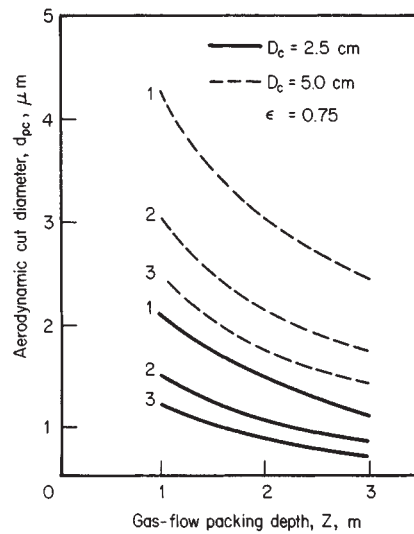


FIG. 14-119 Aerodynamic cut diameter for a typical packed-bed entrainment separator as a function of packing size, bed depth, and three gas velocities: curve 1–1.5 m/s, curve 2–3.0 m/s, and curve 3–4.5 m/s. To convert meters to feet, multiply by 3.281; to convert centimeters to inches, multiply by 0.394. [Calvert, *J. Air Pollut. Control Assoc.*, **24**, 929 (1974).]

alternate directions, which increases voidage, reduces sheltering and increases target efficiency per layer, and gives a lower pressure drop per unit length; and (3) spiral-wound layers which reduce pressure drop by one-third, but fluid creep may lead to higher entrainment. Some small manufacturers of plastic meshes may offer other weaves claimed to be superior. The filament size can vary from about 0.15 mm (0.006 in) for fine-wire pads to 3.8 mm (0.15 in) for some plastic fibers. Typical pad thickness varies from 100 to 150 mm (4 to 6 in), but occasionally pads up to 300 mm (12 in) thick are used. A typical wire diameter for standard stainless mesh is 0.28 mm (0.011 in), with a finished mesh density of 0.15 g/cm³ (9.4 lb/ft³). A lower mesh density may be produced with standard wire to give 10 to 20 percent higher flow rates.

Figure 14-120 presents an early calculated estimate of mesh efficiency as a fraction of mist-particle size. Experiments by Calvert (R-12) confirm the accuracy of the equation of Bradie and Dickson (*Joint Symp. Proc. Inst. Mech. Eng./Yorkshire Br. Inst. Chem. Eng.*, 1969, pp. 24–25) for primary efficiency in mesh separators:

$$\eta = 1 - \exp(-2/3)\pi al\eta_i \quad (14-232)$$

where η is the overall collection efficiency for a given-size particle; l is the thickness of the mesh, cm, in the direction of gas flow; a is the surface area of the wires per unit volume of mesh pad, cm²/cm³; and η_i , the target collection efficiency for cylindrical wire, can be calculated from Fig. 17-39 or the impaction data of Golovin and Putnam [*Ind. Eng. Chem.*, **1**, 264 (1962)]. The factor 2/3, introduced by Carpenter and Othmer [*Am. Inst. Chem. Eng. J.*, **1**, 549 (1955)], corrects for the fact that not all the wires are perpendicular to the gas flow and gives the projected perpendicular area. If the specific mesh surface area a is not available, it can be calculated from the mesh void area ϵ and the mesh wire diameter d_w in cm, $a = 4(1 - \epsilon)/d_w$.

York and Poppele (R-17) have stated that factors governing maximum allowable gas velocity through the mesh are (1) gas and liquid density, (2) liquid surface tension, (3) liquid viscosity, (4) specific wire surface area, (5) entering-liquid loading, and (6) suspended-solids content. York (R-18) has proposed application of the Souders-Brown equation [Eq. (14-226)] for correlation of maximum allowable gas velocity with values of K for most cases of 0.1067 m/s to give U in m/s (0.35 ft/s). When liquid viscosity or inlet loading is high or the liquid is dirty, the value of K must be reduced. Schroeder (M.S. thesis, Newark College of Engineering, 1962) found lower values for K necessary when liquid surface tension is reduced such as by the presence of surfactants in water. Ludwig (*Applied Process Design for Chemical and Petrochemical Plants*, 2d ed., vol. I, Gulf, Houston, 1977, p. 157) recommends reduced K values of (0.061 m/s) under vacuum at an absolute pressure of 6.77 kPa (0.98 lbf/in²) and $K = 0.082$ m/s at 54 kPa (7.83 lbf/in²) absolute. Most manufacturers suggest setting the design velocity at three-fourths of the maximum velocity to allow for surges in gas flow.

York and Poppele (R-17) have suggested that total pressure drop through the mesh is equal to the sum of the mesh dry pressure drop

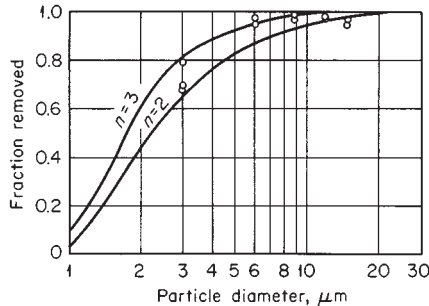


FIG. 14-120 Collection efficiency of wire-mesh separator; 6-in thickness, 98.6 percent free space, 0.006-in-diameter wire used for experiment points. Curves calculated for target area equal to 2 and 3 times the solids volume of packing. To convert inches to millimeters, multiply by 25.4.

plus an increment due to the presence of liquid. They considered the mesh to be equivalent to numerous small circular channels and used the D'Arcy formula with a modified Reynolds number to correlate friction factor (see Fig. 14-121) for Eq. (14-233) giving dry pressure drop.

$$\Delta P_{dry} = flap_g U_g^2 / 981 \epsilon^3 \quad (14-233)$$

where ΔP is in cm of water; f is from Fig. (14-121); ρ_g is the gas density, g/cm³; U_g is the superficial gas velocity, cm/s; and ϵ is the mesh porosity or void fraction; l and a are as defined in Eq. (14-232). Figure 14-121 gives data of York and Poppele for mesh crimped in the same and alternating directions and also includes the data of Satsangee, of Schuring, and of Bradie and Dickson.

The incremental pressure drop for wet mesh is not available for all operating conditions or for mesh of different styles. The data of York and Poppele for wet-mesh incremental pressure drop, ΔP_l , in cm of water, are shown in Fig. 14-122 or parameters of liquid velocity L/A , defined as liquid volumetric flow rate, cm³/min per unit of mesh cross-sectional area in cm²; liquid density ρ_L is in g/cm³.

York generally recommends the installation of the mesh horizontally with upflow of gas as in Fig. 14-110f; Calvert (R-12) tested the mesh horizontally with upflow and vertically with horizontal gas flow. He reports better drainage with the mesh vertical and somewhat higher permissible gas velocities without reentrainment, which is contrary to past practice. With horizontal flow through vertical mesh, he found collection efficiency to follow the predictions of Eq. 14-232 up to 4 m/s (13 ft/s) with air and water. Some reentrainment was encountered at higher velocities, but it did not appear serious until velocities exceeded 6.0 m/s (20 ft/s). With vertical upflow of gas, entrainment was encountered at velocities above and below 4.0 m/s (13 ft/s), depending on inlet liquid quantity (see Fig. 14-123). Figure 14-124 illustrates the onset of entrainment from mesh as a function of liquid loading and gas velocity and the safe operating area recommended by Calvert. Measurements of dry pressure drop by Calvert gave values only about one-third of those predicted from Eq. (14-233). He found the pressure drop to be highly affected by liquid load. The pressure drop of wet mesh could be correlated as a function of $U_g^{1.65}$ and parameters of liquid loading L/A , as shown in Fig. 14-125.

As indicated previously, mesh efficiency drops rapidly as particles decrease in size below 5 μm. An alternative is to use two mesh pads in series. The first mesh is made of fine wires and is operated beyond the

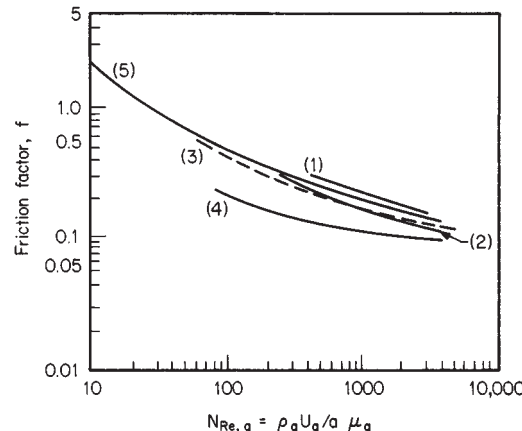


FIG. 14-121 Value of friction factor f for dry knitted mesh for Eq. (14-233). Values of York and Poppele [*Chem. Eng. Prog.*, **50**, 421 (1954)] are given in curve 1 for mesh crimped in the alternating direction and curve 2 for mesh crimped in the same direction. Data of Bradie and Dickson (*Joint Symp. Proc. Inst. Mech. Eng./Yorkshire Br. Inst. Chem. Eng.*, 1969, pp. 24–25) are given in curve 3 for layered mesh and curve 4 for spiral-wound mesh. Curve 5 is data of Satsangee (M.S. thesis, Brooklyn Polytechnic Institute, 1948) and Schuring (D.Ch.E. dissertation, Brooklyn Polytechnic Institute, 1946). (From Calvert, Yung, and Leung, NTIS Publ. PB-248050, 1975.)

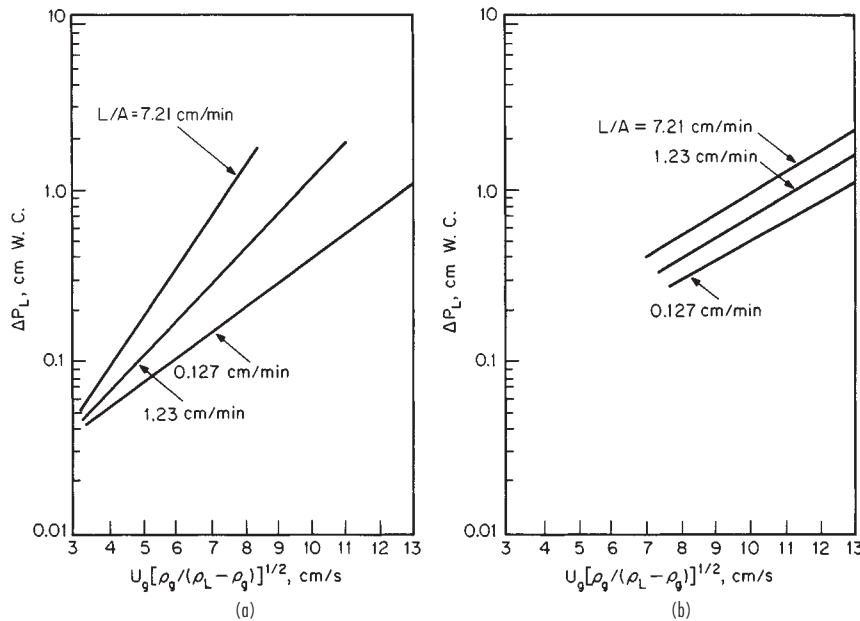


FIG. 14-122 Incremental pressure drop in knitted mesh due to the presence of liquid (a) with the mesh crimps in the same direction and (b) with crimps in the alternating direction, based on the data of York and Popple [Chem. Eng. Prog., **50**, 421 (1954)]. To convert centimeters per minute to feet per minute, multiply by 0.0328; to convert centimeters per second to feet per second, multiply by 0.0328. (From Calvert, Yung, and Leung, NTIS Publ. PB-248050, 1975.)

flood point. It results in droplet coalescence, and the second mesh, using standard wire and operated below flooding, catches entrainment from the first mesh. Coalescence and flooding in the first mesh may be assisted with water sprays or irrigation. Massey [Chem. Eng. Prog., **53**(5), 114 (1959)] and Coykendall et al. [J. Air Pollut. Control Assoc., **18**, 315 (1968)] have discussed such applications. Calvert (R-12) presents data on the particle size of entrained drops from mesh as a function of gas velocity which can be used for sizing the secondary collector. A major disadvantage of this approach is high pressure drop, which can be in the range from 25 cm (10 in) of water to as high as 85 cm (33 in) of water if the mist is mainly submicrometer.

Wet Scrubbers Scrubbers have not been widely used for the collection of purely liquid particulate, probably because they are generally more complex and expensive than impaction devices of the types previously discussed. Further, scrubbers are no more efficient than the former devices for the same energy consumption. However,

scrubbers of the types discussed in Sec. 17 and illustrated in Figs. 17-48 to 17-55 can be used to capture liquid particles efficiently. Their use is primarily indicated when it is desired to accomplish simultaneously another task such as gas absorption or the collection of solid and liquid particulate mixtures.

Table 20-41 [Chemical Engineers' Handbook, 5th ed.], showing

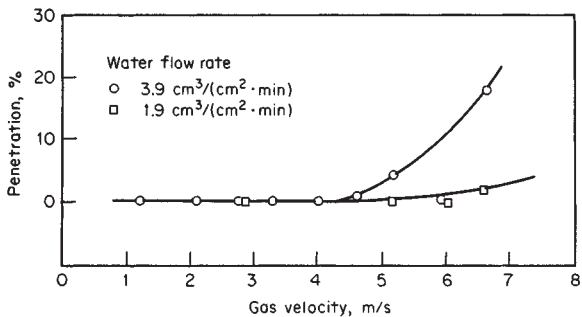


FIG. 14-123 Experimental data of Calvert with air and water in mesh with vertical upflow, showing the effect of liquid loading on efficiency and reentrainment. To convert meters per second to feet per second, multiply by 3.281; to convert cubic centimeters per square centimeter-minute to cubic feet per square foot-minute, multiply by 0.0328. (Calvert, Yung, and Leung, NTIS Publ. PB-248050, 1975.)

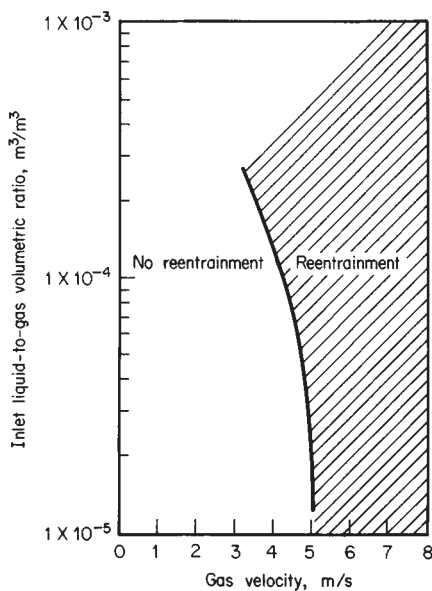


FIG. 14-124 Effect of gas and liquid rates on onset of mesh reentrainment and safe operating regions. To convert meters per second to feet per second, multiply by 3.281. (Calvert, Yung, and Leung, NTIS Publ. PB-248050, 1975.)

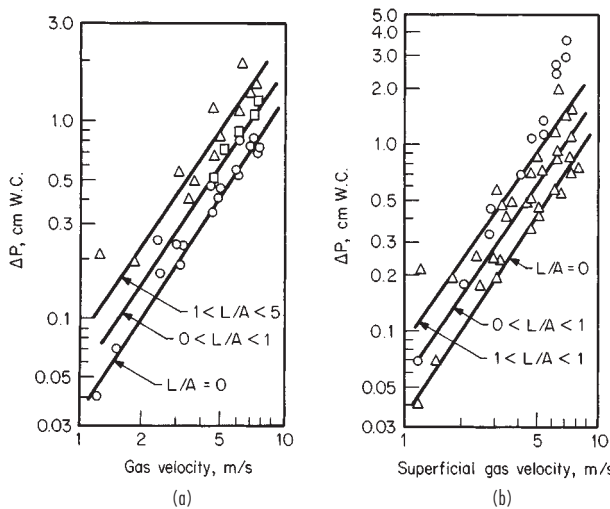


FIG. 14-125 Experimental pressure measured by Calvert as a function of gas velocity and liquid loading for (a) horizontal gas flow through vertical mesh and (b) gas upflow through horizontal mesh. Mesh thickness was 10 cm with 2.8-mm wire and void fraction of 98.2 percent, crimped in alternating directions. To convert meters per second to feet per second, multiply by 3.281; to convert centimeters to inches, multiply by 0.394. (*Calvert, Yung, and Leung, NTIS Publ. PB-248050, 1975.*)

the minimum size of particles collectible in different types of scrubbers at reasonably high efficiencies, is a good selection guide. Cyclonic spray towers (Fig. 17-52) can effectively remove liquid particles down to around 2 to 3 μm . Figures 20-112 and 20-113 (*Chemical Engineers' Handbook*, 5th ed.), giving target efficiency between spray drop size and particle size as calculated by Stairmand or Johnstone and Roberts, should be considered in selecting spray atomization for the most efficient tower operation. Figure 14-126 gives calculated particle cut size as a function of tower height (or length) for vertical countercurrent spray towers and for horizontal-gas-flow, vertical-liquid-flow cross-current spray towers with parameters for liquid drop size. These curves are based on physical properties of standard air and water and should be used under conditions in which these are reasonable

approximations. Lack of uniform liquid distribution or liquid flowing down the walls can affect the performance, requiring empirical correction factors. Calvert (B-10) suggests that a correction factor of 0.2 be used in small-diameter scrubbers to account for the liquid on the walls, i.e., let $Q_L/Q_g = 0.2 (Q_L/Q_g)_{\text{actual}}$. Many more complicated wet scrubbers employ a combination of sprays or liquid atomization, cyclonic action, baffles, and targets. These combinations are not likely to be more efficient than similar devices previously discussed that operate at equivalent pressure drop. The vast majority of wet scrubbers operate at moderate pressure drop [8 to 15 cm (3 to 6 in) of water or 18 to 30 cm (7 to 12 in) of water] and cannot be expected to have high efficiency on particles smaller than 10 μm or 3 to 5 μm respectively. Fine and submicrometer particles can be captured efficiently only in wet scrubbers having high energy input such as venturi scrubbers, two-phase eductor scrubbers, and flux-force-condensation scrubbers.

Venturi Scrubbers One type of venturi scrubber is illustrated in Fig. 17-48. Venturi scrubbers have been used extensively for collecting fine and submicrometer solid particulate, condensing tars and mists, and mixtures of liquids and solids. To a lesser extent, they have also been used for simultaneous gas absorption, although Lundy [*Ind. Eng. Chem.*, **50**, 293 (1958)] indicates that they are generally limited to three transfer units. They have been used to collect submicrometer chemical incinerator fume and mist as well as sulfuric and phosphoric acid mists. The collection efficiency of a venturi scrubber is highly dependent on the throat velocity or pressure drop, the liquid-to-gas ratio, and the chemical nature of wettability of the particulate. Throat velocities may range from 60 to 150 m/s (200 to 500 ft/s). Liquid injection rates are typically 0.67 to 1.4 $\text{m}^3/1000 \text{ m}^3$ of gas. A liquid rate of 1.0 m^3 per 1000 m^3 of gas is usually close to optimum, but liquid rates as high as 2.7 m^3 (95 ft³) have been used. Efficiency improves with increased liquid rate but only at the expense of higher pressure drop and energy consumption. Pressure-drop predictions for a given efficiency are hazardous without determining the nature of the particulate and the liquid-to-gas ratio. In general, particles coarser than 1 μm can be collected efficiently with pressure drops of 25 to 50 cm of water. For appreciable collection of submicrometer particles, pressure drops of 75 to 100 cm (30 to 40 in) of water are usually required. When particles are appreciably finer than 0.5 μm , pressure drops of 175 to 250 cm (70 to 100 in) of water have been used.

One of the problems in predicting efficiency and required pressure drop of a venturi is the chemical nature or wettability of the particulate, which on 0.5- μm -size particles can make up to a threefold difference in required pressure drop for its efficient collection. Calvert

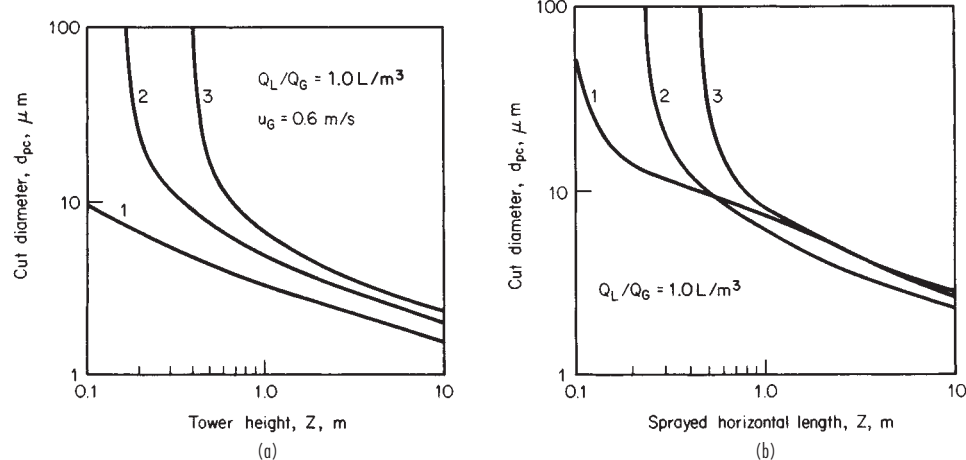


FIG. 14-126 Predicted spray-tower cut diameter as a function of sprayed length and spray droplet size for (a) vertical countercurrent towers and (b) horizontal-cross-flow towers per Calvert [*J. Air Pollut. Control Assoc.*, **24**, 929 (1974)]. Curve 1 is for 200- μm spray droplets, curve 2 for 500- μm spray, and curve 3 for 1000- μm spray. Q_L/Q_G is the volumetric liquid-to-gas ratio, L liquid/ m^3 gas, and u_G is the superficial gas velocity in the tower. To convert liters per cubic meter to cubic feet per cubic foot, multiply by 10^{-3} .

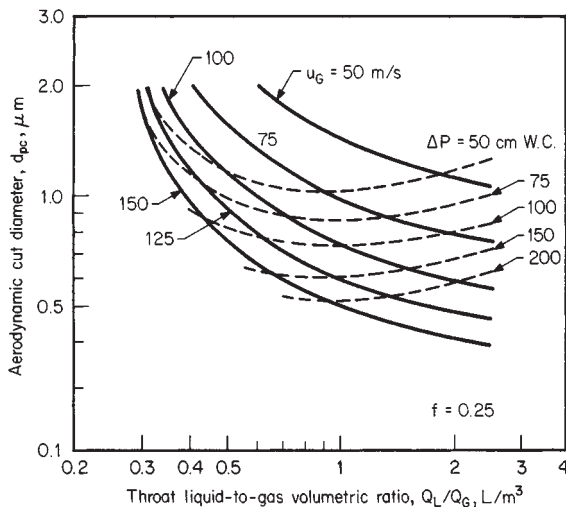


FIG. 14-127 Prediction of venturi-scrubber cut diameter for hydrophobic particles as functions of operating parameters as measured by Calvert [Calvert, Goldshmid, Leith, and Mehta, NTIS Publ. PB-213016, 213017, 1972; and Calvert, J. Air Pollut. Control Assoc., **24**, 929 (1974).] u_g is the superficial throat velocity, and ΔP is the pressure drop from converging to diverging section. To convert meters per second to feet per second, multiply by 3.281; to convert liters per cubic meter to cubic feet per cubic foot, multiply by 10^{-3} ; and to convert centimeters to inches, multiply by 0.394.

(R-9, R-10) has represented this effect by an empirical factor f , which is based on the hydrophobic ($f=0.25$) or hydrophilic ($f=0.50$) nature of the particles. Figure 14-127 gives the cut diameter of a venturi scrubber as a function of its operating parameters (throat velocity, pressure drop, and liquid-to-gas ratio) for hydrophobic particles. Figure 14-129 compares cut diameter as a function of pressure drop for an otherwise identically operating venturi on hydrophobic and hydrophilic particles. Calvert (R-9) gives equations which can be used for constructing cut-size curves similar to those of Fig. 14-127 for other values of the empirical factor f . Most real particles are neither completely hydrophobic nor completely hydrophilic but have f values lying between the two extremes. Phosphoric acid mist, on the basis of data of Brink and Contant [Ind. Eng. Chem., **50**, 1157 (1958)] appears to have a value of $f=0.46$. Unfortunately, no chemical-test methods have yet been devised for determining appropriate f values for a particulate in the laboratory.

Pressure drop in a venturi scrubber is controlled by throat velocity. While some venturis have fixed throats, many are designed with variable louvers to change throat dimensions and control performance for changes in gas flow. Pressure-drop equations have been developed by Calvert (R-13, R-14, R-15), Boll [Ind. Eng. Chem. Fundam., **12**, 40 (1973)], and Hesketh [J. Air Pollut. Control Assoc., **24**, 939 (1974)]. Hollands and Goel [Ind. Eng. Chem. Fundam., **14**, 16 (1975)] have developed a generalized pressure-drop equation.

The Hesketh equation is empirical and is based upon a regression analysis of data from a number of industrial venturi scrubbers:

$$\Delta P = U_{gt}^2 \rho_g A_t^{0.155} L^{0.78} / 1270 \quad (14-234)$$

where ΔP is the pressure drop, in of water; U_{gt} is the gas velocity in the throat, ft/s; ρ_g is the gas density, lb/ft³; A_t is the throat area, ft²; and L is the liquid-to-gas ratio, gal/1000 acf.

Calvert (R-15) critiqued the many pressure-drop equations and suggested the following simplified equation as accurate to ± 10 percent:

$$\Delta P = \frac{2\rho_e U_g^2}{981g_c} \left(\frac{Q_t}{Q_g} \right) [1 - x^2 + \sqrt{(x^4 - x^2)^{0.5}}] \quad (14-235)$$

where

$$x = (3l_t C_{Dl} \rho_g / 16d_l \rho_l) + 1 \quad (14-236)$$

ΔP is the pressure drop, cm of water; ρ_e and ρ_g are the density of the scrubbing liquid and gas respectively, g/cm³; U_g is the velocity of the gas at the throat inlet, cm/s; Q_t/Q_g is the volumetric ratio of liquid to gas at the throat inlet, dimensionless; l_t is the length of the throat, cm; C_{Dl} is the drag coefficient, dimensionless, for the mean liquid diameter, evaluated at the throat inlet; and d_l is the Sauter mean diameter, cm, for the atomized liquid. The atomized-liquid mean diameter must be evaluated by the Nukiyama and Tanasawa [Trans. Soc. Mech Eng. (Japan), 4, 5, 6 (1937-1940)] equation:

$$d_l = \frac{0.0585}{U_g} \left(\frac{\sigma_e}{\rho_e} \right)^{0.5} + 0.0597 \left[\frac{\mu_e}{(\sigma_e \rho_e)^{0.5}} \right]^{0.45} \left(\frac{\rho_e}{Q_g} \right)^{1.5} \quad (14-237)$$

where σ_e is the liquid surface tension, dyn/cm; and μ_e is the liquid viscosity; P . The drag coefficient C_{Dl} should be evaluated by the Dickinson and Marshall [Am. Inst. Chem. Eng. J., **14**, 541 (1968)] correlation $C_{Dl} = 0.22 + (24/N_{Re})^2 (1 + 0.15 N_{Re}^{0.6})$. The Reynolds number, N_{Re} , is evaluated at the throat inlet considerations as $d_l G_e / \mu_g$.

All venturi scrubbers must be followed by an entrainment collector for the liquid spray. These collectors are usually centrifugal and will have an additional pressure drop of several centimeters of water, which must be added to that of the venturi itself.

Other Scrubbers A liquid-ejector venturi (Fig. 17-53), in which high-pressure water from a jet induces the flow of gas, has been used to collect mist particles in the 1- to 2-μm range, but submicrometer particles will generally pass through an eductor. Power costs for liquid pumping are high if appreciable motive force must be imparted to the gas because jet-pump efficiency is usually less than 10 percent. Harris [Chem. Eng. Prog., **42**(4), 55 (1966)] has described their application. Two-phase eductors have been considerably more successful on capture of submicrometer mist particles and could be attractive in situations in which large quantities of waste thermal energy are available. However, the equivalent energy consumption is equal to that required for high-energy venturi scrubbers, and such devices are likely to be no more attractive than venturi scrubbers when the thermal energy is priced at its proper value. Sparks [J. Air Pollut. Control Assoc., **24**, 958 (1974)] has discussed steam ejectors giving 99 percent collection of particles 0.3 to 10 μm. Energy requirements were 311,000 J/m³(8,250 Btu/scf). Gardenier [J. Air Pollut. Control Assoc., **24**, 954 (1974)] operated a liquid eductor with high-pressure (6900- to 27,600-kPa) (1000- to 4000-lbf/in²) hot water heated to 200°C (392°F) which flashed into two phases as it issued from the jet. He obtained 95 to 99 percent collection of submicrometer particulate. Figure 14-128 shows the water-to-gas ratio required as a function of particle size to achieve 99 percent collection.

Effect of Gas Saturation in Scrubbing If hot unsaturated gas is introduced into a wet scrubber, spray particles will evaporate to cool and saturate the gas. The evaporating liquid molecules moving away from the target droplets will repel particles which might collide with them. This results in the forces of diffusiophoresis opposing particle

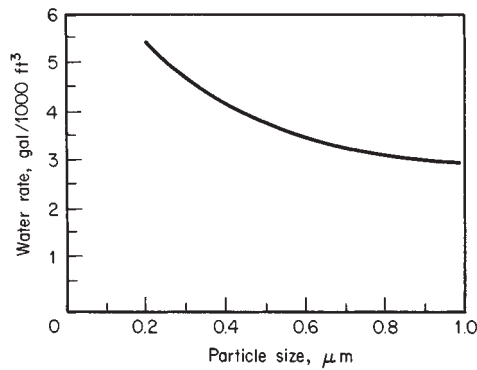


FIG. 14-128 Superheated high-pressure hot-water requirements for 99 percent collection as a function of particle size in a two-phase eductor jet scrubber. To convert gallons per 1000 cubic feet to cubic meters per 1000 cubic meters, multiply by 0.134. [Gardenier, J. Air Pollut. Control Assoc., **24**, 954 (1974).]

collection. Semrau and Witham (*Air Pollut. Control Assoc. Prepr.* 75-30.1) investigated temperature parameters in wet scrubbing and found a definite decrease in the efficiency of evaporative scrubbers and an enhancement of efficiency when a hot saturated gas is scrubbed with cold water rather than recirculated hot water. Little improvement was experienced in cooling a hot saturated gas below a 50°C dew point.

Energy Requirements for Inertial-Impaction Efficiency Semrau [*J. Air Pollut. Control Assoc.*, 13, 587 (1963)] proposed a "contacting-power" principle which states that the collecting efficiency of a given size of particle is proportional to the power expended and that the smaller the particle, the greater the power required. Mathematically expressed, $N_T = \propto P_T^\gamma$, where N_T is the number of particulate transfer units achieved and P_T is the total energy expended within the collection device, including gas and liquid pressure drop and thermal and mechanical energy added in atomizers. N_T is further defined as $N_T = \ln [1/(1 - \eta)]$, where η is the overall fractional collection efficiency. This was intended as a universal principle, but the constants \propto and γ have been found to be functions of the chemical nature of the system and the design of the control device. Others have pointed out that the principle is applicable only when the primary collection mechanism is impaction and direct interception. Calvert (R-10, R-12) has found that plotting particle cut size versus pressure drop (or power expended) as in Fig. 14-129 is a more suitable way to develop a generalized energy-requirement curve for impaction devices. The various curves fall close together and outline an imaginary curve that indicates the magnitude of pressure drop required as particle size decreases bound by the two limits of hydrophilic and hydrophobic particles. By calculating the required cut size for a given collection efficiency, Fig. 14-129, can also be used as a guide to deciding between different collection devices.

Subsequently, Calvert (R-19, p. 228) has combined mathematical modeling with performance tests on a variety of industrial scrubbers and has obtained a refinement of the power-input/cut-size relationship as shown in Fig. 14-130. He considers these relationships sufficiently reliable to use this data as a tool for selection of scrubber type and performance prediction. The power input for this figure is based solely on gas pressure drop across the device.

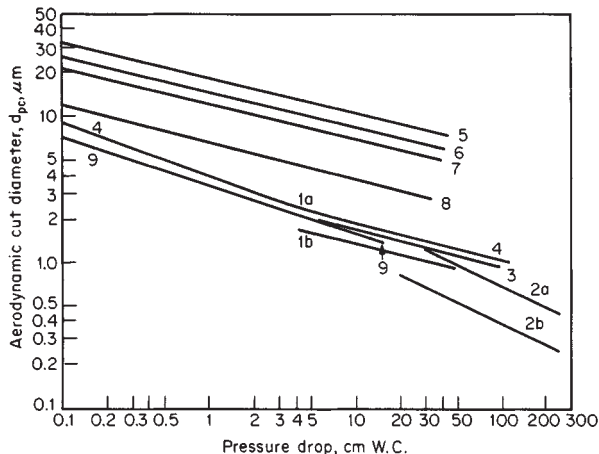


FIG. 14-129 Typical cut diameter as a function of pressure drop for various liquid-particle collectors. Curves 1a and b are single-sieve plates with froth density of 0.4 g/cm³; 1a has sieve holes of 0.5 cm and 1b holes of 0.3 cm. Curves 2a and b are for a venturi scrubber with hydrophobic particles (2a) and hydrophilic particles (2b). Curve 3 is an impingement plate, and curve 4 is a packed column with 2.5-cm-diameter packing. Curve 5 is a zigzag baffle collector with six baffles at $\theta = 30^\circ$. Curve 7 is for six rows of staggered tubes with 1-cm spacing between adjacent tube walls in a row. Curve 8 is similar, except that tube-wall spacing in the row is 0.3 cm. Curve 9 is for wire-mesh pads. To convert grams per cubic centimeter to pounds per cubic foot, multiply by 62.43; to convert centimeters to inches, multiply by 0.394. [Calvert, J. Air Pollut. Control Assoc., 24, 929 (1974); and Calvert, Yung, and Leung, NTIS Publ. PB-248050, 1975.]

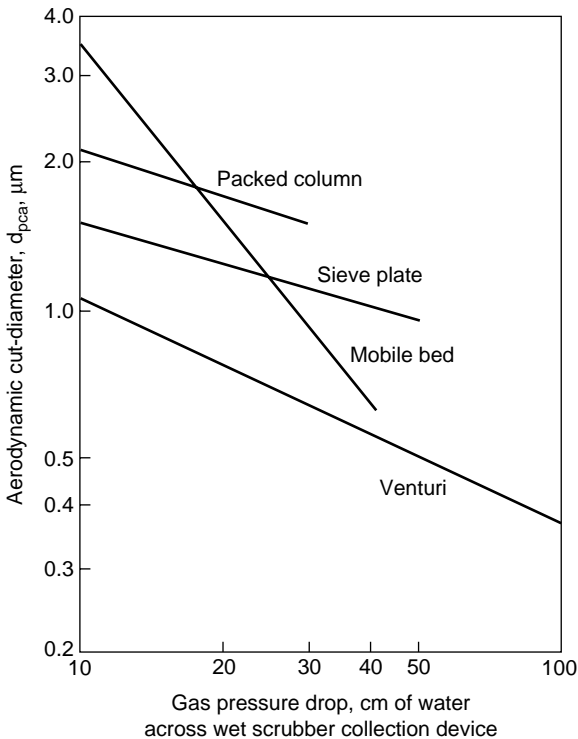


FIG. 14-130 Calvert's refined particle cut-size/power relationship for particle inertial impaction wet collectors. Ref. (R-19) by permission.

Collection of Fine Mists Inertial-impaction devices previously discussed give high efficiency on particles above 5 μm in size and often reasonable efficiency on particles down to 3 μm in size at moderate pressure drops. However, this mechanism becomes ineffective for particles smaller than 3 μm because of the particle gaslike mobility. Only impaction devices having extremely high energy input such as venturi scrubbers and a flooded mesh pad (the pad interstices really become miniature venturi scrubbers in parallel and in series) can give high collection efficiency on fine particles, defined as 2.5 or 3 μm and smaller, including the submicrometer range. Fine particles are subjected to brownian motion in gases, and diffusional deposition can be employed for their collection. Diffusional deposition becomes highly efficient as particles become smaller, especially below 0.2 to 0.3 μm. Table 14-20 shows typical displacement velocity of particles. Randomly oriented fiber beds having tortuous and narrow gas passages are suitable devices for utilizing this collection mechanism. (The diffusional collection mechanism is discussed in Sec. 17 under "Gas-Solids Separations.") Other collection mechanisms which are efficient for fine particles are electrostatic forces and flux forces such as thermophoresis and diffusiophoresis. Particle growth and nucleation methods are also applicable. Efficient collection of fine particles is important because particles in the range of 2.0 to around 0.2 μm are the ones which penetrate and are deposited in the lung most efficiently. Hence, particles in this range constitute the largest health hazard.

Fiber Mist Eliminators These devices are produced in various configurations. Generally, randomly oriented glass or polypropylene fibers are densely packed between reinforcing screens, producing fiber beds varying in thickness usually from 25 to 75 mm (1 to 3 in), although thicker beds can be produced. Units with efficiencies as high as 99.9 percent on fine particles have been developed (see *Chemical Engineers' Handbook*, 5th ed., p. 18-88). A combination of mechanisms interacts to provide high overall collection efficiency. Particles larger than 2 to 3 μm are collected on the fibers by inertial impaction

14-94 GAS ABSORPTION AND GAS-LIQUID SYSTEM DESIGN

TABLE 14-20 Brownian Movement of Particles*

Particle diameter, μm	Brownian displacement of particle, $\mu\text{m/s}$
0.1	29.4
0.25	14.2
0.5	8.92
1.0	5.91
2.5	3.58
5.0	2.49
10.0	1.75

*Brink, *Can. J. Chem. Eng.*, **41**, 134 (1963). Based on spherical water particles in air at 21°C and 1 atm.

and direct interception, while small particles are collected by brownian diffusion. When the device is designed to use this latter mechanism as the primary means, efficiency turndown problems are eliminated as collection efficiency by diffusion increases with residence time. Pressure drop through the beds increases with velocity to the first power since the gas flow is laminar. This leads to design capability trade-offs. As pressure drop is reduced and energy is conserved, capital increases because more filtering area is required for the same efficiency.

Three series of fiber mist eliminators are typically available. A spray-catcher series is designed primarily for essentially 100 percent capture of droplets larger than 3 μm . The high-velocity type is designed to give moderately high efficiency on particles down to 1.0 μm as well. Both of these types are usually produced in the form of flat panels of 25- to 50-mm (1- to 2-in) thickness. The high-efficiency type is illustrated in Fig. 14-131. As mist particles are collected, they coalesce into a liquid film which wets the fibers. Liquid is moved horizontally through the bed by the gas drag force and downward by gravity. It drains down the downstream retaining screen to the bottom of the element and is returned to the process through a liquid seal. Table 14-21 gives typical operating characteristics of the three types of collectors. The application of these devices to sulfuric acid plants and other process gases has been discussed by Brink (see *Chemical Engineers' Handbook*, 5th ed., pp. 18-89, 18-90).

Solid particulates are captured as readily as liquids in fiber beds but can rapidly plug the bed if they are insoluble. Fiber beds have frequently been used for mixtures of liquids and soluble solids and with soluble solids in condensing situations. Sufficient solvent (usually water) is atomized into the gas stream entering the collector to irrigate the fiber elements and dissolve the collected particulate. Such fiber beds have been used to collect fine fumes such as ammonium nitrate and ammonium chloride smokes, and oil mists from compressed air.

Electrostatic Precipitators The principles and operation of electrical precipitators are discussed in Sec. 17 under "Gas-Solids Separations." Precipitators are admirably suited to the collection of fine mists and mixtures of mists and solid particulates. Tube-type precipitators have been used for many years for the collection of acid mists and the removal of tar from coke-oven gas. The first practical installation of a precipitator by Cottrell was made on sulfuric acid mist in 1907. Most older installations of precipitators were tube-type rather than plate-type. However, recently two plate-type wet precipitators employing water sprays or overflowing weirs have been introduced by Mikropul Corporation [Bakke, *J. Air Pollut. Control Assoc.*, **25**, 163 (1975)] and by Fluid Ionics. Such precipitators operate on the principle of making all particles conductive when possible, which increases the particle migration velocity and collection efficiency. Under these conditions, particle dielectric strength becomes a much more impor-

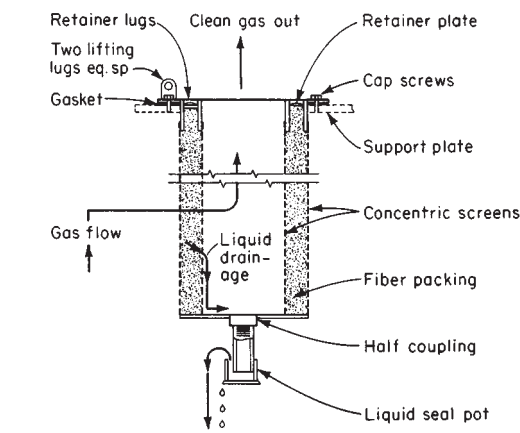


FIG. 14-131 Monsanto high-efficiency fiber-mist-eliminator element. (Monsanto Company.)

tant variable, and particles with a low dielectric constant such as condensed hydrocarbon mists become much more difficult to collect than water-wettable particles. Bakke (U.S.-U.S.S.R. Joint Work. Group Symp.: Fine Particle Control, San Francisco, 1974) has developed equations for particle charge and relative collection efficiency in wet precipitators that show the effect of dielectric constant. Wet precipitators can also be used to absorb soluble gases simultaneously by adjusting the pH or the chemical composition of the liquid spray. The presence of the electric field appears to enhance absorption. Wet precipitators have found their greatest usefulness to date in handling mixtures of gaseous pollutants and submicrometer particulate (either liquid or solid, or both) such as fumes from aluminum-pot lines, carbon anode baking, fiberglass-fume control, coke-oven and metallurgical operations, chemical incineration, and phosphate-fertilizer operations. Two-stage precipitators are used increasingly for moderate-volume gas streams containing nonconductive liquid mists which will drain from the collecting plates. Their application on hydrocarbon mists has been quite successful, but careful attention must be given to fire and explosion hazards.

Electrically Augmented Collectors A new area for enhancing collection efficiency and lowering cost is the combining of electrostatic forces with devices using other collecting mechanisms such as impaction and diffusion. Cooper (Air Pollut. Control Assoc. Prepr. 75-02.1) evaluated the magnitude of forces operating between charged and uncharged particles and concluded that electrostatic attraction is the strongest collecting force operating on particles finer than 2 μm . Nielsen and Hill [*Ind. Eng. Chem. Fundam.*, **15**, 149 (1976)] have quantified these relationships, and a number of practical devices have been demonstrated. Pilat and Meyer (NTIS Publ. PB-252653, 1976) have demonstrated up to 99 percent collection of fine particles in a two-stage spray tower in which the inlet particles and water spray are charged with opposite polarity. The principle has been applied to retrofitting existing spray towers to enhance collection.

Klugman and Sheppard (Air Pollut. Control Assoc. Prepr. 75-30.3) have developed an ionizing wet scrubber in which the charged mist particles are collected in a grounded, irrigated cross-flow bed of Tellerette packing. Particles smaller than 1 μm have been collected

TABLE 14-21 Operating Characteristics of Various Types of Fiber Mist Eliminators as Used on Sulfuric Acid Plants*

	High efficiency	High velocity	Spray catcher
Controlling mechanism for mist collection	Brownian movement	Impaction	Impaction
Superficial velocity, m/s	0.075-0.20	2.0-2.5	2.0-2.5
Efficiency on particles greater than 3 μm , %	Essentially 100	Essentially 100	Essentially 100
Efficiency on particles 3 μm and smaller, %	95-99+	90-98	15-30
Pressure drop, cm H ₂ O	12-38	15-20	1.0-2.5

*Brink, Burggrabe, and Greenwell, *Chem. Eng. Prog.*, **64**(11), 82 (1968). To convert centimeters to inches, multiply by 0.394.

with 98 percent efficiency by using two units in series. Dembinsky and Vicard (Air Pollut. Control Assoc. Prepr. 78-17.6) have used an electrically augmented low-pressure [5 to 10 cm (2 to 4 in) of water] venturi scrubber to give 95 to 98 percent collection efficiency on submicrometer particles.

Particle Growth and Nucleation Fine particles may be subjected to conditions favoring the growth of particles either through condensation or through coalescence. Saturation of a hot gas stream with water, followed by condensation on the particles acting as nuclei when the gas is cooled, can increase particle size and ease of collection. Addition of steam can produce the same results. Scrubbing of the humid gas with a cold liquid can bring diffusiophoresis into play. The introduction of cold liquid drops causes a reduction in water-vapor pressure at the surface of the cold drop. The resulting vapor-pressure gradient causes a hydrodynamic flow toward the drop known as Stefan flow which enhances the movement of mist particles toward the spray drop. If the molecular mass of the diffusing vapor is different from the carrier gas, this density difference also produces a driving force, and the sum of these forces is known as diffusiophoresis. A mathematical description of these forces has been presented by Calvert (R-9) and by Sparks and Pilat [Atmos. Environ., 4, 651 (1970)]. Thermal differences between the carrier gas and the cold scrubbing droplets can further enhance collection through thermophoresis. Calvert and Jhaseri [J. Air Pollut. Control Assoc., 24, 946 (1974)]; and NTIS Publ. PB-227307, 1973]) have investigated condensation scrubbing in multiple-sieve plate towers.

Submicrometer droplets can be coagulated through brownian diffusion if given ample time. The introduction of particles 50 to 100 times larger in diameter can enhance coagulation, but the addition of a broad range of particle sizes is discouraged. Increasing turbulence will aid coagulation, so fans to stir the gas or narrow, tortuous passages such as those of a packed bed can be beneficial. Sonic energy can also produce coagulation, especially the production of standing waves in the confines of long, narrow tubes. Addition of water and oil mists can sometimes aid sonic coagulation. Sulfuric acid mist [Danser, Chem. Eng., 57(5), 158 (1950)] and carbon black [Stokes, Chem. Eng. Prog., 46, 423 (1950)] have been successfully agglomerated with sonic energy. Frequently sonic agglomeration has been unsuccessful because of the high energy requirement. Most sonic generators have very poor energy-transformation efficiency. Wegrzyn et al. (U.S. EPA Publ. EPA-600/7-79-004C, 1979, p. 233) have reviewed acoustic agglomerators. Mednikov (U.S.S.R. Akad. Soc. Moscow, 1963) suggested that the incorporation of sonic agglomeration with electrostatic precipitation could greatly reduce precipitator size.

Other Collectors Tarry particulates and other difficult-to-handle liquids have been collected on a dry, expendable phenol formaldehyde-bonded glass-fiber mat (Goldfield, *J. Air Pollut. Control Assoc.*, 20, 466 (1970)) in roll form which is advanced intermittently into a filter frame. Superficial gas velocities are 2.5 to 3.5 m/s (8.2 to 11.5 ft/s), and pressure drop is typically 41 to 46 cm (16 to 18 in) of water. Collection efficiencies of 99 percent have been obtained on submicrometer particles. Brady [*Chem. Eng. Prog.*, 73(8), 45 (1977)] has discussed a cleanable modification of this approach in which the gas is passed through a reticulated foam filter that is slowly rotated and solvent-cleaned.

In collecting very fine (mainly submicron) mists of a hazardous nature where one of the collectors previously discussed has been used as the primary one (fiber-mist eliminators of the Brownian diffusion type and electrically augmented collectors are primarily recommended), there is the chance that the effluent concentration may still be too high for atmospheric release when residual concentration must be in the range of 1–2 µm. In such situations, secondary treatment may be needed. Probably removal of the residual mist by adsorption will be in order. See "Adsorption," Sec. 16. Another possibility might be treatment of the remaining gas by membrane separation. A separator having a gas-permeable membrane that is essentially nonliquid-permeable could be useful. However, if the gas-flow volumes are appreciable, the device could be expensive. Most membranes have low capacity (requiring high membrane surface area) to handle high gas-permeation capacity. See "Membrane Processes," Sec. 29.

Continuous Phase Uncertain Some situations exist such as in

two-phase gas-liquid flow where the volume of the liquid phase may approach being equal to the volume of the vapor phase, and where it may be difficult to be sure which phase is the continuous phase. Svrek and Monnery [*Chem. Eng. Prog.*, 89(10), 53–60 (Oct. 1993)] have discussed the design of two-phase separation in a tank with gas-liquid separation in the middle, mist elimination in the top, and entrained gas-bubble removal from the liquid in the bottom. Monnery and Svrek [*Chem. Eng. Prog.*, 90(9), 29–40 (Sept. 1994)] have expanded the separation to include multiphase flow, where the components are a vapor and two immiscible liquids and these are also separated in a tank. A design approach for sizing the gas-liquid disengaging space in the vessel is given using a tangential tank inlet nozzle, followed by a wire mesh mist eliminator in the top of the vessel for final separation of entrained mist from the vapor. Design approaches and equations are also given for sizing the lower portion of the vessel for separation of the two immiscible liquid phases by settling and separation of discontinuous liquid droplets from the continuous liquid phase.

LIQUID-PHASE CONTINUOUS SYSTEMS

Practical separation techniques for gases dispersed in liquids are discussed. Processes and methods for dispersing gas in liquid have been discussed earlier in this section, together with information for predicting the bubble size produced. Gas-in-liquid dispersions are also produced in chemical reactions and electrochemical cells in which a gas is liberated. Such dispersions are likely to be much finer than those produced by the dispersion of a gas. Dispersions may also be unintentionally created in the vaporization of a liquid.

GENERAL REFERENCES: Adamson, *Physical Chemistry of Surfaces*, 4th ed., Wiley, New York, 1982. Akers, *Foams*, Academic, New York, 1976. Bikerman, *Foams*, Springer-Verlag, New York, 1973. Bikerman, et al., *Foams: Theory and Industrial Applications*, Reinhold, New York, 1953. Chremisinoff, ed., *Encyclopedia of Fluid Mechanics*, vol. 3, Gulf Publishing, Houston, 1986. Kerner, *Foam Control Agents*, Noyes Data Corp., Park Ridge, NJ, 1976. Rubel, *Antifoaming and Defoaming Agents*, Noyes Data Corp., Park Ridge, NJ, 1972. Rosen, *Surfactants and Interfacial Phenomena*, 2d ed., Wiley, New York, 1989. Sonntag and Strenge, *Coagulation and Stability of Disperse Systems*, Halsted-Wiley, New York, 1972. Wilson, ed., *Foams: Physics, Chemistry and Structure*, Springer-Verlag, London, 1989. "Defoamers" and "Foams", *Encyclopedia of Chemical Technology*, 4th ed., vols. 7, 11, Wiley, New York, 1993–1994.

Types of Gas-in-Liquid Dispersions Two types of dispersions exist. In one, gas bubbles produce an unstable dispersion which separates readily under the influence of gravity once the mixture has been removed from the influence of the dispersing force. Gas-liquid contacting means such as bubble towers and gas-dispersing agitators are typical examples of equipment producing such dispersions. More difficulties may result in separation when the gas is dispersed in the form of bubbles only a few micrometers in size. An example is the evolution of gas from a liquid in which it has been dissolved or released through chemical reaction such as electrolysis. Coalescence of the dispersed phase can be helpful in such circumstances.

The second type is a stable dispersion, or foam. Separation can be extremely difficult in some cases. A pure two-component system of gas and liquid cannot produce dispersions of the second type. Stable foams can be produced only when an additional substance is adsorbed at the liquid-surface interface. The substance adsorbed may be in true solution but with a chemical tendency to concentrate in the interface such as that of a surface-active agent, or it may be a finely divided solid which concentrates in the interface because it is only poorly wetted by the liquid. Surfactants and proteins are examples of soluble materials, while dust particles and extraneous dirt including traces of nonmiscible liquids can be examples of poorly wetted materials.

Separation of gases and liquids always involves coalescence, but enhancement of the rate of coalescence may be required only in difficult separations.

Separation of Unstable Systems The buoyancy of bubbles suspended in liquid can frequently be depended upon to cause the bubbles to rise to the surface and separate. This is a special case of gravity settling. The mixture is allowed to stand at rest or is moved along a

14-96 GAS ABSORPTION AND GAS-LIQUID SYSTEM DESIGN

TABLE 14-22 Terminal Velocity of Standard Air Bubbles Rising in Water at 20°C*

Bubble diameter, μm	10	30	50	100	200	300
Terminal velocity, mm/s	0.061	0.488	1.433	5.486	21.95	49.38

*Calculated from Stokes' law. To convert millimeters per second to feet per second, multiply by 0.003281.

flow path in laminar flow until the bubbles have surfaced. Table 14-22 shows the calculated rate of rise of air bubbles at atmospheric pressure in water at 20°C (68°F) as a function of diameter. It will be observed that the velocity of rise for 10- μm bubbles is very low, so that long separating times would be required for gas which is more finely dispersed.

For liquids other than water, the rise velocity can be approximated from Table 14-22 by multiplying by the liquid's specific gravity and the reciprocal of its viscosity (in centipoises). For bubbles larger than 100 μm , this procedure is erroneous, but the error is less than 15 percent for bubbles up to 1000 μm . More serious is the underlying assumption of Table 14-22 that the bubbles are rigid spheres. Circulation within the bubble causes notable increases in velocity in the range of 100 μm to 1 mm, and the flattening of bubbles 1 cm and larger appreciably decreases their velocity. However, in this latter size range the velocity is so high as to make separation a trivial problem.

In design of separating chambers, static vessels or continuous-flow tanks may be used. Care must be taken to protect the flow from turbulence, which could cause back mixing of partially separated fluids or which could carry unseparated liquids rapidly to the separated-liquid outlet. Vertical baffles to protect rising bubbles from flow currents are sometimes employed. Unseparated fluids should be distributed to the separating region as uniformly and with as little velocity as possible. When the bubble rise velocity is quite low, shallow tanks or flow channels should be used to minimize the residence time required.

Quite low velocity rise of bubbles due either to small bubble size or to high liquid viscosity can cause difficult situations. With low-viscosity liquids, separation-enhancing possibilities in addition to those previously enumerated are to sparge the liquid with large-diameter gas bubbles or to atomize the mixture as a spray into a tower. Large gas bubbles rising rapidly through the liquid collide with small bubbles and aid their coalescence through capture. Atomizing of the continuous phase reduces the distance that small gas bubbles must travel to reach a gas interface. Evacuation of the spray space can also be beneficial in promoting small-bubble growth and especially in promoting gas evolution when the gas has appreciable liquid solubility. Liquid heating will also reduce solubility.

Surfaces in the settling zone for bubble coalescence such as closely spaced vertical or inclined plates or tubes are beneficial. When clean low-viscosity fluids are involved, passage of the undegassed liquid through a tightly packed pad of mesh or fine fibers at low velocity will result in efficient bubble coalescence. Problems have been experienced in degassing a water-based organic solution that has been passed through an electrolytic cell for chemical reaction in which extremely fine bubbles of hydrogen gas are produced in the liquid within the cell. Near-total removal of hydrogen gas from the liquid is needed for process safety. This is extremely difficult to achieve by gravity settling alone because of the fine bubble size and the need for a coalescing surface. Utilization of a fine fiber media is strongly recommended in such situations. A low-forward liquid flow through the media is desirable to provide time for the bubbles to attach themselves to the fiber media through Brownian diffusion. Spielman and Goren [*Ind. Eng. Chem.*, **62**(10), (1970)] reviewed the literature on coalescence with porous media and reported their own experimental results [*Ind. Eng. Chem. Fundam.*, **11**(1), 73 (1972)] on the coalescence of oil-water liquid emulsions. The principles are applicable to a gas-in-liquid system. Glass-fiber mats composed of 3.5-, 6-, or 12- μm diameter fibers, varying in thickness from 1.3 to 3.3 mm, successfully coalesced and separated 1- to 7- μm oil droplets at superficial bed velocities of 0.02 to 1.5 cm/s (0.00067 to 0.049 ft/s).

In the deaeration of high-viscosity fluids such as polymers, the material is flowed in thin sheets along solid surfaces. Vacuum is applied to increase bubble size and hasten separation. The Versator (Cornell Machine Co.) degasses viscous liquids by spreading them

into a thin film by centrifugal action as the liquids flow through an evacuated rotating bowl.

Separation of Foam Foam is a colloidal system containing relatively large volumes of dispersed gas in a relatively small volume of liquid. Foams are thermodynamically unstable with respect to separation into their components of gas and vapor, and appreciable surface energy is released in the bursting of foam bubbles. Foams are dynamic systems in which a third component produces a surface layer that is different in composition from the bulk of the liquid phase. The stabilizing effect of such components (often present only in trace amounts) can produce foams of troubling persistence in many operations. (Foams which have lasted for years when left undisturbed have been produced.) Bendure [TAPPI, **58**(2), 83 (1975)], Keszthelyi [*J. Paint Technol.*, **46**(11), 31 (1974)], Ahmad [*Sep. Sci.* **10**, 649 (1975)], and Shedlovsky ("Foams," *Encyclopedia of Chemical Technology*, 2d ed., Wiley, New York, 1966) have presented concise articles on the characteristics and properties of foams in addition to the general references cited at the beginning of this subsection.

Foams can be a severe problem in chemical-processing steps involving gas-liquid interaction such as distillation, absorption, evaporation, chemical reaction, and particle separation and settling. It can also be a major problem in pulp and paper manufacture, oil-well drilling fluids, production of water-based paints, utilization of lubricants and hydraulic fluids, dyeing and sizing of textiles, operation of steam boilers, fermentation operations, polymerization, wet-process phosphoric acid concentration, adhesive production, and foam control in products such as detergents, waxes, printing inks, instant coffee, and glycol antifreeze.

Foams, as freshly generated, are gas emulsions with spherical bubbles separated by liquid films up to a few millimeters in thickness. They age rapidly by liquid drainage and form polyhedrals in which three bubbles intersect at corners with angles of approximately 120°. During drainage, the lamellae become increasingly thinner, especially in the center (only a few micrometers thickness), and more brittle. This feature indicates that with some foams if a foam layer can be tolerated, it may be self-limiting, as fresh foam is added to the bottom of the layer with drained foam collapsing on the top. (A quick-breaking foam may reach its maximum life cycle in 6 s. A moderately stable foam can persist for 140 s.) During drainage, gas from small foam bubbles, which is at a high pressure, will diffuse into large bubbles so that foam micelles increase with time. As drainage proceeds, weak areas in the lamella may develop. However, the presence of a higher concentration of surfactants in the surface produces a lower surface tension. As the lamella starts to fail, exposing bulk liquid with higher surface tension, the surface is renewed and healed. This is known as the *Marangoni effect*. If drainage can occur faster than Marangoni healing, a hole may develop in the lamella. The forces involved are such that collapse will occur in milliseconds without concern for rupture propagation. However, in very stable foams, electrostatic surface forces (zeta potential) prevent complete drainage and collapse. In some cases, stable lamella thicknesses of only two molecules have been measured.

Drainage rate is influenced by surface viscosity, which is very temperature-sensitive. At a critical temperature, which is a function of the system, a temperature change of only a few degrees can change a slow-draining foam to a fast-draining foam. This change in drainage rate can be a factor of 100 or more; thus increasing the temperature of foam can cause its destruction. An increase in temperature may also cause liquid evaporation and lamella thinning. As the lamellae become thinner, they become more brittle and fragile. Thus, mechanical deformation or pressure changes, which cause a change in gas-bubble volume, can also cause rupture.

Bendure indicates 10 ways to increase foam stability: (1) increase bulk liquid viscosity, (2) increase surface viscosity, (3) maintain thick

walls (higher liquid-to-gas ratio), (4) reduce liquid surface tension, (5) increase surface elasticity, (6) increase surface concentration, (7) reduce surfactant-adsorption rate, (8) prevent liquid evaporation, (9) avoid mechanical stresses, and (10) eliminate foam inhibitors. Obviously, the reverse of each of these actions, when possible, is a way to control and break foam.

Physical Defoaming Techniques Typical physical defoaming techniques include mechanical methods for producing foam stress, thermal methods involving heating or cooling, and electrical methods. Combinations of these methods may also be employed, or they may be used in conjunction with chemical defoamers. Some methods are only moderately successful when conditions are present to reform the foam such as breaking foam on the surface of boiling liquids. In some cases it may be desirable to draw the foam off and treat it separately. Foam can always be stopped by removing the energy source creating it, but this is often impractical.

Thermal Methods Heating is often a suitable means of destroying foam. As indicated previously, raising the foam above a critical temperature (which must be determined experimentally) can greatly decrease the surface viscosity of the film and change the foam from a slow-draining to a fast-draining foam. Coupling such heating with a mechanical force such as a revolving paddle to cause foam deformation is frequently successful. Other effects of heating are expansion of the gas in the foam bubbles, which increases strain on the lamella walls as well as requiring their movement and flexing. Evaporation of solvent may occur causing thinning of the walls. At sufficiently high temperatures, desorption or decomposition of stabilizing substances may occur. Placing a high-temperature bank of steam coils at the maximum foam level is one control method. As the foam approaches or touches the coil, it collapses. The designer should consider the fact that the coil will frequently become coated with solute.

Application of radiant heat to a foam surface is also practiced. Depending on the situation, the radiant source may be electric lamps, Glowbar units, or gas-fired radiant burners. Hot gases from burners will enhance film drying of the foam. Heat may also be applied by jetting or spraying hot water on the foam. This is a combination of methods since the jetting produces mechanical shear, and the water itself provides dilution and change in foam-film composition. Newer approaches might include foam heating with the application of focused microwaves. This could be coupled with continuous or intermittent pressure fluctuations to stress lamella walls as the foam ages.

Cooling can also destroy foam if it is carried to the point of freezing since the formation of solvent crystals destroys the foam structure. Less drastic cooling such as spraying a hot foam with cold water may be effective. Cooling will reduce the gas pressure in the foam bubbles and may cause them to shrink. This is coupled with the effects of shear and dilution mentioned earlier. In general, moderate cooling will be less effective than heating since the surface viscosity is being modified in the direction of a more stable foam.

Mechanical Methods Static or rotating breaker bars or slowly revolving paddles are sometimes successful. Their application in conjunction with other methods is frequently better. As indicated in the theory of foams, they will work better if installed at a level at which the foam has had some time to age and drain. A rotating breaker works by deforming the foam, which causes rupture of the lamella walls. Rapidly moving slingers will throw the foam against the vessel wall and may cause impact on other foam outside the envelope of the slinger. In some instances, stationary bars or closely spaced plates will limit the rise of foam. The action here is primarily one of providing surface for coalescence of the foam. Wettability of the surface, whether moving or stationary, is frequently important. Usually a surface not wetted by the liquid is superior, just as is frequently the case of porous media for foam coalescence. However, in both cases there are exceptions for which wettable surfaces are preferred. Shkodin [*Kolloidn. Zh.*, **14**, 213 (1952)] found molasses foam to be destroyed by contact with a wax-coated rod and unaffected by a clean glass rod.

Goldberg and Rubin [*Ind. Eng. Chem. Process Des. Dev.*, **6** 195 (1967)] showed in tests with a disk spinning vertically to the foam layer that most mechanical procedures, whether centrifugation, mixing, or blowing through nozzles, consist basically of the application of shear stress. Subjecting foam to an air-jet impact can also provide a source

of drying and evaporation from the film, especially if the air is heated. Other effective means of destroying bubbles are to lower a frame of metal points periodically into the foam or to shower the foam with falling solid particles.

Pressure and Acoustic Vibrations These methods for rupturing foam are really special forms of mechanical treatment. Change in pressure in the vessel containing the foam stresses the lamella walls by expanding or contracting the gas inside the foam bubbles. Oscillation of the vessel pressure subjects the foam to repeated film flexing. Parlow [Zucker, **3**, 468 (1950)] controlled foam in sugar-sirup evaporators with high-frequency air pulses. It is by no means certain that high-frequency pulsing is necessary in all cases. Lower frequency and higher amplitude could be equally beneficial. Acoustic vibration is a similar phenomenon causing localized pressure oscillation by using sound waves. Impulses at 6 kHz have been found to break froth from coal flotation [Sun, *Min. Eng.*, **3**, 865 (1958)]. Sonntag and Strenge (*Coagulation and Stability of Disperse Systems*, Halsted-Wiley, New York, 1972, p. 121) report foam suppression with high-intensity sound waves (11 kHz, 150 dB) but indicate that the procedure is too expensive for large-scale application. The Sontrifuge (Teknika Inc., a subsidiary of Chemineer, Inc.) is a commercially available low-speed centrifuge employing sonic energy to break the foam. Walsh [*Chem. Process.*, **29**, 91 (1966)], Carlson [*Pap. Trade J.*, **151**, 38 (1967)], and Thorhildsen and Rich [*TAPPI*, **49**, 95A (1966)] have described the unit.

Electrical Methods As colloids, most foams typically have electrical double layers of charged ions which contribute to foam stability. Accordingly, foams can be broken by the influence of an external electric field. While few commercial applications have been developed, Sonntag and Strenge (op. cit., p. 114) indicate that foams can be broken by passage through devices much like electrostatic precipitators for dusts. Devices similar to two-stage precipitators having closely spaced plates of opposite polarity should be especially useful. Sonntag and Strenge, in experiments with liquid-liquid emulsions, indicate that the colloid structure can be broken at a field strength of the order of $8 \text{ to } 9 \times 10^5 \text{ V/cm}$.

Chemical Defoaming Techniques Sonntag and Strenge (op. cit., p. 111) indicate two chemical methods for foam breaking. One method is causing the stabilizing substances to be desorbed from the interface, such as by displacement with other more surface-active but nonstabilizing compounds. Heat may also cause desorption. The second method is to carry on chemical changes in the adsorption layer, leading to a new structure. Some defoamers may act purely by mechanical means but will be discussed in this subsection since their action is generally considered to be chemical in nature. Often chemical defoamers act in more than one way.

Chemical Defoamers The addition of chemical foam breakers is the most elegant way to break a foam. Effective defoamers cause very rapid disintegration of the foam and frequently need be present only in parts per million. The great diversity of compounds used for defoamers and the many different systems in which they are applied make a brief and orderly discussion of their selection difficult. Compounds needed to break aqueous foams may be different from those needed for aqueous-free systems. The majority of defoamers are insoluble or nonmiscible in the foam continuous phase, but some work best because of their ready solubility. Lichtman (*Defoamers*, 3d ed., Wiley, New York, 1979) has presented a concise summary of the application and use of defoamers. Rubel (*Antifoaming and Defoaming Agents*, Noyes Data Corp., Park Ridge, N.J., 1972) has reviewed the extensive patent literature on defoamers. Defoamers are also discussed extensively in the general references at the beginning of this subsection.

One useful method of aqueous defoaming is to add a nonfoam stabilizing surfactant which is more surface-active than the stabilizing substance in the foam. Thus foam stabilized with an ionic surfactant can be broken by the addition of a very surface-active but nonstabilizing silicone oil. The silicone displaces the foam stabilizer from the interface by virtue of its insolubility. However, it does not stabilize the foam because its foam films have poor elasticity and rupture easily.

A major requirement for a defoamer is cost-effectiveness. Accordingly, some useful characteristics are low volatility (to prevent strip-

14-98 GAS ABSORPTION AND GAS-LIQUID SYSTEM DESIGN

ping from the system before it is dispersed and does its work), ease of dispersion and strong spreading power, and surface attraction-orientation. Chemical defoamers must also be selected in regard to their possible effect on product quality and their environmental and health suitability. For instance, silicone antifoam agents are effective in textile jet dyeing but reduce the fire retardancy of the fabric. Mineral-oil defoamers in sugar evaporation have been replaced by specifically approved materials. The tendency is no longer to use a single defoamer compound but to use a formulation specially tailored for the application comprising carriers, secondary antifoam agents, emulsifiers, and stabilizing agents in addition to the primary defoamer. Carriers, usually hydrocarbon oils or water, serve as the vehicle to support the release and spread of the primary defoamer. Secondary defoamers may provide a synergistic effect for the primary defoamer or modify its properties such as spreadability or solubility. Emulsifiers may enhance the speed of dispersion, while stabilizing agents may enhance defoamer stability or shelf life.

Hydrophobic silica defoamers work on a basis which may not be chemical at all. They are basically finely divided solid silica particles dispersed in a hydrocarbon or silicone oil which serves as a spreading vehicle. Kulkarni [*Ind. Eng. Chem. Fundam.*, **16**, 472 (1977)] theorizes that this mixture defoams by the penetration of the silica particle into the bubble and the rupture of the wall. Table 14-23 lists major types of defoamers and typical applications.

Other Chemical Methods These methods rely chiefly on destroying the foam stabilizer or neutralizing its effect through methods other than displacement and are applicable when the process will permit changing the chemical environment. Forms stabilized with alkali esters can be broken by acidification since the equivalent free acids do not stabilize foam. Foams containing sulfated and sulfonated ionic detergents can be broken with the addition of fatty-acid soaps and calcium salts. Several theories have been proposed. One suggests that the surfactant is tied up in the foam as double calcium salts of both the sulfonate and the soap. Another suggests that calcium soaps oriented in the film render it inelastic.

Ionic surfactants adsorb at the foam interface and orient with the

charged group immersed in the lamellae and their uncharged tails pointed into the gas stream. As the film drains, the charged groups, which repel each other, tend to be moved more closely together. The repulsive force between like charges hinders drainage and stabilizes the film. Addition of a salt or an electrolyte to the foam screens the repulsive effect, permits additional drainage, and can reduce foam stability.

Foam Prevention Chemical prevention of foam differs from defoaming only in that compounds or mixtures are added to a stream prior to processing to prevent the formation of foam either during processing or during customer use. Such additives, sometimes distinguished as antifoam agents, are usually in the same chemical class of materials as defoamers. However, they are usually specifically formulated for the application. Typical examples of products formulated with antifoam agents are laundry detergents (to control excess foaming), automotive antifreeze, instant coffee, and jet-aircraft fuel. Foaming in some chemical processes such as distillation or evaporation may be due to trace impurities such as surface-active agents. An alternative to antifoam agents is their removal before processing such as by treatment with activated carbon [Pool, *Chem. Process.*, **21**(9), 56 (1958)].

Automatic Foam Control In processing materials when foam can accumulate, it is often desirable to measure the height of the foam layer continuously and to dispense defoamer automatically as required to control the foam. Other corrective action can also be taken automatically. Methods of sensing the foam level have included electrodes in which the electrical circuit is completed when the foam touches the electrode [Nelson, *Ind. Eng. Chem.*, **48**, 2183 (1956); and Browne, U.S. Patent 2,981,693, 1961], floats designed to rise in a foam layer (Carter, U.S. Patent 3,154,577, 1964), and change in power input required to turn a foam-breaking impeller as the foam level rises (Yamashita, U.S. Patent 3,317,435, 1967). Timers to control the duration of defoamer addition have also been used. Browne has suggested automatic addition of defoamer through a porous wick when the foam level reaches the level of the wick. Foam control has also been discussed by Kroll [*Ind. Eng. Chem.*, **48**, 2190 (1956)].

TABLE 14-23 Major Types and Applications of Defoamers

Classification	Examples	Applications
Silicones	Dimethyl silicone, trialkyl and tetraalkyl silanes	Lubricating oils; distillation; fermentation; jam and wine making; food processing
Aliphatic acids or esters	Mostly high-molecular-weight compounds; diethyl phthalate; lauric acid	Papermaking; wood-pulp suspensions; water-based paints; food processing
Alcohols	Moderate- to high-molecular-weight monohydric and polyhydric alcohols; octyl alcohol; C-12 to C-20 alcohols; lauryl alcohol	Distillation; fermentation; papermaking; glues and adhesives
Sulfates or sulfonates	Alkali metal salts of sulfated alcohols, sulfonic acid salts; alkyl-aryl sulfonates; sodium lauryl sulfate	Nonaqueous systems; mixed aqueous and nonaqueous systems; oil-well drilling muds; spent H ₂ SO ₄ recovery; deep-fat frying
Amines or amides	Alkyl amines (undecyloctyl and diamyl methyl amine); polyamides (acyl derivatives of piperazine)	Boiler foam; sewage foam; fermentation; dye baths
Halogenated compounds	Fluochloro hydrocarbons with 5 to 50 C atoms; chlorinated hydrocarbons	Lubrication-oil and grease distillation; vegetable-protein glues
Natural products	Vegetable oils; waxes, mineral oils plus their sulfated derivatives (including those of animal oils and fats)	Sugar extraction; glue manufacture; cutting oils
Fatty-acid soaps	Alkali, alkaline earth, and other metal soaps; sodium stearate; aluminum stearate	Gear oils; paper stock; paper sizing; glue solutions
Inorganic compounds	Monosodium phosphate mixed with boric acid and ethyl carbonate; disodium phosphate; sodium aluminate, bentonite and other solids	Distillation; instant coffee; boiler feedwater; sugar extraction
Phosphates	Alkyl-alkalene diphosphates; tributyl phosphate in isopropanol	Petroleum-oil systems; foam control in soap solutions
Hydrophobic silica	Finely divided silica in polydimethyl siloxane	Aqueous foaming systems
Sulfides or thio derivatives	Metallic derivatives of thio ethers and disulfides, usually mixed with organic phosphite esters; long-chain alkyl thiienyl ketones	Lubricating oils; boiler water